LANDSCAPE STRUCTURE, REGIMES, AND THE CO-EVOLUTION OF HYDROLOGIC SYSTEMS

BY

CIARAN JOSEPH HARMAN

DISSERTATION

Submitted in partial fulfillment of the requirements
for the degree of Doctor of Philosophy in Civil Engineering
in the Graduate College of the
University of Illinois at Urbana-Champaign, 2011

Urbana, Illinois

Doctoral Committee:

Professor Murugesu Sivapalan, Chair and Director of Research
Professor Praveen Kumar
Professor Albert J. Valocchi
Professor P. Suresh C. Rao, Purdue University
Assistant Professor Kathleen Lohse, Idaho State University

Abstract

In this dissertation I discuss approaches to building hydrologic understanding in a changing world that go beyond the construction of models of ever-greater complexity. These approaches aim to develop insight into the relationship between catchment properties and hydrologic dynamics using reduced-complexity models, and by looking for patterns that reveal emergent relationships between hydrologic systems and the landscapes they are embedded in. The dissertation proposes a framework for thinking about hydrologic systems in a changing world based on seeking a synthesis between the search for mechanistic descriptions of landscape *processes*, and the search for explanations for emergent landscape *patterns*.

The dissertation is divided into two parts. The first describes a series of studies considering controls on the propagation of hydrologic variability through the landscape. One discusses the propagation of water and solutes through the vadose zone, another the lateral movement of water through a hillslope, and the third the accumulated effect of many hillslopes on the recession of flows at a watershed outlet. Each case builds on parsimonious representations of hydrologic processes to distill analytical results in terms of landscape and climate properties. These analytical results are used to define 'regimes' of hydrologic behavior in which particular properties play decisive roles in the hydrologic system. The studies demonstrate that the regime framework yields insight into controls on the aggregate behavior of hydrologic system that can be used to develop 'closure relations' capable of representing the effects of unresolved landscape structure on hydrologic fluxes without resolving them explicitly.

The second part of the dissertation is concerned with how the landscape structure controlling the hydrologic dynamics has come to be the way it is, and the role that hydrologic variability plays in its evolution. This question is pursued at a range of scales, using modeling and data analysis. Inter-annual water balance variability across the climates and geologies of the continental US are examined for patterns in the dynamics of co-evolved landscapes. A simple model is then used to illustrate how catchment water-balance is affected by feedbacks between the lateral redistribution of water and the spatial organization of vegetation along the network.

This work illustrates how insights into why and how landscape hydrology varies from place to place

and through time can be built through a focus on the behavior that emerges from small-scale dynamics, conditioned by the over-arching climate, geology and the contingencies of history. These insights point the way to a new paradigm for hydrology that treats hydrologic systems as integrated wholes that have evolved through time, and will continue to change in the future.

. . . for Mum and Dad, of course

Acknowledgments

Many people have contributed directly and indirectly to this dissertation. I have mentioned at the start of each chapter some of the people that I directly collaborated with to create each piece, but there are many others whose insights and support have also helped me along the way. I must first pay tribute to Siva Sivapalan, who has been a mentor for me for many years now. Siva gave me excellent fundamental training many years ago when I was an undergraduate, and has given me extraordinary opportunities in the past 6 years as a graduate student. Few students are blessed with advisors so dedicated, generous and supportive.

Partly as a result of the opportunities that Siva gave me, I owe a debt of thanks to many others who have given me support and guidance over the years: Praveen Kumar for his deep, quantitative reasoning about systems, and for challenging my thinking when I get sloppy, Suresh Rao for his gentle, inspirational, Guru-like nature (that hides a quick, hard-headed intelligence), Peter Troch for his long-standing support for my work and for me personally, Kathleen Lohse, who supported for my crazy ideas, showed me the tools and gave me the resources I needed to execute them, Matt Reeves for being willing to work effectively *pro-bono* to follow an idea where it led, and Sally Thompson, who is an inspiration, a bench-mark and a great friend.

There are many others who deserve a mention. My office-mates Juan Quijano and Venkat Srinivasan (from whose always-interesting and probing conversations I had to hide to complete this dissertation); everyone involved in the 2009 Summer Hydrologic Synthesis Institute, especially Stefano Zanardo, Mary Yaeger, Nandita Basu, Gavan McGrath and Marwan Hassan; all the people who have looked after the bureaucratic side of things that I have little patience for, especially Jennifer Wilson (who is also a great friend), Mary Pearson and Robin Ray. I have had dear friends here in Champaign-Urbana that have made life outside of work fun: James Ivaska, Patrick Mustain, An-Phong Le, Jeff Comer, Megan Kniepkamp, Michelle Schmidt (and the whole Schmidt family), Nic Zea, Walter Frei and many others.

In the end, none of this would have been possible without the love and support of my parents, Liz and Frank Harman, and my sister Nicole. They have always been there to help me see what is really important, and remind me that it isn't always work. I am looking forward to spending some time now with them on the things that really matter.

The work in this dissertation was funded by the the NSF-funded Hydrologic Synthesis project, "Water Cycle Dynamics in a Changing Environment: Advancing Hydrologic Science through Synthesis" (NSF Grant EAR-0636043, M. Sivapalan, PI), NSF grant EAR09-11205 "Biotic alteration of soil hydrologic properties and feedback with vegetation dynamics in water limited ecosystems" (PI: Sivapalan), and NSF grant ATM06-28687 "Interactions Between Water, Energy and Carbon Dynamics as Predictors of Canopy to Ecosystem Scale Vegetation Pattern and Function in a Changing Environment".

Table of Contents

List of Tables . . . . . **x**

List of Figures . . . . . **xi**

Chapter 1 Five ways of thinking: Towards a new epistemology for landscape hydrology under change **1**
1.1 Introduction 2
1.2 Hydrologic Drivers, Structure, Dynamics, and Science 4
1.3 Five ways of thinking in hydrology 8
1.3.1 Forms 9
1.3.2 Mechanisms 9
1.3.3 Regimes 10
1.3.4 Co-evolution 11
1.3.5 Functions 12
1.3.6 Spiraling towards a synthesis of world-views 12
1.4 Outline of this dissertation 13

I Regimes and Processes **16**

Chapter 2 Climate, soil and vegetation controls on the temporal variability of vadose zone transport - Simplified modeling framework **17**
2.1 Introduction 18
2.2 Event-based model of solute transport in the root zone 20
2.2.1 Soil water storage dynamics 21
2.2.2 Solute transport and degradation 24
2.2.3 Typical results for various solutes, soils, climates 26
2.2.4 Validation of the model against HYDRUS 1-D 28
2.3 Conclusions 34
2.4 Acknowledgments 34

Chapter 3 Climate, soil and vegetation controls on the temporal variability of vadose zone transport - Probabilistic analysis **35**
3.1 Introduction 36
3.2 Solute leaching as a stochastic process 37
3.2.1 Distribution of transport event sizes and waiting times 38
3.2.2 Framework for deriving the PDF of transit times and delivery ratios 40
3.2.3 Analytical solution for $\phi = 0$ 44
3.2.4 Approximate solution for $\phi > 0$ 46
3.3 Discussion 50
3.3.1 Sensitivity to climate and soil properties 50
3.3.2 Classification of realistic scenarios 56

3.4 Conclusions . . . 59
3.5 Acknowledgments . . . 60

Chapter 4 A subordinated kinematic wave equation for heavy-tailed flow responses from heterogeneous hillslopes . . . 61
4.1 Introduction . . . 62
4.1.1 The closure problem . . . 62
4.1.2 Effects of heterogeneity on hillslope-scale hydrologic response . . . 64
4.2 Theoretical development . . . 66
4.2.1 Kinematic wave equation . . . 67
4.2.2 Subordination of the kinematic wave equation . . . 69
4.3 Numerical simulations of hillslope flow . . . 73
4.4 Results . . . 75
4.4.1 Linearity of hillslope response . . . 75
4.4.2 Single impulse response . . . 77
4.4.3 Event response . . . 80
4.5 Discussion . . . 81
4.6 Conclusions . . . 84
4.7 Acknowledgments . . . 85

Chapter 5 Power-law catchment-scale recessions arising from heterogeneous linear small-scale dynamics . . . 86
5.1 Introduction . . . 87
5.1.1 Recession curves and catchment properties . . . 87
5.1.2 Aims of this work . . . 89
5.2 Theory . . . 90
5.2.1 Linear reservoir approximation . . . 90
5.2.2 Impulse responses . . . 91
5.2.3 Steady-state recharge . . . 97
5.2.4 Periodic recharge . . . 99
5.3 Application to data . . . 101
5.3.1 Comparison with Panola recession data . . . 101
5.3.2 Comparison to published datasets of b exponents . . . 104
5.4 Discussion . . . 106
5.4.1 The recession slope curve as a signature of spatial and temporal variability . . . 106
5.4.2 Relationship to the hydraulic interpretation of the recession . . . 107
5.5 Conclusions . . . 108
5.6 Acknowledgments . . . 109

II Functional patterns and Co-evolution 110

Chapter 6 Functional patterns of elasticity of fast and slow runoff components to precipitation change in the continental United States . . . 111
6.1 Introduction . . . 112
6.1.1 Space-for-time and time-for-time approaches to understanding water-balance sensitivity 113
6.1.2 Outline of this work . . . 115
6.2 Methods . . . 116
6.2.1 Sensitivity in the Ponce and Shetty framework . . . 117
6.2.2 The MOPEX dataset: parameter estimation and uncertainty . . . 118
6.3 Results . . . 120
6.3.1 Sensitivity of streamflow components to precipitation . . . 120
6.3.2 Robustness of functional parameters and sensitivity results . . . 123
6.3.3 Controls of the functional parameters on sensitivity . . . 123

6.4 Discussion: functional controls on climate sensitivity . . . 125
6.5 Discussion: Comparison with other predictions of climate sensitivity . . . 128
6.6 Conclusions . . . 130
6.7 Acknowledgments . . . 133

Chapter 7 Scaling of ecohydrologically mediated water balance partitioning . . . 134
7.1 Introduction . . . 135
7.2 A simple model of water balance and vegetation coupling on a hierarchical flowpath network 137
7.2.1 Model formulation . . . 137
7.2.2 Solution of governing equations in a link of the network . . . 141
7.2.3 Solving the model along the network . . . 142
7.3 Discussion . . . 143
7.3.1 Vegetation and water balance patterns along the network . . . 143
7.3.2 Controls of landscape and vegetation parameters on subsidy-based patterns . . . 146
7.3.3 Effects on climate sensitivity of water balance . . . 148
7.4 Conclusions . . . 150

Chapter 8 Conclusions . . . 152
8.1 Major contributions of the dissertation . . . 152
8.2 Future research . . . 153

References . . . 157

Vita . . . 171

List of Tables

1.1 Properties of the five ways of thinking about hydrology 8

2.1 Soil properties used for the example simulations, and for validation of the model against HYDRUS. 27
2.2 Climate properties for the example simulations 27
2.3 Pesticide properties for the example simulations 28

3.1 Dimensionless numbers characterizing the hydrologic and solute transport behavior of four soil/climate combinations and four common pesticides. The first two, ϕ and γ represent the aridity index, the storage capacity of the soil relative to the average storm, respectively. Λ is a function of the water balance (see Section 3.3). $\kappa\Lambda^2$ determines whether the transport through the soil is dominated by the mean travel time or large, rare events. $R\gamma$ is a measure of the number of storms required to transport the solute through the soil. The products $k\mu_T$ and $k\mu_{T0}$ are the Damkŏhler numbers for the cases with and without evapotranspiration. . . 58

4.1 Parameters of the subordinated kinematic wave equation fitted to mean impulses responses from ensemble hillslope simulations with various degrees of heterogeneity. [a]Natural log of the standard deviation of K in the random hillslope fields. [b]Tail index of stable subordinator. [c]Temporal shift applied to piston during calibration. [d]Effective velocity $[L/t^\gamma]$ of subordinated solution: ratio of v and s, where $v = 0.12$ [m/hr] for all single impulse realizations. 83

5.1 Parameters of the bounded power-law distribution fitted to the Panola recession data. 102

6.1 Overview of the estimated parameters for the Ponce and Shetty model and derived elasticities for the MOPEX dataset. Minimum, mean, maximum and standard deviation of the best estimates are shown, indicating the distribution across all the sites of the (individual sites' best estimate of) parameters and elasticities. The median absolute and relative error refer to the median level (between sites) of the uncertainty in sites' parameter and elasticity estimates. 122

List of Figures

1.1 Five ways of thinking about hydrology, arranged in a spiral that alternates between Newtonian and Darwinian thought. 8

2.1 Representation of water and solute dynamics in the HEIST model. The infiltration $I(t_i)$ from rainfall event i forms a sharp wetting front that displaces antecedent moisture in the profile. After redistribution the upper part of the profile has a maximum water content at field capacity θ_{fc} and the lower part is unchanged. The transport of the solute load centered at depth ξ_j depends on the difference between the infiltration $I(t_i)$ and the storage deficit in the soil above it $SD(\xi_j, t_i^-)$. Evapotranspiration $E(t_i)$ is removed from the profile between one storm and the next, creating this storage deficit. 22

2.2 Typical transport and degradation of four pesticides in coarse and fine soils under a humid climate and a semi-arid climate, as given by the parameters in Tables 1, 2 and 3. As the pesticides move down through the soil profile they are degraded (indicating by the fading lines) and spend longer at a particular depth before being mobilized by the flow again, and "jumping" to a deeper point, or being leached out of the domain. 29

2.3 Comparison of the cumulative drainage from the base of the (free draining) vadose zone predicted by HYDRUS (solid line) and the current model with two values of ϵ. Insets show detail of the behavior over the first year of the simulation. These results indicate that the model does a good job at replicating the timing and magnitude of drainage events, though the precise value of α required to match HYDRUS is uncertain. 32

2.4 Comparison of the cumulative leaching of pesticide loads from the base of the vadose zone predicted by HYDRUS (solid line) and the current model with various values of θ_R. These results indicate that the model also does a good job at replicating the timing and magnitude of leaching events, though, again, the precise value of the effective parameter required to match HYDRUS is uncertain. 33

3.1 Numerical experiments indicate that the waiting times between transport events are not Poissonian except for small values of γ and ϕ. They also become increasingly power-law with depth. The solid line gives the PDF of the waiting times between infiltration events (an exponential with rate parameters λ_p). 41

3.2 Transport distance in each "jump" (see Figure 2.2) follows a exponential distribution with a mean given by $\alpha/R\theta_{fc}$. This appears to hold throughout the profile, and for all combinations of γ and ϕ. 42

3.3 Probability density function of the transit time T for solute fronts for the special case of no evapotranspiration ($\phi = 0$), normalized by the storm arrival rate λ_p. The atom of probability at $T = 0$ is not shown. Three cases of the shape parameter $R\gamma$ are shown: 1, 5, 20. 45

3.4 Relationships between the effective parameters observed in 400 random simulations (normalized by their original values) λ_e/λ_p and γ_e/γ and the ratio λ_d/λ_p. Two very simple relationships emerge: the effective mean jump rate λ_e is very closely approximated by λ_d, and the effective storage parameter γ_e scales with $(\lambda_d/\lambda_p)^{\frac{1}{2}}$. 47

3.5 Comparison of mean and variance of the travel time distribution predicted by eqs. 3.9, with those derived from 400 random simulations. The inset plots show the same relationships with the parameters λ_p and γ replaced with the effective parameters λ_e and γ_e. The water balance E/P in each simulation is represented by the tone of the dots. These results show that the moments of the travel time distribution are very well characterized by the derived expressions when the effective parameters are used. 48
3.6 Examples of the ability of equation 3.11 to predict the PDF of the delivery ratio for bromacil. When the original parameters are used, representing the case with no evapotranspiration, delivery ratio is overestimated (dashed line). When evapotranspiration is accounted for using the effective parameters, equation 3.11 provides an excellent prediction of the PDF of pesticide delivery (solid line). 49
3.7 Contours of the ratio $\Lambda = \sqrt{\lambda_p/\lambda_d}$ as a function of the soil ratio γ and the aridity index ϕ. This ratio controls the increase in travel time due to the effect of evapotranspiration. 52
3.8 Contours of the normalized mean and CV of the arrival time distributions as a function of γ and ϕ. Darker colors represent larger values. 53
3.9 Contours of the variance of delivery ratio as a function of ϕ and γ for various values of the retardation coefficient R and normalized decay rate κ. 54
3.10 Contours of mean delivery ratio $< M/M_0 >$ as a function of ϕ and γ for various values of the retardation coefficient R and normalized decay rate κ. 55
3.11 Each darker pair of bars in the figure above gives the mean (center of the bar) and standard deviation (length of the bar) of the travel time (in days) predicted by the numerical model (background bar in each pair) and its analytical approximation (foreground bar), Equation 3.19, for various pesticides under the four example scenarios. Ligher bars show the mean and standard deviation when the effects of evapotranspiration are neglected (lighter pair of bars, back bar is numerical result, front bar is analytical approximation). 56
3.12 Mean (center of the bar) and standard deviation (length of the bar) of the delivery ratio predicted by the numerical model (lower bar in each pair) and its analytical approximation, Equation 3.21, (upper bar) for the example scenarios. Ligher bars show the mean and standard deviation when the effects of evapotranspiration are neglected (lighter pair of bars, lower bar is numerical result, upper bar is analytical approximation). 57

4.1 Impulse response obtained by randomizing the velocity of a piston according to a log-normal distribution with various σ parameters. This approximates the subsurface discharge response of a hillslope comprised of strips (from ridge to base) of diffferent soil materials. Though unrealistic, it demonstrates how the same underlying kinematic-wave like behaviour can produce piston-like, exponential-like and power-law-like behavior, depending on the degree of spatial variability. 65
4.2 Schematic depicting how recharge impulses distributed along a hillslope (left) with constant velocity produce a piston flow response at the base of a hillslope (right), where the magnitude of the piston is Rv/L with duration L/v. An impulse at an arbitrarily initial location x_s has an arrival time t_s of $(L - x_s)/v$. 70
4.3 Kinematic wave solutions for (left) values of γ ranging from 0.1 (highly heterogeneous) to 1 (homogenous, classic piston) with s held constant at 1 and (right) for values of s ranging from 10^{-4} to 10^3 with γ held constant at 0.9. The subordinated solution at early time has a slope equal to $-1+\gamma$ under the influence of the piston impulse and transitions to a slope of $-1-\gamma$ after depletion of the piston impulse input. Times of transition between the two slopes are directly related to s and inversely related to γ. 73
4.4 Examples of random K fields with $\sigma_{LogK} = 5$ given correlation length scales (relative to the domain size) of 1/20, 1/10 and 1/5. The 'Combined' case was computed by averaging the three previous fields, thereby containing multiple correlation lengths. 74

4.5 Evidence for the approximate linearity of the subsurface flow response described by the Boussinesq equation in highly heterogeneous conductivity fields. The left plot of each pair shows the impulse response, and the right shows the response to a arbitrary input predicted by the full Boussinesq model (solid line) and predicted by convolving the impulse response with the (dashed line) recharge input. Details given in the text. 76
4.6 Discharge results with time for (top to bottom) $\sigma_{LogK} = 1$, 5, and 10 and (left to right) $\hat{L}_K = 1/5$, 1/10, 1/20 and the combined case. Solid line is the log mean, and dashed lines are ± 1 standard deviation of the log transformed values. 77
4.7 Mean discharge for (top to bottom) $\sigma_{\ln K} = 1$, 5, and 10 for each of the correlation length cases. The correlation length seems to have very little effect on the ensemble (geometric) mean discharge, but does affect the standard deviation of discharge; $\pm 1\sigma$ is plotted in light gray for correlation lengths $L/5$ and $L/20$. 78
4.8 Ensemble mean discharge for σ_{LogK} values of 1, 3, 5 and 10, respectively, along with best fit subordinated wave equation, plotted on log-log axes. Note that the absence of heavy tails in the $\sigma_{LogK} = 1$ case excludes the use of the kinematic wave equation. However, its solution is provided for comparison. Insets show same data in with linear axes. 79
4.9 Simulated discharge from 100 generated heterogeneous hillslopes ($\sigma_{\log K} = 5$, 'combined' correlation lengths) subject to a 24 hour recharge event, and the prediction provided by the subordination approach (black line). Gray lines give individual realizations of Q, dark gray is their geometric mean. The recharge event is shown at the top. 81
4.10 Empirical relationship between heterogeneity and tail index of the γ-stable subordinator. . . 82

5.1 Left to right, the pdf $f(V)$, unit hydrograph $IUH(t)$ and recession slope curve $g(t)$ for the case where $f(V)$ is a Gamma distribution (equation 5.5). All axes are made dimensionless using the V_0 parameter. Values of α are 0.2 (dotted line), 1 (dash-dot), 5 (dashed line). Example power-laws with exponents 1 and 2 are plotted in gray on the right plot. 92
5.2 Derived relationships between variability in catchment properties and the recession slope curve exponent b. Curves are shown for the case of a Gamma distribution (left) following impulses (dashed line, equation 5.8) and following steady-state recharge (dash-dot line, equation 5.8), for a Lognormal distribution following an impulse (center, exponents estimated), and for a bounded power-law following an impulse (right, equations 5.21 and 5.25) with various values of κ. 93
5.3 Same as Figure 5.1, but for the Lognormal distribution (equation 5.9. Values of σ are 0.3 (dotted line), 1 (dash-dot), 3 (dashed line). 93
5.4 Same as Figure 5.1, but for the bounded power-law distribution (equation 5.22). Values of γ are -1.5 (dotted line), -0.99 (dash-dot), and 2 (dashed line). Example power-laws with exponents 1,2 and 3 are plotted in gray on the right plot. 96
5.5 Comparison of the exponent of the recession slope curve predicted by equation (21) (solid line) and fitted to the early part ($t = 1/V_0$ to $10/V_0$) of the recession slope curve when $f(V)$ follows a bounded power law distribution. 97
5.6 Control of the variability of recharge events on the recession slope curve. For Gamma distributions of V with low variability (left plot) the recession following an impulse, following periodic recharge and following steady-state recharge are all similar. For larger degrees of variability (center, right), the recession curves following impulse and steady-state recharge become different. The recession curves following periodic recharge depend on the inter-storm period. Results are for $\alpha = \{2, 1, 1/2\}$, $V_0 = 1$ day^{-1}, $P_0 = 1$mm day^{-1}, $t_r = 3$ days, $Q_0 = 1$mm, $R_0 = 1$mm day^{-1}. 100
5.7 Recession data from the Panola Mountain Research Watershed compared to (dashed line) the multiple linear reservoir model of *Clark et al.* (2009), and the generalization to an ensemble proposed in this work with (solid line) a Gamma distribution of V and assuming initially steady state recharge, and (dash-dot line) bounded power-law distribution of V and assuming an impulse of recharge with no initial storage in the catchment. 102

5.8 Comparison of the cumulative densities of V fitted to the Panola data in *Clark et al.* (2009) and in this work. . . . 103
5.9 Comparison of observed values of the recession slope curve exponents, values obtained from approximate solutions of the Boussinesq equation, and values obtained from ensembles of linear reservoirs with various distributions of V. Values of b from Panola (diamonds) and *Tague and Grant* (2004) (stars), k_K (circles) from *Kirchner* (2009), k_C from *Chapman* (1999), k_W from *Wittenberg* (1999). . . . 105
5.10 The hydraulic theory and the theory presented here both provide explanations for the same phenomenon, though based on different assumptions about the relative importance of the heterogeneity and hydraulics in controlling the phenomenon. Consequently, neither gives full account of the behavior of real catchments, in which both these factors are likely relevant. . . . 107

6.1 Relationships between elasticity and the humidity index, P/E_P. Elasticity is higher for total flow and both components in the arid sites, and converges to a common value in humid sites. Three relationships cited in *Dooge* (1992) are plotted for comparison. . . . 121
6.2 Elasticity of runoff components in the continental US. . . . 122
6.3 Relationship beween the predicted elasticity and the functional parameters (normalized by P). Differences between sites' sensitivity is mostly explained by differences in their threshold parameters $\lambda_s W_P$ and $\lambda_u V_P$. The upper potential W_P and V_P have less relative control. . . . 124
6.4 The thresholds for runoff production (normalized by annual precipitation) are directly correlated with the Horton index. Absolute uncertainty in the threshold parameters is shown by the tone (uncertainty greater than 0.15 is given by an asterix). . . . 124
6.5 Quick flow as a function of precipitation for two very similar sites that differ mainly in their quick flow thresholds. See text for a discussion. . . . 126
6.6 Relationship between the elasticity and the Horton index. Curves are gvien by equation 6.20. Black lines use thresholds predicted by regression, while the grey lines show the sensitivity when the thresholds are set to zero. The dashed, solid and dash-dot lines represent different values of $W_P/\overline{P}$. Values used are representative of median (4.5) 10^{th} percentile (2.7) and 90^{th} percentile (10.1) in the MOPEX data. . . . 127
6.7 Comparison of estimated elasticity from the P&S model with the non-parametric approach of *Sankarasubramanian et al.* (2001). The non-parametric approach predicts lower elasticities at the upper and lower end of the distribution. Tone represents the relative uncertainty (light tone is higher relative uncertainty). . . . 129

7.1 Virgin forest cover in the US at the time of colonization appears to follow a gradient from complete absence to complete presence across the continent, and was strongly organized by the river network in mesic climates. The self-similarity of this vegetation coverage is reflected in the historical forest cover of the state of Illinois. Interestingly, despite the high level of clearing and land disturbance in Illinois, contemporary patterns also preserve the remnants of this spatial pattern, although the degree to which this reflects water availability, the suitability of riverine land for agriculture or deliberate land management practices is unclear. Images sourced from *Greeley* (1925), *Iverson* (1991) and Google Earth (USDA Farm Service Imagery, ©2010 Digital Globe, ©2010 Google). Figure by Sally Thompson. . . . 138
7.2 A) Vegetation mediates partitioning at a point. Flow paths in the catchment may be visualized as a network of links (each represented by a 'slab' in this figure). A downslope subsidy U_S provided by the sum of contributions from up-gradient contributing areas. The subsidy and the local wetting W are partitioned into vaporization V and an additional downslope contribution as mediated by local vegetative cover and properties. Local vegetation cover B controls partitioning and depends on water availability. . . . 139

7.3 Model output for a system with $N = 511$ links, and $\beta = 0.5$, $R = 2.5$ (a dry system), $D = 1.5$ (Q_0/V_{max}), and $G = 0.2$ (V_B/V_{max}). (A) The proportion of the area with upgradient contributing areas of different amounts (from 256 external links with area 1 to a single link with area 511 at the outlet), (B) vegetation index B, locally and averaged over the accumulated areas, as a function of accumulated area (closed symbols: water limited, open symbols: energy limited), and (C) Horton index for the accumulated areas (total V / total W) as a function of the accumulated area along the flowpath leading to each link in the system 144
7.4 Contours of the difference in Horton index H (calculated at the system outlet) between the case with self-organized vegetation and the case with uniform vegetation, as a function of the three dimensionless ratios that determine the dynamics. 147
7.5 Sensitivity of the Horton Index to changes in aridity as a function of the drainage efficiency D. The multiple regimes of sensitivity are driven by a) thresholds in the capacity for vegetation to survive, b) the threshold between water stressed and unstressed transpiration and c) the symmetry of a perfectly bifurcating network, such that switching of either threshold induced by a change in D occurs synchronously at all links of a given order. In a more random network, the transitions between these regimes would be damped and would tend to confine the sensitivity of $(\frac{dH_k}{dR})/G$ to near zero at whole-catchment scales 149

Chapter 1

Five ways of thinking: Towards a new epistemology for landscape hydrology under change

[1] *This introductory chapter to the dissertation serves two purposes. Firstly, a broad framework for thinking about hydrology in a changing world is developed. This framework then motivates and contextualizes the work presented in subsequent chapters.*

1.1 Introduction

Hydrology as a discipline was largely motivated by applied engineering problems, and has played a vital social role in providing drinking water and irrigation supplies, and mitigating the threats of floods and droughts (*Dooge*, 1988). The signature motivating task for hydrology over its recent history has been prediction (*Dooge*, 1986; *Sivapalan*, 2003a). The dominant mode of hydrologic prediction has treated the landscape as a vast boundary-value problem, and progress in hydrologic prediction was for many years synonymous with increasing the number of equations coupled together in a model, and increasing the spatial and temporal resolution over which they are solved (*McDonnell et al.*, 2007). While such high-resolution models serve an important, even vital, role in hydrologic science – particularly to aid our understanding in particular places where sufficient data exists to parametrize the models – such models are only a tool for building an integrated understanding of watersheds, and do not represent that understanding themselves. More than two decades ago *Dooge* (1986) bemoaned the preoccupation within hydrology with building ever-more complex models at the expense of a parsimonious understanding of catchments, and argued for the formulation of a body of meso-scale hydrologic theory that was applicable directly at the scales of interest for prediction. This body of theory has not materialized in the intervening years, though many ways forward have been proposed (*Beven*, 2006, 2008; *Blöschl*, 2006; *Kirchner*, 2006; *Kumar*, 2007; *McDonnell et al.*, 2007; *Schaefli et al.*, 2010; *Sivapalan*, 2003a, 2009; *Troch et al.*, 2009b). The limits of the present approach have been foreseen for many years, but there is little agreement amongst hydrologists about how best to deal with them. The increasing awareness of these issues has led to a growing sense of crisis in the hydrologic community (*Sivapalan*, 2003a, 2009; *Blöschl and Zehe*, 2005; *Kirchner*, 2006; *Beven*, 2006, 2008).

The accelerating pace of global change – both in the climate and the landscape – is raising new challenges for prediction, even as these older ones persist. Models are required that can predict outside the range of observed variability (*Wagener et al.*, 2010). Under these changing conditions models that can be calibrated to mimic past behavior cannot be assumed to predict future responses with similar accuracy. This is partly because the structure of the landscape itself is being altered by human and natural forces. These changes cascade through the landscape ecology, geomorphology, soils (amongst other thing), driving changes in the

[1] The concepts presented in this introductory chapter were developed by Ciaran Harman, but have benefited considerably from discussions with many others, particularly Murugesu Sivapalan and Sally Thompson. All figures, tables and data were created by Ciaran Harman unless otherwise indicated.

properties of the landscape that control hydrologic fluxes. These changes happen at all scale, from changes in pore structure due to traffic compaction to changes in vegetation across whole catchments, making prediction of their effects at the scale of prediction difficult. There has been a recognition that facing the applied challenges of the future will require a deeper understanding of the interconnected earth system (*Committee on Opportunities in the Hydrologic Sciences and Technology Board*, 1991; *Wagener et al.*, 2010; *Paola et al.*, 2006).

Further difficulties arise from the imperfect representation of hydrologic processes in predictive models. Calibrated parameters generally represent the emergent effects of unresolved properties and processes in the landscape. Changes in the climatic forcing may drive changes in these unresolved features (by shifting spatio-temporal patterns of water storage in the landscape, and altering the partitioning between different flow pathways), altering the values of the 'effective' properties (*Sivapalan*, 2005a, 2003b; *Kirchner*, 2006; *Harman*, 2007b).

A common component to these problems is the difficulty in understanding and faithfully representing the relationships between the (possibly changing) properties of the landscape and the hydrologic fluxes across spatial and temporal scales. These problems persist despite the on-going analysis of scale issues in hydrology for many years (*Blöschl and Sivapalan*, 1995). Finding upscaled closure relationships (*Reggiani et al.*, 1999, 1998) for hydrologic modeling that are faithful to the unresolved components of the landscape is now well recognized as an extremely important endeavor for watershed hydrology (*Beven*, 2006). The need to couple hydrologic processes to other earth surface processes complicates this challenge even further.

These are big challenges, and will be answered through a combination of many different approaches. A conceptual framework for thinking about these problems is needed to provide a context for different approaches and to establish the links between them. This framework must be broad enough that it can encompass the diversity of empirical and theoretical efforts that gives hydrology its strength, but to be useful it must also provide clear structure, and not be so general as to be diffuse.

These challenges to the *status quo* of hydrologic science are the primary motivation for the work presented in this dissertation. In this introduction I propose a framework for thinking about hydrologic systems. Each component of the dissertation that follows can be located within this framework, and each represents an approach to understanding the integrated behavior of hydrologic system, either through up-scaling from small-scale processes, or by considering the feedbacks between the hydrologic system and other landscape processes. Despite the variable subject matter of each chapter, the framework presented here provides a consistent thread of ideas that runs through the entire dissertation.

The framework is based on the idea that hydrologic science is fundamentally concerned with the in-

teractions between the structure of the earth surface, the drivers of mass and energy, and the hydrologic dynamics that arise from their interaction. In Section 2 of this chapter these terms are defined and used to further discuss the challenges facing hydrologic science. Section 3 then lays out the framework in terms of five ways of thinking about the relationship between structure, drivers and dynamics. Together these five ways constitute a path towards a synthesis of Newtonian and Darwinian world views, as suggested by *Harte* (2002). Finally, in Section 4 the work that makes up the bulk of the dissertation is introduced and placed in this framework.

1.2 Hydrologic Drivers, Structure, Dynamics, and Science

A defining feature of hydrology, and one that makes it challenging and fascinating, is its mandate to understand how water flows through the landscapes that exist in the world (including their atmosphere). This distinguishes it from other sciences such as fluid mechanics that deal with flows in well-controlled or prescribed conditions. The challenges for hydrology do not arise from the mechanics of the flow itself. Rather they arise from the interaction of the flow dynamics and the vastly complex structure of the real-world landscapes, driven by the fluxes of mass and energy operating at larger scales (*Sivapalan*, 2005b). Indeed, this interaction is at the heart of the whole discipline.

Consider: an ecologist, a geomorphologist and a hydrologist are standing on a hill, overlooking a watershed, and are asked to describe the landscape they see before them. The ecologist, depending on his or her particular interests, might describe the food-web that connects the organisms, the niches they inhabit, the patterns of succession that are driving change. The geomorphologist might describe the erosional, transportational and depositional zones of the landscape, point out relic terraces and channels, and areas of active gullying. If there were earth scientists of other persuasions present (structural geologists, pedologists, atmospheric scientists etc), they could tell their own stories. What does the hydrologist describe?

Some hydrologists might be tempted to say, with some justification, 'I see everything that you see, and more'. Water is deeply connected with almost all earth surface processes. The movement of water is controlled by the topography of the earth, the hydraulic properties of the soils and rocks, the transpiration of plants, the energy available from the sun and the atmosphere, and more. Together these determine the flow pathways that are available to storage and transmit water, and the mass and energy that drives the flow through them. To understand the hydrology of the landscape we must understand the *structure* and *drivers* controlling the flow of water, and in turn shaped by it. Water is essential to life, and is a major determinant of ecological organization, particularly in dry parts of the world. The ability of water to

dissolve and transport minerals and nutrients gives it an important role in the physical and biogeochemical organization of soils. Water does the lion's share of the (non-human created) geomorphic work that shapes the land surface. Since water touches almost everywhere, in most of the world the hydrologic structure of the landscape *is* the landscape. Understanding this structure therefore requires that the scope of hydrology be expanded and integrated with a broader earth science.

From another perspective though, hydrology is not (and surely cannot try to be) the study of the landscape in its entirety. That may the role of earth system science as a whole, but hydrologists study water. If the hydrologist were able (by wearing an elaborate pair of spectacles) to see through all the other structures that exist in the landscape they might see only the *hydrologic dynamics* of the water itself: stored here, flowing there, streams of it dividing in some places between different fates, and converging towards a shared fate in others. Adopting an even more omniscient perspective, the hydrologist would also see temporal and spatial patterns of variability in these dynamics at all scales. Collectively, these hydrologic dynamics are what hydrology as a discipline has sought to understand, both for their own sake, and for the good of humanity. The original, applied purpose of hydrology was to predict and manage the dynamics of water, and this purpose will continue to be a motivating force.

These two visions of the hydrology of a landscape, while inseparable in reality, have played different roles in the development of hydrologic science. The purely statistical approach to flood frequency developed in the middle of last century depends only on a characterization of hydrologic dynamics, and not on the structure of the landscape whatsoever. On the other hand, the use of complex, high resolution hydrologic models for prediction relies on being able to measure and characterize hydrologic structure and then use this information to predict dynamics. Models that incorporate additional landscape processes, such as vegetation growth and phenology, allow the structure to change over time. The most advanced current models (such as MLCan (*Drewry et al.*, 2010) and RHESSys (*Tague and Band*, 2004)) allow for feedbacks between the dynamics and structure, and include more of the previously exogenous drivers of the system as endogenous responses to larger scale drivers.

Furthermore, the concepts of hydrologic drivers, structure and dynamics can be used to clarify the challenges faced by this current paradigm of hydrologic prediction.

1. *It is difficult and expensive to measure drivers, structure and dynamics with sufficient accuracy.* The "gold standard" representations of flow and transport (such as Richards equation and the St. Vernant Equation) were originally formulated in laboratory-scale experiments. Physically measuring the structure of the landscape at a scale sufficiently fine to parameterize these models is – for the most part – currently unfeasible. The space-time structure of the drivers is also very hard to measure - space-time rainfall fields

in complex terrain being a particularly challenging example. Predictions are therefore subject to wide uncertainties, particularly predictions under conditions that are different than those previously observed, or when predictions of unobserved internal states is needed. The application of such models to ungauged catchments (that is, most of them) may be simply fanciful.

2. *We don't know how to map the landscape structure, with its unresolved details and interactions with dynamics, onto model structure.* Rather than use models resolved at scales too fine to measure, hydrologic models are typically based on resolving the larger-scale landscape structure (such as using a TIN or resolving individual hillslopes). These fluxes between these elements must be parameterized in some way, such as by 'closure laws' in the Representative Elementary Watershed approach of *Reggiani et al.* (1998). However, it remains an open question how to appropriately map the landscape structure that we can measure onto the model structure. Lacking this, model structures are chosen without a rigorous basis for choosing, and the parameters they rely on are unconstrained. Hydrologists must resort to calibrating their models and spending considerable energy on uncertainty analysis.

3. *The structure of the landscape and drivers are changing.* Global and regional climates are changing, and humans are transforming the land surface at a rapid pace. Both types of changes cascade through the coupled systems (socio-economic, ecological, hydrologic, geomorphic, pedologic, and others) that control the structure of the landscape, and feed back on the drivers. Attempts to account for these interactions by constructing models of ever more complexity must specify an even greater number of parameters and initial conditions, and so the uncertainty of their predictions is exacerbated, rather than reduced.

4. *The feedbacks between the structure, drivers and dynamics (and between different components of the structure) introduce systematic unpredictability into the system.* High-dimensional systems with multiple feedbacks have the potential to exhibit high inherent unpredictability and instability. These manifest in such phenomena as multiple basins of attraction, chaos, thresholds, irreversibility, and bifurcations. These complexities compound the problems previously noted, and challenge our ability to use complex, process-based models for long-term prediction.

These issues arise in the context of one particular approach to thinking about hydrologic systems – one in which the ability to predict everything, everywhere, all the time would represent complete knowledge. However, this need not be the only way of thinking – other 'epistemologies' of hydrologic science are possible. *Harte* (2002) discussed the problems facing earth system science more generally, and suggested that progress might come from finding a synthesis between 'Newtonian' and 'Darwinian' epistemologies. These terms should not be taken too literally – they do not refer directly to the works of these two great scientists, but act as shorthand for two ways of understanding the world that dominate the disciplines they helped create.

In the specific context of hydrology the meaning of the terms 'Newtonian' and 'Darwinian' is perhaps more clearly carried by referring to 'Processes' and 'Patterns'. These terms also tie the present discussion more closely to previous discussions by *Sivapalan* (2005a).

The Process approach of physics seeks to represent natural processes in isolation from each other and 'out of time', divorced from their historical context. This reductionism produces simpler, more universal representations of the processes. Its aim is create models that predict the outcome of experiments or future events (to the extent that quantum physics, chaotic dynamics and random processes allow). The behavior of complex systems, composed of many interacting parts, can then be predicted by connecting together many of these representations and solving with the appropriate boundary and initial conditions. 'Understanding' a system in this world-view implies the ability to predict. The parts of hydrologic science that have focused on the development of predictive hydrologic models arise from this approach.

The alternative Pattern-based mode has been less represented in hydrologic science over recent decades. This world-view more closely resembles the view of ecology, and seeks to understand complex phenomena viewed in their totality. Landscapes are systems with histories, whose evolution has been conditioned by their environment and by the networks of interdependency they embody. Understanding in this world-view is not synonymous with prediction, but with explanation. A self-consistent explanation for an observed phenomena that accounts for its observed properties need not be a just-so story: it is a form of scientific theory, from which it is possible to deduce hypotheses capable of being tested against new data.

Hydrologic science conducted within this epistemology treats catchments and the hydrologic structure and dynamics they embody as complex phenomena that must be accounted for by some explanatory theory. Landscapes abound with beautiful, fascinating patterns in space and time. Clods of mud, water and life are not randomly distributed – they are arranged into patterns. The existence of these patterns are what make hydrologic theory possible and, in this opinion, interesting. There are some who have suggested that the only problems in hydrology are the characterization of appropriate boundary and initial conditions for models. Spatial and temporal patterns in the landscape are mere 'grist to the mill', useful for parametization and calibrating models (*Sivapalan*, 1997) . This amounts to a denial that there is any value in seeking out patterns embedded in the hydrologic structure and dynamics of landscapes and finding explanations for them. This seems to be a blinkered, myopic view of hydrology, and one that limits hydrology's future. The alternative, Darwinian world-view is represented in the early modern hydrologic literature, particularly in the perceptual thinking about landscape hydrology exemplified in the work of Robert Horton (see *Beven*, 2004a,b,c, for a discussion), but has suffered a long decline (*Beven*, 2008). The framework offered below seeks a renewal of efforts to observe the hydrology of the landscape, place these observations in an explanatory

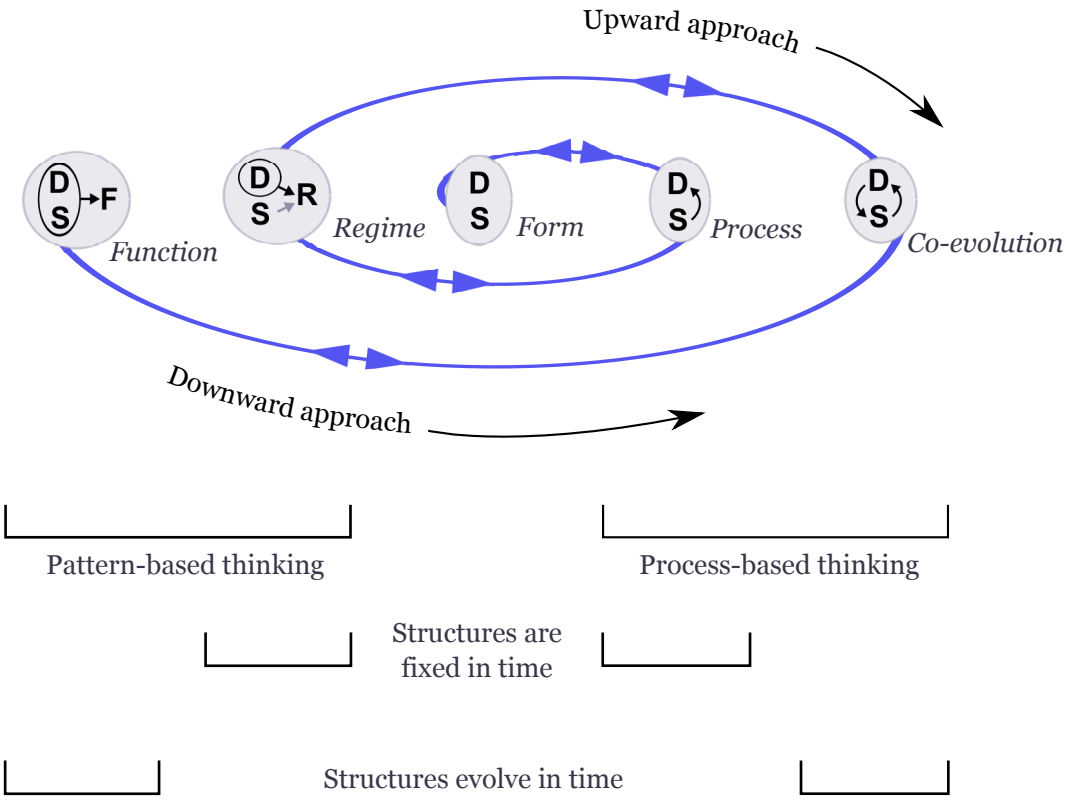

Figure 1.1: Five ways of thinking about hydrology, arranged in a spiral that alternates between Newtonian and Darwinian thought.

Mode	World-view	Role of Structure	Objective
Form	Empirical	-	Observe Structure and Dynamics
Mechanism	Newtonian	Fixed	Predict Dynamics
Regime	Darwinian	Independent variable	Explain Dynamics
Co-evolution	Newtonian	Changes	Predict Structure and Dynamics
Function	Darwinian	Co-dependent variable	Explain Structure and Dynamics

Table 1.1: Properties of the five ways of thinking about hydrology

context, and use them to make better predictions.

1.3 Five ways of thinking in hydrology

Building on these two world-views, it is possible to discern a richer classification of ways of thinking about hydrology by considering the role of structure, drivers and dynamics in the Pattern and Process modes of thought (Figure 1.1, Table 1.3). Attempting to do so serves two purposes. Firstly it clarifies the structure of hydrologic thought, clearly showing where new opportunities for advancement lie. Secondly, we can identify pathways between the modes of thought that might lead to a synthesis. The first, *Form*, is rooted in

the empiricism; two more *Mechanism* and *Co-evolution* are derived from understanding Processes and their interactions, and using them to predict, and two *Regime* and *Function* seek Patterns and try to explain them. In each case though the objective is to develop an understanding of the *aggregate* behavior of hydrologic systems, seeking the kind of synthesis that *Harte* (2002) advocates. Each of these modes is explained below.

1.3.1 Forms

As outlined above, Form refers to scientific questions and research concerned with the empirical observation, measurement and documentation of the structure, drivers and dynamics of hydrological systems. The observation of the world as it is is the foundation of scientific understanding. In hydrology this understanding is based on the observation of patterns in the dynamics of the hydrologic systems, and associations between these patterns and the structure and drivers of the landscapes that generate them.

Research into Form generates basic data and is concerned with developing new observational techniques, characterizing observational uncertainties, and developing infrastructure and methods to manage and interrogate data. Methods and infrastructure are already being developed to deal with the flood of physical data being generated by new technologies able to make observations at increasingly fine spatial and temporal resolution through satellite data and distributed sensor technologies. Data on human structures in the landscape, including non-physical structures such as legal frameworks, economic values, and political boundaries are also needed to characterize these systems, and will have to be obtained and integrated into hydrologic datasets in collaboration with social scientists and economists. Key conceptual questions in the Form mode are related to what quantities should be observed, how to optimize resources available for observations across the landscape, and how to make justifiable comparisons between observations taken from different sites, times and scales, so that together they can contribute to the development of higher-level understanding.

1.3.2 Mechanisms

Mechanism related questions aim to generate mechanistic (quantitative and physically based) descriptions of hydrologic dynamics in terms of landscape structure and climatic drivers. Practically speaking, this means finding mathematical descriptions of mass, energy, momentum and information transport and transformation, and testing these descriptions against data. Mechanistic descriptions of core hydrological mechanisms at a local scale (evapotranspiration, overland flow, channel flow, porous media flow) have been extensively studied, but there remain considerable challenges to develop closure relations capable of representing lateral fluxes (*Reggiani et al.*, 1999, 1998; *Beven*, 2006), and vertical exchanges with the atmosphere at larger scales

in a way that is faithful to the underlying landscape structure. Gaps in mechanistic understanding are particularly great at the interfaces between hydrological processes and other Earth system sciences, such as the link between plant physiology and transpiration, and flow and transport mechanisms near weathering interfaces. The representations that may work at small scales cannot be naively averaged to produce a larger-scale laws (*Beven*, 2006). Different structures in the landscape appear at different scales and may exert the dominant control on the behavior, such as the transition from hillslope to channel controls on catchment behavior (*Robinson et al.*, 1995). These structures interact in non-trivial ways with the dynamics of flow (*Harman and Sivapalan*, 2009a), producing effects that must be captured in upscaled mechanistic representations.

1.3.3 Regimes

The Regime approach treats patterns of hydrologic dynamics as phenomena to be understood, described, and explained. Patterns in the dynamics of a hydrologic system (be it a soil pore or a whole watershed) – such as the dominance of a particular flow process, spatial or temporal changes in dominant processes (gradual or sudden), and shifts in the drivers of flow from local to non-local controls – arise due to complex sets of interactions between the landscape structure and the dynamics itself across many scales, and can be observed in signatures in the measurable hydrologic variables (*Wagener et al.*, 2007; *Western et al.*, 2004; *Farmer et al.*, 2003). In the Regime approach, explanations that account for the variations in these signatures through space and time are sought in terms of the structure of the landscape, the structure of the inputs/outputs of water and energy from the atmosphere, and the processes that are triggered by the interaction of these. The term 'Regimes' in this sense corresponds to a mode of interaction between landscape and climate structure that lead to a pattern of dynamics. The concept is exactly analogous to the way that the relative importance of viscous and inertial forces determines whether a flow is in the laminar or turbulent regime. There has already been considerable work done in hydrology devising ways to express the relative importance of different processes in dimensionless numbers in a manner analogous to the Reynolds number (*Berne et al.*, 2005; *Harman and Sivapalan*, 2009d, for instance).

A sound understanding of regimes will improve our ability to identify dominant processes from the available data, and guide further data collection. It is the conceptual basis for developing the kind of comparative hydrology that might lead to a consistent method for catchment classification (*Wagener et al.*, 2007). Furthermore, regimes may help us develop closure relations. Closure relations must capture the net effect of the driver-structure-dynamics interactions within an REW, and so in addition to being scale-dependent, they are also 'regime-dependent' (*Harman and Sivapalan*, 2009d).

Note that the regime approach still treats landscape structure as an 'independent variable' in the explanations of process dominance, and in the use of regimes for pattern-based prediction. It examines how structure produces patterns in the dynamics, but does not consider the converse. For that we must expand the domain of inquiry, and shift to the co-evolutionary and functional perspectives.

1.3.4 Co-evolution

The Co-evolutionary mode is concerned with the mechanistic understanding of the evolution of hydrologic structure of the landscape, and the role that hydrologic dynamics plays in that evolution. We seek to combine understanding of hydrologic processes with other land-forming and life-sustaining processes, such as geomorphic, pedogenic, ecologic and atmospheric dynamics over multiple time and space scales. The objective is to be able to make reasonable predictions of system behavior, and to understand the limits on predictability created by complex interactions and historical contingencies. The co-evolution of landscape structures and dynamics arises from feedbacks between these dynamics in the landscape, as well as feedbacks with the hydrology itself. These feedbacks can generate complex behavior like stable and unstable modes, oscillations, resilience, chaos, feedbacks. A primary motivation for developing co-evolutionary models is the analysis of these behaviors.

Given the vast network of potential interactions in the landscape, mechanistic relationships with minimal degrees of complexity are required to proceed with this analysis. Two broad classes of relationships are needed:

- *Structural evolution*: Relationships are required to predict the evolution of the structure in terms of the hydrologic dynamics and as determined by other external factors.
- *Process-coupling*: Constituent laws must be developed that map the changes in the structure to changes in the parameters of the closure laws needed to model the dynamics.

Both of these are concerned with the development of new hydrologic relations that connect across disciplines. The description of structural evolution mechanisms in co-evolutionary models suffers the same problem of developing 'closure laws' as the hydrologic models examined in process mode. This point has been made by *Dietrich et al.* (2003) with regard to 'Transport Laws' for geomorphic change. An additional complication arises from the need to consider the coupling between processes that interact over a wide range of time scales. Hydrologic processes operating at the timescales of individual storms play an important role in landscape evolutionary processes that accumulate over millennia. This multi-scale coupling presents an intriguing challenge for developing hydrologic theory.

1.3.5 Functions

The function mode is concerned with the patterns and phenomena that arise from the co-evolution of landscape structure, drivers and dynamics. These patterns can most easily be observed when the structure, drivers and regimes of many catchments are considered together, such as in the Budyko Curve and the Abrahams Curve. The objective in the function mode is to seek out and find coherent, cogent explanations for these patterns, and learn from them. Just as the regime mode considers phenomena that arise from hydrologic mechanisms, the function viewpoint considers phenomena that arise from co-evolution. In contrast to the Regime mode of thought, in the Function mode the landscape structure (or at least, some critical part of it) is no longer treated as an independent variable when we seek an explanation. We seek explanations that account for observed patterns in the structure and dynamics simultaneously. Explanatory theories at the functional level draw on high-level principles. A mechanism like self-organized criticality (*Dietrich et al.*, 2003) or constructal theory (*Bejan*, 2000) (or perhaps some sort of evolution by natural selection) might provide an explanation at the function level: they explain at a very fundamental way why we observed the functional patterns we do. The function approach tackles the deepest questions in hydrology about why hydrologic structures and dynamics come to be organized the way they are, and is vital to developing and understanding of how catchments will change over time.

1.3.6 Spiraling towards a synthesis of world-views

Consider an example that might clarify the relationship between these modes of thought. An observation of Form tells us what is occurring at a particular time and place – perhaps we observe macropore flow at the face of a trench of a type similar to that of *Tromp-van Meerveld and McDonnell* (2006a). The Pattern perspective seeks out patterns in this behavior and looks for explanations for why they exist. The Regime mode places the observations in a broader hydrologic context – we observe that this hillslope (and perhaps others nearby) macropore flow is triggered when storm-sizes exceed some threshold (*Tromp-van Meerveld and McDonnell*, 2006b; *Tromp-van Meerveld et al.*, 2008). The Function mode expands this view further to consider the association between the pattern and the landscape structure: we might observe that this kind of threshold-triggered lateral macropore flow often occurs in soil-mantled hillslopes in forests (*Uchida et al.*, 2005). Such an observation suggests some functional 'purpose' that the macropores have played in the evolution of the landscape, perhaps ensuring landscape stability by rapidly releasing incoming precipitation to the stream before elevated pore pressures can trigger landslides (*Uchida et al.*, 2001) (although it should also be noted that subsurface erosion through soil pipes can also be a cause of landslides, (*Nieber and Sidle*, 2008)). A quantitative expression of this pattern would provide a basis for making predictions about the

occurrence and role of preferential flow in un-gauged watersheds.

Such predictions would not be process-based, but rather pattern-based. A process-based model of preferential flow might resolve individual macropores (*Nieber and Sidle*, 2010), or represent their effects through a dual permeability model (*Gerke*, 2006). To develop a co-evolutionary model of this process the formation, maintenance and destruction of preferential flow networks (perhaps due to biological processes like root turnover and burrowing) would have to be represented and coupled to the hydrologic dynamics.

Ultimately however, a complete understanding must come by finding a synthesis between these approaches. The regimes of threshold-triggered preferential flow must be shown to arise naturally in mechanistic representations of the process under the appropriate circumstances. Hillslope-scale representations of subsurface lateral flow that incorporate this threshold-switching might then be developed with parameters that relate to measurable properties of the hillslope. Furthermore the functional patterns of association between the occurrence of the flow process and landscape properties must be be shown to arise naturally in co-evolutionary models when the appropriate processes are incorporated. These relationships can then be used to make predictions about the effects of landscape and climate change on macropore flow.

1.4 Outline of this dissertation

This framework is intentionally broad and represents a very diverse range of approaches. The work presented in this dissertation represents a portion of these. In keeping with the framework, none of the pieces of work are concerned with the behavior of one particular watershed. Rather, the objective is to utilize the framework developed above to develop generalized understandings of the aggregate behavior of hydrologic systems at the scale of soils, hillslopes and small watersheds. In each chapter a particular approach is applied at a particular scale. The work is divided into two parts.

The first part considers how the landscape structure and climate properties control the propagation of hydrologic variability through the landscape. In the context of the framework presented above, the work is primarily concerned with understanding Regimes and Mechanisms. Small-scale processes are connected to aggregate hydrologic behavior using simplified models and stochastic or simplified representations of the inputs of water.

In Chapter 2 and Chapter 3, the role of climate, soil and vegetation on the travel time of sorbing, reactive solutes through the vadose zone is examined. A simplified representation of the transport process based on piston-flow is developed and validated, and then used to translate the stochastic variability of rainfall into probability density functions of the travel time through the vadose zone, and fractional delivery of degrading

solutes to the underlying soils. These results are applied to examine how pesticide leaching risk is determined by the regimes of climate, soil and vegetation controls.

In Chapter 4 a closure relationship for shallow saturated subsurface flow through a steep, heterogeneous hillslope is developed using concepts from heavy-tailed stochastic processes and fractional calculus. Results of a spatially-explicit model of the process show that heterogeneous conductivity fields impose a distribution of timescales on the flow of water through the system. This effect is then shown to be captured elegantly by a time-fractional kinematic wave equation, which can be solved to yield an impulse response function predicting the discharge at hillslope scales without explicit resolution of the fine-scale heterogeneity.

Chapter 5 considers the effects of spatial heterogeneity at the catchment scale in the context of stream-flow recession curves. It is argued that the widely-adopted explanations of the apparent power-law nature of these curves based on the hydraulics of a single 'effective' hillslope pay inadequate attention to the role of spatial variability in the catchment. It is shown that this power-law type behavior can in fact arise purely from the spatial variability of the catchment properties - an insight with important implications for how we interpret and predict stream-flow.

The second part of the dissertation is concerned with functional patterns and co-evolution of aggregate hydrologic systems. These pieces of work seek to understand how the landscape structure that controls the hydrologic dynamics has come to be the way it is, and the expression of this evolution in functional patterns observed across places. This question is pursued at a range of scales, using a combination of modeling and data analysis.

Chapter 6 presents an analysis of functional patterns in catchment-scale water balance dynamics across many catchments in the continental US. This work applies a model of annual water balance partitioning based on a 'functional' conceptualization of watershed hydrologic dynamics that has demonstrated wide applicability (*Sivapalan et al.*, 2010). Spatial and climatic patterns in the sensitivity of precipitation demonstrate the central role that the non-linear 'threshold' component of the functional model plays in inter-annual variability in catchment partitioning, especially in arid catchments. Finding the connection between the emergent functional parameters and the co-evolved landscape structure and regimes remains a challenge.

In Chapter 7 the concept of co-evolution and functional patterns is illustrated at the watershed scale using a simple steady-state model. This model illustrates how feedback between a) vegetation as a driver of evapotranspiration and b) the control of water availability on vegetation distribution, can generate non-trivial spatial scaling and organization in both vegetation distribution and catchment water balance along a convergent network of flowpaths. The resulting self-organization generated spatial dependence in vegetation density and water balance along the network. The model suggested how these patterns depended on climate,

vegetation and landscape properties, and provided a theoretical framework to connect water balances at patch and catchment scales.

Finally Chapter 8 summarizes the findings from this work and discusses future research opportunities within the framework presented here.

Part I

Regimes and Processes

Chapter 2

Climate, soil and vegetation controls on the temporal variability of vadose zone transport - Simplified modeling framework

[1] *Temporal patterns of solute transport and transformation through the vadose zone are driven by the stochastic variability of water fluxes. This is determined by the hydrologic filtering of precipitation variability into infiltration, storage, drainage and evapotranspiration. In this work we develop a framework for examining the role of the hydrologic filtering, and in particular the effect of evapotranspiration, in determining the travel time and delivery of sorbing, reacting solutes transported through the vadose zone by stochastic rainfall events. We describe a 1-D vertical model in which solute pulses are tracked as point loads transported to depth by a series of discrete infiltration events. Numerical solutions of this model compare well to the Richards equation-based HYDRUS model for some typical cases.*

2.1 Introduction

The complex, transient, non-linear transport and transformation processes operating in the vadose zone determine the timing and magnitude of the delivery of surface-applied solutes to groundwater (*Raats*, 1981; *Rao et al.*, 1990; *Wang et al.*, 2009). Through these processes, the vadose zone acts as a hydrologic filter for the variability of the climatic signals, coupled with a bio-geochemical filter to retard and attenuate solute inputs (*Rao et al.*, 2010). Understanding this filtering is important for assessing the risks associated with groundwater contamination of surface-applied solutes, such as pesticides (*Rao and Davidson*, 1980; *Rao et al.*, 1985; *Gustafson*, 1989; *van Der Werf*, 1996; *Arias-este et al.*, 2008). An important control on this temporal filtering is the reduction of soil water content by vegetation through root water uptake, and the replenishing of this water content by the stochastic inputs of infiltration (*Struthers et al.*, 2006, 2007; *McGrath et al.*, 2007). A full understanding of the temporal patterns of solute delivery through the vadose zone therefore depends not only on the processes of solute transport and degradation, but also the way these processes are controlled by the stochastic variability of the climate and the hydrologic filtering of this variability in the vadose zone.

In previous work, several authors have examined solute transport through the root zone by assuming for simplicity that the flow is steady, thus neglecting the episodic (stochastic) transport processes (*Rao et al.*, 1985). In this work we examine the role of evapotranspiration on delaying, and making more variable, the transport of solutes carried through the vadose zone by the propagation of wetting fronts, using a low-dimensional model of this transport that lends itself ultimately to a semi-analytical solution.

Surface applied solutes can migrate very rapidly to groundwater through preferential flow pathways, such as macropores, or more slowly through the bulk of the unsaturated zone (*Flury*, 1996). While preferential

[1] This work has been submitted for publication to Water Resources Research as: Harman, C J, P S C Rao, N B Basu, G S Mcgrath, P Kumar, and M Sivapalan, Climate, soil and vegetation controls on the temporal variability of vadose zone transport. All figures, tables and data were created by Ciaran Harman unless otherwise indicated.

flow can be important for leaching, the vast majority of chemical is transported through the slower flow pathways (*McGrath et al.*, 2007). It is therefore important to understand the capacity of the latter domain to store and release these solutes. In this domain, the solutes are rarely flushed through the vadose zone in a single infiltration event. Rather, multiple events are required to carry a surface applied solute through the vadose zone in a series of events, during which the solutes are mobilized by the flow (*Wang et al.*, 2009). The depth to which water will infiltrate the soil and carry these solute loads through the profile is driven in part by the antecedent conditions of soil water content, as well as by the rainfall characteristics and the hydraulic properties of the soil. Thus the reduction of water content by root water uptake may serve to increase the residence time of solutes, particularly as they progress deeper through the profile and require larger events to mobilize them (*Destouni*, 1991). The time delays associated with episodic and retarded transport through the vadose zone allow for various bio-geochemical processes to transform and attenuate the solute pulses. For example, the degradation of pesticides in the vadose zone is vital to reducing groundwater contamination (*Flury*, 1996).

The effects of transient infiltration on the travel time distribution of solutes through the vadose zone has been investigated extensively to determine whether this transport can be approximated by equivalent steady-state flows (*Wierenga*, 1977). *Russo et al.* (1989a,b) suggested that solutes may travel faster through a soil profile under transient flow, while *Destouni* (1991) suggested that when the effects of root-water uptake are accounted for, equivalent steady-state flows could be used to predict the solute break-through curve. *Foussereau et al.* (2001) examined flow in a heterogeneous vadose-saturated zone system and found that while equivalent steady flow could predict the spatial structure of a solute plume, uncertainty in the timing of the solute breakthrough from the vadose zone was dominated by the variability in the rainfall. More recently *Russo and Fiori* (2008) found that at hillslope scales (where the water table was sufficiently deep) transport through soils could be conceptualized as occurring in two zones: a highly transient near-surface zone and a deep zone where flow was quasi-steady. *Fiori and Russo* (2008) found that the transient flows had little effect on the flow-corrected travel time distribution of a solute migrating through a heterogeneous hillslope. In other words, the transient flow determined the absolute travel time, but did not create additional dispersion. Such equivalent steady-state flows have been used to predict contaminant leaching risks (*Rao et al.*, 1985). In short, these studies suggest that the transience of flow created by the hydrologic variability of the vadose zone is an important determinant on the absolute travel time of a solute, but has only a small effect, if any, on the dispersion of an individual solute pulse.

Rao et al. (1990) suggested a simplified framework for modeling solute transport through the vadose zone that is useful for investigating the role of hydrologic-biogeochemical filtering. In this approach, solute pulses

are tracked as point loads undergoing retardation (linear, reversible, equilibrium sorption) and first-order degradation. The pulses are transported through the vadose zone in a series of discrete jumps associated with infiltration events, whose size depends on the amount of infiltration relative to the deficit of water storage created by evapotranspiration, as well as the solute and soil properties.

The discrete jumps in the *Rao et al.* (1990) approach can be conceptualized as a stochastic process, similar to a random walk, whose jump sizes and the waiting time between jumps are driven by the stochastic rainfall process modified by the retardation and hydrologic filtering. This suggests that this approach to solute transport can be coupled to the stochastic soil water models to predict the delivery of reactive solutes through the vadose zone probabilistically in terms of the soil, climate and vegetation properties.

In this work we will use the approach of *Rao et al.* (1990) and the stochastic soil water theory described above to investigate the temporal filtering of reactive solute delivery to the base of the vadose zone. Of particular interest is how the controls on this filtering affect the likely values (and variability) of the travel time through the vadose zone and the consequent degradation of solutes undergoing transformations with first-order kinetics. We will use a numerical implementation of the *Rao et al.* (1990) approach, which allows results to be obtained for specific cases without further assumptions. We will also provide analytical and semi-analytical solutions for the probability density functions (PDF), mean and variance of quantities of interest which provide deeper insight to the shifting importance of different controls across a range of conditions. These results can be seen as an extension of the work of *Jury and Gruber* (1989), except that here we neglect the effects of dispersion, but account for the effects of evapotranspiration.

In this chapter we develop this model in more detail and provide examples of typical numerical results and a validation against HYDRUS (*Šimůnek et al.*, 2009), a full Richards-equation based solution.

2.2 Event-based model of solute transport in the root zone

The vadose zone model developed here is a low-dimensional model that combines a soil water framework amenable to the stochastic models developed in *Milly* (1993) and *Rodriguez-Iturbe et al.* (1999) with the solute transport model of *Rao et al.* (1990). For convenience we will refer to this model as "HEIST" (*HEIST Event-based Infiltration and Solute Transport model*). The model is intended to provide insights into the dynamics of the upper part of the vadose zone where root-water uptake is a significant part of the water balance. For simplicity we assume a homogeneous profile of soil and root properties. The soil water content varies throughout the profile and through time, as a result of the inputs from infiltration and losses from drainage and evapotranspiration. We adopt constant values of the sorption and degradation solute properties

(defined below), which must be regarded as effective properties.

2.2.1 Soil water storage dynamics

Soil water mass balance in a uniform soil at a depth z is typically expressed as (Laio 2006, Molz 1981):

$$\frac{\partial\theta(z,t)}{\partial t} = -\frac{\partial q(z,t)}{\partial z} - U(z,t) \tag{2.1}$$

where $\theta(z,t)$ is the volumetric soil water content, $q(z,t)$ is the soil water flux, and $U(z,t)$ is the rate of uptake of water by plants. At the upper boundary of the soil ($z = 0$) the flux $q(z,t)$ into the soil is the infiltration rate $I(t)$, which is the rainfall rate reduced by losses to interception and surface runoff. Typically the solution of this equation under variable $I(t)$ requires numerical modeling due to the non-linear dependence of $q(z,t)$ on the soil water content and hydraulic potential gradients in the soil, and the dependence of $U(z,t)$ on atmospheric water demand and the regulation of stomatal conductance by vegetation.

Here we will adopt a significantly simpler approach that is similar to other vertically extended stochastic soil water models that have been used for similar purposes recently, such as *Schenk* (2008), *Guswa et al.* (2004) and *Laio et al.* (2006). This approach is motivated by the observation that the infiltration and redistribution of rainfall in well-drained soils operates on a much shorter timescale than the time between storm events. We can therefore treat the infiltration and subsequent redistribution of water in the soil profile as an event that occurs effectively instantaneously. The infiltrated water forms a sharp 'wetting front', below which water content is unaffected by the advancing front (this model is therefore most appropriate in soils that drain quickly, such as those with low clay content). This approach is similar to that assumed by the Green and Ampt infiltration model (*Green and Ampt*, 1911) and the multiple wetting front model of *Struthers et al.* (2006), and was investigated by *Milly* (1985), who found that it was appropriate in soils where the second derivative of the hydraulic conductivity with respect to soil moisture is strictly positive, a condition that is usually satisfied. The position of the wetting front after redistribution is determined by assuming that it effectively ceases to advance once the water content of the soil profile above it reaches some threshold value θ_{fc}. This value represents the water content at which the hydraulic conductivity of the redistributing front becomes in some sense 'small', compared to the process of evapotranspiration. In Section 2.2.4 we will test the ability of the model to reproduce the water-balance and solute dynamics, and the values of θ_{fc} required to do so. This model is given in precise terms below, and is illustrated in Figure 2.1. Given an initial water content profile $\theta(z, t_i^-)$ (where t_i^- indicates the time just prior to the storm at time t_i), the effect of the infiltration and redistribution of the volume of water $I(t_i)$ is to raise the water

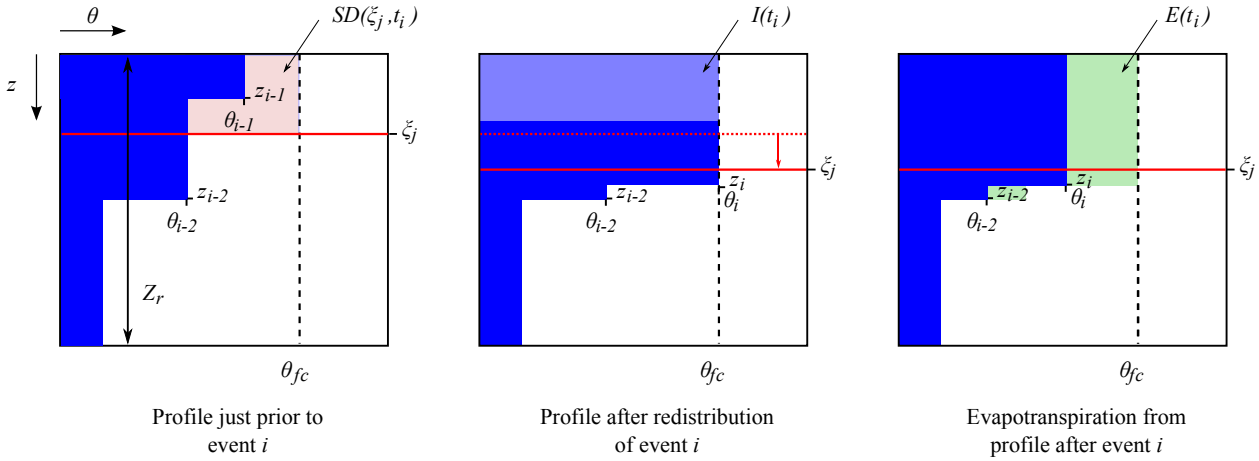

Figure 2.1: Representation of water and solute dynamics in the HEIST model. The infiltration $I(t_i)$ from rainfall event i forms a sharp wetting front that displaces antecedent moisture in the profile. After redistribution the upper part of the profile has a maximum water content at field capacity θ_{fc} and the lower part is unchanged. The transport of the solute load centered at depth ξ_j depends on the difference between the infiltration $I(t_i)$ and the storage deficit in the soil above it $SD(\xi_j, t_i^-)$. Evapotranspiration $E(t_i)$ is removed from the profile between one storm and the next, creating this storage deficit.

content of the surface soils to θ_{fc} down to a depth z_i given by:

$$I(t_i) = \int_0^{z_i} (\theta_{fc} - \theta(z, t_i^-))dz \tag{2.2}$$

In other words, the infiltrated water fills the deficit between θ_{fc} and the initial water profile $\theta(z, t_i^-)$. Note that (as shown in Figure 2.1) the water at the lower edge of the wetting front will be composed of "old water" that has been displaced down the profile. Drainage through a reference plane at the base of the root zone Z_r occurs when the sum of the initial soil water content and the infiltrating water is greater than the total storage above the reference plane at field capacity $Z_r\theta_{fc}$.

The infiltration amount $I(t_i)$ must be related to the rainfall depth $P(t_i)$ by considering the precipitation intensity and the constraints imposed by the infiltration capacity of the soil. We can incorporate this effect while retaining the instantaneous description of the process by using a model of the infiltration capacity as a function of total infiltration. Here we use the Green and Ampt model, modified to account for the profile of water content. This model, like the framework described above, assumes a sharp wetting front of infiltration, driven by gravity. The infiltration rate over the course of a storm is given by a linear approximation of the water potential gradient between the soil just below the wetting front and the ponded surface. The modification simply involves allowing the water potential below the wetting front to vary over the course of the infiltration event in line with the actual profile of water content $\theta(z, t_i^-)$, rather than have a fixed value.

Between storm events i and $i+1$ evapotranspiration removes an amount of water $E(t_i)$ from the profile (Figure 2.1). We will neglect soil evaporation and consider only the effect of root water uptake on $E(t_i)$. Root density distributions for annual crops (to which pesticides are commonly applied) are more likely to decline exponentially with depth, and grow deeper with time over the growing season (*Bengough et al.*, 2006). Here we neglect such effects. For the purposes of examining the role of evapotranspiration on solute transport, we will define the reference plane Z_r as the base of the root zone and assume that the root properties are uniform over the profile. The model of evapotranspiration must determine both the quantity of water to be removed from the root zone between one storm event and the next, and from where in the profile the water is removed. Many models of different complexity exist in the literature. We adopt two alternative approaches here so that the results will be comparable to two other soil water models. The first is the simpler approach used in the stochastic soil water models (*Porporato et al.*, 2004), which determines the uptake rate as limited by a maximum rate ET_{max}, and reduced below this maximum by a function of the average water content of the profile, that is:

$$E(t_i) = ET_{max} \int_{t_i}^{t_{i+1}} f[\bar{\theta}(t)]dt \tag{2.3}$$

where

$$f[\bar{\theta}(t)] = \begin{cases} 0 & \bar{\theta}(t) < \theta_{pwp} \\ \dfrac{\bar{\theta}(t) - \theta_{pwp}}{\theta_{fc} - \theta_{pwp}} & \theta_{pwp} < \bar{\theta}(t) < \theta_{fc} \\ 1 & \bar{\theta}(t) > \theta_{fc} \end{cases} \tag{2.4}$$

and

$$\bar{\theta}(t) = \frac{1}{Z_r} \int_0^{Z_r} \theta(z,t)dz \tag{2.5}$$

The depth of water $E(t_i)$ is removed from the profile by removing it first from the wetting front with the highest water content (which is always at the surface) until the water content equals that of the next wettest front; extraction then continues from both these fronts, and sequentially deeper ones, until $E(t_i)$ is met. Note that this scheme results in a non-uniform distribution of root water uptake that preferentially removes water from the wetter upper parts of the soil, although we have not specified a non-uniform root depth distribution.

The second model follows the *Feddes et al.* (1978) model used in HYDRUS (*Šimůnek et al.*, 2009), which will be used to validate the solute transport model. This model also assumes as an input a maximum rate of evapotranspiration ET_{max}. We chose to use the simplest version of the model, without uptake compensation.

In this model root water uptake is determined from each point in the profile as a function of water potential $\psi(z,t)$, rather than water content:

$$E(t_i) = \frac{ET_{max}}{Z_r} \int_{t_i}^{t_{i+1}} \int_0^{Z_r} U[\psi(z,t)]\, dz\, dt \tag{2.6}$$

where

$$U[\psi(z,t)] = \begin{cases} 0 & \psi(z,t) < \psi_{pwp} \\ \dfrac{\psi(z,t) - \psi_{pwp}}{\psi_{fc} - \psi_{pwp}} & \psi_{pwp} < \psi(z,t) < \psi_{fc} \\ 1 & \psi(z,t) > \psi_{fc} \end{cases} \tag{2.7}$$

and $\psi(z,t)$ is determined from the water content using an appropriate water retention function, such as the the Brooks-Corey formulation. Note that we neglect the role of root stress under very wet conditions that appears in the *Feddes et al.* (1978) model, as we are primarily concerned with well-drained soils.

2.2.2 Solute transport and degradation

Solutes are assumed to be transported through the soil by the advective flux of water, neglecting diffusion and dispersion. Observed solute spreading arises from processes at three scales: 1) molecular diffusion at scales of a few centimeters due to concentration gradients; 2) hydrodynamic dispersion at scales of <1m, due to variations in local flow velocity; and 3) macrodispersion at the scale of several meters due to spatial heterogeneity in hydraulic properties and flow pathways. Here we will neglect all these forms of spreading in order to focus on the range of travel times created by the effects of variable climate inputs on infiltrating water. Our analysis is therefore valid for cases with large Peclet numbers, and provides systematic underestimates for high dispersion cases. This approach is further justified by the observations cited previously that the transient water dynamics have little effect on the shape of the solute plume, and primarily affect the timing of the solute delivery, which is captured here by the arrival of the point load at the base of the root zone (*Destouni*, 1991; *Foussereau et al.*, 2001; *Russo and Fiori*, 2008; *Fiori and Russo*, 2008).

Under these assumptions, *Rao et al.* (1990) suggested the following piston model of the transport of reactive solute point loads through the vadose zone. Let us assume that a storm event at time t_i carries into the soil a mass of solute M_i. This mass may be carried by the rainfall (e.g. wet deposition), or released and leached into the soil from some surface source zone (e.g. applied fertilizers, nutrients, pesticides). The point load mass is carried into the soil by the infiltrating water, and its final position after redistribution, ξ_i, is

proportional to the depth of wetting front penetration $I(t_i)/\theta_{fc}$, and inversely proportional to a retardation factor R that accounts for the effects of linear equilibrium reversible sorption/desorption processes:

$$\xi_i(t_i) = \frac{I(t_i)}{R\theta_{fc}} \tag{2.8}$$

The retardation factor for pesticides is a function of the soil bulk density ρ_b, organic matter fraction f_{OC}, equilibrium sorption co-efficient (normalized to organic carbon), K_{OC}, and soil water content θ:

$$R = 1 + \frac{\rho_b f_{OC} K_{OC}}{\theta} \tag{2.9}$$

R varies from 1 to ∞, representing no retardation ($K_{OC} = 0$) to complete sorption ($K_{OC} = \infty$) respectively (*Rao et al.*, 1990). Here we are assuming that soil organic matter is the primary sorption domain, but this definition can easily be altered to allow for sorption to other soil components, and to explicitly consider non-linear sorption isotherm models. The retardation factor, as defined here, is a function of soil water content. We will make the assumption that an effective retardation factor can be obtained which represents the retardation that occurs during transport. This assumption will be tested in Section 2.2.4.

After being transported into the soil, solute point loads are transported deeper into the soil by a series of wetting fronts that propagate from rainfall events. The volume of water that transports a point load is reduced due to the storage deficit created by evapotranspiration above the point load. The storage deficit above a point load at depth ξ_j at time t_i is defined as (see figure 2.1):

$$SD(\xi_j, t_i^-) = \int_0^{\xi_j} (\theta_{fc} - \theta(z, t_i^-))dz \tag{2.10}$$

Therefore the infiltration at time t_i, $I(t_i)$, will advect a point load initially at point $\xi_j(t_i^-)$ to a depth given by:

$$\xi_j(t_i^+) = \xi_j(t_i^-) + \begin{cases} \dfrac{I(t_i) - SD(\xi_j(t_i^-), t_i^-)}{R\theta_{fc}} & I(t_i) > SD(\xi_j(t_i^-), t_i^-) \\ 0 & otherwise \end{cases} \tag{2.11}$$

Thus, each rainfall pulse infiltrating into the soil profile has to be larger than the soil water deficit SD above the current solute pulse location before further solute displacement occurs. As a consequence, the effective events that cause solute transport at depth in the profile are a filtered form of the rainfall events arriving at the surface.

The point loads are lost from the root zone when they cross the reference plane Z_r. The age of the point

load when it is lost from the system is given by $T_i = t_e - t_i$, the difference in the time of the infiltration event that carried it into the soil t_i and t_e, the time of the event that carried it past the reference plane Z_r. Note that if a point load is carried completely through the system in one event, $T_i = 0$. When the retardation and degradation are absent ($R = 1$ and $k_d = 0$) the solute load represents a non-reactive tracer, and its age T_i can be regarded as being representative of the age of the water carrying it through the system, allowing the water leaving the system to be 'dated'.

Many solutes undergo complex biotic and abiotic transformations that alter their mass in the soil due to intra- and extra-cellular microbial transformations, inorganic reactions with the soil constituents, and uptake by plants (*Flury*, 1996; *Jury*, 1982; *Rao et al.*, 1990). Here we assume a simple first-order transformation model, with a rate constant k, to approximate the solute loss during transport through the soil profile. The mass remaining after a point load (with initial mass M_i) has traversed the vadose zone is then given by:

$$M_e = M_i \exp(-kT_i) \tag{2.12}$$

Where there are multiple transformation pathways, k represents the pooled loss through all loss pathways. If all loss processes are first-order, we can treat k as the sum of their individual contributions. We can define the *delivery ratio* DR as the ratio of the point load of solute mass of solute that enters the soil at t_i, and the mass that is advected past the reference depth Z_r at t_e:

$$DR = \frac{M_e}{M_i} = \exp(-kT_i) \tag{2.13}$$

This is also known as the "Attenuation Factor" (*Rao et al.*, 1985). In principle it is possible to extend the present analysis by invoking more complex models and by considering the fate of various by-products of degradation. However our initial goal here is to consider the interaction between retardation, degradation and episodic transport to illustrate the hydrologic and biogeochemical filtering of the root zone.

2.2.3 Typical results for various solutes, soils, climates

Example results illustrating this model were obtained using a similar set of parameters as that used by *Jury and Gruber* (1989). The root zone was assumed to be homogeneous. Soil parameters are given in Table 2.1 for a coarse soil with low organic carbon content, such as a sandy loam soil, and a finer soil with larger organic carbon content and a deeper biologically active zone.

Following the stochastic approach of *Rodriguez-Iturbe et al.* (1999) and others, we will assume that rainfall can be represented by a marked Poisson process with arrival rate λ_p, and an exponential distribution of event

Table 2.1: Soil properties used for the example simulations, and for validation of the model against HYDRUS.

Parameter		Coarse	Fine	Unit
Bulk density	ρ_b	1.5	1.2	g/cm^3
Organic carbon	f_C	0.2	1	$\%w/w$
Depth	Zr	500	1000	mm
Field capacity	θ_{fc}	10	20	$\%v/v$
Wilting point	θ_{pwp}	4.56	6.04	$\%v/v$
Saturated water content	θ_{sat}	0.395	0.451	$\%v/v$
Air entry pressure	Ψ_a	478	121	mm
Saturated hydraulic conductivity	K_{sat}	15.2	0.601	m/day
Brooks-Corey exponent	n	0.375	0.282	–

Table 2.2: Climate properties for the example simulations

Parameter		Humid	Semi-arid	Unit
Storm frequency	λ_p	0.3	0.047	$1/day$
Storm depth	α	8.5	23	mm
Maximum evapotranspiration	ET_{max}	600	1000	$mm/year$

sizes with mean depth α. These parameters and ET_{max} were fixed constants for these simulations. Climate properties are given in Table 2.2.3 for (1) a humid climate, with low potential evapotranspiration and small frequent storms, representative of the Marine climates of the Atlantic coast of the US, and (2) a semi-arid climate, with large, infrequent storms, such as might be found in the south-western US.

The migration through the root zone of four pesticides, applied to these hypothetical soils once a year, was examined. To focus on the transformations within the root zone, the dynamics of pesticide degradation following application and prior to the first storm were neglected. A unit mass of each pesticide was assumed to enter the soil in the first storm following application. These pesticides have a variety of properties, and were selected because of their widespread use and potential to contaminate the environment (see Table 2.2.3). Pesticide profiles are available from EXTOXNET (pmep.cce.cornell.edu/profiles/extoxnet/), and are also available in *Hornsby et al.* (1996). Atrazine is a widely used herbicide in the United States, but is banned in the European Union. It has moderate sorption properties and an intermediate decay rate. Atrazine (A) is moderately toxic to humans, and has been classified as possibly carcinogenic by the United States Environmental Protection Agency. Bromacil (B) is also a herbicide, and is similarly moderately toxic and possibly carcinogenic. However, it is more weakly sorbing than atrazine, and has a longer half-life in the environment. Ethylene dibromide (ED) is a fungicide and a fuel additive. It is highly toxic, carcinogenic, weakly sorbing, volatile, and resistant to degradation. (Note that we do not account for vapor losses in the current model, which are likely to be particularly significant for Ethylene Dibromide.) Oxamyl (Ox), an insecticide, is extremely toxic and very weakly sorbing, but degrades quickly.

Figure 2.2 illustrates how soil and climate properties affect pesticide transport through the root zone. All

Table 2.3: Pesticide properties for the example simulations

Parameter		Atrazine	Bromacil	Ethylene Dibromide	Oxamyl	Unit
OC sorption	K_{OC}	160	72	44	6	cm^3/g
Degradation rate	$1/k_d$	92	505	5266	9	$days$

of the pesticides leach quickly through the coarse soil in both climates, though only B and ED (which have half-lives > 300 days) reach the reference depth Z_r without significant degradation. The higher retardation and faster degradation of A (half-life $= \log(2)/k_d \sim 64$ days) reduce its delivery in the humid climate, and greatly reduce its delivery in the dry climate. Oxamyl degrades so quickly (half-life ~ 6 days) that it only reaches the base if a sufficiently large storm (or series of storms) occur soon after application. This can occur under both climates, because the semi-arid climate has large average storms, and the humid climate has a high average initial water content so the storms driving the transport need not be so large.

The results from the finer soil reveal a striking ability of evapotranspiration to delay transport compared to the coarse, and a stronger contrast between the climates for the more persistent pesticides. The A and O both degrade near the surface of the soil profile in both climates. In a humid climate, B reaches the base of the vadose zone after about 200 days of transport with some moderate degradation, and ED arrives in slightly less time with almost none. In the semi-arid climate though, the low transport rates in the lower vadose zone delay the transport further, leading to a long residence time and the potential for accumulation in the soil profile. Thus, the strongest potential for contamination are for chemicals B and ED, and in coarse soil. However, even for these pesticides, retention within the root zone for fine soils and semi-arid climate may be long enough to significantly reduce leaching risks.

2.2.4 Validation of the model against HYDRUS 1-D

The model described above was compared to a standard numerical model of variably saturated flow and transport for validation and to compare its predictions with those of a Richards' equation solver.

HYDRUS 1-D is a well established model of variably saturated flow based on the Richards' equation, capable of modeling the transport of sorbing, degrading solutes (*Šimůnek et al.*, 2009). To make an appropriate comparison to HEIST, the dispersivity parameters in HYDRUS were set to zero. Increasing dispersivity (i.e. smaller Peclet numbers) would lead to a divergence between the models, particularly as the dispersion length scale approached the dimension of the soil profile depth.

The HYDRUS and HEIST models differ greatly in their complexity, and as a result it is difficult to make perfect comparisons. In two instances the HEIST model uses effective parameter values that do not appear in the HYDRUS model. These are the threshold water content θ_{fc} and the retardation factor R. The

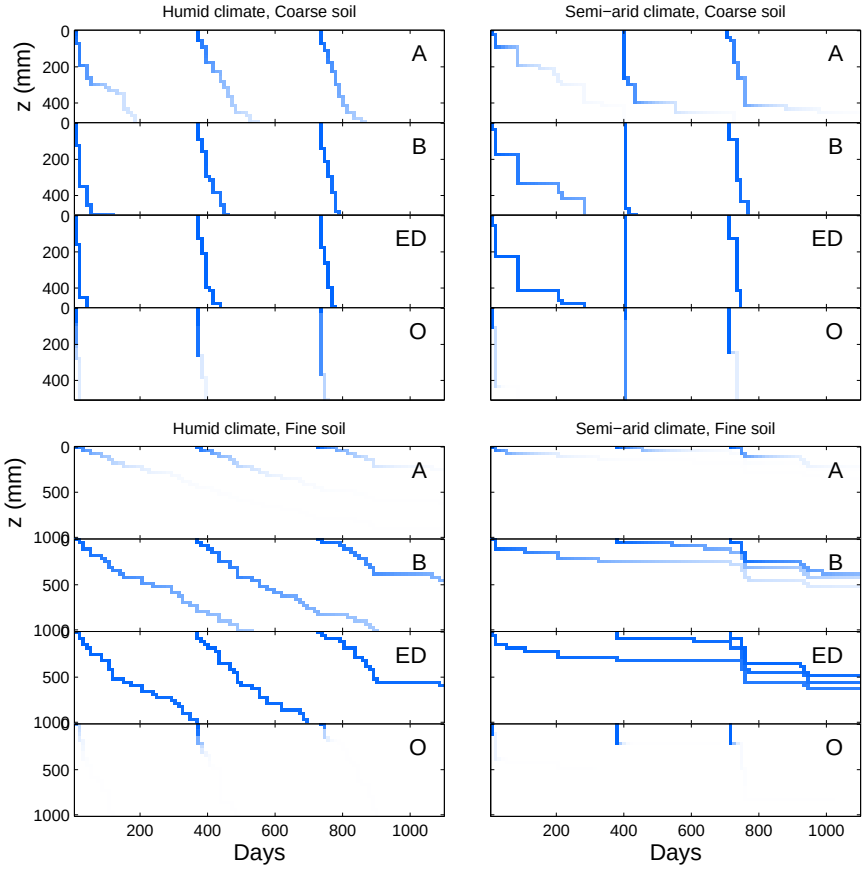

Figure 2.2: Typical transport and degradation of four pesticides in coarse and fine soils under a humid climate and a semi-arid climate, as given by the parameters in Tables 1, 2 and 3. As the pesticides move down through the soil profile they are degraded (indicating by the fading lines) and spend longer at a particular depth before being mobilized by the flow again, and "jumping" to a deeper point, or being leached out of the domain.

threshold water content is the water content at which drainage rates become "small", and the retardation factor is determined by the equilibrium sorption at some effective water content during transport.

In the HYDRUS model the water content and conductivity are controlled by the chosen soil characteristic curves (we have chosen to use the Brooks-Corey formulation for simplicity). We can define a connection between the threshold water content of HEIST and the Brooks-Corey parameters in HYDRUS only by considering the process competing against drainage in the water balance: evapotranspiration. Using the maximum rate ET_{max}, we can predict that the appropriate threshold water content (i.e. that which provides the best match to the Richards' equation solution) is that at which the hydraulic conductivity falls to some multiple of the potential evapotranspiration. That is $K(\theta) = \epsilon ET_{max}$, where ϵ is some dimensionless positive number close to 1. Substituting this into the Brooks-Corey relationship, we obtain:

$$\theta_{fc} = \theta_{sat}(\epsilon \frac{ET_{max}}{K_{sat}})^{1/(2b+3)} \tag{2.14}$$

The selection of an effective water content for the retardation factor is more complex. Recall that under steady flow conditions the retardation factor is given by:

$$R = 1 + \frac{\rho_b f_{OC} K_{OC}}{\theta_{SS}} \tag{2.15}$$

where θ_{SS} is the steady-state water content. In the transient flow conditions this steady-state value must be replaced by an effective water content θ_R. The appropriate value of θ_R will be a function of the water content at which transport occurs, which is in turn a function of the variability of the soil water content in time, and the profile of soil water content relative to the solute loads (and may also vary with depth). We cannot determine this water content a priori at this stage, and must examine the behavior under a number of different values.

HYDRUS was set up with parameters used in the previous Section (Tables 1, 2 and 3) to produce four scenarios: two climates (wet and dry) and two soil types (fine and coarse). The models were both run for 25 years on the same generated series of storms. The input timeseries of rainfall for HYDRUS were constructed from the timeseries of event magnitudes and interstorm durations used in HEIST by assuming that the duration of rainfall events is exponentially distributed with a mean equal to 10% of the mean time between storms, $1/\lambda_p$. Rapid changes in boundary conditions created by rectangular storm events were found to produce numerical instability in HYDRUS and so the input timeseries were smoothed with a Gaussian smoothing filter to produce storms that increase and decrease in intensity over several hours. Pesticides were added annually to the first storm of each year by imposing a fixed concentration boundary

condition of 1 unit mass per m^3 for the duration of the storm.

The results are presented in terms of the cumulative discharge and pesticide leaching as a function of time in Figure 2.3 and Figure 2.4. Cumulative values are presented to simultaneously illustrate the ability of HEIST to capture both the overall partitioning of water (into drained versus transpired fractions) and pesticides (into degraded versus leached fractions), and the pattern of the population of individual drainage events. Because of the instantaneous, event-based nature of HEIST it is not reasonable to compare the hydrographs and chemographs of individual events.

The results show that in all four cases the HEIST model is able to very closely match the HYDRUS water balance – and the timing of drainage events – when ϵ is set to a value in the range of 1-2 (Figure 2.3). The match is closer, and depends less on the value of ϵ in the wet climate cases. In the coarse/dry and especially the fine/dry cases the drainage events are highly intermittent and have a large range of drainage volumes. Nevertheless the HEIST model is able to reproduce this behavior.

The results for the pesticide leaching loads are similarly encouraging (Figure 2.4). In many cases HEIST is able to reproduce the total mass of pesticide and the timing of its delivery very well. The best results were for solutes with lower degradation rates, including Atrazine (whose half-life is 64 days). The appropriate values for θ_R in most cases seem to fall in the range of 0.5 to 1 times θ_{fc}. Variations in θ_R have the greatest effect in the cases of atrazine and bromacil, the more strongly sorbing solutes. The total delivery is most sensitive to θ_R in the fine/dry case, where transport through the profile is dominated by a small number of events and the soil water content will explore a wide range of values due to the high evapotranspiration. The predictions are very strong in the case of ethylene dibromide, which is less sorbing and slowly degrading.

The timing of the delivery of oxamyl is well represented by HEIST, but the total loads are not. This is a direct result of the very rapid degradation of this compound. In HYDRUS the solute is delivered to the lower boundary of the solution domain over a period of time as the soil water content in the profile redistributes after a storm event. The degradation that occurs within the profile during this time reduces the mass of solute finally leached from the system. On the other hand the delivery of the solute load occurs instantaneously in HEIST, and so less degradation occurs in the profile and the cumulative load predicted by HEIST is higher than that of HYDRUS. Further model results showed that HEIST overpredicted total oxamyl loads in the absence of any retardation ($R = 1$), showing that the discrepancy does indeed arise from the assumption of instantaneous delivery in HEIST.

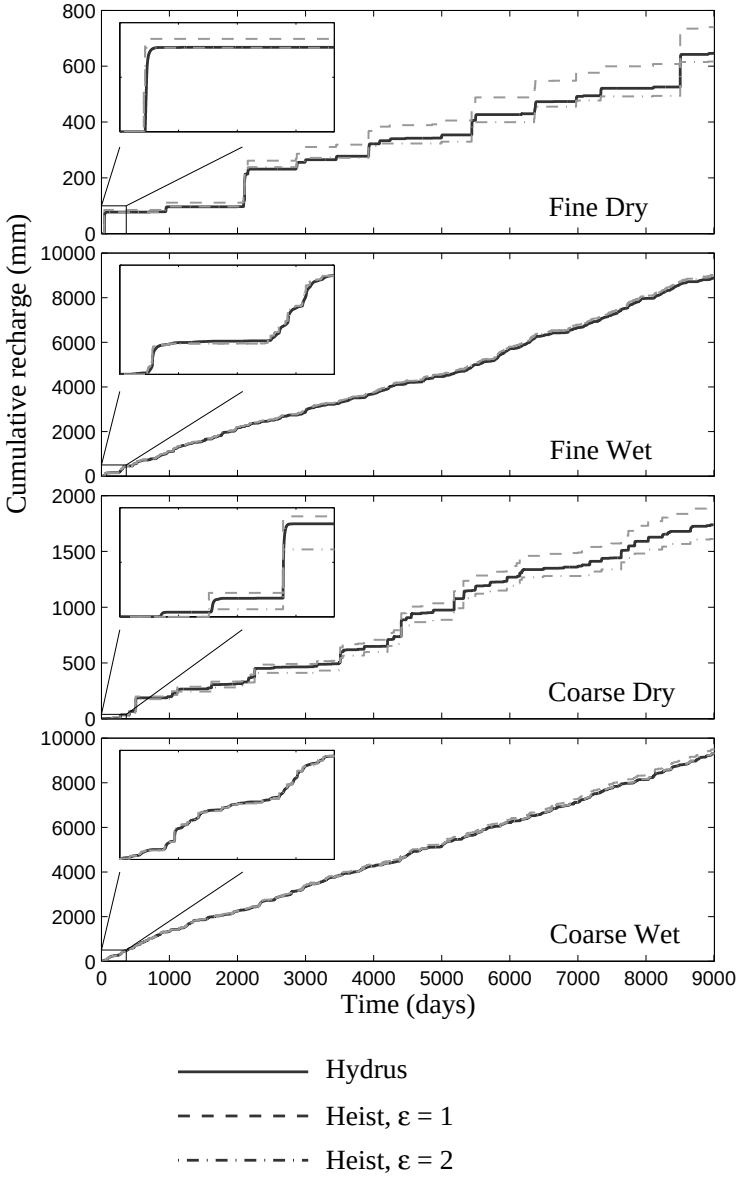

Figure 2.3: Comparison of the cumulative drainage from the base of the (free draining) vadose zone predicted by HYDRUS (solid line) and the current model with two values of ϵ. Insets show detail of the behavior over the first year of the simulation. These results indicate that the model does a good job at replicating the timing and magnitude of drainage events, though the precise value of α required to match HYDRUS is uncertain.

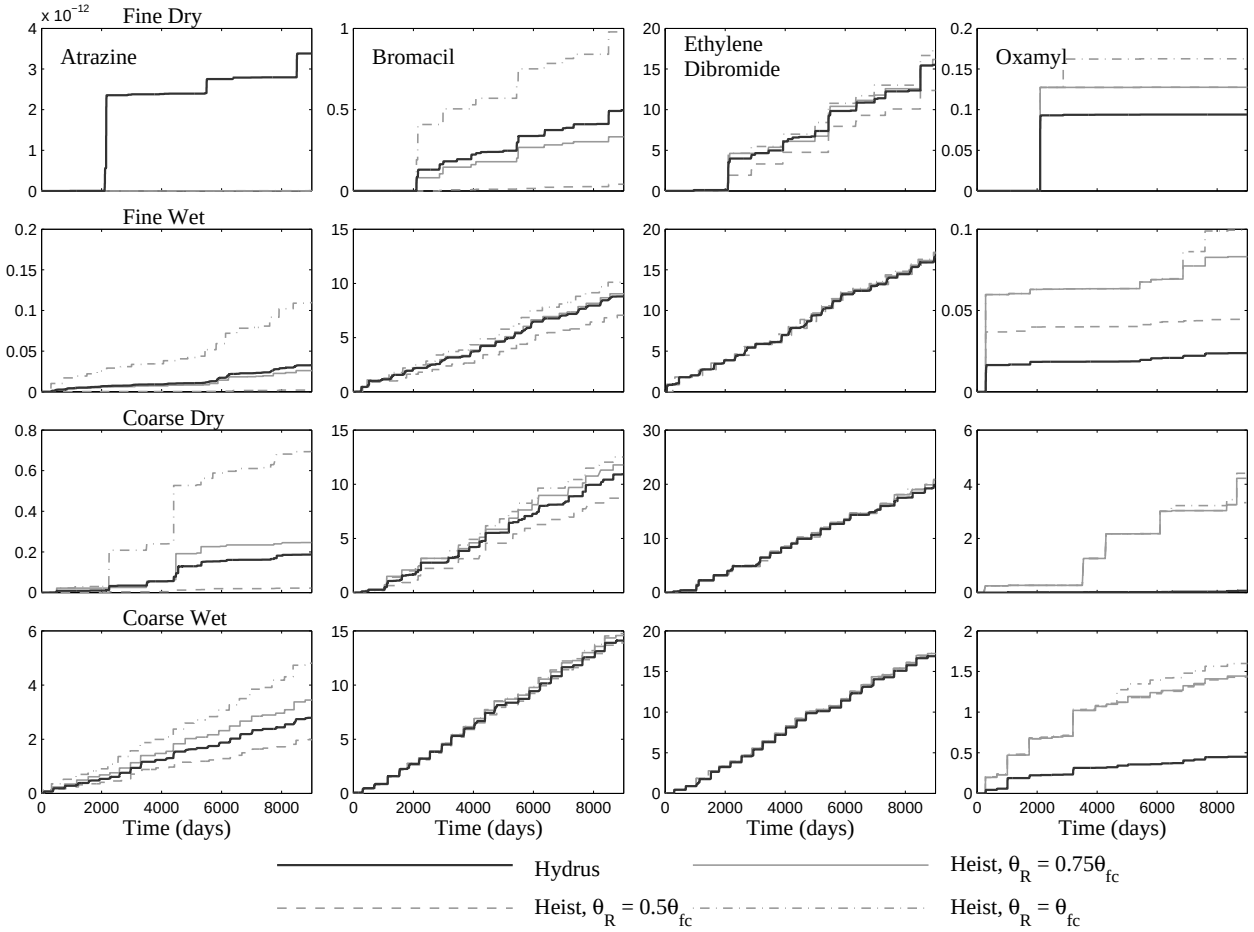

Figure 2.4: Comparison of the cumulative leaching of pesticide loads from the base of the vadose zone predicted by HYDRUS (solid line) and the current model with various values of θ_R. These results indicate that the model also does a good job at replicating the timing and magnitude of leaching events, though, again, the precise value of the effective parameter required to match HYDRUS is uncertain.

2.3 Conclusions

This work has used simple modeling approach to gain insight into the control of evapotranspiration on the travel time and delivery of reactive solutes through the vadose zone. We developed a piston-displacement model of 1-D retarded, reactive solute transport through a homogeneous soil profile. The model was compared to HYDRUS 1-D (*Šimůnek et al.*, 2009) and was shown to capture the dynamics of solute transport through the vadose zone relatively well if appropriate values of soil water parameters θ_{fc} and θ_R are used. Methods for estimating θ_{fc} were developed, and issues associated with the accurate identification of θ_R were discussed.

2.4 Acknowledgments

Work on this chapter commenced during the Summer Institute organized at the University of British Columbia (UBC) during June-July 2009 as part of the NSF-funded Hydrologic Synthesis project, "Water Cycle Dynamics in a Changing Environment: Advancing Hydrologic Science through Synthesis" (NSF Grant EAR-0636043, M. Sivapalan, PI). The work was completed with support from NSF grant EAR09-11205 "Biotic alteration of soil hydrologic properties and feedback with vegetation dynamics in water limited ecosystems" (PI: Sivapalan). The work was conducted in collaboration with Suresh Rao, Nandita Basu, Gavan Mcgrath, Praveen Kumar, and Murugesu Sivapalan. Thanks also to Al Valocchi and Stefano Zanardo for their fruitful discussions of these ideas.

Chapter 3

Climate, soil and vegetation controls on the temporal variability of vadose zone transport - Probabilistic analysis

[1]*Building on the model described in the previous chapter, we utilize existing theory of the stochastic dynamics of soil water to derive analytical and semi-analytical expressions for the PDFs of solute travel time and delivery. The moments of these PDFs directly relate the mean and variance of expected travel times to the water balance, and show how evapotranspiration tends to reduce (and make more uncertain) the mass of a degrading solute delivered to the base of the vadose zone. These expressions also provide insight to the shifting importance of different controls across a range of conditions. Results suggest that in dry climates, rare large storms can be an important mechanism for leaching to groundwater. The framework suggests a classification of different modes of subsurface process dominance in the hydrologic filtering.*

3.1 Introduction

The previous chapter described a parsimonious modeling framework for solute transport through the vadose zone and showed that this model was able to reproduce the behavior of more sophisticated models quite well. Here we will build on this model to examine the extent to which the stochastic variability in the rainfall amounts influences the expected travel time of a solute, and the exact nature of this influence. Many previous studies that have examined these controls have been restricted to relatively humid systems, where the effects of evapotranspiration on the transport behavior may be small (*Destouni*, 1991). Those who have used an analytical approach tend to neglect the effects of evapotranspiration. *Jury and Gruber* (1989) used the transfer function approach to examine the effect of climate variability on the travel time through the vadose zone. The transfer function predicts the solute delivery as a function of the total infiltration. Convolving this with the probability density function (PDF) of the total infiltration (conditional on time since solute application) gives the PDF of the travel time, but neglects the effect of evapotranspiration noted above. A recent exception is *McGrath et al.* (2008, 2010), who used recent advances in stochastic modeling of the coupling of soil water and climate to directly examine the role of the hydrologic filtering on solute delivery to groundwater. They used a simple stochastic soil water model to assess the risk of pesticide leaching through preferential flow channels, based on the assumption that preferential flow was initiated when mean soil water content or rainfall intensity exceeded a threshold.

The stochastic soil water content models utilized by *McGrath et al.* (2008, 2010) provide an elegant framework for investigating how soil, climate and vegetation properties control soil water variability and how this variability affects coupled processes. The approach was pioneered by *Eagleson* (1978) and *Milly* (1993) and was later expanded by *Rodriguez-Iturbe et al.* (1999) and others (see for example *Laio et al.*,

[1]This work has been submitted for publication to Water Resources Research as: Harman, C J, P S C Rao, N B Basu, G S Mcgrath, P Kumar, and M Sivapalan, Climate, soil and vegetation controls on the temporal variability of vadose zone transport. All figures, tables and data were created by Ciaran Harman unless otherwise indicated.

2001b; *Porporato et al.*, 2001). In these works, precipitation is represented as a stochastic process (a marked Poisson process) with known properties. Simplified representations of soil water dynamics parametrized with measurable properties of the soil, climate and vegetation (such as potential evapotranspiration, root zone depth and soil hydraulic properties) can then be used to derive analytical expressions for key aspects of soil hydrologic variability. Expressions have been derived for the PDF of soil water content (*Laio et al.*, 2001b), duration of plant water stress (*Porporato et al.*, 2001), mean frequency of recharge (*Botter et al.*, 2007), and other properties. The power of these approaches is in the way they reveal the dynamic variability of the vadose zone hydrology, the relative importance of different controls on that variability, and the relationship between the controls and other quantities of interest, such as the ecosystem functional behavior. Consequently, they can also provide a first-order estimate of the direction and magnitude of changes in system dynamics under changing climatic conditions (*Porporato et al.*, 2004).

Despite this power, this stochastic soil water approach has not been applied to examine controls on the dynamics or functional behavior of reactive solute transport and transformations through the soil profile (as opposed to the preferential flow-triggering examined by *McGrath et al.* (2008, 2010)). An impediment to using the stochastic approach for solute transport through the vadose zone is the need to resolve the travel time from the soil surface to the water table. Most applications of this type of stochastic soil water model have treated the root zone in a lumped way, and have not considered the vertical variations in soil water content. *Guswa et al.* (2004) examined the validity of this assumption for ecohydrologic applications and found it to provide a reasonable approximation of the water balance dynamics. An exception is *Laio et al.* (2006), who developed a vertically extended stochastic soil water content model and used it to predict optimal root distribution (*Laio*, 2006).

The model presented in the previous chapter is of a similar order of complexity as the stochastic soil water approach, and relies on compatible assumptions of soil water content dynamics. Here we develop a semi-analytical solution to the stochastic model dynamics, and test it against the numerical solutions. Then we discuss the results, focusing on what is revealed about the role of hydrologic filtering on the timing and delivery of solutes through the vadose zone, and the role of climate, soils and vegetation in controlling this filtering.

3.2 Solute leaching as a stochastic process

The filtering of the solutes through the vadose zone illustrated in Figure 2.2 is determined by the combination of soil, climate and solute properties, and in particular from the spatial and temporal hydrologic variability

of the vadose zone. Our simulations suggest that the roles played by climate and soil properties have a complex set of interactions. Motivated by the desire to get a broader view of this interaction, we will seek expressions for the PDF of the residence time and delivery ratio of such surface-applied sorbing, degrading solutes to these properties that explicitly incorporates climatic and soil properties. We start by examining the distribution of transport event sizes and waiting times using the numerical model. Using the results, we will then lay out a general framework for the derivation under some simple assumptions, and then derive the results under the special case that there is no evapotranspiration. The expressions obtained are similar to that of *Jury and Gruber* (1989). We then utilize the results of a Monte-Carlo simulation with the HEIST model to obtain a semi-analytical expressions for the PDF of travel times where evapotranspiration creates variations in the water content with depth. This semi-analytical model will then be evaluated against the numerical HEIST approach developed in the preceding section.

3.2.1 Distribution of transport event sizes and waiting times

Here, we will develop expressions for the distribution of jump sizes and waiting times of transport events through the vadose zone. To do so we will make use of the class of stochastic soil water models derived from the work of *Rodriguez-Iturbe et al.* (1999). This model uses a lumped conceptualization of soil water in which the vadose zone is treated as a single unit. Although the model described above resolves the vertical profile of soil water, drainage events are only triggered when an infiltrating event raises the average water content of the whole profile above the threshold value θ_{fc}. Consequently, when averaged over the depth Z_r, the dynamics of soil water in the above model operate identically to the stochastic soil water models cited earlier, so long as the correct parametrization of the loss processes are adopted, as described in the model development above. We shall ignore the residual from water content and assume that the reduction function for evapotranspiration is from $f(0) = 0$ to $f(\theta_{fc}/\theta_{sat}) = 1$. We can therefore use results from those models as needed here.

To proceed, we note that the paths traced by the solutes in Figure 2.2 appear to have the form of a random walk with strictly positive jump sizes. The jumps $\{\zeta_i\}$ are the transport events driven by infiltration past each depth. The intervals between jumps $\{\tau_i\}$ are the waiting times between transport events. To obtain the PDF of travel times through the vadose zone, it is therefore necessary to determine the appropriate distributions for the jump sizes, $f_\zeta(\zeta)$, and waiting times $f_\tau(\tau)$.

Unlike previous random walk approaches (*Jury and Gruber*, 1989; *McGrath*, 2007), the distribution of jumps and intervals in the transport through the vadose zone may not be independent of the position ξ_j in the profile. The variations in the distributions with depth are bounded at the surface by the distri-

bution of infiltration events, and at the base by the distribution of leaching events from the vadose zone. The distribution at the base differs from that of the surface due to the soil water deficits created by the evapotranspiration of soil water between events.

Recent work provides a basis for developing expressions for these distributions. *Porporato et al.* (2004) showed that these dynamics are a function of just two dimensionless parameters, which we will use here to express the required results. Recast here in a convenient form, the first is the aridity index ϕ, and is the ratio of the maximum evapotranspiration rate and the rainfall rate:

$$\phi = \frac{ET_{max}}{\alpha \lambda_p} \tag{3.1}$$

The second is γ, the ratio of the potential storage in the vadose zone ($Z_r \theta_{fc}$) and the average depth of the storm events (α):

$$\gamma = \frac{Z_r \theta_{fc}}{\alpha} \tag{3.2}$$

It can be shown that the magnitudes of the drainage events will follow the same exponential distribution as the infiltration events (*Botter et al.*, 2007), (*Rodriguez-Iturbe et al.*, 1999). This effect is related to the "memoryless" property of the exponential distribution. For an exponentially distributed set of random variables X, the PDF of $X - c$ for all $X > c$ is identical to the PDF of X. Another way to express this is that the conditional probability $P(X > x|X > c)$ is equal to the probability $P(X > x - c)$ for $x > c > 0$, when X is an exponentially distributed random variable. In essence, the effect of the unsaturated zone is simply to alter the frequency of events (filtering those events that are $< c$ in the previous example), but not their magnitude. If this is the case, the distribution of jump sizes, $f_\zeta(\zeta)$, can be found simply by noting that the transport of the solutes depends on the water content at field capacity and the retardation factor (as given in Equation 2.11) such that:

$$f_\zeta(\zeta) = \frac{R\gamma}{Z_r} \exp(-R\gamma \frac{\zeta}{Z_r}) \tag{3.3}$$

This result is very powerful, and simplifies the analysis.

Botter et al. (2007) also derived an expression for the mean of the waiting times between leaching events based on the assumption that infiltration at the surface follows a marked Poisson process with an exponential distribution of event magnitudes. *McGrath et al.* (2007) further derived expressions for the first n moments of the waiting time distribution between leaching events. These expressions suggested that when the ratio ϕ/γ is sufficiently small (*Botter et al.* (2007) suggests it should be less than 0.1), the distribution of waiting

times between recharge events can be approximated by an exponential distribution with a rate parameter λ_d given by:

$$\lambda_d = \lambda_p \frac{e^{-\gamma} \gamma^{\frac{\gamma}{\phi}} \phi/\gamma}{\Gamma\left(\frac{\gamma}{\phi}\right) - \Gamma\left(\frac{\gamma}{\phi}, \gamma\right)} \tag{3.4}$$

where $\Gamma(a)$ is the gamma function and $\Gamma(a, z)$ is the incomplete gamma function (*Abramowitz and Stegun*, 1972).

McGrath et al. (2007) observed that for larger γ/ϕ (called β in their notation) the distribution of waiting times becomes less and less like a exponential distribution, and instead exhibits a clustering behavior that is amplified when ϕ is close to 1. This clustering arises from the increased probability of short waiting times when the soil water content is close to the maximum capacity, and more likely long waiting times when soil water content is low.

Numerical tests were conducted using the model for a variety of values of γ and ϕ to determine the validity of assuming an exponential distribution of jump sizes and waiting times. Figure 3.2 strongly supports the assumption that the jump sizes are in fact exponentially distributed throughout the profile with a mean given by $\alpha/R\theta_{fc}$. However, Figure 3.1 suggests a more complex picture for the waiting time distribution. For humid climates ($\phi < 1$) and small γ (< 1) the distribution does appear to follow an exponential distribution with rate constant λ_d (given by the red line). However in deeper and drier soils this approximation does not hold, particularly in the deeper parts of the soil. The shorter waiting times seem to follow an exponential distribution with the same arrival rate as the infiltration λ_p. However the tail of the distribution appears to follow a power-law with an exponent that decreases deeper in the profile, and as γ and ϕ increase.

Proceeding toward an analytical derivation of the PDF, these results suggest that an exponential distribution of jump sizes is justified for this model, but that the assumption of an exponential distribution of waiting times may lead to inaccurate results in some cases.

3.2.2 Framework for deriving the PDF of transit times and delivery ratios

In the interest of obtaining an analytical result we will assume that the water flux past a point ξ is a Poisson process with the same mean volume throughout the profile, but a rate that depends on the depth $\lambda(\xi) \leq \lambda_p$. Under these conditions we can make the following arguments to derive the PDF of travel times T through the vadose zone. Wetting fronts enter the vadose zone and traverse it in a series of independent steps that are drawn from an exponential distribution with parameter $\alpha/(\theta_{fc}R)$. From the properties of such a process, we can say that the number of steps n required for a front to reach the base is given by a Poisson distribution

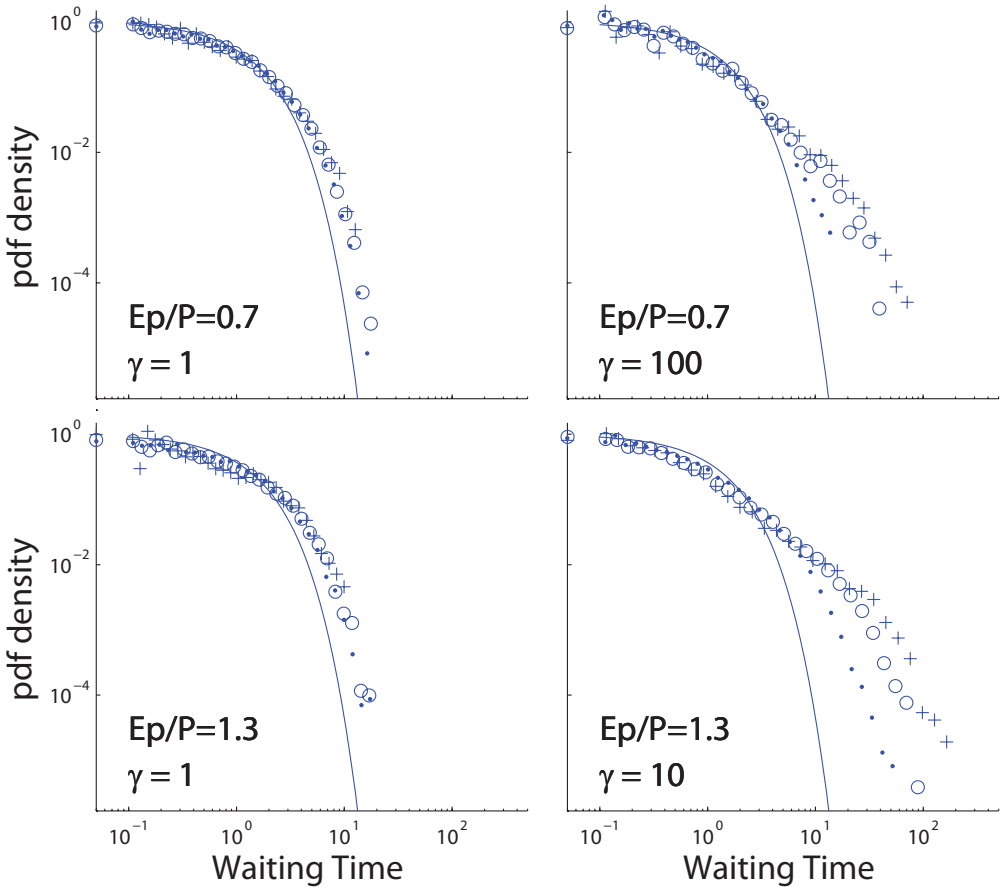

Figure 3.1: Numerical experiments indicate that the waiting times between transport events are not Poissonian except for small values of γ and ϕ. They also become increasingly power-law with depth. The solid line gives the PDF of the waiting times between infiltration events (an exponential with rate parameters λ_p).

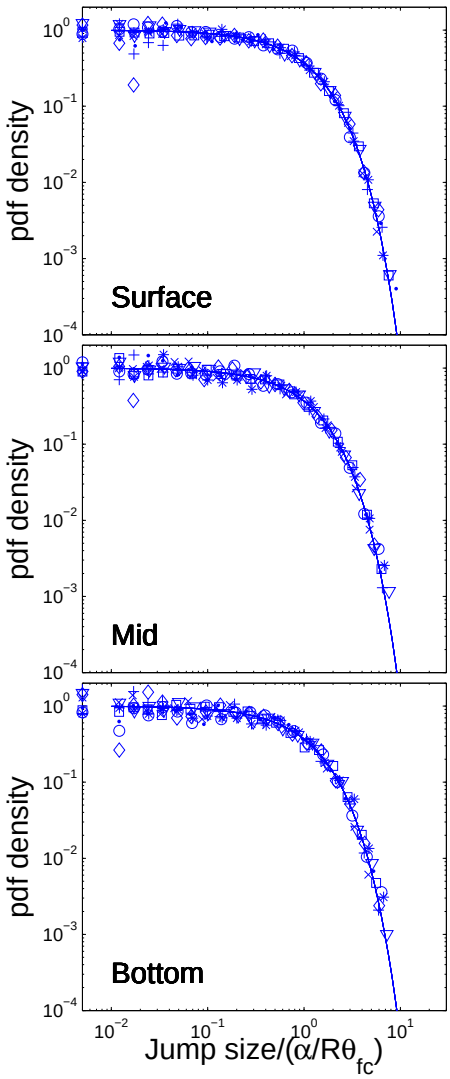

Figure 3.2: Transport distance in each "jump" (see Figure 2.2) follows a exponential distribution with a mean given by $\alpha/R\theta_{fc}$. This appears to hold throughout the profile, and for all combinations of γ and ϕ.

with parameter $R\gamma$, and the position ξ of a step is uniformly distributed throughout the column.

Note that the probability that the front takes exactly zero steps to reach the base is equal to $\exp(-R\gamma)$. This is the probability that an event will completely "flush" the system, transporting the new wetting front, and all the solute fronts stored in the vadose zone, through the reference plane at the base of the vadose zone. Furthermore, when R is large the probability that the solute will reach the base in a finite amount of time approaches zero.

The waiting time for any particular step τ_i can be found by randomizing the value of ξ in the wetting front arrival rate according to a uniform distribution on $[0, Z_r]$:

$$f_{\tau_i} = \frac{1}{Z_r} \int_0^{Z_r} \lambda(\xi) e^{-\lambda(\xi)\tau_i} d\xi \tag{3.5}$$

If $n-1$ steps are required to traverse the vadose zone then the total travel time T_n is the sum of the $n-1$ values of τ_i. The distribution of the sum of n random variables is given by the n-fold convolution of the PDF of each value:

$$f_{T_n} = \left(\underbrace{f_{\tau_i} * f_{\tau_i} * \ldots * f_{\tau_i}}_{n} \right) (T_n) \tag{3.6}$$

where $*$ is the convolution operator. Finally, the number n is itself a random variable with a Poisson distribution with parameter $R\gamma$. To obtain the distribution of the travel times T we must therefore randomize the value of n in the distribution of the n-step travel time f_{T_n}.

$$f_T(T) = \sum_{n=0}^{\infty} f_{T_n} \frac{e^{-R\gamma}(R\gamma)^n}{n!} \tag{3.7}$$

These steps can be followed to obtain a PDF of T so long as a) the function $\lambda(\xi)$ can be specified, b) closed forms of the integrals can be found, and c) a form for f_{T_n} can be found for arbitrary n. This is a serious challenge.

Laio et al. (2006) developed a vertically extended stochastic soil water content model to predict how the PDF of soil water content varies with depth. They derived a general expression for $\lambda(z)$, and an explicit solution for the case of a uniform root profile. However, this expression could not be carried through the above steps to produce an analytical solution for $f_T(T)$. In the following section we derive an analytical expression for when $\phi = 0$, and an approximate solution for $\phi \neq 0$.

3.2.3 Analytical solution for $\phi = 0$

One case where an analytical solution can be found is where there is no evapotranspiration. In that case, the storage deficit is always zero and the same amount of water flows past every point in the profile, so the function $\lambda(\xi)$ is constant at $\lambda(\xi) = \lambda_p$. Thus f_{τ_i} is simply an exponential distribution with parameter λ_p. The sum of n independent, identically distributed exponential random variables is given by a Gamma distribution with a shape parameter n and a scale parameter equal to the rate constant of the underlying exponential distribution. Therefore we can determine the PDF of the amount of time T each solute front spends in the vadose zone by randomizing the shape parameter of a gamma distribution according to the Poisson distribution, as given above. This yields:

$$f_T(T) = \begin{cases} \dfrac{\exp(-R\gamma - T\lambda_p)}{T}\sqrt{T\lambda_p R\gamma} I_1\left(2\sqrt{T\lambda_p R\gamma}\right) & T > 0 \\ \exp(-R\gamma) & T = 0 \end{cases} \tag{3.8}$$

where $I_1(z)$ is the modified Bessel Function of the first kind. The PDF of (*Jury and Gruber*, 1989) differs from that presented here in that they assume a gamma distribution of infiltrating volumes (rather than exponential) and account for the waiting time between solute application and the first storm. In this distribution λ_p operates as scale parameter, and $R\gamma$ controls the shape of the distribution. Figure 3.3 shows the control of the shape parameter on this distribution. When $R\gamma$ is close to 1, many of the events have $T = 0$, and the distribution for $T > 0$ drops off quickly. When $R\gamma$ is larger, it becomes increasingly symmetrical, approximating a normal distribution. The mean and variance of the distribution are given by:

$$\mu_T = \frac{R\gamma}{\lambda_p} \qquad \sigma_T^2 = \frac{2R\gamma}{\lambda_p^2} \tag{3.9}$$

These moments can be derived as a special case of the PDF derived by (*Jury and Gruber*, 1989) when the waiting time between solute application and the first storm is neglected (see *McGrath* (2007)).

If the fronts carry a solute subject to first-order degradation, then the proportion of mass remaining when the front exits the system to the initial mass M/M_0 (which we shall refer to as the delivery ratio DR) is a function of the transit time T and the degradation rate constant k (Equation 2.13). Since T is a random variable DR is also a random variable, and since the PDF of T is known (under the approximations given above), we can also determine the PDF of DR. In general if a random variable Y is a monotonically decreasing function $y = g(x)$ of another random variable X, then their distributions $f_Y(y)$ and $f_X(x)$ are related by:

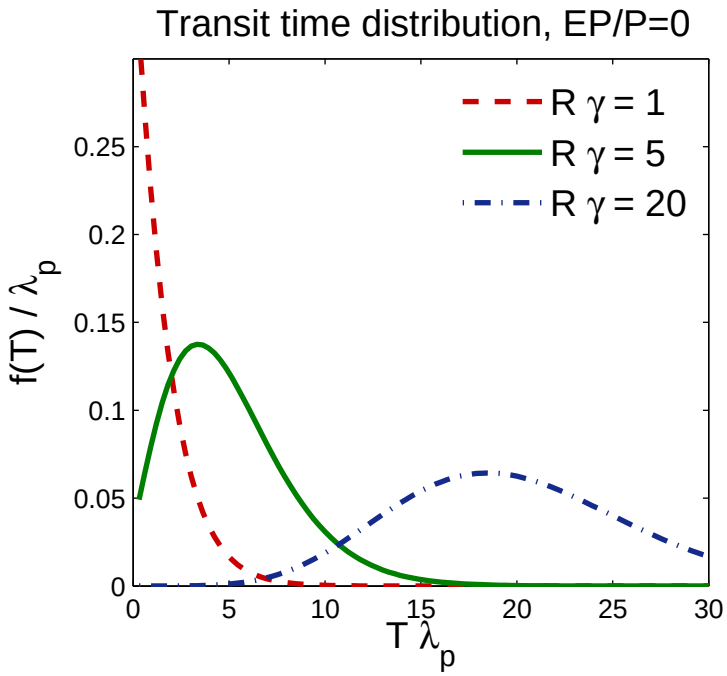

Figure 3.3: Probability density function of the transit time T for solute fronts for the special case of no evapotranspiration ($\phi = 0$), normalized by the storm arrival rate λ_p. The atom of probability at $T = 0$ is not shown. Three cases of the shape parameter $R\gamma$ are shown: 1, 5, 20.

$$f_Y(y) = -f_X(g^{-1}(y))\frac{d(g^{-1}(y))}{dy} \tag{3.10}$$

where $x = g^{-1}(y)$. Here Equation 2.13 is g and Equation 3.8 is f_X. Thus we can find the PDF of DR as:

$$f_{DR}(DR) = {}_0\tilde{F}_1\left(2, -\frac{R\gamma}{k_d/\lambda_p}\log(DR)\right)\frac{R\gamma}{k_d/\lambda_p}e^{-R\gamma}DR^{\frac{1}{k_d/\lambda_p}-1} \tag{3.11}$$

plus an atom of probability at $DR = 1$ equal to $exp(-R\gamma)$, corresponding to the events that flush the solute all the way through the soil. The function ${}_0\tilde{F}_1$ is the regularized confluent hypergeometric function (*Abramowitz and Stegun*, 1972). The nth raw moment of the delivery ratio is given by:

$$\mu_n = \exp\left(-\frac{R\gamma n k_d}{\lambda_p + n k_d}\right) \tag{3.12}$$

So that the mean and variance are given by:

$$\mu_{DR} = \exp\left(-\frac{R\gamma k_d}{\lambda_p + k_d}\right) \tag{3.13}$$

$$\sigma^2_{DR} = \exp\left(-\frac{2R\gamma k_d}{\lambda_p + 2k_d}\right) - \exp\left(-\frac{2R\gamma k_d}{\lambda_p + k_d}\right) \tag{3.14}$$

3.2.4 Approximate solution for $\phi > 0$

When $\phi > 0$ the storage deficit created by evapotranspiration will reduce the frequency with which wetting fronts reach a depth z in the soil, leading to the more complex distributions shown in Figure 3.1. However it is possible that effective values of the mean waiting time, λ_e and shape parameter $R\gamma_e$ can be found. Here we explore this possibility by comparing the analytical results obtained above to HEIST. By rearranging the expression for the mean and variance of the travel time we can obtain expressions to infer the effective parameter values:

$$\lambda_e = \frac{2\mu_T}{\sigma^2_T} \tag{3.15}$$

$$R\gamma_e = \frac{2\mu^2_T}{\sigma^2_T} \tag{3.16}$$

The numerical model was run for 400 combinations of random soil and climate parameters to ensure that the effective parameter gave reasonable results over the full parameter range. The retardation factor was set at 1. All parameters were sampled independently to ensure maximum coverage of the parameter space. Rainfall parameters were sampled from distributions fitted to the data in *Hawk and Eagleson* (1992). ET was sampled from a gamma distribution with mean 1000mm and standard deviation 500mm. Soil depths were sampled from a log-normal distribution with scale parameter 1 meter and shape parameter 2.5. Soil properties were obtained by choosing % sand uniformly from 0 to 100, and % clay uniformly from 0 to the minimum of 20 or $100 - \%$sand. Field capacity and wilting point were assumed to correspond with the water contents at 33kPa and 1500kPa obtained from the pedotransfer functions of *Saxton and Rawls* (2006).

It was found that the effective parameters inferred from the numerical results showed consistent and simple relationships with the ratio λ_d/λ_p (Figure 3.4). The effective jump rate λ_e is very close to λ_d. The effective γ_e varies in a way that is very close to:

$$\frac{\gamma_e}{\gamma} = \left(\frac{\lambda_d}{\lambda_p}\right)^{\frac{1}{2}} \tag{3.17}$$

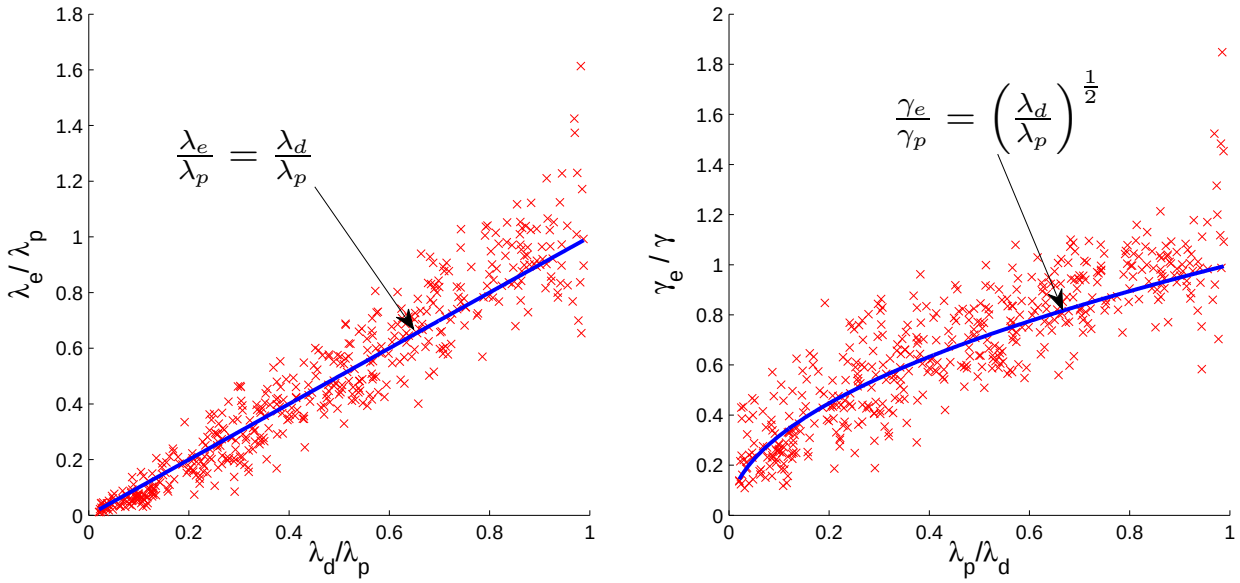

Figure 3.4: Relationships between the effective parameters observed in 400 random simulations (normalized by their original values) λ_e/λ_p and γ_e/γ and the ratio λ_d/λ_p. Two very simple relationships emerge: the effective mean jump rate λ_e is very closely approximated by λ_d, and the effective storage parameter γ_e scales with $(\lambda_d/\lambda_p)^{\frac{1}{2}}$.

These relationship are remarkably simple, and suggest that it may be possible to derive closed-form analytical solutions for the travel-time distribution that do not rely on these approximate relationships.

We would like to be able to use these effective parameters in the expressions for the PDF and moments of the travel time and delivery ratio derived above. In using these effective parameters, it is necessary to consider the role of the atom of probability $\exp(-R\gamma)$ that appears in the expression for the travel time and delivery ratio PDFs. These atoms refer to the case where a storm event flushes the solute load completely through the system, and are therefore not affected by the antecedent soil water storage. The value of γ used to calculate the probability of this occurrence should therefore not be replaced with the effective value γ_e. However, this creates an inconsistency in the PDF, such that its zeroth moment many not be unity. To correct this, we must introduce a correction C that scales the main part of the PDF:

$$C = \frac{1 - e^{R\gamma}}{1 - e^{R\gamma_e}} \tag{3.18}$$

This factor is slightly greater than 1 in most cases, and can usually be neglected. It is only significant when ϕ and γ are both very large. By neglecting this factor we can indeed substitute the effective parameters into the expressions for the moments of the travel time distribution and delivery ratio derived for the case with $\phi = 0$.

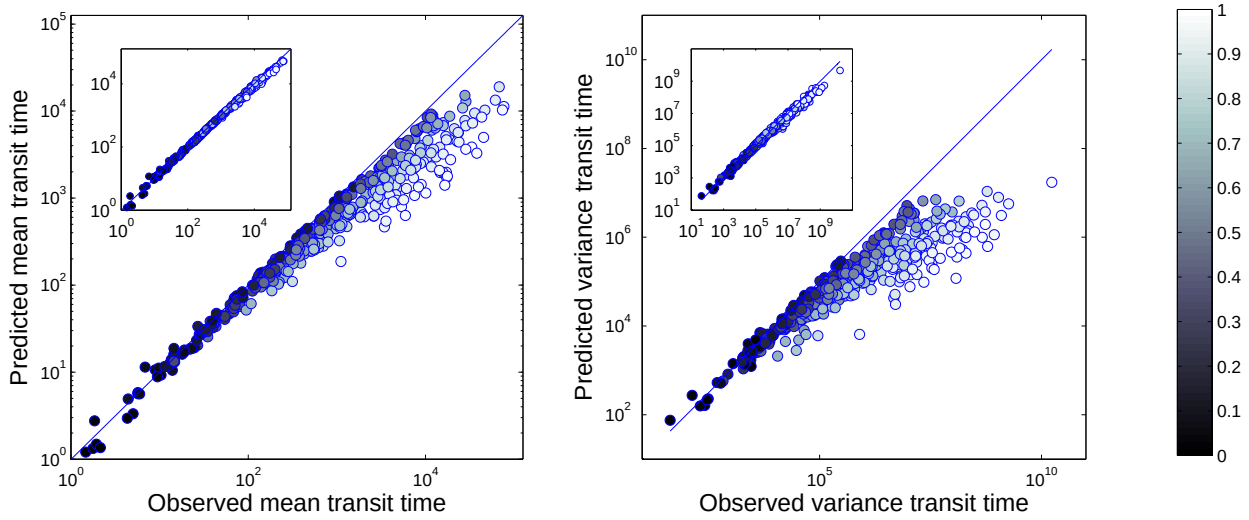

Figure 3.5: Comparison of mean and variance of the travel time distribution predicted by eqs. 3.9, with those derived from 400 random simulations. The inset plots show the same relationships with the parameters λ_p and γ replaced with the effective parameters λ_e and γ_e. The water balance E/P in each simulation is represented by the tone of the dots. These results show that the moments of the travel time distribution are very well characterized by the derived expressions when the effective parameters are used.

Figure 3.5 shows that the approximate analytical expressions provide an excellent prediction of the first two moments of the distribution. The figure compares the sample mean and variance $\bar{T}$ and S_T^2 observed over many simulations to the mean and variance μ_T and σ_T^2 obtained from Equation 3.9 using the original parameters, as well as those obtained by using the effective parameter values in 3.9. The results show that, as would be expected, when $\phi > 0$ the original parameters significantly underestimate the mean and the variance of the age distribution. In such cases the reduction of the average load velocity due to evapotranspiration is not accounted for. The effects are strongest for the drier sites (light dots). On the other hand the effective parameter value give an excellent prediction.

Using the effective parameters in the PDF of the delivery ratio, equation 3.11, gives a very close match to the numerical results (Figure 3.6). These results show that the semi-analytical solution obtained by using the effective parameters is able to correctly characterize the behavior of the numerical model over a wide range of conditions.

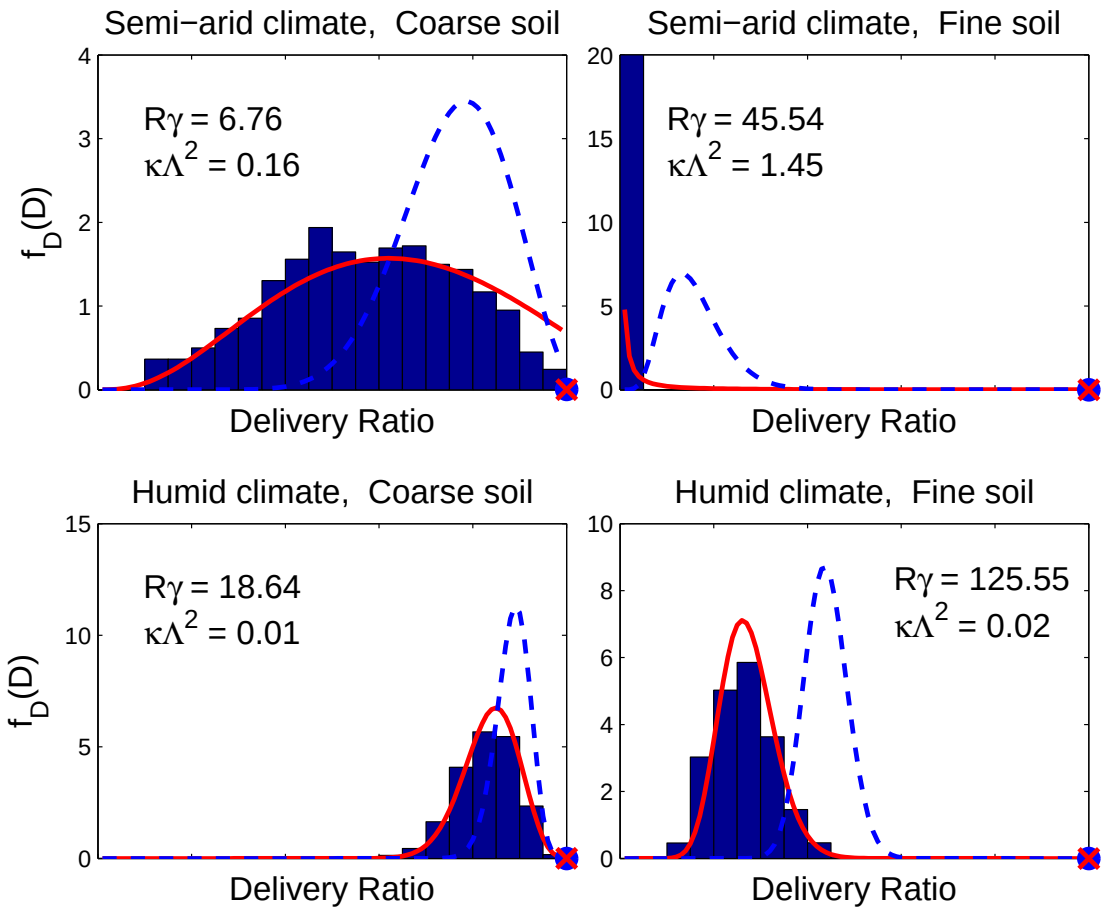

Figure 3.6: Examples of the ability of equation 3.11 to predict the PDF of the delivery ratio for bromacil. When the original parameters are used, representing the case with no evapotranspiration, delivery ratio is overestimated (dashed line). When evapotranspiration is accounted for using the effective parameters, equation 3.11 provides an excellent prediction of the PDF of pesticide delivery (solid line).

3.3 Discussion

3.3.1 Sensitivity to climate and soil properties

The numerical model and semi-analytical result presented above provides a framework for assessing the controls of climate, soils and solute properties on the residence time and delivery ratio of solutes in the vadose zone. We can introduce two new dimensionless numbers that will allow us to further isolate the essential controls. Firstly, we define Λ as the ratio $\sqrt{\lambda_p/\lambda_d}$. The effective parameters determined above can then be defined relative to their original values as $\lambda_e = \lambda_p/\Lambda^2$ and $\gamma_e = \gamma/\Lambda$. Second we define κ as the ratio of the degradation rate and the frequency of storms k_d/λ_p. With these ratios, and assuming $C \sim 1$, we can re-write the moments of the travel time and delivery ratio as:

$$\mu_T = \frac{R\gamma\Lambda}{\lambda_p} \tag{3.19}$$

$$\sigma_T^2 = \frac{2R\gamma\Lambda^3}{\lambda_p^2} \tag{3.20}$$

and

$$\mu_{DR} = e^{-\frac{R\gamma\kappa\Lambda}{\kappa\Lambda^2+1}} \tag{3.21}$$

$$\sigma_{DR}^2 = e^{-\frac{2R\gamma\kappa\Lambda}{2\kappa\Lambda^2+1}} - e^{-\frac{2R\gamma\kappa\Lambda}{\kappa\Lambda^2+1}} \tag{3.22}$$

Note that we can express the moments of the travel time as the product of a 'wet travel time', μ_{T0}, which is the travel time when there is no evapotranspiration, and a deceleration factor, which is simply Λ, that accounts for the effect of evapotranspiration:

$$\mu_T = \Lambda\mu_{T0} \tag{3.23}$$

$$\sigma_T^2 = \Lambda^3\sigma_{T0}^2 \tag{3.24}$$

Also, note that the products $k_d\mu_T$ and $k_d\mu_{T0}$ are the so-called "Damkŏhler numbers" (*Rao et al.*, 2010) of the cases with and without evapotranspiration. Λ can also be interpreted as the effect of the evapotranspiration on this number, which has been used to characterize the reactive transport of solutes through the soil (*Kuntz and Grathwohl*, 2009). The value of Λ^{-2} is equal to the ratio of the mean rate of infiltration $\lambda_p\alpha$ and

drainage $\lambda_d\alpha$. Alternatively $\Lambda^2 = (1-H)^{-1}$, where H is the local value of the Horton index $ET/\alpha\lambda_p$ (*Troch et al.*, 2009b), the ratio of evapotranspiration and infiltration. It is common in simple pesticide risk analysis to estimate mean travel time using a mean leaching rate calculated from the water balance (*Wang et al.*, 2009). Expressed in the terms used in this chapter, the mean travel time under the mean rate of recharge determined from the water balance would be $R\gamma/\lambda_d = \Lambda^2\mu_{T0}$. The actual mean travel time determined here, μ_T, can be expressed as $R\gamma/\sqrt{\lambda_d\lambda_p} = \Lambda\mu_{T0}$. The factor $\sqrt{\lambda_d\lambda_p}$, which appears as a result of the choice of expressions for the effective parameters, can be interpreted as the geometric mean of the rate parameters at the surface and base of the soil. Thus we see that the evapotranspiration causes the mean travel time to lie between that predicted by the mean infiltration and recharge rates.

The ratio Λ is shown in Figure 3.7. For small γ, the effects of ET are minor, as the soil water storage is not large enough (compared to the average storm depth), for the antecedent soil water conditions to have a significant control. In humid systems ($\phi < 1$), the effects are also small, and become insensitive to variations in larger values of γ. In these cases, the potential for water to be removed by evapotranspiration between storms is generally less than the size of the storm events, and so most (but not all) storms bring the soil profile to field capacity and initiate drainage. In more arid systems though ($\phi > 1$) the system can dry out between storms. The accumulated infiltration from a closely spaced run of multiple storms is required to initiate drainage. For larger values of γ, the total depth of infiltration required increases, and so Λ (and μ_T/μ_{T0} and σ_T/σ_{T0}) increase with γ.

We can visualize the effect of evapotranspiration on the travel time by plotting contours of the mean and coefficient of variation (CV) of the travel times, normalized so that they are functions of only γ and ϕ: that is $\lambda_p\mu_T/R = \gamma\Lambda$ and $\sigma_T/\mu_T/\sqrt{R} = 2\Lambda/\gamma$ (Figure 3.8). The normalized mean increases with γ, and with the effect of Λ shown in Figure 3.7. In humid climates the relative variability of the travel time decreases with larger γ. When γ is less than ≈ 1 (shallow soils or large storms) the value of $\lambda_p\mu_T/R$ is also less than 1, indicating that average travel times are less than R/λ_p, which is R times the average time between storms. These cases are dominated by the flushing events (which have travel times of zero). Under humid climates the effects of Λ is small, and so the travel time is mainly a function of γ. Under dry climates Λ, and therefore the travel time, becomes very large, for instance reaching $> 10^7$ for $\gamma = 100$ and $\phi = 3$. The variability also increases greatly. In these cases recharge is simply so rare that solutes remain in the soil for very long periods, and their travel time is determined by (highly variable in time) rare events.

A front moving at the average leaching rate will have a delivery ratio given by $\mu = \exp(-k_d\mu_T)$. The expression for the mean delivery ratio given in Equation 3.21 reduces to this when $k_d/\lambda_d \ll 1$, that is when degradation rates are slow compared with the leaching rate. However, when degradation rates are large

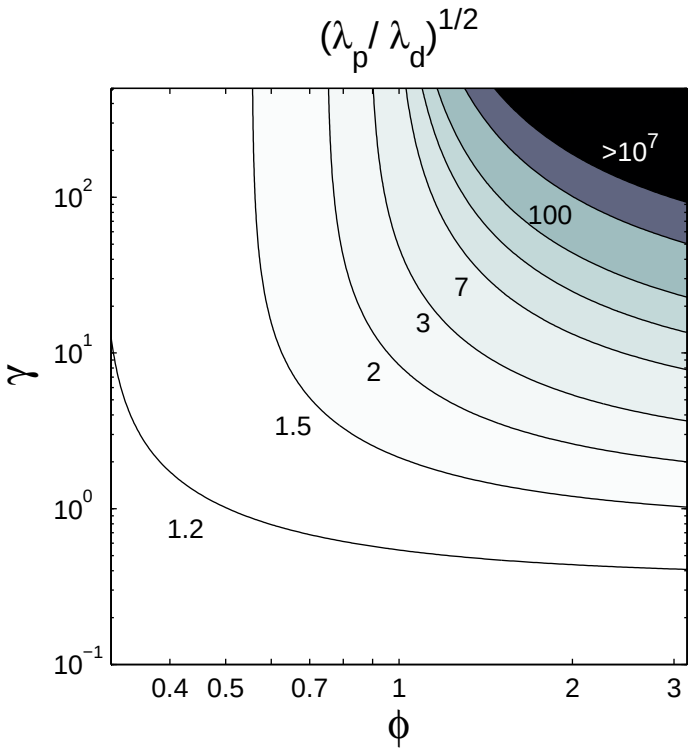

Figure 3.7: Contours of the ratio $\Lambda = \sqrt{\lambda_p/\lambda_d}$ as a function of the soil ratio γ and the aridity index ϕ. This ratio controls the increase in travel time due to the effect of evapotranspiration.

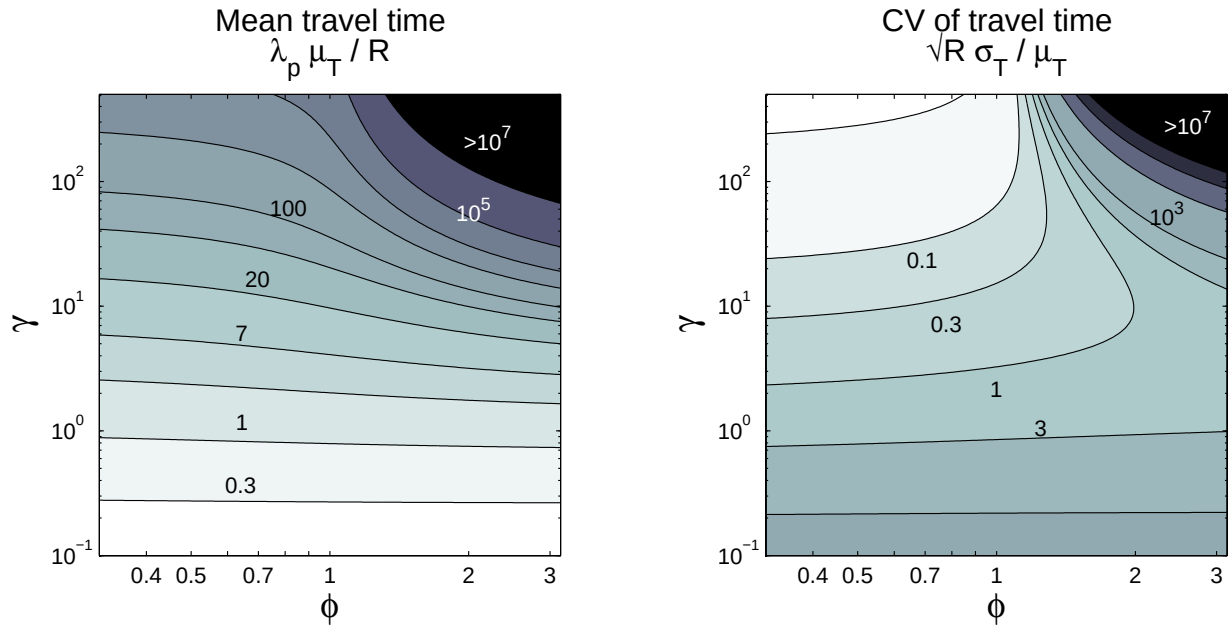

Figure 3.8: Contours of the normalized mean and CV of the arrival time distributions as a function of γ and ϕ. Darker colors represent larger values.

$k_d/\lambda_d \gg 1$, the mean delivery ratio is given by $\mu = \exp(R\gamma)$, which is simply the probability that an rainfall event will "flush" the vadose zone, and carry the solute from the surface to the base in a single event. This critical ratio can also be written as $k_d/\lambda_d = \kappa\Lambda^2$.

We can see this dependence in a contour plot of the mean and variance (as functions of ϕ and γ, Equation 3.21) of the delivery ratio for fixed values of κ and R (Figure 3.10 and 3.9). When κ is 1 (top row in each figure), indicating a degradation rate similar to the rate of storm interarrivals, the delivery ratio is small and there is low sensitivity to ϕ. In these cases κ will always be larger than 1, and so the delivery ratio is close to zero except for those times where there is an event that flushes the whole soil column. Therefore the average delivery ratio depends primarily on γ, since this parameter controls the frequency of the flushing events. The variance is greatest for those values of γ where the mean is changing most rapidly with respect to γ, which is around 1 for $R = 1$ and around 3 for $R = 3$.

When κ is small (bottom row in each figure), the product $\kappa\Lambda^2$ can be less than 1 provided Λ is not too large. Consequently the delivery ratio tends to be larger, and more strongly dependent on the climate. In these cases the ability of evapotranspiration to effectively slow down the transport of a solute through the vadose zone (and thus increase μ_T) becomes important. For a value of γ around 10, the delivery ratio at a humid site (say $\phi = 0.3$) will be around 90% on average, while at an arid site ($\phi = 3$) it will be close to 0%. The variance tends to be smaller for small κ than for $\kappa = 1$, but is also greatest for the regions where the

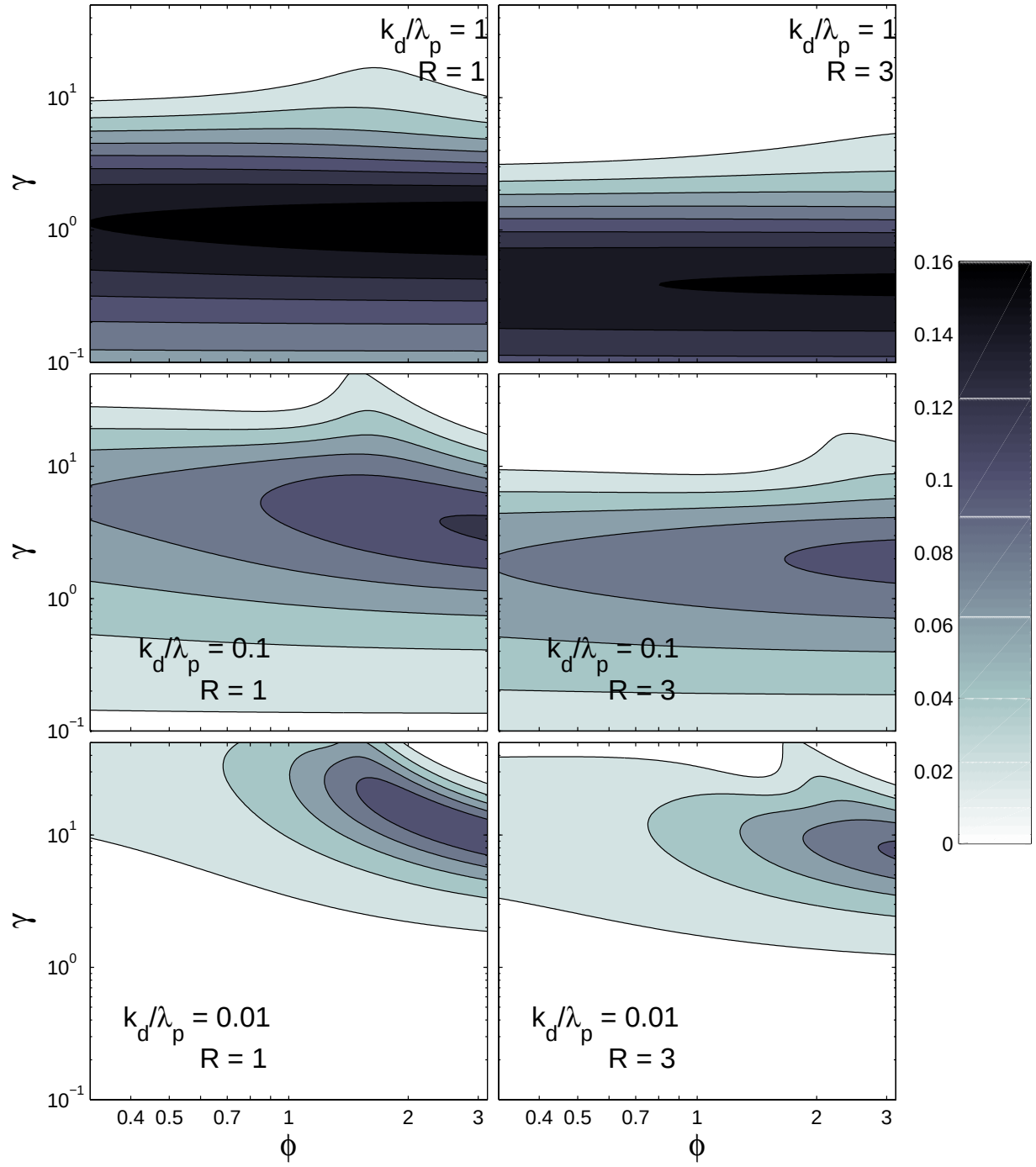

Figure 3.9: Contours of the variance of delivery ratio as a function of ϕ and γ for various values of the retardation coefficient R and normalized decay rate κ.

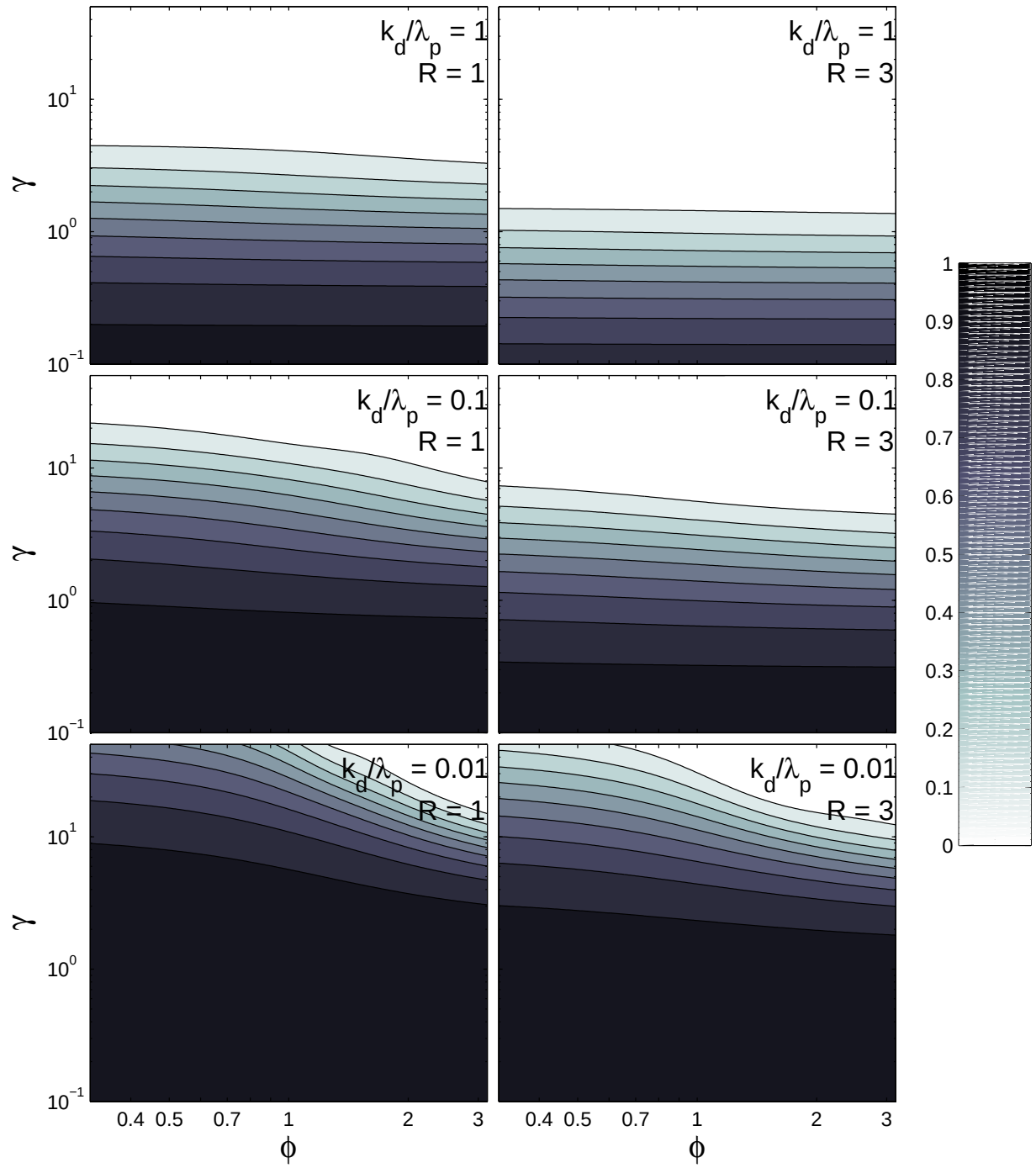

Figure 3.10: Contours of mean delivery ratio $< M/M_0 >$ as a function of ϕ and γ for various values of the retardation coefficient R and normalized decay rate κ.

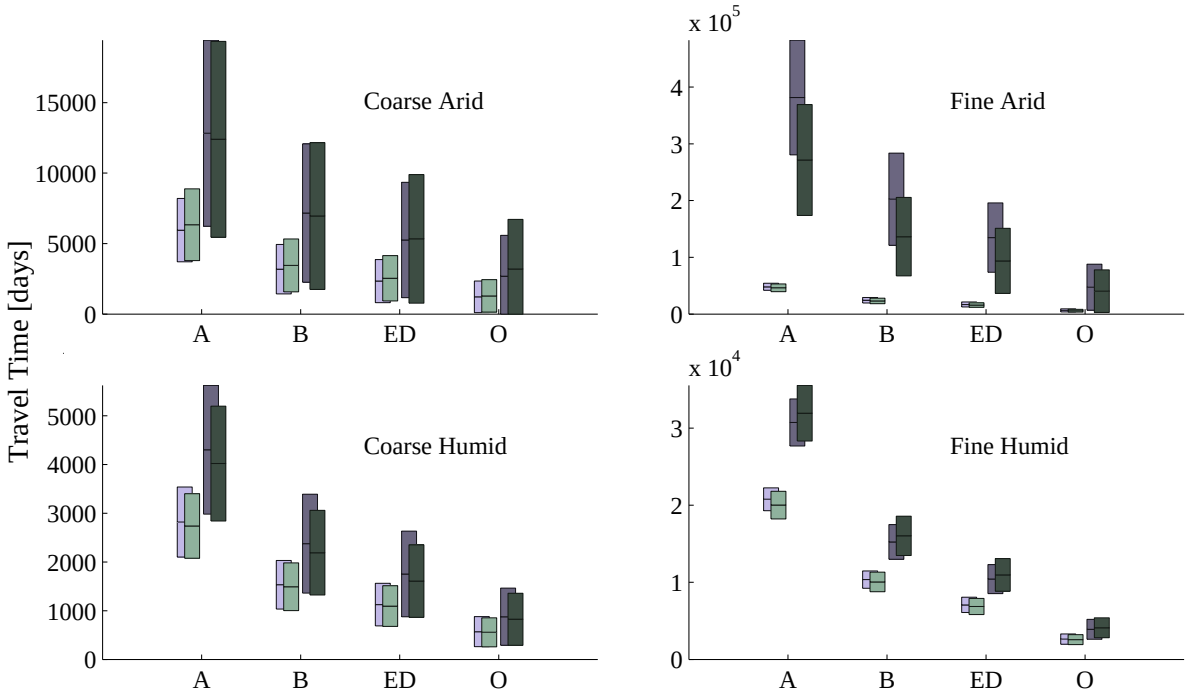

Figure 3.11: Each darker pair of bars in the figure above gives the mean (center of the bar) and standard deviation (length of the bar) of the travel time (in days) predicted by the numerical model (background bar in each pair) and its analytical approximation (foreground bar), Equation 3.19, for various pesticides under the four example scenarios. Ligher bars show the mean and standard deviation when the effects of evapotranspiration are neglected (lighter pair of bars, back bar is numerical result, front bar is analytical approximation).

mean in changing rapidly with γ. It tends to increase with ϕ.

3.3.2 Classification of realistic scenarios

The framework presented here is useful for interpreting and classifying the different controls on travel times and help us to better understand the scenarios presented in Section 2.2.3. Table 3.3.2 shows the value of various dimensionless numbers calculated from the parameters of the example scenarios. Figures 3.11 and 3.12 show the mean and standard deviation of the transit time and delivery ratio for the example scenarios calculated both numerically and with the analytical solutions.

We can classify these scenarios based on whether the mean delivery ratio is primarily controlled by the mean travel time (when $\kappa\Lambda^2 < 0.5$), or by the flushing events (when $\kappa\Lambda^2 > 2$) or by a combination of both $0.5 < \kappa\Lambda^2 < 2$ (the choice of 0.5 and 2 is somewhat arbitrary). We will refer to these as *mean-time limited*, *fast-time limited* and *co-limited* cases respectively.

The slow degrading compounds B and ED tend to be mean-time limited, apart from B in the fine, dry case which is co-limited. In contrast, oxamyl tends to be fast-time or co-limited due its rapid degradation

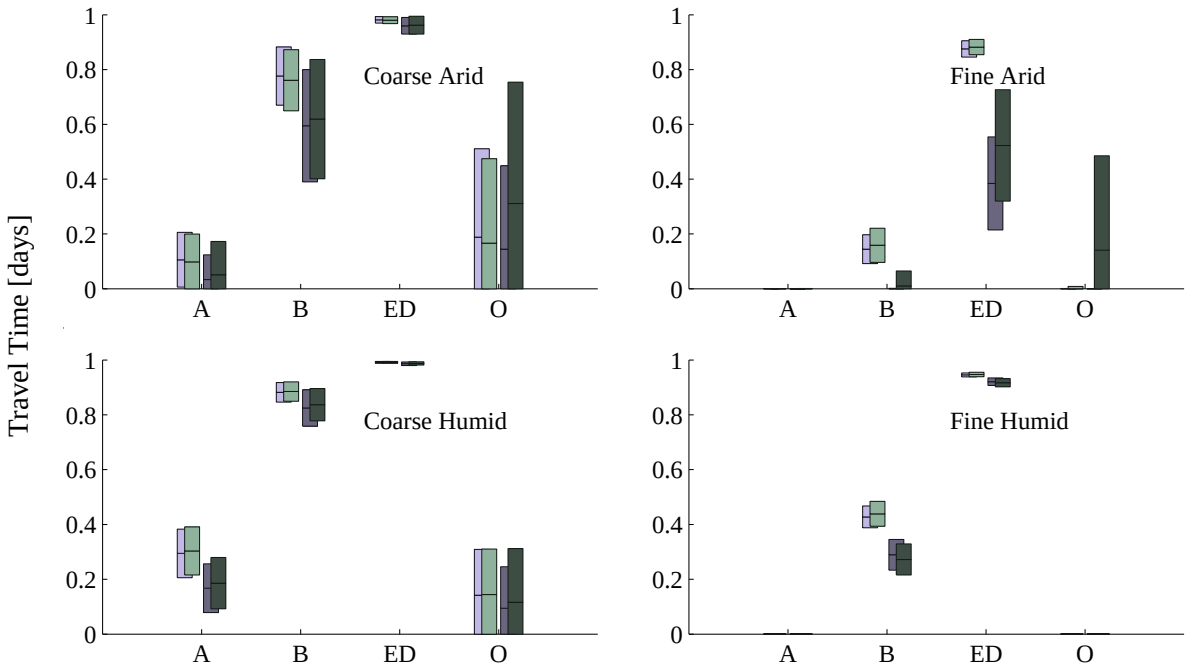

Figure 3.12: Mean (center of the bar) and standard deviation (length of the bar) of the delivery ratio predicted by the numerical model (lower bar in each pair) and its analytical approximation, Equation 3.21, (upper bar) for the example scenarios. Ligher bars show the mean and standard deviation when the effects of evapotranspiration are neglected (lighter pair of bars, lower bar is numerical result, upper bar is analytical approximation).

				Atrazine				Bromacil				Ethylene Dibromide				Oxamyl			
	ϕ	γ	Λ	$\kappa\Lambda^2$	$R\gamma$	$k\mu_T$	$k\mu_{T0}$	$\kappa\Lambda^2$	$R\gamma$	$k\mu_T$	$k\mu_{T0}$	$\kappa\Lambda^2$	$R\gamma$	$k\mu_T$	$k\mu_{T0}$	$\kappa\Lambda^2$	$R\gamma$	$k\mu_T$	$k\mu_{T0}$
Coarse Humid	0.65	5.9	1.5	0.078	34	1.8	*1.2*	0.014	19	0.18	*0.12*	0.001	14	0.013	*0.009*	0.83	7.000	3.9	*2.7*
Coarse Arid	2.5	2.1	2.0	0.88	12	5.6	*2.9*	0.16	6.8	0.56	*0.28*	0.015	5	0.039	*0.02*	9.4	2.5	12	*6.2*
Fine Humid	0.65	24	1.6	0.092	250	14	*9.0*	0.017	130	1.3	*0.83*	0.002	86	0.087	*0.054*	0.98	32	20	*12*
Fine Arid	2.5	8.6	5.9	7.9	91	120	*21*	1.4	46	11	*1.9*	0.14	31	0.74	*0.13*	84	12	170	*29*

Table 3.1: Dimensionless numbers characterizing the hydrologic and solute transport behavior of four soil/climate combinations and four common pesticides. The first two, ϕ and γ represent the aridity index, the storage capacity of the soil relative to the average storm, respectively. Λ is a function of the water balance (see Section 3.3). $\kappa\Lambda^2$ determines whether the transport through the soil is dominated by the mean travel time or large, rare events. $R\gamma$ is a measure of the number of storms required to transport the solute through the soil. The products $k\mu_T$ and $k\mu_{T0}$ are the Damkŏhler numbers for the cases with and without evapotranspiration.

rate. Atrazine exhibits all three classes of behavior depending on climate and soil type. Mean-time limitation is more common in the humid climate. In the dry climate the coarse soil tends to produce more mean-limited behavior, and the fine soil more fast-limited behavior.

The actual delivery ratios that occur in these scenarios depend on the transit time and/or flushing probability. The numerical model predicts mean transit times varying from 35 day for weakly sorbing oxamyl in the coarse, humid case, to 52 years for atrazine in the fine soil, dry climate case. The difference from the case with no evapotranspiration is a factor of about 1.5 in the first case to more than 10 in the second. The latter case has a large degree of variability, in the order of 3.8 years, though in relative terms this is less than 10% of the mean travel time. The largest relative variability occurs for oxamyl in the coarse dry case, where the relatively small value of $R\gamma$ (2.5) means that flushing events are relatively common (about 8% of storms). The large value of $\kappa\Lambda^2$ (9.4) also suggests that these events control the expected delivery ratio.

3.4 Conclusions

In this work we have used a range of modeling approaches to gain insight into the control of evapotranspiration on the travel time and delivery of reactive solutes through the vadose zone. The numerical model developed in the previous chapter was combined with stochastic soil water models to derive semi-analytic expressions for the PDF of solute travel time and delivery ratio. These expressions were found to predict the results of the piston-displacement model very well.

The resulting expressions were used to obtain the following insights:

1. The results suggest that the mean and variance of the travel time are increased by the action of evapotranspiration in a way that is related to the water balance of the soil profile. In particular, the mean travel time was found to be determined by the geometric mean of the time-averaged infiltration at the top of the soil profile and recharge rates at the base. This effect could be expressed as a function of a dimensionless ratio Λ.

2. The distribution of the delivery ratio was found to be dependent on Λ and a second dimensionless number κ. For small values of κ the delivery ratio is mean-time dependent: the mean delivery ratio approaches that predicted by the mean travel time. However for large values of κ the delivery ratio is affected by the probability of a single large event carrying the solute all the way through the system. For such fast-time dependent solutes these relatively rare events may be the primary mechanism for transport to groundwater systems.

3. The results were used to classify the controls on the delivery of 4 common pesticides applied to 4 soil-climate combinations. Under the humid climate, the slower degrading compounds atrazine, bromacil and ethylene dibromide were found to be mean-time dependent. Under dry climates their behavior was mixed or even fast-time dependent depending on the soil type. Under dry climates the fast degrading oxamyl was fast-time dependent, but under a humid climate it was mixed.

The results of this work could be used to better understand the risk of pesticide leaching, and the controls on it, though the methods are not limited to pesticides. It can also be used to assess the risks posed by climate change, which may alter the frequency of storm events, their magnitude, or the evapotranspiration, or all of these. An increase in total storm depth with little increase in total precipitation would correspond to a decrease in γ. The results here suggest that this could lead to an increase in the delivery ratio in a dry area, but may have less significance in a wet area.

Our focus in this chapter are systems without significant preferential flow, and in which infiltration produces fairly uniform wetting fronts. However, the approach can be potentially modified to consider such effects.

3.5 Acknowledgments

Work on this chapter commenced during the Summer Institute organized at the University of British Columbia (UBC) during June-July 2009 as part of the NSF-funded Hydrologic Synthesis project, "Water Cycle Dynamics in a Changing Environment: Advancing Hydrologic Science through Synthesis" (NSF Grant EAR-0636043, M. Sivapalan, PI). The work was completed with support from NSF grant EAR09-11205 "Biotic alteration of soil hydrologic properties and feedback with vegetation dynamics in water limited ecosystems" (PI: Sivapalan). The work was conducted in collaboration with Suresh Rao, Nandita Basu, Gavan Mcgrath, Praveen Kumar, and Murugesu Sivapalan. Thanks also to Al Valocchi and Stefano Zanardo for their fruitful discussions of these ideas.

Chapter 4

A subordinated kinematic wave equation for heavy-tailed flow responses from heterogeneous hillslopes

[1]*Analytical expressions of hillslope-scale subsurface stormflow discharge are currently restricted to hillslopes with homogeneous or mildly heterogeneous conductivity fields. In steep, straight hillslopes with uniform recharge these exhibit a classical piston flow response, which arises from an assemblage of impulses all moving at a constant velocity but with different starting locations. Heterogeneity within a hillslope soil creates variations in the down-slope velocity of these impulses, which may lead to non-piston flow responses with either exponential or heavy (power-law) tails. The presence of heavy tails suggests that heterogeneity imparts a temporal memory on the motion of the impulses. Using this assumption, a subordinated kinematic wave equation is proposed for moderately to highly heterogeneous hillslopes. This equation convolves the piston response from a homogenous hillslope with a stable subordinator. The stable subordinator randomizes the time that impulses spend in motion and produces non-piston solutions with heavy tails. Through comparisons of synthetic data generated from numerical hillslope simulations with physically realistic parameters, this equation faithfully reproduces both early and late time characteristics of heavy-tailed flow responses from moderate to highly heterogenous hillslopes. A systematic evaluation of hillslope responses under different degrees of heterogeneity revealed a quantitative link between the statistical properties of the heterogeneous random fields and the parameters of the subordination framework. This suggests that the subordinator can be parameterized with the physical measurement of hillslope properties.*

4.1 Introduction

4.1.1 The closure problem

Modeling the flow of water through natural landscapes is necessary for accurate hydrologic prediction, as well as prediction of fluxes of pollutants, nutrients, pathogens and sediments. However, the heterogeneity present in these landscapes makes these predictions very difficult. It is practically infeasible to fully characterize the heterogeneity of the landscape properties at a sufficiently small scale to be commensurate with the well-known physical theories that describe hydrologic fluxes, such as Darcy's Law (*McDonnell et al.*, 2007). A key challenge for advancing hydrology therefore is developing 'closure relations' (*Reggiani et al.*, 1999, 2000) – descriptions of hydrologic fluxes at some integral scale (such as a hillslope) in terms of parameters that are physically meaningful at those scales. These closure relations must then account for the effects of the spatial heterogeneity on the fluxes without the need to resolve the flows at smaller (sub-hillslope) scales explicitly

[1]An edited version of this work has been published as: Harman, C J, D M Reeves, B Baeumer, and M Sivapalan, 2010, A subordinated kinematic wave equation for heavy-tailed flow responses from heterogeneous hillslopes. *Journal of Geophysical Research - Earth Surface* 115, F00A08, doi:10.1029/2009JF001273.

(*Sivapalan*, 2005b; *Beven*, 2006).

One such hydrologic flux is subsurface saturated lateral flow through hillslopes. This class of subsurface flow is typically characterized as occurring in steep terrain, where highly permeable surface soils are underlain by relatively impermeable bedrock or other aquitard. Recharge from the unsaturated zone reaches this layer and flows in a saturated layer under the influence of topographic and hydraulic gradients.

Mathematical formulations describing this flow at the scale of the hillslope have been developed for the case of no heterogeneity based on upscaling the point-scale laws that are assumed to describe the flux (*Beven*, 1981; *Brutsaert*, 1994; *Berne et al.*, 2005; *Paniconi et al.*, 2003; *Troch et al.*, 2004, 2003, 2002). These models might be called 'zero-dimensional' since they predict behavior at the scale of the whole hillslope, and do not require that a differential equation be solved numerically to obtain the internal dynamics of the hillslope. Early work by *Beven* (1981) investigated the behavior for the restricted case of steep slopes and small saturated thickness where the topographic gradients dominate the flow. In these cases the solution behaves as a kinematic wave, in which flow velocity is everywhere proportional to the base gradient, and hydraulic gradients are relatively minor. This produces a piston-flow-like discharge response at the base of the hillslope. The later work of *Brutsaert* (1994) and others considered a wider range of circumstances, including more complex hillslope geometry. However, in all these cases the hydraulic properties of the soils are assumed to be uniform.

Presently, there are few similar 'zero-dimensional' hillslope-scale analytical models that account for the effect of spatial heterogeneity on transient hillslope-scale responses to recharge. In general, the large fluctuations in local water potential and flux associated with transient unconfined flow over a sloping base make it difficult to apply standard stochastic groundwater approaches. A perturbation type approach was adopted by *Dogrul et al.* (1998) to derive ensemble-average partial differential equations (PDEs) from the one-dimensional form of the modified Boussinesq equation, but found that these equations poorly represented the late-time water table profiles produced by flow simulations with relatively mild heterogeneous hydraulic conductivity fields ($\sigma_{LogK} \leq 1.2$). Subsequent work by Kavvas and colleagues has led to the development of the Watershed Environmental Hydrology (WEHY) model (*Kavvas et al.*, 2004; *Chen et al.*, 2004), which implements an upscaled conservation equation of two-dimensional, unconfined subsurface flow to account for random changes in hydraulic conductivity. Most recently, *Cayar and Kavvas* (2008) developed a mixed Eulerian-Lagrangian-Fokker-Planck equation based on the traditional Boussinesq equation to describe one-dimensional, unconfined subsurface flow through heterogeneous media. This approach was not applied to the case of a sloping base.

4.1.2 Effects of heterogeneity on hillslope-scale hydrologic response

Soils properties can vary a great deal over a range of scales, including the scale of a hillslope. For instance, *Mallants et al.* (1996) found that the saturated hydraulic conductivity of a well-drained colluvial subsoil in Belgium varied by up to 897% along a 31m transect. Recently, *Harman* (2007a) (see also *Harman and Sivapalan* (2009b,c)) used a numerical model to study flow through heterogeneous hillslopes and found that the presence of heterogeneity produced response curves that fundamentally differ from those with uniform properties. Consequently, descriptions of the hillslope-scale response to recharge based on descriptions of flow through uniform hillslopes (such as the use of 'effective' parameters) have been found to be unlikely to give good predictions in cases with significant heterogeneity. *El-kadi and Brutsaert* (1985) used a simple numerical model to investigate whether an effective K value could be found that would reproduce the behavior of a modeled heterogeneous hillslope, but found (as *Dagan* (1982) did for the confined case) that the 'effective' value was not constant over time. *Binley et al.* (1989) obtained effective values of K for certain cases of simulated flow through heterogeneous hillslopes, but found that they varied between storm events, and were unable to find any relation between the effective values and the moments of the spatial distributions of K. *Fiori and Russo* (2007) used a full 3-D Richards equation solver to investigate the hillslope subsurface flow response and concluded that discharge from heterogeneous hillslopes is more sensitive to temporal variability in recharge inputs than homogeneous hillslopes due to the role of preferential pathways in transmitting recharge impulses.

In the modeling study of *Harman and Sivapalan* (2009c), the responses in relatively steep hillslopes ranged from classical piston flow in homogeneous soils, to non-piston responses characterized by either exponential or heavy-tailed flow recessions in heterogeneous soils. *Harman and Sivapalan* (2009c) suggested that the heterogeneous hillslope response could be explained by deviations in the velocity of flow above and below the constant velocity of the uniform case. It is well understood that the randomization of a parameter of a probability distribution (or in this case, the randomization of the velocity controlling the arrival time at the hillslope base) can give rise to distributions that do not resemble the parent distribution (e.g. *Ganti et al.*, 2009; *Stark et al.*, 2009; *Hill et al.*, 2010). This provides an intuitive (if not completely rigorous) explanation for the exponential and heavy-tailed responses observed by *Harman and Sivapalan* (2009c). For example, consider a piston-like respose of a hillslope to an impulse of recharge (i.e. an instantaneous unit hydrograph, or IUH) given by:

$$IUH(t) = \frac{H(t) - H(t - L/V)}{L/V} \tag{4.1}$$

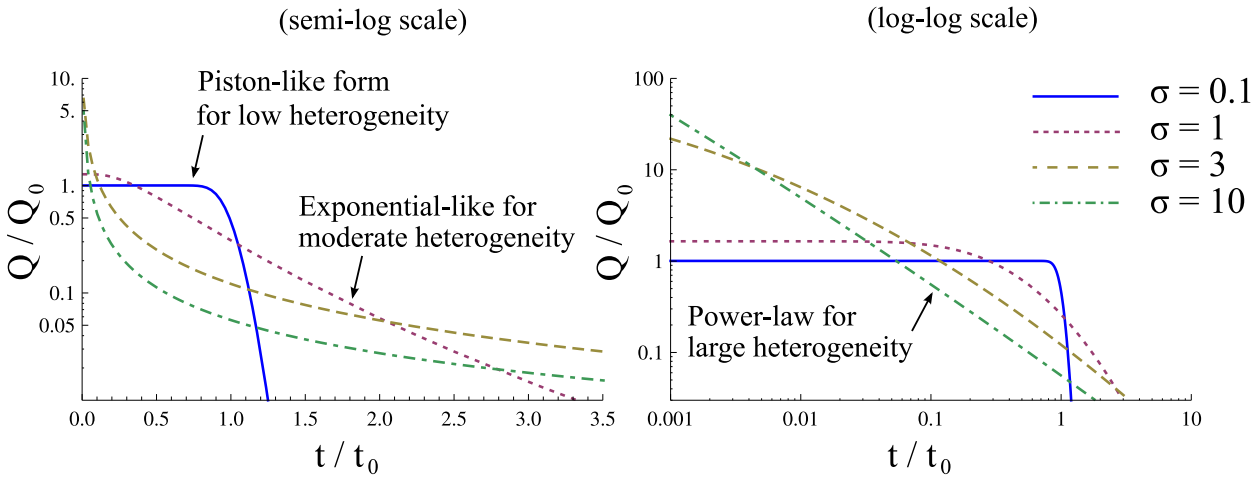

Figure 4.1: Impulse response obtained by randomizing the velocity of a piston according to a log-normal distribution with various σ parameters. This approximates the subsurface discharge response of a hillslope comprised of strips (from ridge to base) of diffferent soil materials. Though unrealistic, it demonstrates how the same underlying kinematic-wave like behaviour can produce piston-like, exponential-like and power-law-like behavior, depending on the degree of spatial variability.

where $H()$ is the Heaviside step-function, L is the hillslope length, and V is the kinematic wave velocity. If the velocity V is randomized according to a log-normal distribution $f(V;\mu,\sigma)$ (as is typically found for the spatial variability of hydraulic conductivity) with parameters $\mu = \log V_0$ and σ, the resulting IUH becomes:

$$IUH(t) = \int_0^\infty f(V;\mu,\sigma)\frac{H(t) - H(t - L/V)}{L/V}dV \tag{4.2}$$

$$= \frac{V_0}{2L}e^{\frac{\sigma^2}{2}}\text{Erfc}\left(\frac{\log\left(\frac{tV_0}{L}\right) + \sigma^2}{\sqrt{2}\sigma}\right) \tag{4.3}$$

where Erfc() is the complementary error function. Figure 4.1 shows the form of this response for a variety of values of σ, representing different degrees of heterogeneity. This clearly shows that for small σ the piston-like response is preserved. For moderate σ the response becomes exponential, while for large heterogeneity, it becomes a power-law. Field studies of flow from hillslopes mostly report exponentially-tailed recessions (*Whipkey*, 1966, 1967; *Dunne*, 1978) suggesting perhaps that the degree of heterogeneity required to produce heavy tails is not common, or that such heterogeneous hillslopes are not selected for field studies.

Although illustrative, this simple mixing of distributions is inadequate to describe the behavior of heavy-tailed recessions, since it effectively assumes that the response is composed of an ensemble of pistons operating in parallel, each with a different characteristic velocity. In reality, an impulse of water moving through a heterogeneous hillslope will encounter a series of high and low conductivity areas which act as a series of time

filters to the arrival of impulses at the base of a hillslope. Thus, the distribution of impulse arrivals is an integrated response that reflects the sum of waiting times applied to impulses traveling through a multitude of velocity zones. Heavy-tailed flow recessions imply heavily-tailed distributions of waiting times applied to individual impulses. The sum of independent and identically distributed (*iid*) heavy-tailed quantities (i.e., waiting times) converge in the limit to a Lévy-stable probability distribution (*Feller*, 1971; *Meerschaert et al.*, 2001), which exhibit heavy tails. This rationale for heavy-tailed behavior has recently been used by *Ganti et al.* (2009), *Ganti et al.* (in press), *Hill et al.* (2010) and *Stark et al.* (2009) in the context of sediment transport.

This work describes the development of an analytical framework built upon this heavy-tailed time filtering that faithfully reproduces both the early- and late-time characteristics of heavy-tailed flow responses from heterogeneous hillslopes. Through the use of a mathematical technique termed *subordination*, the arrival of flow impulses at the base of a hillslope is randomized by replacing clock time with 'operational time', i.e. the time a flow impulse spends in motion. This process accounts for varying degrees of heterogeneity by incorporating, in the scaling limit, a heavy-tailed probability density of operational times with recharge impulses whose motion in linear (unsubordinated) time is governed by a kinematic wave equation.

A subordinated kinematic wave approach offers hope both as a closure relation for this flux, and as a template for the further development of closure relations of other fluxes. In this work we test this proposed method against numerical hillslope simulations of flow through random fields with various degrees of heterogeneity and several correlation length scales. This paper describes the theoretical development, parameterization and application of a subordinated kinematic wave equation to synthetic hillslope data. A quantitative link between the statistical properties of the heterogeneous random fields and the subordination framework is established through a systematic evaluation of flow responses given various degrees of heterogeneity.

4.2 Theoretical development

To demonstrate the potential utility of the time subordination approach, we restrict our attention to the particular phenomenon of subsurface lateral flow over an impermeable base. In particular, we assume that the slope of this base is sufficiently steep that the topographic gradient is the dominant driver of flow. This allows us to ignore certain non-linearities in the flow (as discussed below), and base the theory on the kinematic wave equation proposed by *Beven* (1981), a simplified form of the modified Boussinesq equation. We will also make the assumption that recharge is uniform over the hillslope. In future work we hope to be

able to relax some of these assumptions and broaden the framework.

The solution of the kinematic wave equation for a uniform, rectangular hillslope is a piston-like flow of impulse arrivals at the base of a hillslope. This condition simplifies application of the subordination approach, as a continuum of operational times can be assigned to individual impulses that would otherwise move at a constant velocity. Details of the kinematic wave equation, its applicability to steep hillslopes and subordination are provided below.

4.2.1 Kinematic wave equation

The Boussinesq description of lateral subsurface flow is based on a form of Darcy's law vertically integrated over the saturated zone, under the assumption that flow is primarily oriented parallel to an impervious hillslope base. Continuity in the saturated zone requires that:

$$\phi_d \frac{\partial h}{\partial t} = r - \nabla(\vec{q}) \tag{4.4}$$

where $h = h(x, y, t)$ is the thickness of the aquifer at a point given by co-ordinates (x, y) defined in the plane of the sloping base, at time t; ϕ_d is the drainable porosity and $r = r(x, y, t)$ is the recharge rate. The components of the flux $\vec{q} = \vec{q}(x, y, t)$ in the i direction are given by:

$$q_i = -K_i h \left(\frac{dh}{dx_i} \cos\theta_i - \sin\theta_i \right) \tag{4.5}$$

which is a function of the hydraulic conductivity K_i, water table gradient dh/dx_i, and angle of depression θ_i in the i direction. Note that equation (4.4) is a modified form of the traditional Boussinesq equation which is purely diffusional and does not include a convective term.

The resulting equation is a non-linear PDE due to the multiplication of the h and dh/dx terms in the expression for the flux. However, conditions have been described under which this non-linearity can be ignored, most recently by *Harman and Sivapalan* (2009b). The dh/dx term describes the component of the potential gradient driving flow given by the gradient of the aquifer thickness. When the ratio of the mean aquifer thickness $\bar{h}$ and the product of hillslope length L and slope $\tan\theta$ is small:

$$\bar{\eta} = \frac{\bar{h}}{L \tan\theta} \ll 1 \tag{4.6}$$

the potential gradient driving the flux is dominated by the topographic gradient. The expression for flux in the downslope direction in a straight, uniform hillslope (with i subscripts dropped, since flow is only

downslope), then reduces to:

$$q = Kh\sin\theta \tag{4.7}$$

and the PDE is then linear. We can re-write this in terms of the velocity of an impulse moving through the hillslope v as:

$$q = vh\phi_d \tag{4.8}$$

where the velocity is defined by

$$v = \frac{K\sin\theta}{\phi_d}. \tag{4.9}$$

Considering only 1-D flow down the hillslope, the conservation equation for flow can then be written as:

$$\frac{\partial h}{\partial t} = -v\frac{\partial h}{\partial x} + \frac{r}{\phi_d}. \tag{4.10}$$

Beven (1981) used this approximation to derive an expression for the response of a sufficiently steep rectangular hillslope (with uniform conductivity) to an impulse of recharge applied uniformly across the hillslope. The discharge per unit depth of recharge is given by:

$$IUH_0(t) = \begin{cases} \dfrac{K\sin\theta}{L} & \text{for } 0 < t < \dfrac{L}{v} \\ 0 & \text{otherwise} \end{cases}. \tag{4.11}$$

Because the system is linear, this result is the impulse response function (or unit hydrograph), and the output of the system for an arbitrary timeseries of (spatially uniform) recharge inputs $r(t)$ can be obtained by convolving the unit hydrograph, equation (4.11), with the input:

$$\begin{aligned} Q_0(t) =& \int_{-\infty}^{\infty} r(\tau) IUH_0(t-\tau)d\tau \\ =& r(t) \star IUH_0(t) \end{aligned} \tag{4.12}$$

where the $\star$ represents the convolution operator. A build-up of storage in low-conductivity areas within heterogeneous hillslopes can create large gradients in the aquifer thickness, violating the assumption that these gradients have a negligible influence on flow. However, *Harman and Sivapalan* (2009c) demonstrated that these gradients do not have a significant effect on the flow when the condition in equation (4.6) is met. If we can assume that the behavior is still linear, it should be possible to find a new unit hydrograph for a heterogeneous conductivity field IUH_K that allows us to obtain the discharge result for arbitrary input in

the same manner as for the uniform K field:

$$Q_K(t) = r(t) \star IUH_K(t). \tag{4.13}$$

We test this assumption using synethetic data generated from a numerical model that solves the full Boussinesq equation (equations 4.4, 4.5). The model is run first for an impulse of recharge to produce a 'unit hydrograph', and then for a hypothetical time-variable recharge event of 24 hours duration. By convolving the unit hydrograph with the recharge event, it should be possible to obtain a similar discharge timeseries as the numerical model if the hillslope is behaving linearly, and a different response if the linearity assumption is not valid.

4.2.2 Subordination of the kinematic wave equation

The kinematic wave equation (equation 4.7) provides a basis for the development of an analytical framework for modeling flow through heterogeneous hillslopes. According to equation 4.7, the flux q [L/t] at the base of a hillslope for an instantaneous and evenly distributed recharge impulse of magnitude R for a hillslope of length L is a piston of magnitude Rv/L with duration L/v (Figure 4.2). The piston flow response arises from a collection of flow impulses at the hillslope base, where the impulses all move at the same velocity but have different starting locations. The arrival time of an individual impulse t_i with a travel distance of $L - x_i$, where x_i is the initial location and values of x increases in the direction of flow, is equal to $\frac{L-x_i}{v}$ (Figure 4.2). The study by *Harman* (2007a) demonstrates that the motion of impulses within heterogeneous hillslopes is not subject to a constant or equivalent velocity. Rather, impulses are subject to a wide range of velocities as they migrate through a hillslope, and flow responses of heterogeneous hillslopes signify an assemblage of both fast and slow arrival times. As a consequence, the flow behavior of heterogeneous hillslopes clearly violates the equivalent velocity assumption of a piston. By randomizing the time the impulses spend in motion, and consequently arrival times t_i of impulses at the base of a hillslope via subordination, we broaden the applicability of equation 4.7 which was previously limited to only the least heterogeneous hillslopes.

Subordination is a standard tool in the theory of Markov and Lévy processes (e.g. *Baeumer and Meerschaert*, 2007; *Bertoin*, 1996; *Bochner*, 1949; *Feller*, 1971; *Meerschaert and Scheffler*, 2004, 2008; *Sato*, 1999). The process of subordination refers to the replacement of linear time with operational time (e.g. *Baeumer and Meerschaert*, 2007; *Meerschaert and Scheffler*, 2004, 2008). In our work, operational time refers to the random amount of time that a flow impulse 'operates' or participates in the motion process. Other earth science applications of subordination include transport of sediment particles in river systems (*Ganti et al.*, in press) and transport of solutes through heterogeneous aquifers subject to differential advec-

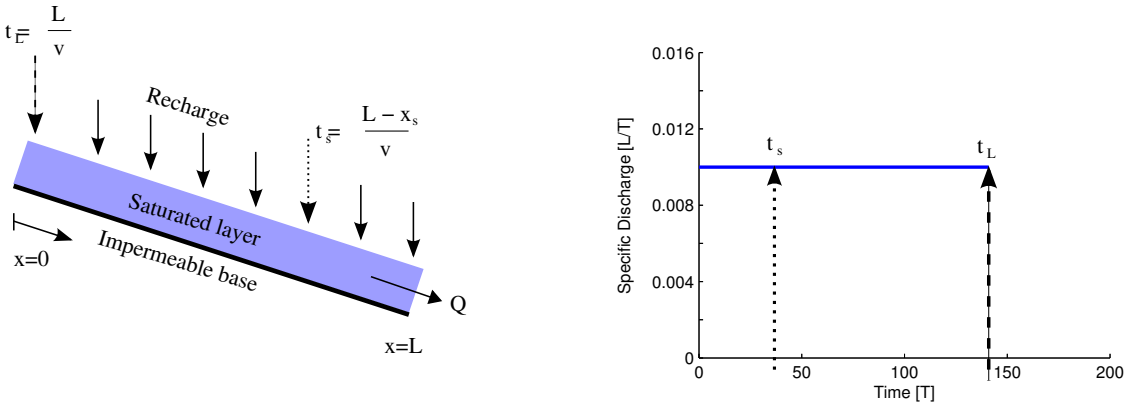

Figure 4.2: Schematic depicting how recharge impulses distributed along a hillslope (left) with constant velocity produce a piston flow response at the base of a hillslope (right), where the magnitude of the piston is Rv/L with duration L/v. An impulse at an arbitrarily initial location x_s has an arrival time t_s of $(L-x_s)/v$.

tion (*Baeumer et al.*, 2001) or retention in immobile zones (e.g. *Baeumer and Meerschaert*, 2007; *Benson and Meerschaert*, 2009; *Schumer et al.*, 2003).

We focus our application on hillslope flow responses with heavy-tails (i.e., exhibit a linear decay of flux over time on a log-log plot). The heavy-tails imply that the heterogeneity within a hillslope soil exerts a strong time influence on the motion of flow impulses; i.e. the time between motions is heavy tailed. However, it is well known that the classical advection-diffusion equation fails to take into account the heavy-tails in the waiting times or the velocities of transport (e.g. see *Benson et al.*, 2000, 2001, among many others). It has been specifically shown that the governing equation for the transport with a heavy-tailed distribution with a power-law decay in the tails of waiting times and/or transport distances can be recast into a fractional advection-dispersion equation (e.g. *Meerschaert et al.*, 1999; *Meerschaert and Scheffler*, 2001; *Schumer et al.*, 2003). Specifically, it has been shown that heavy-tails in waiting times can be taken into account by time fractional derivatives and heavy-tails in travel distances by space-fractional derivatives (e.g. *Benson et al.*, 2001; *Ganti et al.*, 2009; *Schumer et al.*, 2003, 2009). In the above case we focus our attention on heavy-tailed waiting times and in the scaling limit these motions (without recharge) satisfy the fractional-in-time differential equation:

$$\frac{\partial^\gamma H}{\partial t^\gamma} = -\frac{v \partial H}{s \partial x} \tag{4.14}$$

where the fractional time derivative of order γ and scale factor s (with units of $[\mathrm{t}^{\gamma-1}]$) describe an inverse stable distribution of waiting times between impulse motion. Note that the selection of a stable subordinator is motivated by mathematical limit theorems that describe the convergence of the sum of *iid* heavy-tailed random variables to a Lévy-stable density [*Meerschaert and Scheffler*, 2001]. In order to incorporate recharge $r(x,t)$ which modifies $\partial h/\partial t$, equation (4.14) needs to be recast (differentiating $(1-\gamma)$ times both sides in

t) to expose a first order temporal derivative on the left hand side (*Baeumer et al.*, 2005):

$$\frac{\partial}{\partial t}H(x,t) = -\frac{\partial^{1-\gamma}}{\partial t^{1-\gamma}}\frac{v\partial}{s\partial x}H(x,t) + \frac{r(x,t)}{\phi_d}. \tag{4.15}$$

Note that equation (4.15) is a generalized form of equation (4.10). Equations (4.10) and (4.15) are equivalent for the special case of $\gamma = 1$ and $s = 1$ which describes piston flow through a homogenous hillslope. The function H is given by:

$$H(x,t) = \frac{r}{\phi_d} \star \int_0^\infty h(x,u)p(u,t)\,du \tag{4.16}$$

where h is the piston flow solution to an impulse, and $p(u,t)$ is an inverse stable density of index gamma; i.e.

$$p(u,t) = \frac{t}{s^{1/\gamma}\gamma u^{1+1/\gamma}} g_\gamma\left(\frac{t}{(su)^{1/\gamma}}\right), \tag{4.17}$$

where g_γ is a standard stable density ($\int_0^\infty e^{-\lambda t} g_\gamma(t)\,dt = \exp(-\lambda^\gamma)$). Our approach essentially randomizes the response for a homogenous hillslope Q_0, equation (4.11), with a heavy-tailed subordinator to generate unit responses for heterogeneous hillslopes Q_K (equation (4.13)).

We can find the discharge (flux) F at a point x by looking at the rate of change of total mass to the right of x:

$$F(t,x) = \frac{\partial}{\partial t}\int_x^\infty H(\xi,t)\,d\xi = \frac{r}{\phi_d} \star \int_0^\infty \frac{1}{(su)^{1/\gamma}} g_\gamma\left(\frac{t}{(su)^{1/\gamma}}\right) \frac{\partial}{\partial u}\int_x^\infty h(\xi,u)\,d\xi\,du. \tag{4.18}$$

To model the flux of impulses at the base of a hillslope the following steps are required. First, an instantaneous recharge flux f_0 is distributed evenly for all x along a hillslope of length L according to:

$$f_0(x) = \frac{R}{L}\Phi(L-x)\Phi(x) \tag{4.19}$$

where R is total recharge applied to the entire hillslope, and $\Phi(\cdot)$ is the Heaviside step function. Then $r(x,t) = \delta(t)f_0(x)$. As $h(x,t) = \delta(x-vt)$, we obtain:

$$\begin{aligned} \frac{r}{\phi_d} \star \frac{\partial}{\partial u}\int_x^\infty h(\xi,u)\,d\xi =& r \star \frac{\partial}{\partial u}\Phi(vu-x) = r \star v\delta(vu-x) \\ =& v f_0(vu). \end{aligned} \tag{4.20}$$

Hence equation (4.18) becomes:

$$\begin{aligned} F(t,L) &= \int_0^{(L/v)} \frac{Rv}{L\phi_d} g_\gamma \left(\frac{t}{(su)^{1/\gamma}} \right) (su)^{-1/\gamma} \, du \\ &= \int_0^{s(L/v)} \frac{Rv/s}{L\phi_d} g_\gamma \left(\frac{t}{u^{1/\gamma}} \right) u^{-1/\gamma} \, du \end{aligned} \tag{4.21}$$

where an $x = L$ substitution describes the flux of recharge impulses at the base of the hillslope and v/s is an effective velocity used in calibration to the numerical data. Dividing this by the size of the original impulse gives the dimensionless unit hydrograph (equation 4.13):

$$IUH_K(t) = \frac{F(t,L)}{R} = \int_0^{s(L/v)} \frac{v/s}{L\phi_d} g_\gamma \left(\frac{t}{u^{1/\gamma}} \right) u^{-1/\gamma} \, du. \tag{4.22}$$

Parameters γ and s will depend on the properties of the hillslope, though analytical expressions for this relationship have not been derived at this time. Solutions to the subordinated kinematic wave equation (equation 4.21) for a wide range of γ are shown in Figure 4.3. Values of γ describe the tail index of a $\gamma-$stable subordinator used to regulate the times that the piston impulses participate in the motion process. As values of γ decrease, more probability mass is shifted to the tail of the subordinator and the likelihood of extreme events increases. This translates into shorter amounts of time that the recharge impulses actively spend in motion, greater impulse arrival times at the hillslope base, and greater deviations from the homogeneous piston flow response (Figure 4.3). If heterogeneity imparts a temporal memory on the motion of recharge impulses in hillslopes, then increases in the heterogeneity should be linked to decreases in γ.

The mass of the initial piston impulse is conserved by equation (4.21) for all parameter values. The subordinated solution at early time has a decay rate of $-1 + \gamma$. Once the piston impulse is depleted, the decay of the subordinated solutions is more rapid (i.e., steeper slope) and transitions to $-1 - \gamma$. Transition times between the two slopes depend on values of both γ and s. For example, the transition time for $\gamma = 0.9$ when $s = 1$ is close to the duration of the classical piston (γ=1) (Figure 4.3). Lower values of γ temporally spread the mass of the piston, and slope transitions are not observed in Figure 4.3 when $\gamma \leq 0.3$.

Calibration of the analytical solutions to data is facilitated by changing values of s to apply a temporal scale to the velocity of the piston input. This temporal scale changes the velocity of the piston, thereby changing the magnitude and duration of the piston input (Figure 4.3). The quotient of v and s can be viewed as an overall or 'effective' velocity, where $s > 1$ and $s < 1$ represent lower and greater velocities than originally assigned to the piston, respectively (Figure 4.3). If $s = 1$, the original piston velocity and effective velocity are equal. This method of varying s allows us to efficiently calibrate the subordinated solution to

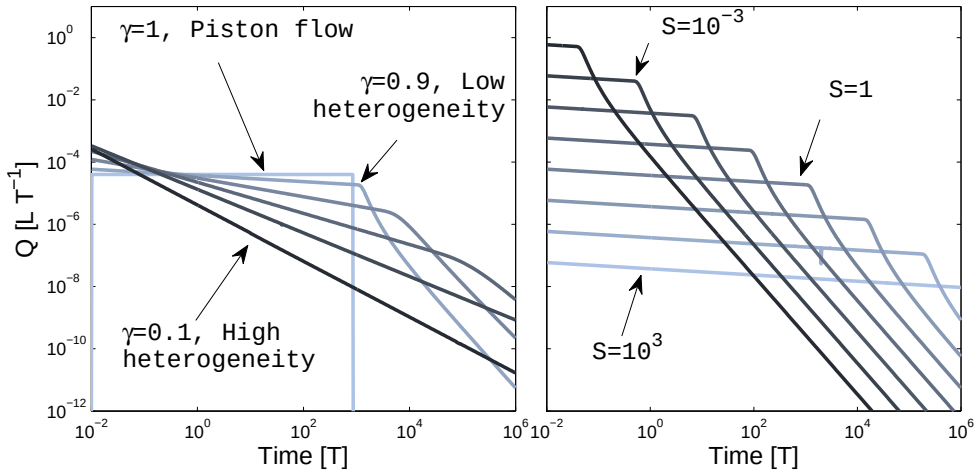

Figure 4.3: Kinematic wave solutions for (left) values of γ ranging from 0.1 (highly heterogeneous) to 1 (homogenous, classic piston) with s held constant at 1 and (right) for values of s ranging from 10^{-4} to 10^{3} with γ held constant at 0.9. The subordinated solution at early time has a slope equal to $-1+\gamma$ under the influence of the piston impulse and transitions to a slope of $-1-\gamma$ after depletion of the piston impulse input. Times of transition between the two slopes are directly related to s and inversely related to γ.

the numerical data without changing the piston parameters directly. Since the hydraulic conductivity fields are random and all other hillslope parameters are held equal, the use of s is equivalent to dividing the mean piston K value (and hence v) by s.

4.3 Numerical simulations of hillslope flow

Numerical simulations of hillslope flow are used to provide synthetic data for three purposes: (1) to verify that the linearity of the kinematic wave condition that is known to hold when the conductivity field is uniform also holds for variable conductivity fields; (2) to determine whether the subordination approach can be used to simulate the effect of heterogeneous conductivity fields on the impulse-response of a hillslope; and (3) to determine whether the fitted impulse response can be used as an instantaneous unit hydrograph (IUH) to reproduce the discharge from a hillslope subject to a realistic recharge event.

The response of hillslopes to impulses and time-variable recharge events were generated using the model described in *Harman and Sivapalan* (2009b) and *Harman and Sivapalan* (2009c). This model solves the full Boussinesq equation (4.4 and 4.5) on a 64×64 square grid using a finite volume scheme with adaptive timestepping. The simulated hillslope used for most of the simulations measured 100m×100m and had a constant slope of 0.1m/m, with a zero flux boundary condition at the upper boundary, periodic boundary conditions on the left and right (i.e. flux out of one side enters the other side, and gradients are calculated as

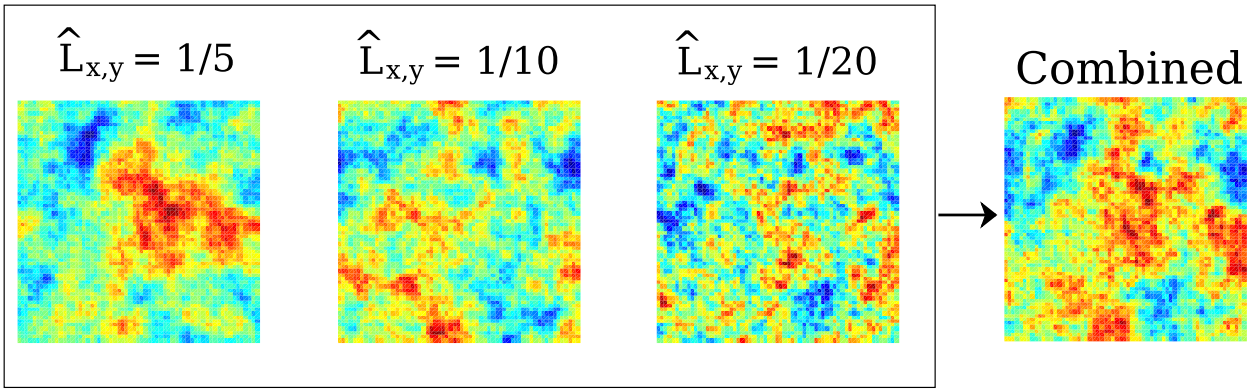

Figure 4.4: Examples of random K fields with $\sigma_{LogK} = 5$ given correlation length scales (relative to the domain size) of 1/20, 1/10 and 1/5. The 'Combined' case was computed by averaging the three previous fields, thereby containing multiple correlation lengths.

though indentical hillslopes lay side-by-side), and a kinematic boundary condition at the base (i.e., constant potential gradient). The soil drainable porosity was set at 0.34 and the mean log conductivity $\langle \log K \rangle$ at 0.1m/hr. These physically realistic values were chosen for convenience, rather than to represent any particular hillslope.

The natural log of the field of conductivity values was assumed to have a Gaussian distribution. Four types of correlation structure for the log conductivity were used (Figure 4.4). Three were random exponential fields with correlation lengths (normalized by the domain size) of 1/20, 1/10, and 1/5 representing short, intermediate, and long range correlations, respectively. A fourth ('combined') case with multiple correlation lengths was constructed by averaging the values of $\log K$ from three independently generated correlation fields with correlation lengths of 1/20, 1/10, and 1/5. The incorporation of multiple correlation lengths into a single field was motivated by studies of subsurface heterogeneity that report spatial variations in K on a multitude of scales (e.g. *Neuman and Federico*, 2003, and references therein). Though studies of subsurface heterogeneity within hillslope soils are limited, *Kirchner et al.* (2001) reported a characteristic dispersion length scale for the Plynlimon catchment that approached the entire length of the hillslope. This finding suggests, since the dispersion length scale is directly influenced by the length scale of variability of the hydraulic conductivity field, that the Plynlimon hillslope soils exhibit spatial variability in K at all scales up to the length of the entire hillslope. Note that the averaging of the three fields was performed on the Gaussian random variables before exponentiating. Three degrees of variability in $\log K$ were used initially: $\sigma_{\log K} = 1$, 5, and 10. A fourth value of $\sigma_{\log K} = 3$ was added later exclusively for the combined correlation length case.

For the impulse responses, 100 realizations of each type of heterogeneity field were simulated. The hillslopes were initialized with a uniform 34mm of drainable water (or a saturated thickness of 100mm) at

time zero and allowed to drain with no further input. This corresponds to a dimensionless thickness of $\bar{\eta} = 0.01$, making the flow strongly controlled by the topographic gradient, and in the kinematic range of dynamics (*Harman and Sivapalan*, 2009b). Simulated discharge was calculated at logarithmically spaced points in time ranging from 1 second to several years (though due to computational constraints in the $\sigma_{\log K} = 10$ case not all 100 runs completed the full duration). The ensemble geometric mean and standard deviation was calculated at each point in time.

The discharge response to a time-variable recharge event was calculated using 100 random field realizations with $\sigma_{\log K} = 5$ and a multiple correlation length structure. The storage in this case at time $t = 0$ was set to zero, and recharge was then applied uniformly over the whole grid from time zero. The same hourly time series of recharge was used in each simulation, generated initially by multiplying a Gaussian bell-curve by a set of 24 uniformly distributed random numbers. Recharge over each 1 hour period was assumed to be constant. Output, consisting of discharge at the base of the hillslope and storage within the random field, was generated and recorded at 1 minute time steps.

4.4 Results

The numerical simulations were used to generate flow responses for heterogenous hillslopes subject to single and multiple impulse events. The simulated hillslope responses serve as synthetic data to test the assumption of linearity in hillslope response, and to ascertain the suitability of, and any potential limitations pertaining to, the use of a subordinated kinematic wave equation for heterogeneous hillslopes. The simulation of flow through hillslopes with a wide range of heterogeneity and correlation structure allows us to systematically investigate flow responses and parameterize equation (4.21).

4.4.1 Linearity of hillslope response

The impulse responses for each realization of the conductivity field were numerically convolved with the time-variable recharge event at a 1 minute time step, and the result compared with the numerically modeled response to the recharge event. The results for six typical realizations of the conductivity fields with $\sigma_{\log K} = 5$ and the combined correlation lengths are shown in Figure 4.5. In every case there is excellent correspondence between the hydrograph predicted by the full non-linear Boussinesq model and that predicted by the convolution of the input with the impulse response. This correspondence would not be possible if non-linear interactions were significant. We can therefore be confident that the assumption of linearity used in the subordinated piston approach is appropriate for hillslopes with $\bar{\eta} \ll 1$.

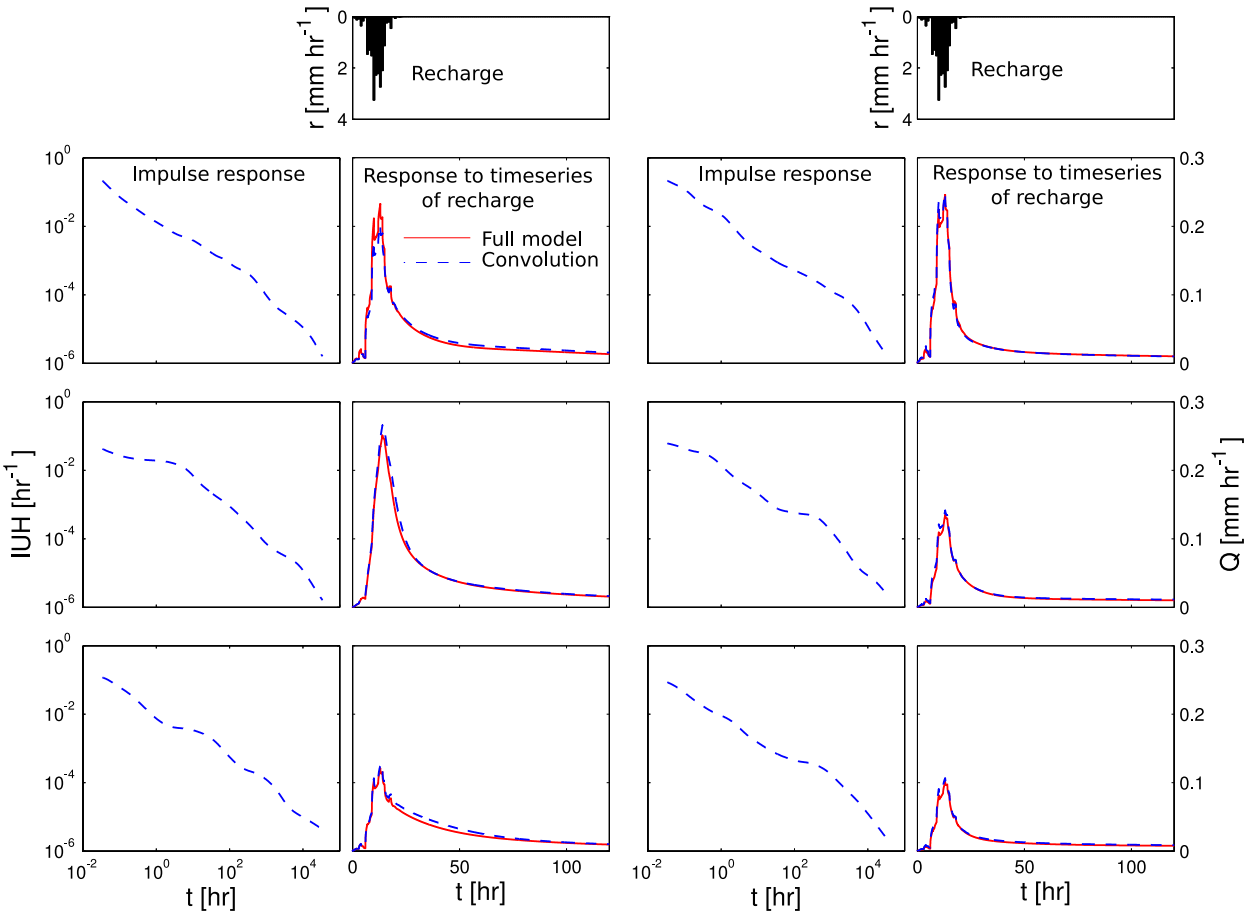

Figure 4.5: Evidence for the approximate linearity of the subsurface flow response described by the Boussinesq equation in highly heterogeneous conductivity fields. The left plot of each pair shows the impulse response, and the right shows the response to a arbitrary input predicted by the full Boussinesq model (solid line) and predicted by convolving the impulse response with the (dashed line) recharge input. Details given in the text.

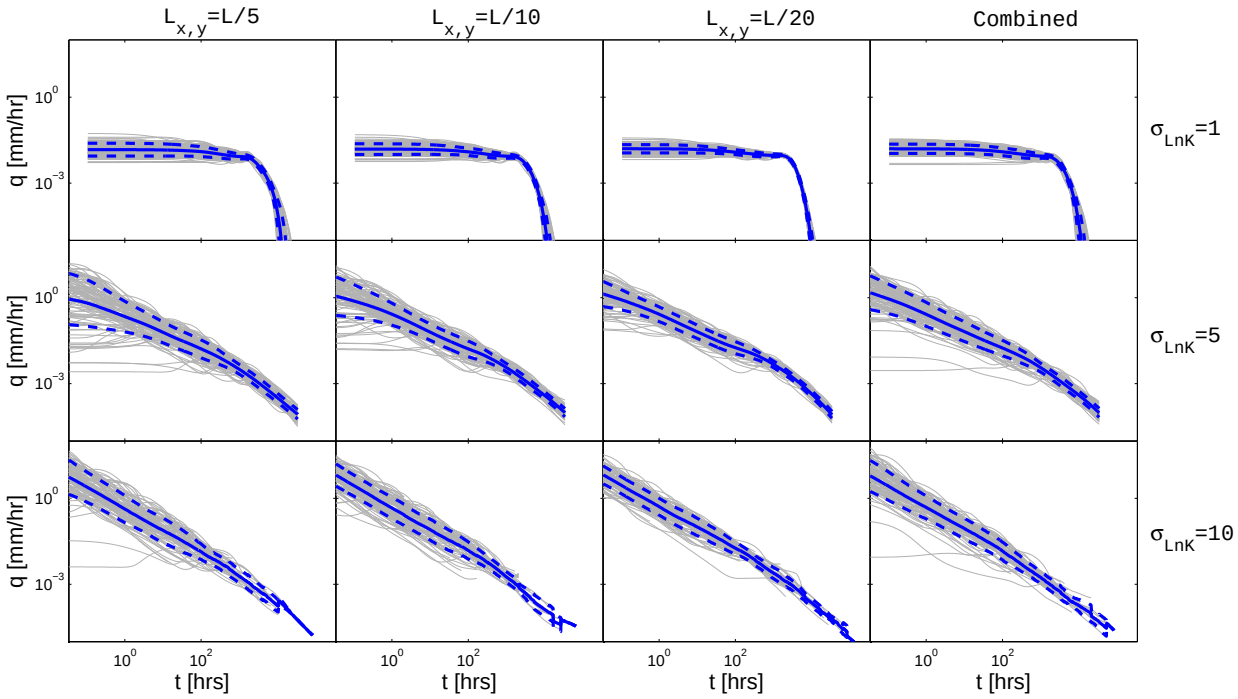

Figure 4.6: Discharge results with time for (top to bottom) $\sigma_{LogK} = 1$, 5, and 10 and (left to right) $\hat{L}_K = 1/5$, 1/10, 1/20 and the combined case. Solid line is the log mean, and dashed lines are ± 1 standard deviation of the log transformed values.

4.4.2 Single impulse response

The single impulse data describe the hillslope response to a single, instantaneous impulse of 34mm applied at $t = 0$, and provide the foundation for our assessment and parameterization of a subordinated kinematic wave equation. Discharge at the hillslope base for all 100 realizations for the initial σ_{LogK} and correlation structures are shown shown in Figure 4.6. We display our results on a logarithmic scale because of the orders of magnitude in simulation time and our interest in heavy-tails.

The mean impulse response is insensitive to the correlation length regardless of σ_{LogK} values. This is clearly evident when the ensemble mean of all cases are plotted together (Figure 4.7). However, the variability around the mean is sensitive to correlation structure, particularly for early time (Figure 4.6). Discharge at early time varies over several orders of magnitude for $\sigma_{\log K} = 1$ for the large correlation length case ($L/5$ or 20m), but is mostly constrained to a single order of magnitude for small correlation length ($L/20$ or 5m). The combined correlation length case has a similar range of values as the large correlation length, but variability in individual realizations (as shown by the ± 1 standard deviation) is generally more tightly constrained. The distribution of log discharge has a negative skew, with more small values far from the mean than large values. Particularly low values tend to have a constant discharge for early times.

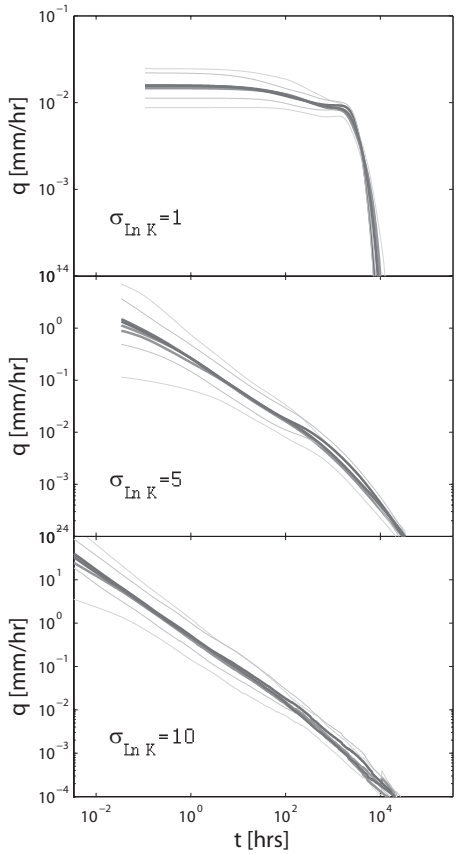

Figure 4.7: Mean discharge for (top to bottom) $\sigma_{\ln K} = 1$, 5, and 10 for each of the correlation length cases. The correlation length seems to have very little effect on the ensemble (geometric) mean discharge, but does affect the standard deviation of discharge; $\pm 1\sigma$ is plotted in light gray for correlation lengths $L/5$ and $L/20$.

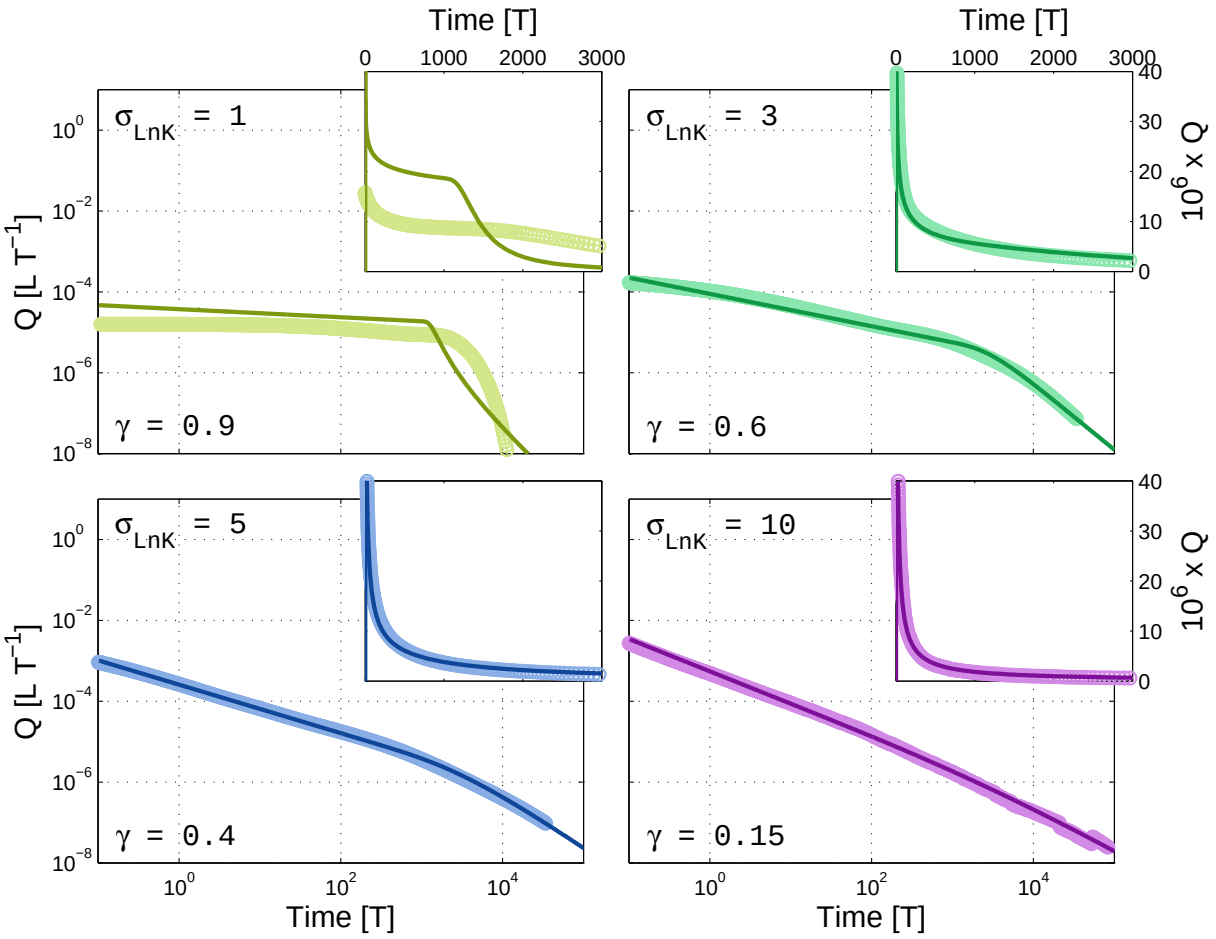

Figure 4.8: Ensemble mean discharge for σ_{LogK} values of 1, 3, 5 and 10, respectively, along with best fit subordinated wave equation, plotted on log-log axes. Note that the absence of heavy tails in the $\sigma_{LogK} = 1$ case excludes the use of the kinematic wave equation. However, its solution is provided for comparison. Insets show same data in with linear axes.

The subordinated solutions were fitted to the ensemble mean discharge of the multiple correlation structure. Mean discharge curves for all correlation structures are more or less equal (Figure 4.8) indicating that the selection of one correlation structure over the others has negligible impact on the results of our study. All best-fit parameters are based on visual inspection with the objective of matching both early- and late-time portions of the flow response (Table 4.5). The piston impulse subject to subordination is defined according to quantifiable properties of the synthetic hillslopes and the impulse including mean K, drainable porosity, slope, and impulse magnitude. These values are held constant for all cases.

Mild heterogeneity is represented by the K fields with $\sigma_{LogK} = 1$ (Figure 4.8, top left). Impulses traveling through these random fields produce near piston flow responses as expected from kinematic wave theory with

a slight exception. Rather than an instantaneous drop occurring exactly at L/v and a flux magnitude of Rv/L, the hillslope response exhibits a slightly lower, near-piston flux along with an exponential tail. Since the numerical simulations conserve mass, the slight decrease in flux from the theoretical piston is caused by the exponential tail. The absence of a power-law tail in the response produced by these fields excludes the use of a subordinated kinematic wave equation. However, a best-match kinematic hillslope equation is included for comparison (Table 4.5). As expected when comparing to an incompatible model (a subordination model with power-law tails versus simulated data with exponential tails), the fit between the subordinated solution and the mild heterogeneity case is poor.

Moderately to highly heterogeneous hillslopes with $\sigma_{LogK} \geq 3$ (Figure 4.8) exhibit heavy-tailed hillslope responses. For these cases, the match between the numerical data and subordinated solutions are excellent. Not only are the early and late time behavior well-represented, the trend of the numerical data supports the subordinated kinematic wave theory that predicts a slope transition from early time decay of $-1+\gamma$ to $-1-\gamma$ at later times once the piston impulse is depleted. The transition between the early and late time regimes represents some 'characteristic' time scale over which the subordinated solution spreads the mass of the piston. If this slope transition did not occur, mass would not be conserved in the subordinated solution. In addition to the excellent fit between the numerical data and subordinated solution, values of γ decrease with increasing heterogeneity (σ_{LogK}). As values of σ_{LogK} increase, decreases in γ are accompanied by decreases in s (Table 4.5). The implications of these observations are discussed later.

4.4.3 Event response

The subordinated kinematic wave equation proved successful for the single impulse case. The next logical step in our analysis is to evaluate subordinated solutions against an event with time-variable recharge. This is more realistic than an instantaneous impulse as storms vary in intensity and have a temporal duration. The flow response to a time-variable recharge event with a total input depth of 20mm distributed over 24 hours with a peak of 3.2mm/hr was simulated for 100 realization of spatial variability in the conductivity field. The case of $\sigma_{LogK} = 5$ was chosen due to computational speed relative to the $\sigma_{LogK} = 10$.

The subordinated solution was generated by subordinating a piston with the subordination parameters, γ and s, obtained from the single impulse, $\sigma_{LogK} = 5$ case (Table 4.5). The subordinated solution provides an excellent prediction of the geometric mean discharge from the hillslope for a recharge event (Figure 4.9). There is a slight under-prediction of the peak, but the recession behavior is very well captured. The peak modeled discharge from the ensemble of hillslopes varies from 0.3mm/hr to 0.002mm/hr, with a geometric mean of 0.096mm/hr. The subordinated solution has a mean peak discharge of 0.080mm/hr. However from

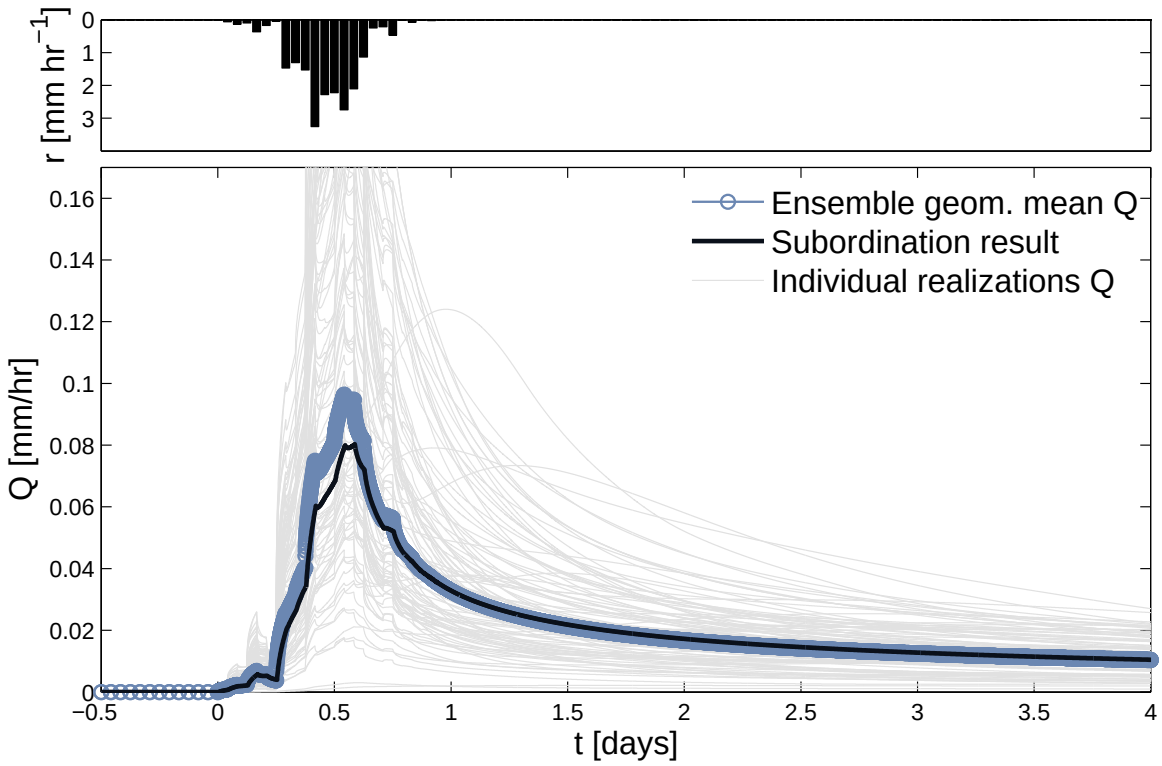

Figure 4.9: Simulated discharge from 100 generated heterogeneous hillslopes ($\sigma_{\log K} = 5$, 'combined' correlation lengths) subject to a 24 hour recharge event, and the prediction provided by the subordination approach (black line). Gray lines give individual realizations of Q, dark gray is their geometric mean. The recharge event is shown at the top.

the end of the recharge event to the end of the modeled period (5 days) the root-mean-square error (RMSE) is less than 3.2x10^{-4}mm/hr. Note that the subordinated solution used for the recharge event input is based on subordination parameters obtained from the impulse flow response with $\sigma_{LogK} = 5$, and not by fitting them to this hydrograph.

4.5 Discussion

The kinematic wave equation was successfully extended to the case of heterogeneous hillslopes through the incorporation of a stable subordinator. Solutions to this equation were found to provide excellent early and late time matches to numerical data for moderately to highly heterogeneous hillslopes ($\sigma_{LogK} \geq 3$) for both single impulse and realistic time-variable recharge event scenarios. Measurable hillslope and impulse parameters in all cases were used to define the piston, and subordinated parameters γ and s were based on matching to early and late time characteristics of the numerical flow data.

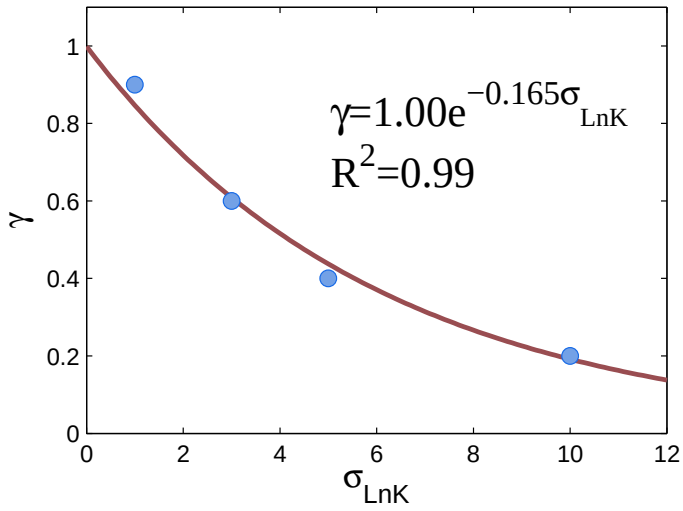

Figure 4.10: Empirical relationship between heterogeneity and tail index of the γ-stable subordinator.

Results from this study have several significant implications. First, the results suggest that a definitive correspondence exists between γ and hillslope heterogeneity. By using the standard deviation of hydraulic conductivity of the random fields as a quantitative measure of heterogeneity, the following proposed relationship:

$$\gamma = 1.00e^{-0.165\sigma_{LogK}} \tag{4.23}$$

suggests a strong ($R^2 = 0.99$) exponential correlation between these parameters (Figure 4.10). We acknowledge that this fit is only based on four data points which may overestimate the correlation. However, this relation albeit preliminary is very exciting and provides a link between heterogeneity and model parameters in a stochastic flow equation. Such links have proved elusive in fractional-derivative extensions to groundwater equations. Only a handful of theoretical contaminant transport studies have linked physical properties of porous and fractured media to the order of spatial (*Benson et al.*, 2000; *Reeves et al.*, 2008a,b) or temporal (*Zhang et al.*, 2007) derivatives in fractional advection-dispersion equations (fADEs). Derivations of fADEs have some similarity with this work as fractional-order derivatives invoke Lévy processes described by γ-stable probability densities.

Second, the predominance of heavy tails in the heterogeneous fields shows that increases in heterogeneity, while influencing early impulse arrivals and piston velocity, predominately increase time delays between impulse motion (i.e., retention). This is demonstrated by the heavy tailed decay of impulse flux simulated at the base of the hillslopes (Figure 4.8). Thus, heterogeneity exerts a strong influence on the characteristic

$\sigma_{\log K}$ [a]	γ [b]	s [c]	$\langle V \rangle$ [d]
1	0.9	1.00	0.12
3	0.6	0.30	0.4
5	0.4	0.07	1.7
10	0.2	0.02	6.0

Table 4.1: Parameters of the subordinated kinematic wave equation fitted to mean impulses responses from ensemble hillslope simulations with various degrees of heterogeneity. [a]Natural log of the standard deviation of K in the random hillslope fields. [b]Tail index of stable subordinator. [c]Temporal shift applied to piston during calibration. [d]Effective velocity $[L/t^{\gamma}]$ of subordinated solution: ratio of v and s, where $v = 0.12$ [m/hr] for all single impulse realizations.

time scale required to dissipate the mass of the piston.

Third, the numerical results suggest that correlation structure does not play a major role in the ensemble flow response, though correlation structure was found to exert minor differences in flow about the mean. An explanation for the insensitivity of correlation structure on flow response is unknown at this time. A suggested rationale is that flow impulses are predominately delayed in heterogeneous hillslopes, and these delays are observed through increases in storage within low velocity zones. If the relative proportion of low velocity zones is equal for random fields with the same value of σ_{LogK}, these fields may have similar storage characteristics regardless of correlation structure.

Finally, it should be noted that although these results are promising, their application is limited to cases where the underlying assumptions are valid. In particular, the assumption of kinematic flow will be valid only in particularly steep, conductive hillslopes. Field studies such as *Dunne* (1978), have long shown that in areas with lower gradients the mounding of the subsurface saturated layer at the hillslope base can create pressure gradients that are a significant driver of lateral flow (see also the model of *Cayar and Kavvas* (2008)). We have also assumed that the soil column is sufficiently deep to accommodate the saturated layer, and so do not make any predictions concerning the location of surface exfiltration (*Dunne et al.*, 1975; *Dunne*, 1978) which can be a significant control on surface saturation (*Ragan*, 1968; *Dunne et al.*, 1975). The assumption of a planar, uniform slope for the base does not reflect the convergent and divergent topographies often found in natural hillslopes, which play an important role in the focusing of flow and the production of surface saturation (*Dunne*, 1978; *Kavvas et al.*, 2004; *Chen et al.*, 2004). Recharge to the hillslope aquifer may not be uniform as we have assumed, and may be correlated in some way to the heterogeneity of aquifer properties, since it also must percolate through the soil medium (e.g. *Maxwell and Kollet*, 2008). Other models including the WEHY model (e.g., *Kavvas et al.*, 2004) allow for spatially-variable recharge.

4.6 Conclusions

A subordinated kinematic wave solution, where the time that flow impulses spend in motion is randomized, faithfully reproduces both the early and late time characteristics of heavy-tailed hillslope flow responses generated by numerical simulations of heterogeneous hillslopes when $\sigma_{LogK} > 1$. Thus, it provides a parameterization of the flow at the scale of the entire hillslope that accounts for the effects of heterogeneity without resolving them explicitly. This is the condition that must be met by the flux closure relations required for Representative Elementary Watershed (REW) -type models (*Reggiani et al.*, 1999, 2000). Ideally, closure relations for hydrologic fluxes will consist of parameters that are physically meaningful and measurable at the scale of the hydrologic element they are designed for. In this case we have shown that the effects of heterogeneity can be accounted for in a hillslope scale closure relationship with the introduction of a stable subordinator that requires only two additional parameters, γ and s. Our results suggest that the subordination parameters are linked to physical properties of the hillslope including mean and log standard deviation of hydraulic conductivity, drainable porosity, hillslope angle and length, and magnitude of recharge impulse. Only a single time shift parameter, representing effective velocity, is needed to calibrate or scale the numerical data to the subordinated solution. Thus, it is possible that the subordination approach offers a closure relationship for kinematic subsurface flow through heterogeneous hillslopes provided that the degree of heterogeneity present in the conductivity field is measurable. Further work is required to test the model against field data from well-studied hillslopes.

This work offers an exciting new avenue for research, particularly as it builds on existing theory developed for the case of uniform hillslopes. Recent work by *Troch et al.* (2004) and *Troch et al.* (2002) (and others) has developed analytical expressions for the unit hydrograph of subsurface flow through hillslopes with a wide range of geometries (including convergent and divergent planforms) and flow dynamics from kinematic wave to fully diffusive. An obvious extension of this work is therefore to examine whether it can be used in such circumstances. If so it could pave the way for a general theory of subsurface flow closure in heterogeneous hillslopes.

The subordination approach may also find application in modeling the vadose zone flow in certain cases. Kinematic wave theory has also been applied to model the infiltration of water into macropores (*Beven*, 2006), and is the basis of the MACRO model of preferential infiltration (*Larsbo et al.*, 2005). These models generally assume a single 'effective' celerity of flow. Perhaps a better match to observed data could be found by using a subordination approach to account for the variability of flow velocities through macropores. This is left for future work.

4.7 Acknowledgments

This work was initiated by discussions at the Working Group meeting "Stochastic Transport and Emergent Scaling on Earth's Surface" in Lake Tahoe, November, 2007. This working group was sponsored by NCED (National Center for Earth-surface Dynamics) an NSF Science and Technology Center funded under contract EAR-0120914, and the Hydrologic Synthesis Activities at the University of Illinois funded by NSF under contract EAR-0636043. The work was done in collaboration with Matt Reeves, Boris Baeumer, and Murugesu Sivapalan. Dr. Michael Church and three anonymous reviewers provided insightful comments improved the quality of this work.

Chapter 5

Power-law catchment-scale recessions arising from heterogeneous linear small-scale dynamics

[1]*Power-law recession behavior has typically been attributed to the hydraulics of subsurface flows in the landscape (e.g. the Boussinesq equation). Many catchments exhibit enormous heterogeneity in their characteristics, such as the permeability of soils, hillslope length and gradient, and soil mantle thickness. In this chapter we demonstrate using a simple linear flow model that the between-hillslope heterogeneity alone can give rise to observed apparently non-linear recession slope curves. The degree of non-linearity (represented by the exponent fitted to the recession slope curve) is shown to increase with the degree of heterogeneity of catchment hydraulic properties. In sufficiently heterogeneous catchments, the recession is also sensitive to the history of recharge events, tending to increase when the past events have built up a storage of water in the 'slow' parts of the catchment. The models based on the catchment heterogeneity were fitted to data from the Panola Mountain Research watershed, yielding a good fit, and allowing us to infer how the heterogeneity in catchment properties varies with scale. The range of exponents explained by this theory overlaps with the range explained by the hydraulics of subsurface flow, which raises doubts about our ability to extract catchment hydraulic parameters on the basis of recession curves so long as the heterogeneity is not accounted for. In general the presented here have enabled us to show how the heterogeneity of landscape characteristics is upscaled and manifested in the apparent non-linear relationship at the catchment scale.*

5.1 Introduction

5.1.1 Recession curves and catchment properties

The patterns, or 'signatures', present in hydrographs offer vital, if narrow, windows into the hydrologic functioning of catchments, but their interpretation depends on the conceptual model adopted (*Sivapalan*, 2005b). One such signature is the recession curve, which refers to the shape of the decline of measured discharge some time after the storm has ended. It has been observed that the rate of change of discharge dQ/dt during the recession at a given discharge Q is often consistent or invariant between storm events (*Brutsaert and Nieber*, 1977). This suggests that it reflects fundamental hydrologic features of the catchment in some way. The relationship $-dQ/dt = g(Q)$ has been called the 'recession slope curve' (*Rupp and Selker*, 2006b). It has often been observed that the recession slope curve follows a power-law of the form $g(Q) = aQ^b$. The exponent b and coefficient a vary from catchment to catchment (*Brutsaert and Nieber*, 1977). Observations of b range from less than 1 to larger than 3 (*Kirchner*, 2009; *Tague and Grant*, 2004; *Chapman*, 1999; *Wittenberg*, 1999). Perhaps because it is simple, easy to estimate and ubiquitous, recession

[1]An edited version of this work has been published as: Harman, C J, M Sivapalan, and P Kumar, 2009, Power law catchment-scale recessions arising from heterogeneous linear small-scale dynamics. *Water Resources Research* 45(9), W09404, doi:10.1029/2008WR007392. Copyright 2009 American Geophysical Union. Reproduced/modified by permission of American Geophysical Union. All figures, tables and data were created by Ciaran Harman unless otherwise indicated.

slope curves have had a significant influence on our understanding of catchment processes such as subsurface discharge to rivers and on the models used to encode that understanding and make predictions (*Brutsaert and Lopez*, 1998; *Szilagyi et al.*, 1998; *Shaw et al.*, 2008; *Rupp and Selker*, 2006a; *Mendoza et al.*, 2003; *Sloan*, 2000; *Manga*, 1999; *Moore*, 1997; *Tallaksen*, 1995; *Troch et al.*, 1993b; *Vogel and Kroll*, 1992; *Zecharias and Brutsaert*, 1988).

The physical origins of the recession slope curve have been subject to considerable study in order to determine whether information about catchment properties can be extracted from them. A common explanation is that they arise from the hydraulics of flow during the discharge of water from a hillslope or riparian aquifer (*Brutsaert and Nieber*, 1977; *Brutsaert*, 1994; *Rupp and Selker*, 2006b; *Brutsaert*, 1994). This explanation is based on derivations from the Boussinesq equation, which can describe saturated flow over a sloping base, and assumes that the catchment-scale behavior follows that of an 'effective hillslope' whose properties are representative (in some sense) of the properties of the collection of landforms that make up a catchment. It is well known, however, that catchment properties are highly heterogeneous, both within and between hillslopes (*Troch et al.*, 2009a). Subsurface discharge from a hillslope depends on the hydraulic and topographic gradients driving flow, soil properties, topography, temporal variability of the recharge from the unsaturated zones, the boundary condition at the base of slope and other factors (*Henderson and Wooding*, 1964; *Beven*, 1982; *Brutsaert*, 1994; *Harman and Sivapalan*, 2009b). A number of studies have investigated the role of internal heterogeneity in these properties on the subsurface discharge from hillslopes, and found that it is indeed significant (*Rupp and Selker*, 2005; *Fiori and Russo*, 2007; *Harman and Sivapalan*, 2009a). However there have been fewer studies of the effects of variability between hillslopes on the shape of the recession slope curve at the catchment scale.

In a recent study of recessions for three nested catchments in the Panola Mountain Research Watershed, *Clark et al.* (2009) showed that variability between hillslope properties was not only significant, it was likely to explain the shape of recession slope curve, and also why this shape changed with scale. They found that recession slope curves from an individual hillslope (0.1ha) had an exponent $b = 1$, suggesting that it in fact behaved as a linear reservoir. However at larger scales (10ha and 41ha) the recession slope curves became increasingly non-linear. *Clark et al.* (2009) showed that it was possible to reproduce this behavior, while maintaining some consistency in the process descriptions, using a model in which discharge from two or three linear reservoirs is summed. Each linear reservoir represented a different component of the landscape (hillslopes, ephemeral riparian aquifers, permanant stream aquifers) and each had a different characteristic timescale, and a different fractional area. *Clark et al.* (2009) found that higher observed exponent could be fitted using a broader range of timescales.

The observations of *Clark et al.* (2009) suggest that the observed b exponents could be attributed at least partly to the heterogeneity of catchment properties. However, the link between the recession exponent and the set of characteristic timescales that represent this variability is not quantified explicitly.

Also, in *Clark et al.* (2009) the empirical recession data from the catchment was fitted to modelled data representing the recession following steady-state recharge. Field estimates of the b exponent are derived from recession data following individual storms, not steady-state recharge (*Clark et al.*, 2009; *Zecharias and Brutsaert*, 1988; *Chapman*, 2003). They therefore reflect the response to recharge of a variety of durations and intensities, and a variety of initial conditions. The influence of this temporal variability on b has not been examined in the context of catchment spatial heterogeneity.

5.1.2 Aims of this work

In this work we aim to develop a general theory based on the conceptual model of *Clark et al.* (2009) that provides a quantitative link between the variability of catchment properties and the recession slope curve exponent b. We will also examine the role of the temporal variability of recharge in controlling this exponent.

We will do so by assuming that the heterogeneity of catchment properties can be captured by a probability density function (pdf) of the characteristic timescales. This simplified conceptual model allows us to develop a simple mathematical theory of discharge from heterogeneous catchments for arbitrary probability distributions. This theory can then be used to establish the connection between the shape of the recession slope curve, the properties of the probability distribution and the type of recharge variability. In particular the link between the exponent b and the coefficient of variation (CV=mean/std deviation) related to the between-hillslope heterogeneity will be examined. The approach we adopt is similar to methods in statistical mechanics known as "superstatistics" for describing the energy states of driven, spatially variable systems (*Touchette and Beck*, 2005; *Beck and Cohen*, 2003). This method essentially involves the randomization of a parameter in a probability distribution relevant to the process according to another distribution that accounts for variability in the catchment properties controlling the process. This method has been used extensively in other disciplines, such as chemical engineering, and even ecology (*Thompson and Katul*, 2008). However, it has not been used in this particular context previously.

Since we do not know what the appropriate distribution of properties is for typical catchments, common and mathematically convenient distributions will be discussed, and methods used in the literature on superstatistics will be used to obtain results for a general class of power-law-tailed distributions. We investigate the effect of temporal variability of recharge on the relationship between b and the catchment heterogeneity first by examining two end-member cases for which analytical expressions can be derived (the

recession following a single impulse, and the recession following steady-state recharge) and second examining the response to periodic recharge events.

The theory is then be tested against the recession slope curves at three catchment scales presented in *Clark et al.* (2009) from the Panola watersheds. We use this theory to examine how the variation in catchment properties varies with scale by fitting the derived expressions for the recession slope curve to the observations, under different assumptions of the mode of recharge forcing and type of distribution of timescales. We also compare the ability of catchment heterogeneity and hydraulic theory to explain the ranges of b exponents reported in literature from catchments around the world. Finally we discuss the implications for catchment modeling and analysis.

5.2 Theory

5.2.1 Linear reservoir approximation

Let us assume that the catchment recession discharge can be approximated by a collection of individual hillslopes that behave like linear reservoirs with various characteristic timescales, arranged in parallel. In a linear reservoir the discharge Q is a linear function of storage S as $Q = S/T$ or $Q = VS$. The timescale T, or alternatively $1/V$, is the characteristic timescale of the response. The observation of *Clark et al.* (2009) provides some empirical justification for this approach. It has also been shown that under certain circumstances the hydraulic theory of subsurface discharge from hillslopes and riparian aquifers does follow this relationship, and in such cases the timescale is proportional to the hillslope length L and drainable porosity ϕ_d, and inversely proportional to the slope Θ and hydraulic conductivity K (*Harman and Sivapalan*, 2009b; *Berne et al.*, 2005):

$$\frac{1}{V} \sim \frac{L\phi_d}{K \sin\Theta} \tag{5.1}$$

The variation in these properties within the catchment can be captured by treating V as a random variable with a probability density function (pdf) $f(V)$ with support $[0, \infty]$,

The impulse-response or 'instantaneous unit hydrograph' (IUH) of single linear reservoir (per unit contributing area) takes the form of an exponential distribution with a timescale $1/V$:

$$IUH_{LR}(t, V) = Ve^{-Vt} \tag{5.2}$$

The IUH function of the ensemble, $IUH(t)$ is the compound distribution of $IUH_{LR}(t, V)$ and $f(V)$ (*Ben-*

jamin and Cornell, 1970). For a finite number of reservoirs n of equal contributing area this is:

$$IUH(t) = \sum_{i=0}^{n} \frac{V_i}{n} e^{-V_i t} \tag{5.3}$$

where the values of V_i are distributed as $f(V)$. In the limit of large n this sum converges to the integral (*Benjamin and Cornell*, 1970):

$$IUH(t) = \int_0^\infty f(V) V e^{-Vt} dV \tag{5.4}$$

The formulation in equation (5.4) is similar to the 'superstatistical' description of a thermally heterogeneous (i.e. non-equilibrium) system used in statistical mechanics (*Beck and Cohen*, 2003; *Touchette and Beck*, 2005). There the integrand is $f(\beta)e^{-\beta E}$, where β is the inverse temperature of a part of the system, and E is an energy state of a particle. The result of the integration is an effective distribution of energy states of the composed system $B(E)$, whose components have mean inverse temperatures distributed as $f(\beta)$. Here the pdf $f(V)$ represents the distribution of inverse timescales, and arises due to the heterogeneity of catchment properties.

Discharge from the catchment can be found by convolving the IUH with the timeseries of recharge. If the catchment has fully drained since previous events and is subjected to a short periods of recharge, the recession will be similar to the shape of the IUH, scaled by the total recharge volume. However this will not be true if the catchment is subjected to extended recharge events, or does not drain fully between them.

5.2.2 Impulse responses

Gamma and Lognormal distributions

A closed form solution for the IUH can be found when $f(V)$ is a Gamma distribution, which takes the form:

$$f(V) = \frac{1}{V_0 \Gamma(\alpha)} e^{-\frac{V}{V_0}} \left(\frac{V}{V_0}\right)^{\alpha-1} \tag{5.5}$$

where $V_0 > 0$ and $\alpha > 0$. Figure 5.1 (left plot) shows this distribution for several values of the shape parameter α. The solution to equation (5.4) in this case is:

$$IUH(t) = \alpha V_0 (1 + tV_0)^{-1-\alpha} \tag{5.6}$$

Figure 5.1 (left plot) shows how the shape of these unit hydrographs varies with α. They take a finite value at $t = 0$ of αV_0 and then converge on a power law with exponent $-1 - \alpha$.

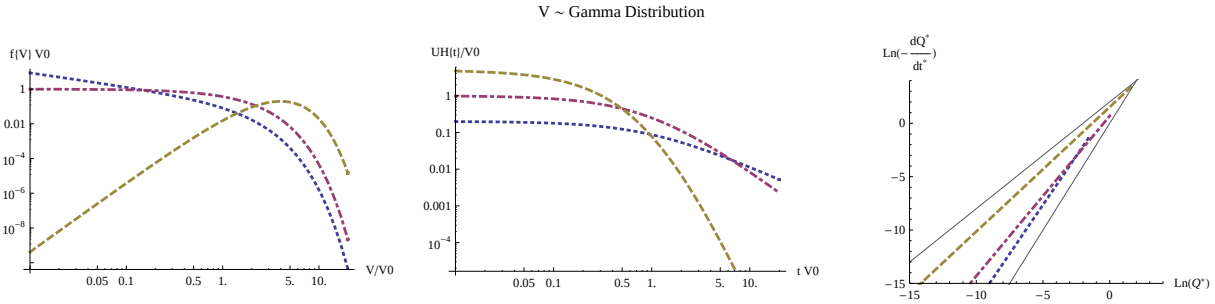

Figure 5.1: Left to right, the pdf $f(V)$, unit hydrograph $IUH(t)$ and recession slope curve $g(t)$ for the case where $f(V)$ is a Gamma distribution (equation 5.5). All axes are made dimensionless using the V_0 parameter. Values of α are 0.2 (dotted line), 1 (dash-dot), 5 (dashed line). Example power-laws with exponents 1 and 2 are plotted in gray on the right plot.

The recession slope curve following an impulse of recharge can be found by convolving the IUH (equation 5.6) with an impulse with total volume Q_0, and eliminating the time variable between the result and its derivative. This yields:

$$-\frac{dQ}{dt} = Q_0 V_0^2 \alpha(\alpha+1)\left(\frac{Q(t)}{Q_0 V_0 \alpha}\right)^{1+\frac{1}{\alpha+1}} \tag{5.7}$$

This is indeed a power-law with a slope that varies between $b = 2$ for $\alpha \to 0$ and $b = 1$ for $\alpha \to \infty$. Figure 5.1 shows the recession slope curves for several values of α. For a Gamma distribution, the coefficient of variation is given by $CV = \alpha^{-1/2}$, and so we can write an expression for the exponent b in terms of the CV as:

$$b = 1 + \frac{CV^2}{1+CV^2} \tag{5.8}$$

This simple result links the observed recession slope curve directly to the variability of the catchment characteristic timescales. It shows that in this case b is 1 for $CV = 0$ and approaches 2 as the CV increases. The variation in b with CV is shown in Figure 5.2.

Similar behavior can be observed for the Log-Normal distribution, which has often been used to describe the distribution of hydraulic conductivity values in catchments:

$$f(V) = \frac{1}{\sqrt{2\pi}V\sigma} e^{-\frac{(\log(V/V_0))^2}{2\sigma^2}} \tag{5.9}$$

Examples of this distribution for various values of σ are shown in Figure 5.3. However, a closed-form solution to the integral in equation (5.4) cannot be found with this distribution. We can plot the impulse response and recession slope curve though using equation (5.3) for large n with V_i drawn from the lognormal distribution, and examples are given in Figure 5.3. When σ is small the behavior is similar to a single linear reservoir, and the recession slope curve approaches $b = 1$. For larger σ the slope approaches $b = 2$, but does not exceed

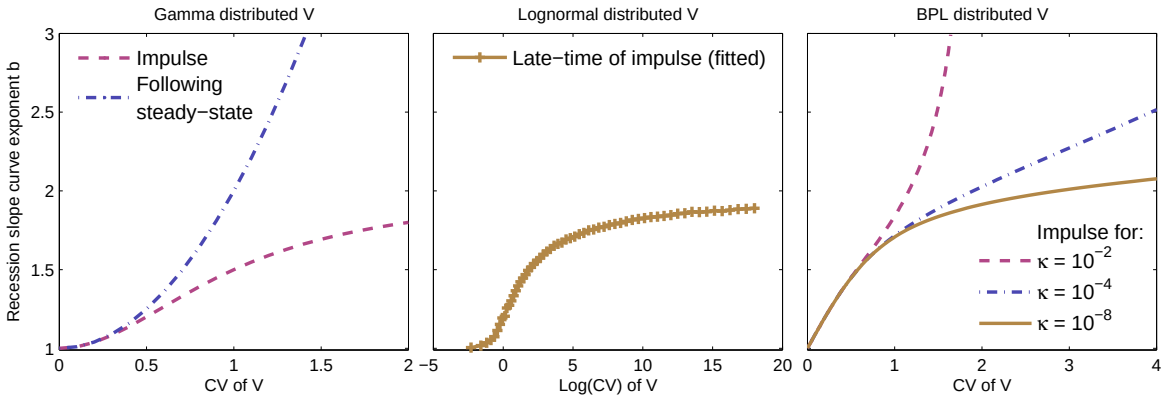

Figure 5.2: Derived relationships between variability in catchment properties and the recession slope curve exponent b. Curves are shown for the case of a Gamma distribution (left) following impulses (dashed line, equation 5.8) and following steady-state recharge (dash-dot line, equation 5.8), for a Lognormal distribution following an impulse (center, exponents estimated), and for a bounded power-law following an impulse (right, equations 5.21 and 5.25) with various values of κ.

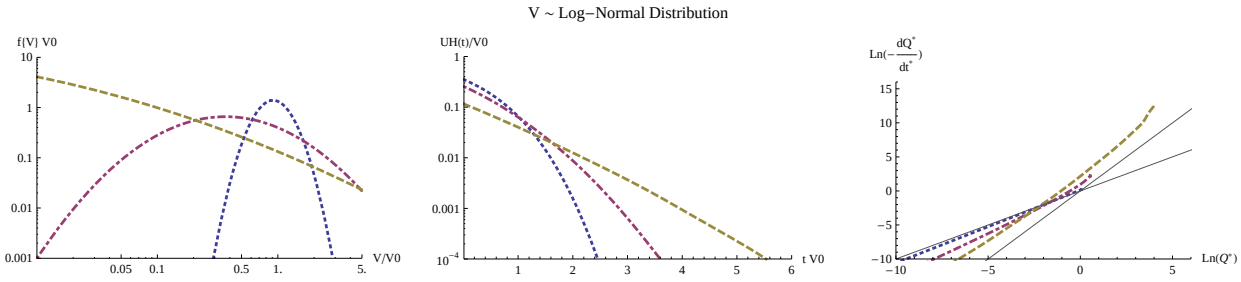

Figure 5.3: Same as Figure 5.1, but for the Lognormal distribution (equation 5.9. Values of σ are 0.3 (dotted line), 1 (dash-dot), 3 (dashed line).

$b = 2$ except for a very brief period at the start of the recession. By fitting a power-law to the late-time behavior for a range of values of the σ parameter, we can estimate the relationship between the CV and the recession slope curve exponent. The CV of a lognormal distribution is related to σ as:

$$CV = \sqrt{e^{\sigma^2} - 1} \tag{5.10}$$

The relationship between b and the CV is shown in Figure 5.2. The value of b at each CV was found to be insensitive to the value of Q_0 and V_0.

General impulse-response behavior for $f(V)$ with power-law tails

We can extend these observations to a general class of distributions of V using methods suggested by the work on superstatistics by *Touchette and Beck* (2005). That work derived expressions for the general classes

of asymptotic behavior of 'effective' Boltzmann factors, but because of the extra factor of V in equation (5.4), their results are not directly applicable here, though the methods still are.

Because the fast ($V \to \infty$) parts of the catchment will drain quickly, the discharge at late time ($t \to \infty$) will depend on the behavior of the 'slow' tail of the distribution ($V \to 0$). We can determine this behavior by noting that equation (5.4) takes the form of a Laplace integral, and using the Laplace, or 'saddle-point' approximation to estimate the value of the integral for large t (*Bender and Orszag*, 1978). We begin by rewriting equation (5.4) as:

$$IUH(t) = \int_0^\infty e^{\Phi(V,t)} dV \tag{5.11}$$

where

$$\Phi(V,t) = -Vt + \log\left[Vf(V)\right] \tag{5.12}$$

We will assume that the value of the integral is dominated by the value of V (denoted V_t) that maximizes the value of $\Phi(V,t)$ at a fixed t. We then take a second-order Taylor series approximation of $\Phi(V,t)$ around V_t:

$$\Phi(V,t) = \Phi(V_t,t) + \frac{1}{2}\Phi''(V_t,t)(V - V_t)^2 \tag{5.13}$$

The first order term has vanished because V_t is a local maxima. We can then approximate equation (5.11) as:

$$IUH(t) \approx e^{\Phi(V_t,t)} \int_0^\infty e^{\frac{1}{2}\Phi''(V_t,t)(V-V_t)^2} dV \tag{5.14}$$

This integral is the well-known Gaussian integral, and converges on the condition that $\Phi''(V_t,t) < 0$ to give:

$$\int_0^\infty e^{\frac{1}{2}\Phi''(V_t,t)(V-V_t)^2} dV = \frac{1}{2}\left[1 + \mathrm{Erf}\left(V_t\sqrt{\frac{-\Phi''(V_t,t)}{2}}\right)\right]\sqrt{\frac{2\pi}{-\Phi''(V_t,t)}} \tag{5.15}$$

where Erf is the error function. We can find V_t by taking $0 = \partial\Phi(V,t)/\partial V$, which gives:

$$t = \frac{1}{V} + \frac{f'(V)}{f(V)} \tag{5.16}$$

Solving for V gives V_t. The timescale $1/V_t$ can be interpreted as the characteristic timescale of the hillslope that is dominating the recession of the impulse response at a particular point in time t.

We can use this general theory to obtain expressions for the asymptotic behavior of the recession slope curves when the distribution of the 'slow' tail of hillslopes follows a power-law, i.e. $f(V) \sim V^\gamma$ as $V \to 0$. The following holds true for all distributions with $\gamma > -1$. The Gamma distribution is one distribution that follows this behavior. Note that it can be shown that this is equivalent to the distribution of $T = 1/V$ going

as $T^{-(\gamma+2)}$ as $T \to \infty$. The value of the characteristic timescale $1/V_t$ in such cases is given by equation (5.16) as:

$$1/V_t = \frac{t}{1+\gamma} \tag{5.17}$$

suggesting that as the catchment drains, the characteristic timescale of the hillslope dominating the discharge response increases linearly in time. The value of $e^{\Phi(V_t,t)}$ then goes as $t^{-1-\gamma}$. The value of $\Phi''(V_t,t)$ is given by:

$$\Phi''(V_t,t) = -\frac{1+\gamma}{V_t^2} \tag{5.18}$$

This is strictly negative only for $\gamma > -1$, which creates the restriction noted above. Substituting this into equation (5.15), the term in the error function becomes independent of V_t and the integral in equation 5.14 goes as t^{-1}. Thus equation (5.14) gives the tailing behavior of the IUH as:

$$IUH(t) \sim t^{-(\gamma+2)} \tag{5.19}$$

That is, the tail of the instantaneous unit hydrograph follows the tail of the distribution of characteristic timescales T. If we assume that following a short period of recharge the tail of the hydrograph for a catchment follows the tail of the IUH, then $Q \sim t^{-2-\gamma}$ and $-dQ/dt \sim t^{-3-\gamma}$. Consequently it follows that:

$$-\frac{dQ}{dt} \sim Q^{1+\frac{1}{\gamma+2}} \tag{5.20}$$

Thus when the 'slow' tail of the distribution of hillslope characteristic timescales follows a power-law with an exponent γ, the tail of the recession slope curve will also follow a power law with an exponent given by:

$$b = 1 + \frac{1}{\gamma+2} \tag{5.21}$$

Note that this result is in full agreement with the result for the particular case of the Gamma distribution in equation (5.7), where $\gamma = \alpha - 1$.

Bounded power-law distribution

For distributions bounded at zero (such as the Gamma distribution), γ must be ≥ -1 for the integral of the pdf to converge. Thus the exponent b of the recession slope curve has an upper bound at 2 for such distributions. However, we can construct a distribution that permits larger b exponents for a significant part of the recession by assuming that the distribution follows a power law as V approaches zero, but is truncated

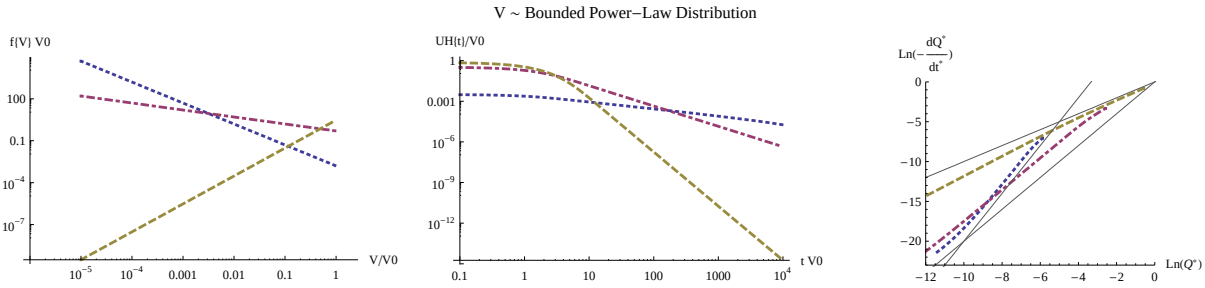

Figure 5.4: Same as Figure 5.1, but for the bounded power-law distribution (equation 5.22). Values of γ are -1.5 (dotted line), -0.99 (dash-dot), and 2 (dashed line). Example power-laws with exponents 1,2 and 3 are plotted in gray on the right plot.

at a finite value for very small V. Consider a distribution given by a power-law over a bounded range of V:

$$f(V) = \frac{1}{V_0}\frac{(\gamma+1)}{1-\kappa^{\gamma+1}}\left(\frac{V}{V_0}\right)^{\gamma} \qquad \kappa V_0 < V < V_0 \tag{5.22}$$

where $V_0 > 0$ is the maximum value of V and $0 < \kappa < 1$ is the size of the minimum relative to V_0. As $\kappa \to 0$ this distribution approximates a power-law pdf that goes as V^{γ} as $V \to 0$ (Figure 5.4). That is, the tails of the distribution of $T = 1/V$ go as $T^{-(\gamma+2)}$). This distribution can be substituted into equation (5.4) and be integrated directly to yield:

$$IUH(t) = \frac{(\gamma+1)}{\kappa^{\gamma+1}-1}(\Gamma(\gamma+2, tV_0) - \Gamma(\gamma+2, tV_0\kappa))V_0(tV_0)^{-\gamma-2} \tag{5.23}$$

where $\Gamma(x, z)$ is the incomplete Gamma function. Examples of this unit hydrograph are given in Figure 5.4. Again if we assume that $Q(t) \approx Q_0 \times IUH(t)$ and $Q'(t) \approx Q_0 \times IUH'(t)$ for the recession, we can plot the recession slope curve as a parametric plot of t. The expression for $IUH'(t)$ is:

$$\begin{aligned} IUH'(t) &= \left(\left(e^{-tV_0} - e^{-tV_0\kappa}\kappa^{\gamma+2}\right)(tV_0)^{\gamma+2} + (\gamma+2)(\Gamma(\gamma+2, tV_0) - \Gamma(\gamma+2, tV_0\kappa))\right) \\ &\quad \times \frac{(\gamma+1)}{(\kappa^{\gamma+1}-1)}V_0^2(tV_0)^{-\gamma-3} \end{aligned} \tag{5.24}$$

The result is shown in Figure 5.4. It shows clearly that exponents of b greater than 2 can occur during the recession up until a time proportional to $1/V_0$, at which point the discharge is dominated by the discharge from the slowest hillslope. The period of time over which this occurs increases with $\kappa \to 0$. In fact, for small κ the b exponent is closely approximated by equation (5.21), even though it was derived strictly for the case of $\gamma > -1$. Figure 5.5 compares the exponent predicted by that equation with the value fitted to bounded power law recession slope curves from times $t = 1/V_0$ to $t = 10/V_0$. The result suggests that equation (5.21)

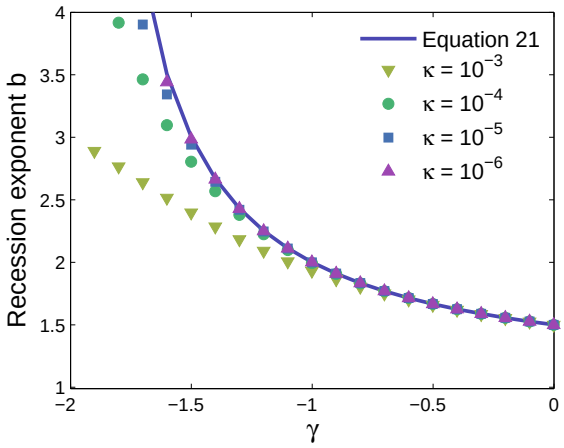

Figure 5.5: Comparison of the exponent of the recession slope curve predicted by equation (21) (solid line) and fitted to the early part ($t = 1/V_0$ to $10/V_0$) of the recession slope curve when $f(V)$ follows a bounded power law distribution.

gives an upper bound to the value of b in this range of times. This bound is approached when $\kappa \to 0$.

The CV of the distribution given in equation (5.22) can be shown to be:

$$CV = \sqrt{\frac{(\gamma+2)^2\left(\kappa^{\gamma+1}-1\right)\left(\kappa^{\gamma+3}-1\right)}{(\gamma+1)(\gamma+3)\left(\kappa^{\gamma+2}-1\right)^2} - 1} \tag{5.25}$$

By combining this with equation (5.21) to eliminate γ, we can obtain a relationship between the CV and this 'potential' value of b. The relationship is shown in Figure 5.2(right) for a number of different values of κ. This relationship is close to linear for small values of the CV, but for larger values it diverges and becomes dependent on the value of κ. That parameter sets the upper bound on the CV by controlling the range of values the distribution can take. The potential value of b becomes large as this upper bound is approached.

5.2.3 Steady-state recharge

Under prolonged constant recharge, a hillslope will (in theory) approach a steady-state in which the discharge is equal to the recharge. If the recharge is then stopped, the discharge will recede with a shape that is different from that of an impulse.

In general we can derive the recession following the cessation of steady-state recharge by convolving the impulse-response $IUH(t)$ with a step function of the form:

$$R(t) = R_0(1 - H(t)) \tag{5.26}$$

where $H(t)$ is the Heaviside step function and R_0 is the rate of discharge for $t < 0$. Recharge for $t > 0$ is zero. Convolution in the time domain is equivalent to multiplication in the frequency domain, so we can compute the discharge by multiplying the Fourier transfer of the impulse response $\mathcal{F}\{IUH(t)\} = \widehat{IUH}(\omega)$ and recharge $\mathcal{F}\{R(t)\} = \hat{R}(\omega)$ and taking the inverse transform:

$$Q = \mathcal{F}^{-1}\{\widehat{IUH} \times \hat{R}\} \tag{5.27}$$

A simple closed-form solution can be found for the case of a Gamma distribution of $f(V)$. The solution is:

$$Q(t) = R_0(1 + tV_0)^{-\alpha} \tag{5.28}$$

Intermediate steps leading to this solution are given at the end of the chapter.

By taking the derivative dQ/dt and eliminating the time derivative between the two equations, we can arrive at an expression for $-dQ/dt$ in terms of Q:

$$\frac{dQ}{dt} = -R_0^{-1/\alpha} V_0 \alpha Q^{1+1/\alpha} \tag{5.29}$$

Thus we see that the recession slope curve in this case is a power law with exponent $b = 1 + 1/\alpha$ and coefficient $a = R^{-1/\alpha}V_0$. Since $\alpha > 0$, the exponent b can take on any value greater than 1. We can invert these relationships to obtain expressions for α and V_0 in terms of a, b and R_0:

$$\alpha = \frac{1}{b-1} \tag{5.30}$$

$$V_0 = a(b-1)R_0^{b-1} \tag{5.31}$$

Using these expressions we can calculate the mean and standard deviation of the characteristic residence times using the following expressions:

$$\mu_V = V_0\alpha = aR_0^{b-1} \tag{5.32}$$

$$\sigma_V = V_0\sqrt{\alpha} = aR_0^{b-1}\sqrt{b-1} \tag{5.33}$$

Estimation of the actual mean and variance requires that an unknown 'effective' steady-state recharge R_0 be determined. We do not currently have a method for identifying this parameter. However, the coefficient of variation (CV) of characteristic timescales (σ_V/μ_V) in such a case is given simply by $CV = \sqrt{b-1}$, or

alternatively:

$$b = 1 + CV^2 \tag{5.34}$$

This relationship is also plotted in Figure 5.2. It shows that for small variance, the difference between the exponent in the steady-state case and the impulse response case is negligible for CV less than around 0.5. For larger values of CV the steady-state case continues to increase, while the impulse response is bounded at $b = 2$.

5.2.4 Periodic recharge

The exponent of the recession slope curve for a more realistic recharge scenario (i.e. a series of storms with finite duration and interstorm period) is likely to lie somewhere between the responses for the impulse and steady state derived above. We can examine this intermediate case by assuming the recharge is periodic with a fixed duration, spacing and intensity. This simple approximation has been used by *Robinson and Sivapalan* (1997) to characterize the way the timescales of a hydrologic system (idealized as a single linear reservoir) interacted with the storm duration, intensity and inter-storm period to control the flood peak.

The response to periodic recharge can be found by convolving the derived impulse-response functions with the recharge timeseries. The example here is for the IUH with V given by a Gamma distribution. Consider a rainfall signal consisting of periods of recharge of constant intensity P_0 for duration t_r separated by an interstorm period t_b. The response of a linear system (with a known IUH function) to such a periodic forcing can be obtained from the Fourier series of the forcing. The Fourier series expansion of this rectangular wave is given by:

$$P(t) = \sum_{m=-\infty}^{\infty} D_m e^{2im\pi \frac{t}{t_r+t_b}} \tag{5.35}$$

where D_m is:

$$D_m = \frac{P_0}{m\pi} \sin\left(m\pi \frac{t_r}{t_r+t_b}\right) \tag{5.36}$$

The discharge response is obtained by multiplying each term by a transfer function $H(s)$ evaluated at $s = im\omega_p$ (where the frequency ω_p is here $2\pi/(t_r + t_b)$):

$$Q(t) = \sum_{m=-\infty}^{\infty} D_m H\left(im\frac{2\pi}{t_r+t_b}\right) e^{2\pi im \frac{t}{t_r+t_b}} \tag{5.37}$$

The transfer function is the Laplace transform of the impulse response function (the IUH). Using the impulse

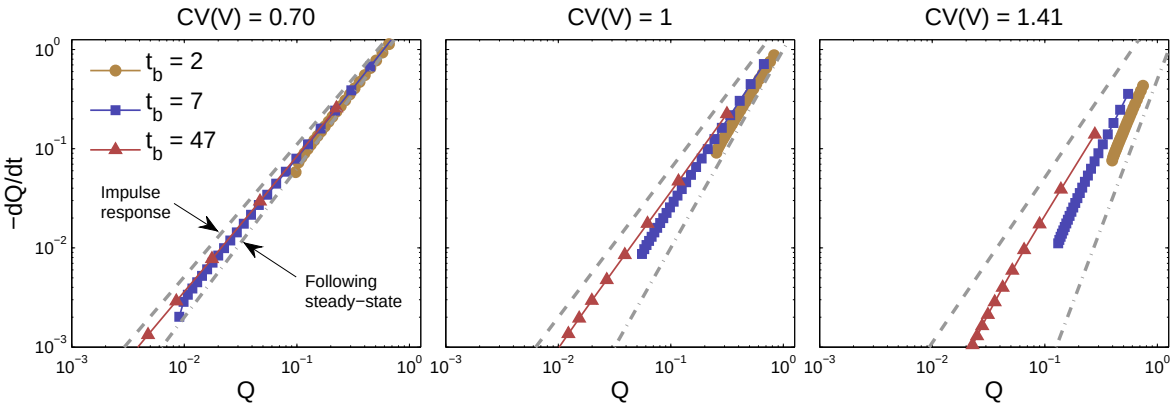

Figure 5.6: Control of the variability of recharge events on the recession slope curve. For Gamma distributions of V with low variability (left plot) the recession following an impulse, following periodic recharge and following steady-state recharge are all similar. For larger degrees of variability (center, right), the recession curves following impulse and steady-state recharge become different. The recession curves following periodic recharge depend on the inter-storm period. Results are for $\alpha = \{2, 1, 1/2\}$, $V_0 = 1$ day^{-1}, $P_0 = 1$mm day^{-1}, $t_r = 3$ days, $Q_0 = 1$mm, $R_0 = 1$mm day^{-1}.

response corresponding to a Gamma distribution of V (equation 5.6) this is:

$$H(s) = \alpha e^{s/V_0} \left(\frac{s}{V_0}\right)^{\alpha} \Gamma\left(-\alpha, \frac{s}{V_0}\right) \tag{5.38}$$

The function describing the rate of change in storage with time can be found by taking the derivative of equation (5.37):

$$-\frac{dQ}{dt} = \sum_{m=-\infty}^{\infty} -\frac{2\pi i m}{t_r + t_b} D_m H\left(im\frac{2\pi}{t_r + t_b}\right) e^{2\pi i m \frac{t}{t_r + t_b}} \tag{5.39}$$

We can plot the recession slope curve by evaluating Equations (5.37) and (5.39) numerically (i.e. for a sufficiently large range of m around zero) for a range of values from $t = t_r/2$ to $t = t_r/2 + t_b$.

Figure 5.6 shows the result for several values of the CV (i.e. several values of α) and t_b. These plots also show the predicted recession slope curve for the asymptotic cases of an impulse or steady-state recharge with the same distribution of V. For the small CV case there is little difference between the limiting cases, and the effect of changing t_b on the exponent is negligible. For larger CV the slopes become steeper, and the effect of the interstorm period becomes pronounced. The shorter interstorm period cases behave more like the steady-state recharge case and exhibit higher slopes, while the longer interstorm period cases behave more like an impulse response and take on smaller slope.

5.3 Application to data

5.3.1 Comparison with Panola recession data

The simple model of *Clark et al.* (2009) represents the heterogeneity in the catchment properties in terms of n discrete linear reservoirs, each with a unique timescale V_i and a fractional area F_i.

$$Q = \sum_{i=1}^{n} F_i V_i S_i \tag{5.40}$$

where S is the storage in the hillslope and n is the number of linear reservoirs. This model is in fact a special case of the model presented above in which $f(V)$ is a discrete distribution. That is,

$$f(V) = \sum_{i=1}^{n} F_i \delta(V_i) \tag{5.41}$$

where $\delta(V)$ is the Dirac Delta function.

Clark et al. (2009) fitted this model to data from a hillslope, a 10ha catchment and a 41ha catchment at the Panola Mountain Research Watershed. The results are shown in Figure 5.7. To fit the model they assumed that the catchments had been subjected to steady-state recharge of constant $R_0 = 25mm/day$. At the hillslope scale the recession slope curve has $b \approx 1$, and they were able to fit a single linear reservoir ($n = 1$, $F_1 = 1$) with $V_1 = 2/day$. For the larger scale catchment the recession slope curve has an exponent around $b = 2$ for large Q and $b = 1$ for lower Q. They added a second linear reservoir with $V_2 = 0.2/day$ and $F_2 = 0.2$ to approximate this behavior. At the largest scale, the recession slope data takes on a convex form, with an average slope around $b = 3$. *Clark et al.* (2009) fitted this data by reducing the fractional area of the second to $F_2 = 0.1$ and adding a third linear reservoir with $F_3 = 0.1$. They showed results for $V_3 = [0.01, 0.05, 0.1]$.

We will fit the results derived above to the Panola data to demonstrate the ability of the catchment heterogeneity to explain the exponents of observed recession slope curves. Since the exponent of the recession slope curve has b as high as 3, we will only use the two cases derived above that can reproduce this behavior:

- The bounded power-law (BPL) distribution with an impulse of recharge
- The Gamma distribution following steady-state recharge

The 10ha and 41ha Panola catchment have riparian aquifers and recharge from groundwater that are likely to store recharge from many previous storms in to the discharge to the stream. It is therefore unlikely that the impulse response-based BPL model will be appropriate, but it is included here for comparison.

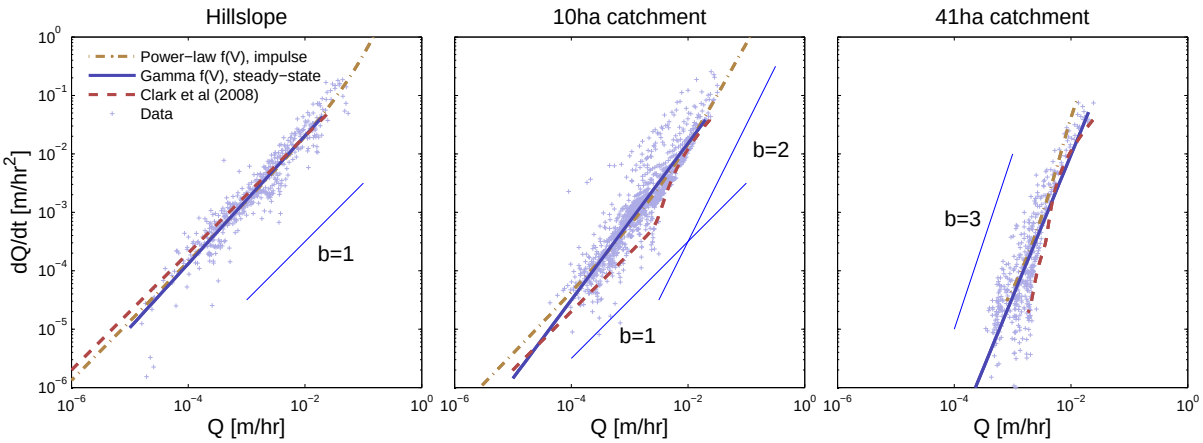

Figure 5.7: Recession data from the Panola Mountain Research Watershed compared to (dashed line) the multiple linear reservoir model of *Clark et al.* (2009), and the generalization to an ensemble proposed in this work with (solid line) a Gamma distribution of V and assuming initially steady state recharge, and (dash-dot line) bounded power-law distribution of V and assuming an impulse of recharge with no initial storage in the catchment.

Table 5.1: Parameters of the bounded power-law distribution fitted to the Panola recession data.

	Bounded Power-law				Gamma		
	Q_0	V_0	κ	γ	R_0	V_0	α
Hillslope	68.7mm	35.2 day^{-1}	3.39%	-1.54	25mm day^{-1}	0.21 day^{-1}	10.6
10ha catchment	68.7mm	35.2 day^{-1}	0.87%	-0.88	25mm day^{-1}	0.71 day^{-1}	2.9
41ha catchment	68.7mm	35.2 day^{-1}	0.0246%	-1.69	25mm day^{-1}	5.1 day^{-1}	0.70

There is no particular reason to choose the Gamma distribution, apart from the mathematical convenience of having an analytical result to work with. However, Gamma distributions provide a launching pad for further investigation.

The Gamma distribution has three parameters α, V_0 and R_0. The value of R_0 used by *Clark et al.* (2009) was adopted (25mm/day), and the values of α and V_0 were obtained by least squares linear regression with the log-transformed values of Q and $-dQ/dt$. The bounded power-law distribution has four parameters: γ, κ, V_0 and Q_0. A single value of Q_0 and V_0 was used across all three catchments, and γ and κ were allowed to vary. The parameters were fitted to the recession data manually.

The fitted results are shown in Figure 5.7. In general the fit to the observed data is excellent. In all cases it is as good or better than the simple one, two or three bucket model of *Clark et al.* (2009). The distribution parameters are given in Table 5.1, and the cumulative distributions for this work and *Clark et al.* (2009) are given in Figure 5.8.

The fitted distributions generally agree with the distributions fitted by *Clark et al.* (2009) (Figure 5.8). The CV of the fitted Gamma distribution (equation 5.34) increases from 0.31 in the hillslope to 1.20 in the

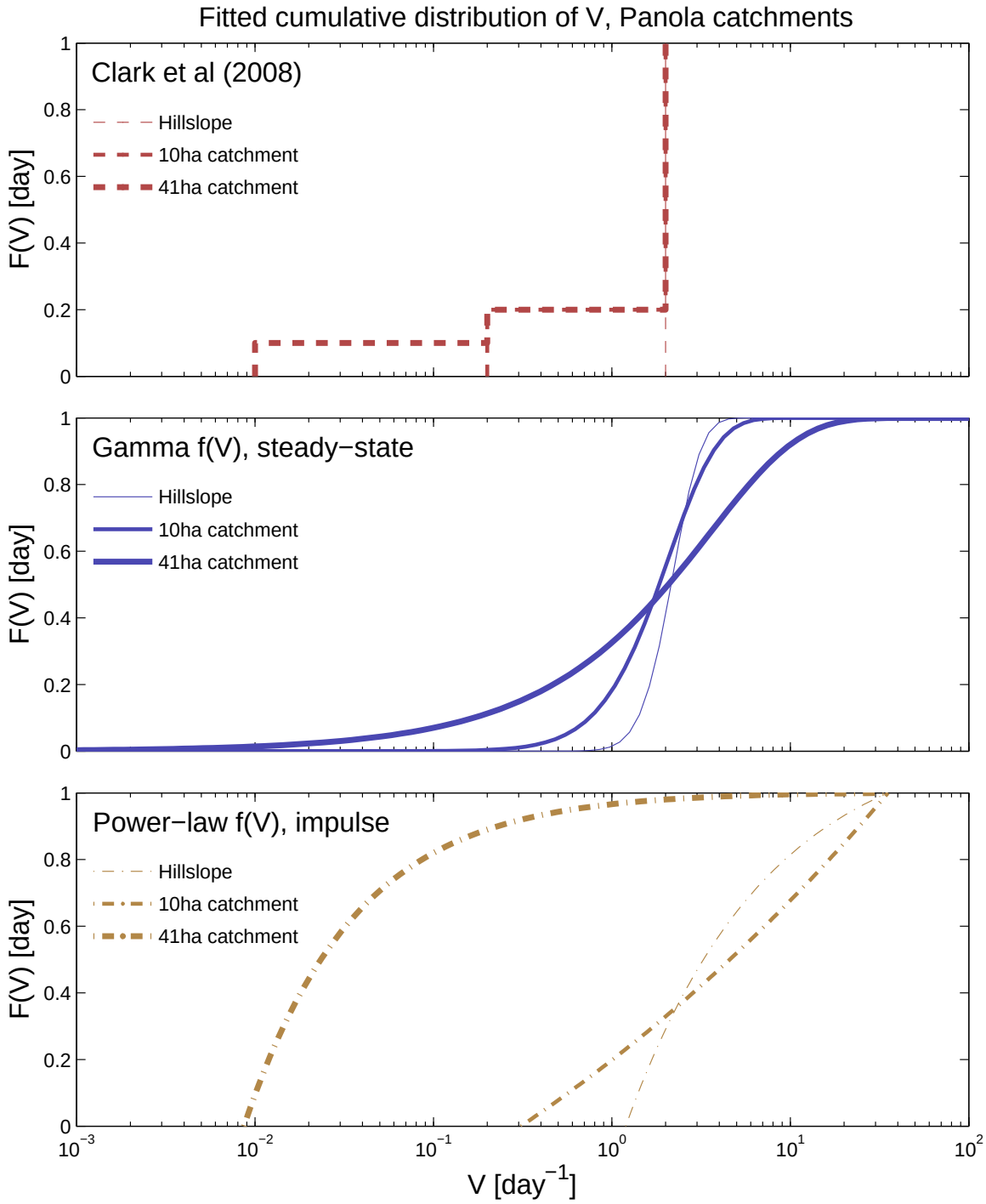

Figure 5.8: Comparison of the cumulative densities of V fitted to the Panola data in *Clark et al.* (2009) and in this work.

41ha catchment, suggesting that at the hillslope scale a narrow range of characteristic timescales controls the response, and at the largest scale there is a much wider range of characteristic timescales controlling the flow. The CV of the fitted BPL distribution (equation 5.25)varies from 1.1 at the small and medium scales, to 6.1 at the large scale. The spread at the large scale can be attributed to low-gradient riparian aquifers and return flow through the bedrock underlying the surrounding hillslopes. These slow-flowing areas can dominate the long-time response, while the parts of the catchment with residence times orders of magnitude shorter dominate the fast response (as suggested by *Clark et al.*, 2009).

There is a striking consistency in the mean of the fitted Gamma distribution across scales. While the values of V_0 and α both vary over more than an order of magnitude, the mean V in each catchment (which is the product of V_0 and α; see equation 5.32) varies much less: Hillslope: 2.2 day^{-1}, 10ha catchment: 2.0 day^{-1}, 41ha catchment: 3.5 day-1. It is important to note that these values are sensitive to the chosen value of R_0, and for different values the consistency between scales is not as striking. The CV of V does not depend on R_0 (equation 5.32).

5.3.2 Comparison to published datasets of b exponents

There are numerous studies that present data on recession slope curves, and collectively they suggest that recessions from natural catchments exhibit a range of values for b. The range of values in some selected studies is shown in Figure 5.9. The techniques and the derivation of the reported values vary. Some studies report values of a and b fitted to the curve directly (e.g. *Tague and Grant*, 2004). Others, including *Wittenberg* (1999) and *Chapman* (1999), have suggested that power-law recession slope curves arise as a result of a non-linear storage-discharge relationship, $Q \sim S^{1/k_W}$ or $Q \sim S^{k_C}$ respectively, and have used these models to derive expressions for the recession slope curve that could be compared to data. More recently *Kirchner* (2009) proposed analyzing $dS/dQ = g(Q)$, and found that this function approximated a power-law $g(Q) \sim Q^{k_K - 1}$ (although a log quadratic function was a closer fit in at least one case). Although there are some differences in their methods, these exponents are all related to each other by:

$$b = k_K = 2 - \frac{1}{k_C} = 2 - k_W \tag{5.42}$$

When $b = 1$ the catchment behaves as a linear reservoir, which produces an exponential recession in time. Values of $b > 2$ imply a negative hyperbolic relationship between storage and discharge (*Kirchner*, 2009). In addition to the observations at Panola cited here, observed values of the recession slope curve exponent b reported in the literature range from less than 1 (transformed using equation (5.42) from data in *Wittenberg*

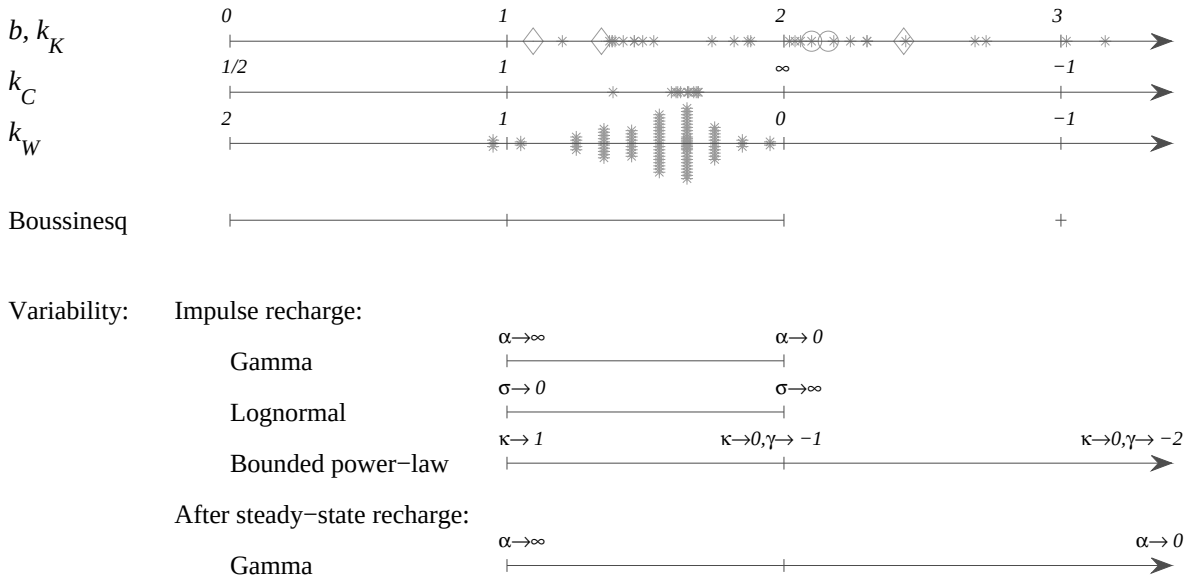

Figure 5.9: Comparison of observed values of the recession slope curve exponents, values obtained from approximate solutions of the Boussinesq equation, and values obtained from ensembles of linear reservoirs with various distributions of V. Values of b from Panola (diamonds) and *Tague and Grant* (2004) (stars), k_K (circles) from *Kirchner* (2009), k_C from *Chapman* (1999), k_W from *Wittenberg* (1999).

(1999)), to higher than 3 (*Tague and Grant*, 2004).

Hydraulic theory based on the Boussinesq equation is able to account for a wide range of these exponents (Figure 5.9). It can be shown that a kinematic wave draining a uniformly thick sloping aquifer has $k_C = 0$ if the thickness is initially uniform and $k_C = 1/2$ (or $b = 0$) if it is initially at steady-state (*Harman and Sivapalan*, 2009b; *Rupp and Selker*, 2005). Linearized forms of the Boussinesq equation applied to the hillslope scale can produce exponents of $b = 3$ for the early stages of drainage and $b = 1$ to 2 for later stages (*Rupp and Selker*, 2006b). *Rupp and Selker* (2005, 2006b) showed that where the hydraulic conductivity of the subsurface decays with depth as a power-law, the exponent is $1 < b < 2$ and depends on the rate of decay.

However, the above derivations suggest that catchment variability can also account for the same exponents. Figure 5.9 shows that the range of observed exponents overlaps with both the range that the heterogeneity can explain and the range that the hydraulic theory of groundwater can explain. The ranges of exponents explained by the hydraulic theory overlaps for impulse-like recharge for Gamma and Lognormal distributions for $1 < b < 2$, and the bounded power-law distribution can explain observations of $b > 2$ as well. For recessions following steady-state recharge the Gamma distribution can account for all $b > 1$. This overlap implies that both the hydraulics of water flow through hillslopes and the heterogeneity in catchment

properties can give rise to similar signatures in the hydrograph.

5.4 Discussion

5.4.1 The recession slope curve as a signature of spatial and temporal variability

The result presented here clearly show that the heterogeneity within catchments alone is capable of producing the apparently non-linear, power-law recession slope curves. The behavior modeled here does not arise as a result of any non-linearity in the flow hydraulics; the underlying flowpaths have been assumed to behave linearly and do not interact with each other. It is simply a result of the heterogeneity of catchment properties, represented in the distribution of timescales in the catchment. These timescales are related to the properties of the soils and the hillslope topography (equation 5.1).

The history of previous events appears to be an important control on the shape of the recession slope curve in heterogeneous catchments. For $f(V)$ following the Gamma distribution, the values of b for different recharge scenarios are similar for small CV, but are bounded at 2 for the impulse case, and unbounded in the steady-state case (Figure 5.2, equations 5.8 and 5.34). In the more realistic situation where the recharge is intermittent over time, the observed value of b lies between the the values given by these equations (Figure 5.6). This result suggests that we would expect the exponent b to change seasonally and interannually as the storage in the slow parts of the catchment vary.

A physical interpretation of the combined control of the spatial variability of properties and the temporal variability of recharge can be constructed as follows. The discharge contributing to the the recession at any particular time is dominated by different parts of the catchment as the recession progresses. As the hillslopes drain after a storm the faster hillslopes (large V) will dominate the initial response, but will drain quickly, leaving the slower (small V) hillslopes to control the later parts of the recession. This shift in dominant timescales creates the apparent non-linearity in the recession slope curve. The rate at which control is passed from the faster to the slower part of the catchment depends on the storage in each part, which may be built up over successive recharge events. Following an impulse the storage in each part of the catchment is the same, and so the control is passed at a constant rate (equation 5.17). Following an extended period of recharge events, storage is built up over time in the slower parts of the catchment (constituting a 'memory' of past events), which reduces the rate of change of discharge at a given discharge (Figure 5.6), leading to steeper recession slope curves.

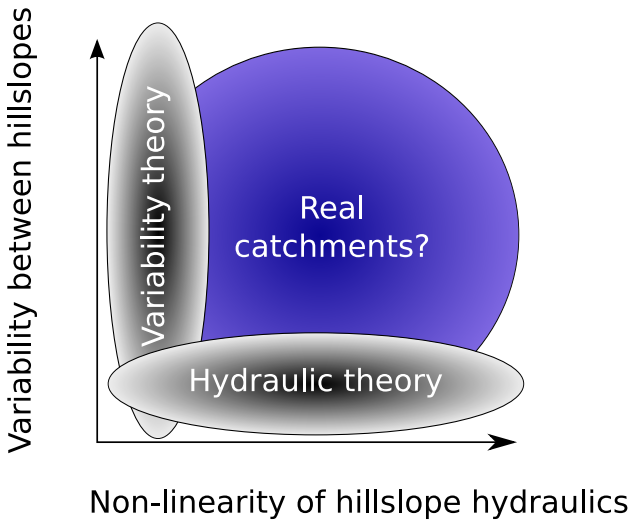

Figure 5.10: The hydraulic theory and the theory presented here both provide explanations for the same phenomenon, though based on different assumptions about the relative importance of the heterogeneity and hydraulics in controlling the phenomenon. Consequently, neither gives full account of the behavior of real catchments, in which both these factors are likely relevant.

5.4.2 Relationship to the hydraulic interpretation of the recession

This interpretation of the physical origins of the recession slope curve is quite different to that provided by the hydraulic theory that has often been given in the past (*Brutsaert and Nieber*, 1977; *Brutsaert*, 1994; *Rupp and Selker*, 2006b; *Brutsaert*, 1994). In the hydraulic interpretation, the exponent of the recession slope curve arises due to the evolution of the water table gradients driving flow through a hillslope through time. If a single 'effective' hillslope is assumed to represent the behavior of all the hillslopes in a catchment, its properties can be determined from inversion of the empirical recession slope curves. This 'effective' hillslope can then be used as a basis for prediction (*Zecharias and Brutsaert*, 1988; *Troch et al.*, 1993a; *Pauwels et al.*, 2002; *Szilagyi et al.*, 1998; *Szilagyi and Parlange*, 1998).

The approach adopted in this work is complementary to the hydraulic approach, which ignores the variability that exists between hillslopes in a watershed and focuses attention exclusively on the flow dynamics (Figure 5.10). The alternative perspective examined in this work uses a simple representation of the flow dynamics in order to focus on the effect of the heterogeneity. Of course in a real catchment neither interpretation alone will do justice to reality: on the one hand the hydraulics of flow are generally more complex than a simple linear reservoir, and on the other hand catchments are highly heterogeneous. The question is more one of dominance. Under which circumstances does variability control the shape of the discharge response, and under which does the hydraulics control?

However the results raise challenges for the inversion problem of determining catchment properties from

hydrographs. If discharge behavior were entirely controlled by the hydraulics of flow, the recession could be used to infer hydraulic properties of catchments (e.g. *Szilagyi et al.*, 1998). However, because the heterogeneity of these properties can explain the same behavior, this inverse calculation cannot be achieved unless a way can be found to separate the effect of the heterogeneity. It may be that there is insufficient information in the hydrograph alone to separate the effects of heterogeneity and hydraulics. Other information may be required, perhaps derived from spatial or using isotope data to estimate travel time distributions.

The approach used here is simplified significantly by the assumptions that the components that make up the catchment (e.g. the individual hillslopes) behave as linear systems with regards to their inputs, and are arranged in parallel. Relaxing either of these assumptions would increase the realism of the description, allowing for a more 'physical' description of the flow hydraulics and catchment structure, but would also make analytical results more difficult to obtain. The central points made above would remain.

5.5 Conclusions

This work has clearly demonstrated that the exponent describing the slope of the recession slope curve, b, can be related to the variability of the hydraulic properties between hillslopes in a catchment and to the variability of recharge. By adopting a simplified representation of the flow through individual hillslopes, explicit expressions have been derived relating b to the coefficient of variation (CV) of the characteristic timescale $1/V$ for several different distributions following both impulses and steady-state recharge.

The derived results were found to be able to fit well to recession data from nested catchments in the Panola Mountain Research Watershed, obtained from *Clark et al.* (2009). This allowed us to make tentative inferences about how the distribution of characteristic timescales in the landscape varied with catchment scale.

It was also shown that the theory derived here can account for almost the full range of observed values of b in the literature. This suggests that both this theory and the hydraulic theory of subsurface discharge are viable explanations for the same hydrologic signature. In reality, both may be contributing to the shape of an observed recession curve.

The approach presented here has enabled us to show how upscaling on the basis of the heterogeneity of landscape characteristics can manifest apparently non-linear behavior at the catchment scale. This is an example of a catchment process being "different in form, not just different in the parameters, from the equations that describe the small-scale physics" (*Kirchner*, 2009) (see also *Kirchner* (2006); *Sivapalan* (2003b); *Savenije* (2001)). The result gives hope that an approach can be found to capture the effects of

more realistic non-linear hydraulics and more complex spatial heterogeneity in catchment-scale models. This would further contribute towards current efforts to develop a comprehensive suite of hydrologic theory that is able to account for the effects of heterogeneity at useful scales (*Blöschl and Sivapalan*, 1995; *McDonnell et al.*, 2007; *Troch et al.*, 2009a).

Key steps leading to equation (5.28)

These results were obtained using Mathematica (Wolfram Research, Inc. *Mathematica* Version 6, Wolfram Research, Inc. Champaign, Illinois 2008). To obtain the Fourier transform of the instantaneous unit hydrograph for the case of a Gamma distribution for $f(V)$, equation (5.6) is first multiplied by the Heaviside step function:

$$\begin{aligned}\widehat{IUH}(\omega) &= \mathcal{F}\left\{H(t)\alpha V_0(1+tV_0)^{-1-\alpha}\right\} \\ &= \frac{\alpha|\omega|^{\alpha}\Gamma(-\alpha)\mathrm{sgn}(\omega)V_0^{-\alpha}}{\sqrt{2\pi}\omega}\left(|\omega|\cos\left(\frac{\pi\alpha}{2}+\frac{|\omega|}{V_0}\right)-i\omega\sin\left(\frac{\pi\alpha}{2}+\frac{|\omega|}{V_0}\right)\right) \\ &\quad +\frac{{}_1F_2\left(1;\frac{1}{2}-\frac{\alpha}{2},1-\frac{\alpha}{2};-\frac{\omega^2}{4V_0^2}\right)}{\sqrt{2\pi}}+\frac{i\omega\,{}_1F_2\left(1;1-\frac{\alpha}{2},\frac{3}{2}-\frac{\alpha}{2};-\frac{\omega^2}{4V_0^2}\right)}{\sqrt{2\pi}(\alpha-1)V_0}\end{aligned} \tag{5.43}$$

The Fourier transform of the recharge forcing is given by:

$$\begin{aligned}\hat{R}(\omega) &= \mathcal{F}\{R_0(1-H(t))\} \\ &= R_0\left(\sqrt{\frac{\pi}{2}}\delta(\omega)-\frac{i}{\sqrt{2\pi}\omega}\right)\end{aligned} \tag{5.44}$$

The result is obtained by taking the inverse transform of the product of these expressions.

5.6 Acknowledgments

This work was supported by by NSF grant ATM 06-28687. Thanks to Jake Peters (USGS), Martyn Clark and David Rupp for supplying the data from the Panola Mountain Research Watershed. Thanks also to the WRR reviewers and editor Amilcare Porporato for their detailed and helpful comments, which led to significant improvements.

Part II

Functional patterns and Co-evolution

Chapter 6

Functional patterns of elasticity of fast and slow runoff components to precipitation change in the continental United States

[1]*Assessing the sensitivity of annual streamflow to precipitation is challenging due to the complexity of the processes that control the water balance. A low-dimensional model can be useful to interrogate data in regional assessments of a large number of catchments, and can provide insights into the broad similarities and differences between catchments' behaviors. This work assesses the sensitivity to precipitation of total annual streamflow, as well as its slow and fast flow components, within the framework of the Ponce and Shetty water balance model. This framework assumes that there are upper limits on the ability of a catchment to store and evaporate water, and there are minimum threshold amounts of precipitation and wetting (precipitation minus fast flow) needed to initiate fast and slow runoff. The flow elasticities (% change in flow per % change in annual precipitation) was estimated for 405 catchments in the MOPEX dataset (including an assessment of parameter uncertainty). The elasticity of total discharge was 2.1 on average across the catchments, which is consistent with other studies. The fast component was higher (≈2.4) and slow flow was lower (≈2.0). Elasticities were highest and most variable in arid areas. The variations in elasticity between sites were shown to be primarily controlled by the two threshold parameters. The thresholds were a high proportion of mean annual precipitation in arid sites where only a small proportion of catchment wetting is released as slow flow. This provides some insight into previous observations that the sensitivity is correlated with climate.*

6.1 Introduction

Quantifying and predicting the effects of environmental change on catchment hydrology is important for socio-economic reasons, but is challenging due to the complexity of the processes that determine how water is partitioned in the landscape (*Wagener et al.*, 2010). Environmental changes do not occur in isolation from one another, and shifts in water balance will arise from both changes in the climatic drivers of catchment hydrology, and from changes in the physical and ecological structure of landscapes, such as those associated with landuse changes. To complicate matters, there are dynamic feedbacks between the climate, hydrologic response and landscape biophysical processes over a wide variety of temporal and spatial scales. Evidence of such changes have already been observed (for instance) where long-term drought has led to the die-off of Piñon Pine in south-western woodlands of North America (*Breshears et al.*, 2005), altering the hydrologic behaviour of these landscapes (*Guardiola-Claramonte et al.*, 2010).

There is a great deal of previous work exploring the sensitivity of annual streamflow to its primary driver, precipitation, using a variety of methods (for instance *Budyko*, 1974; *Schaake*, 1990; *Milly*, 1994;

[1]An edited version of this work has been published as: Harman, C. J., P. A. Troch, and M. Sivapalan. 2011. Functional model of water balance variability at the catchment scale: 2. Elasticity of fast and slow runoff components to precipitation change in the continental United States, *Water Resources Research 47*, W02523, doi:10.1029/2010WR009656. Copyright 2011 American Geophysical Union. Reproduced/modified by permission of American Geophysical Union. All figures, tables and data were created by Ciaran Harman unless otherwise indicated.

Arnell, 1999; *Gellens and Roulin*, 1998; *Sankarasubramanian et al.*, 2001; *Zhang et al.*, 2001; *Woods*, 2003; *Chiew*, 2006; *Yang et al.*, 2007; *Jothityangkoon and Sivapalan*, 2009; *Hurkmans et al.*, 2009, 2010, and many others). These studies show that the sensitivity varies considerably between catchments, due to a wide variety of factors. Those that have considered the partitioning at an annual scale, such as *Budyko* (1974) and *Zhang et al.* (2001), have only considered the the partitioning of precipitation into streamflow and evapotranspiration, while in others the contributions of fast stormflow and slow baseflow are determined by models (and parameters) that operate at faster timescales. Many of these studies use the elasticity of streamflows proposed by *Schaake* (1990) as a basis for analyzing the sensitivity to precipitation.

The annual water balance model of *Ponce and Shetty* (1995b) described in the companion paper to this one *Sivapalan et al.* (2010) (which was itself based on the work of *L'vovich* (1979)) offers a basis for examining the partitioning into fast and slow flow components using functional parameters that have meaning at the annual timescale. These parameters are emergent properties, in the sense that they arise from the multitude of process interactions that control inter-annual variations in water balance. *Sivapalan et al.* (2010) have shown that this model provides robust predictions in catchments across the continental US. That analysis revealed systematic spatial patterns in the annual water balance, and a space-time symmetry in which variations between catchments followed the same functional form as the variations in a single catchment between years.

In this work we will use the *Ponce and Shetty* (1995b) framework to quantify the sensitivity (in terms of the elasticity) of these fast and slow components to interannual variations in precipitation, and determine which of the functional parameters plays the most important role in determining the sensitivity. Moreover, the parameters' simplicity and parsimony allows for easier comparison between a large number of sites and the analysis of patterns of variation between sites. In this way we aim to observe how patterns in the spatial and (long-term) climatic controls on catchment function determine the sensitivity of the streamflow components to (short-term) climate variations (in this case precipitation).

6.1.1 Space-for-time and time-for-time approaches to understanding water-balance sensitivity

In other works the variation in sensitivity seems to be largely associated with differences in aridity (*Budyko*, 1974; *Schaake*, 1990; *Dooge*, 1992). Others have shown that snow cover and the phasing of water and enery inputs are important (*Sankarasubramanian et al.*, 2001; *Milly*, 1994; *Jothityangkoon and Sivapalan*, 2009), as well as the capacity of catchments to store water and the "storminess" of the climate (*Milly*, 1994). *Woods* (2003) developed coupled analytical models of the seasonal and annual water balance of catchments to show

that six dimensionless parameters control hydrological partitioning: (i) climate dryness; (ii) interception capacity relative to rainfall; (iii) combined climate seasonality and root zone storage; (iv) subsurface flow responsiveness; (v) saturated subsurface flow capacity, relative to mean annual rainfall rate; and (vi) a geomorphological exponent controlling the expansion of saturated area fraction. *Zhang et al.* (2001) found that vegetation type showed a consistent effect on annual water balance, with higher evapotranspiration in forested catchments, and more in pasture (see (*Oudin et al.*, 2008) for an alternative perspective), though interannual variations were not examined. *Yang et al.* (2007) analyzed the spatial and temporal variability of annual water-energy balance in 108 non-humid catchments in China and found that besides the annual climate conditions the regional pattern of annual water-energy balance was closely related to the relative infiltration capacity (hydraulic conductivity of the soil versus the average rainfall intensity), relative soil water storage (maximum soil water storage versus potential evapotranspiration), and the average slope of the catchment.

The wide variety of climatic and landscape factors that control water balance greatly complicate the task of assessing regional patterns of sensitivity. The large amount of data required to characterize any particular catchment makes it difficult to use detailed process-based models to do such regional assessments of sensitivity, although they are certainly useful at the scale of individual catchments (*Hurkmans et al.*, 2010, 2009). The level of detail embedded in such models also obscures the fundamental similarities or differences in the ways variability propagates through catchments, controlled by the processes that partition, store and release water (the emergent results of which *Sivapalan* (2005b) called the 'functions' of a catchment), and which control the way the sensitivity varies between catchments.

One alternative to detailed modeling is to use data on the historical sensitivity to inter-annual variations in precipitation as a surrogate for the long term effects (*Risbey and Entekhabi*, 1996). This 'time-for-time' substitution is based on the assumption that the changes in catchment response due to small climate shifts towards a wetter (or drier) climate are reasonably predicted by considering the behavior of catchments in the wetter (or drier) years it currently experiences. Typically the sensitivity is derived from a simple water balance model calibrated to each site (*Němec and Schaake*, 1982; *Schaake*, 1990; *Chiew*, 2006). Such models have typically been applied for predicting changes in the partitioning of annual precipitation into annual evaporation and annual streamflow.

The 'time-for-time' approach ignores the effects that long-term shifts in climate might have on the catchment properties that control the water balance, such as the structure of the ecological community. Another alternative is to use data from an ensemble of catchments to look for patterns in the relationship between long term average metrics of the climate and the partitioning of rainfall into runoff. Comparisons

between catchments are made on the basis of dimensionless similarity indices that characterize the climate drivers and partitioning. The most well-known example of this approach is from *Budyko* (1974), who used long-term data from many catchments around the world to show that scaled evapotranspiration (scaled with respect to mean annual precipitation) depends primarily on the long-term humidity index (ratio of precipitation to potential evapotranspiration). This 'space-for-time' substitution depends on the assumption that the trajectory of short-term (decades to century) responses of catchments to environmental change can be derived from the (dis)similarity between catchments that have been exposed to the projected climate and land cover conditions (e.g. more or less precipitation or conversion from grassland to forested landscapes) over long time periods (centuries to millennia) (*Dooge*, 1992; *Dooge et al.*, 1999).

The *Ponce and Shetty* (1995b) model described in *Sivapalan et al.* (2010) has the advantages of the empirical models described above in that the predictions are based on the observed sensitivity. However, unlike the Budyko formulation or other typical annual water balance models, the L'vovich – Ponce and Shetty formulation enables the partitioning of runoff into quick and slow flow components. Thus it provides more detailed insights into the patterns of climate and landscape controls on water balance. Perhaps most importantly, however, patterns in the functional parameters would allow the model to be used for both space-for-time and time-for-time substitution. These patterns would suggest that the effects of the long-term climate on the emergent properties of the hydrologic systems are encapsulated by the functional parameters. Taking advantage of these patterns of the emergent properties, we could propose that short term variations in climate are characterized by the interannual variability parameterized in the Ponce and Shetty model, while long term variations are described by shifts in the parameters themselves according to the observed between-site patterns.

6.1.2 Outline of this work

The paper is structured as follows. We begin by deriving an elasticity metric of sensitivity within the framework of the Ponce and Shetty model. We then apply these metrics to the MOPEX dataset of US catchments, which has also been used to investigate controls on the water balance in the continental US by *Sivapalan et al.* (2010), *Zanardo et al.* (2010), and *Voepel et al.* (2010). In order to determine the robustness of this elasticity parameter (given the scatter in the fit of the model to the annual water balance data) we then use a Markov-Chain-Monte-Carlo algorithm to determine uncertainty bounds on the sensitivity metrics for each catchment in the database. This analysis is important to establish the credibility of the predicted sensitivities.

We then investigate which of the functional parameters most strongly determine the sensitivity, and

examine the spatial and climatic variations in these parameters. We will examine relationships of these parameters with the humidity index (the ratio of annual precipitation and potential evapotranspiration P/E_P) and the Horton index. The Horton index is a metric of the annual water balance equal to the fraction of the wetting W that goes towards vaporization V (i.e. $H = V/W$) and was the subject of a detailed study by *Troch et al.* (2009b). The results are then compared to previously published analyses of sensitivity.

It is important to note from the start that this framework does not account for many of the other sources of interannual variability, such as variations in temperature and energy inputs more generally, and the timing of rainfall within the year. Temperature in particular may exhibit systematic changes over time that affect hydrologic partitioning. For instance an increase in temperature could increase the vaporization potential and/or increase the slow flow runoff potential. These changes could be accounted for by allowing the parameters (and particularly the vaporization potential in the case of variations in energy inputs) to be functionally dependent on other climatic inputs. However this is beyond the scope of the current work.

6.2 Methods

The Ponce and Shetty (P&S) model was originally described in *Ponce and Shetty* (1995b), and further elaborated in the companion paper to this one (*Sivapalan et al.*, 2010). Readers are referred to those papers for details of the model. In brief though, the model assumes that at an annual time scale all incoming precipitation P is partitioned into a fast component of runoff S and a 'wetting' component W. The wetting component is then further partitioned into a slow component of runoff U and evapotranspiration, which is called vaporization V for reasons of consistency with the previous works. No carry-over storage between years is accounted for. Each of the two partitioning steps is determined by two parameters: 1) an upper limit, known as the wetting potential W_P and vaporization potential V_P, and 2) a threshold for runoff generation, $\lambda_s W_P$ and $\lambda_u V_P$ (we will treat these products as single parameters, which preserves the nomenclature of *Ponce and Shetty* (1995b) but keeps the definition of the threshold independent of the potentials). These parameters all have units of millimeters (volume per catchment area [L^3/L^2]). Total annual discharge (per unit catchment area) is the sum of the components, $Q = S + U$. Note that in practice, the fast and slow components are identified using hourly or daily data and a baseflow separation algorithm, and the totals of each flow component are aggregated at the annual scale. *Troch et al.* (2009b) suggest that the choice of algorithm is not a significant determinant of the water balance at the annual scale.

6.2.1 Sensitivity in the Ponce and Shetty framework

Following *Schaake* (1990) and *Dooge* (1992) we will use the economic metric of 'elasticity' to quantify the sensitivity of catchment water balance to input variability. This metric is generically defined as the percent change in one variable given a unit percent change in another. The use of elasticity is preferable to a simple rate of change, as it elegantly captures the impact of a given change on the normal state of a system. If a decrease in annual precipitation of 10mm leads to a decrease in annual streamflow of 30mm, this might be a negligible change in the humid tropics, but would be highly significant in a semi-arid catchment. This difference would be reflected in different values of the elasticity metric in each catchment. Considering the change in streamflow per change in precipitaion, we can use the approximation of the derivative to write:

$$\Delta Q = \Delta P \frac{\partial Q}{\partial P} \tag{6.1}$$

and similar expressions with U and S substituted for Q, where P is the annual precipitation. Rearranging this relationship we can write:

$$\frac{\Delta S}{S} = \rho_S \frac{\Delta P}{P} \tag{6.2}$$

$$\frac{\Delta U}{U} = \rho_U \frac{\Delta P}{P} \tag{6.3}$$

$$\frac{\Delta Q}{Q} = \rho_Q \frac{\Delta P}{P} \tag{6.4}$$

where the elasticity metrics, ρ, that give the % change in the water balance component per % change in precipitation are defined as:

$$\rho_S = \frac{\partial S}{\partial P} \Big/ \frac{S}{P} \tag{6.5}$$

$$\rho_U = \frac{\partial U}{\partial P} \Big/ \frac{U}{P} \tag{6.6}$$

$$\rho_Q = \frac{\partial Q}{\partial P} \Big/ \frac{Q}{P} \tag{6.7}$$

Note that since $Q = S + U$ and $\partial Q = \partial S + \partial U$, we can write:

$$\frac{\partial Q}{\partial P} = \frac{\partial S}{\partial P} + \frac{\partial U}{\partial P} \tag{6.8}$$

Thus it is possible to obtain the elasticity of the total discharge from its components S and U and their

elasticities:

$$\rho_Q = \frac{S}{S+U}\rho_S + \frac{U}{S+U}\rho_U \tag{6.9}$$

Expressions for the ρ parameters can be found by substituting the P&S model in the definitions and taking the partial derivatives. Note that it remains necessary to specify the precipitation values at which the sensitivity is required. If we specify that we are interested in the sensitivity around the mean $\overline{P}$, the modeled partition values are given by:

$$\overline{S} = \frac{(\overline{P} - \lambda_s W_P)^2}{W_P - 2\lambda_s W_P + \overline{P}} \tag{6.10}$$

$$\overline{W} = \frac{W_P \overline{P} - \lambda_s {W_P}^2}{W_P - 2\lambda_s W_P + \overline{P}} \tag{6.11}$$

$$\overline{U} = \frac{(\overline{W} - \lambda_u V_P)^2}{V_P - 2\lambda_u V_P + \overline{W}} \tag{6.12}$$

where $\overline{P}$ is the mean precipitation. Values of the required partial derivatives with respect to P are then given by:

$$\left.\frac{\partial S}{\partial P}\right|_{\overline{P}} = \frac{2(\overline{P} - \lambda_s W_p)}{W_p - 2\lambda_s W_p + \overline{P}} - \frac{(\overline{P} - \lambda_s W_p)^2}{(W_p - 2\lambda_s W_p + \overline{P})^2} \tag{6.13}$$

$$\left.\frac{\partial W}{\partial P}\right|_{\overline{P}} = \frac{W_p}{W_p - 2\lambda_s W_p + \overline{P}} - \frac{W_p \overline{P} - \lambda_s {W_p}^2}{(W_p - 2\lambda_s W_p + \overline{P})^2} \tag{6.14}$$

$$\left.\frac{\partial U}{\partial P}\right|_{\overline{P}} = \frac{2\frac{\partial W}{\partial P}(\overline{W} - \lambda_u V_p)}{V_p - 2\lambda_u V_p + \overline{W}} - \frac{\frac{\partial W}{\partial P}(\overline{W} - \lambda_u V_p)^2}{(V_p - 2\lambda_u V_p + \overline{W})^2} \tag{6.15}$$

With these equations we can calculate the sensitivity parameter, ρ, evaluated around the mean.

6.2.2 The MOPEX dataset: parameter estimation and uncertainty

The Ponce and Shetty model was applied to 405 catchments from the MOPEX (Model-Parameter Estimation Experiment) dataset (*Schaake et al.*, 2006; *Duan et al.*, 2006) used by *Sivapalan et al.* (2010). This dataset is a standardized collection of up to 50 years of precipitation and flow data from catchments across the US (it is available at www.nws.noaa.gov/oh/mopex). The subset of catchments selected from the database differ slightly from those of the companion paper, in that only catchments with at least 25 years of flow data available were used, and no catchments were excluded on the basis of parameter identifiability. They range in size from 80 to more than 10,000km^2, are distributed across US, but are mostly east of the Rocky Mountains, and are subject to a range of climates, with mean annual precipitation ranging from 436mm to 2380mm and humidity index (precipitation P divided by potential evapotranspiration E_P) ranging from

0.25 to 2.5. Quick and slow flow components were separated in the streamflow data using a one-parameter low-pass filter (see *Sivapalan et al.* (2010) for full discussion), and totals were obtained over the water-year (October 1 to September 30). *Troch et al.* (2009b) demonstrated that the estimation of annual water balance metrics, such as the Horton index, was not highly sensitive to the method of baseflow separation.

While previous work has estimated the P&S parameters for the MOPEX dataset, the uncertainty in these parameters has not been quantified. Uncertainty in the functional parameters arises due to the scatter in the relationship between annual precipitation and the streamflow components. Because of this scatter different combinations of parameters may produce an equally acceptable fit to the data. This uncertainty propagates to the estimates of the elasticity, as these are calculated from the functional parameters. Given that we intend to make predictions of sensitivity of streamflow to climate change, in this work it is important to determine this uncertainty.

Parameters were estimated in a Bayesian framework with uninformative priors, which provides a rigorous framework for assessing uncertainty with a minimum of assumptions. From the initial fit we determined that the errors in the prediction of S and U were close to normally distributed for the MOPEX dataset. For the purposes of the parameter estimation, it was assumed that the observations of S and U were drawn from a normal distribution with pdf $N(x|\{\mu,\sigma^2\})$ in which the mean is given by the P&S model predictions $S = S(P, W_P, \lambda_s W_P)$ and $U = U(P, V_P, \lambda_u V_P)$ and the variances are the unknown variables σ_S^2 and σ_U^2. Note that errors in the prediction of S and U are perfectly inversely correlated with errors in W and V, and so these latter errors can be ignored. The likelihood $L(\Omega|\theta)$ of the observations $\Omega = \{S_1, \ldots, S_n, U_1, \ldots, U_n\}$ given a model $\theta = \{W_P, \lambda_s W_P, V_P, \lambda_u V_P, \sigma_S^2, \sigma_U^2\}$ with input precipitation timeseries $P_1, \ldots, P_n$ is given by the product:

$$L(\Omega|\theta) = \left(\prod_{i=1}^{n} N(S_i|S(P_i, W_P, \lambda_s W_P), \sigma_S^2)\right)\left(\prod_{i=1}^{n} N(U_i|U(P_i, V_P, \lambda_u V_P), \sigma_U^2)\right) \tag{6.16}$$

From Bayes theorem, the *posterior* likelihood of the model given the data $L(\theta|\Omega)$ is given by:

$$L(\theta|\Omega) = \frac{L(\Omega|\theta)L(\theta)}{L(\Omega)} \tag{6.17}$$

where $L(\theta)$ is the *prior* distribution of the parameters, and $L(\Omega)$ is the probability of the observations. As we have no reason to constrain the prior distribution, we will use a uniform prior distribution, and therefore set $L(\theta) = 1$. While $L(\Omega)$ is required to obtain a properly scaled posterior distribution, it is not necessary to evaluate it when using the methods described below.

The posterior distribution was constructed by sampling the parameter space θ using the Metropolis

algorithm (*Kuczera and Parent*, 1998; *Metropolis et al.*, 1953). This algorithm is a Markov chain Monte Carlo technique for efficiently sampling in the vicinity of maximum likelihood, while also providing good coverage of areas of lower likelihood. For each site the algorithm was run to generate a chain of 2500 samples. Convergence was determined as the point in the chain at which the mean over blocks of 250 consecutive samples changed by less than half the standard deviation of the entire chain. Samples prior to convergence of the chain were discarded. This procedure was then repeated to generate a total of 10,000 samples of the (unscaled) posterior likelihood at each site. Finally, by substituting the parameters of each sample into equation 6.2, likelihoods could be associated with values of the elasticity at each site.

The best estimate of each parameter and elasticity was chosen as the maximum likelihood parameter set. The lower and upper uncertainty bounds were defined as the values for which the sum of the likelihoods of lower values was just greater than 5% and 95% of the total. In the remainder of this paper the error is reported in absolute terms as half the range between the upper and lower uncertainty bounds, or in relative terms as a percentage of the maximum likelihood value.

6.3 Results

6.3.1 Sensitivity of streamflow components to precipitation

Results of the parameter estimation and elasticity are summarized in table 6.1. The elasticities ranged from 1.02 to 8.38 for Q, 1.70 to 6.08 for S, and 0.75 to 10.96 for U. Average values of the elasticities across all sites was highest for the quickflow S at 2.38, lowest for the slow flow U at 1.94 and intermediate at 2.08 for Q. However, the variability between sites (measured by the standard deviation across sites) was smallest for the quickflow (0.57), and highest for slow flow (0.88), with variability in the elasticity of total flow between these (0.70). The elasticities of the fast and slow flow components, however, were loosely correlated ($R^2 = 0.62$).

The relationship between the elasticities and the humidity index (P/E_P) is shown in Figure 6.1. The elasticities are generally larger in dry regions, but also show the greatest variability among sites. The scatter seems to be enclosed by two envelopes: an upper bound with a roughly hyperbolic shape that declines with humidity, and a lower bound that is invariant with climate. These bounds appear to converge for humidity index greater than 2, although there are only a handful of sites in the dataset that are that humid. At those sites the elasticites are highly consistent between sites: $\rho_S \approx 1.83$, $\rho_U \approx 1.13$, and $\rho_Q \approx 1.30$.

These climatic patterns create distinct spatial patterns, as shown in Figure 6.2. All three elasticities are highest in a band running north-south along the continental US. The sensitivities in the band between 89°W and 99°W are higher than the national average by 0.60 for Q, 0.51 for S, and 0.66 for U.

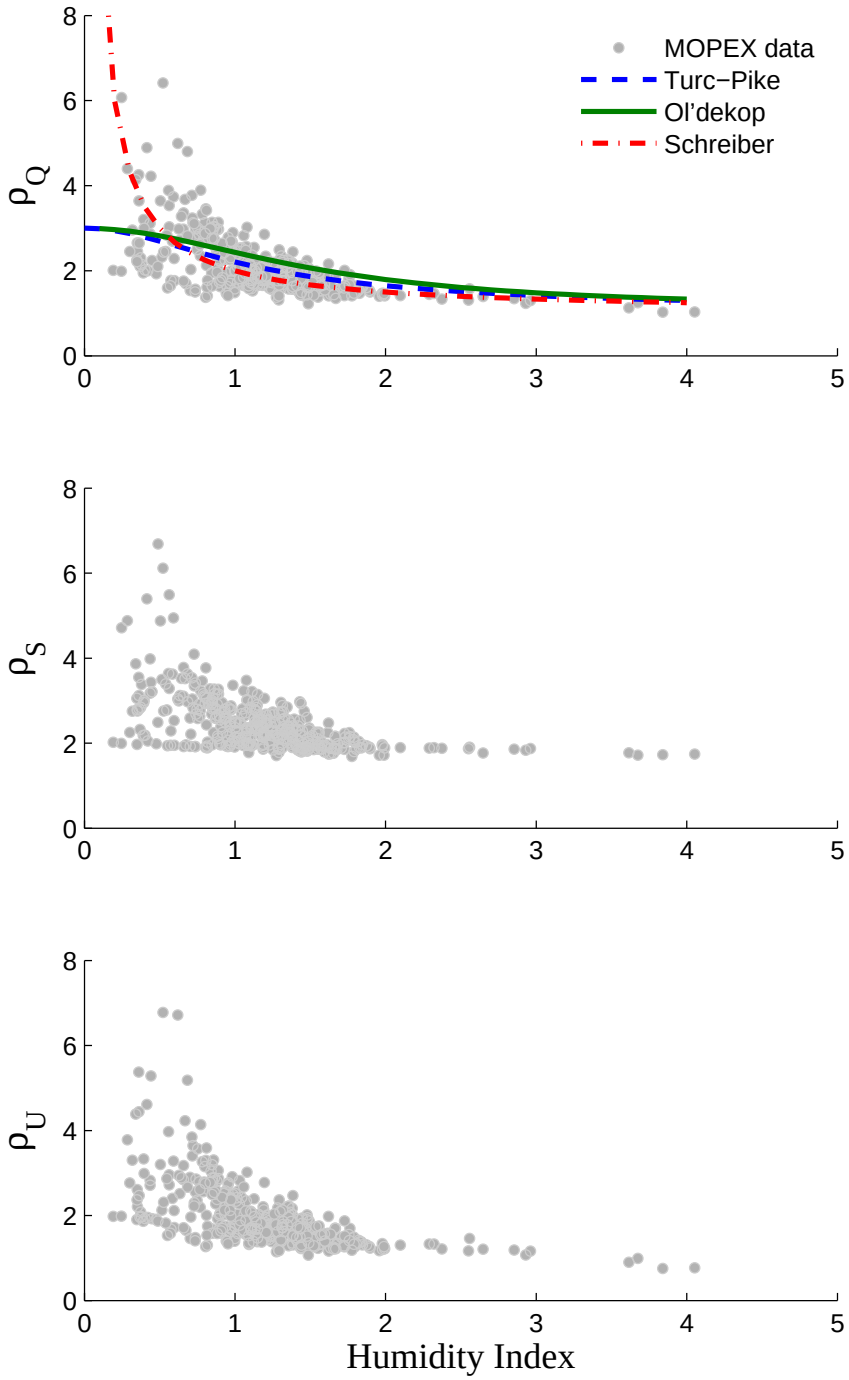

Figure 6.1: Relationships between elasticity and the humidity index, P/E_P. Elasticity is higher for total flow and both components in the arid sites, and converges to a common value in humid sites. Three relationships cited in *Dooge* (1992) are plotted for comparison.

Table 6.1: Overview of the estimated parameters for the Ponce and Shetty model and derived elasticities for the MOPEX dataset. Minimum, mean, maximum and standard deviation of the best estimates are shown, indicating the distribution across all the sites of the (individual sites' best estimate of) parameters and elasticities. The median absolute and relative error refer to the median level (between sites) of the uncertainty in sites' parameter and elasticity estimates.

	Minimum	Mean	Maximum	Std. Dev.	Median Abs. Error	Median Rel. Error (%)
W_P	1746	7635	123200	10386	906	18.9
$\lambda_S W_P$	6.40	181	617	132	84	65.3
V_P	75	3246	117081	10317	364	24.1
$\lambda_U V_P$	7.15	210	617	152	100	69.6
ρ_Q	1.02	2.08	8.38	0.70	0.15	7.98
ρ_S	1.70	2.38	6.08	0.57	0.24	10.28
ρ_U	0.75	1.94	10.96	0.88	0.20	11.79

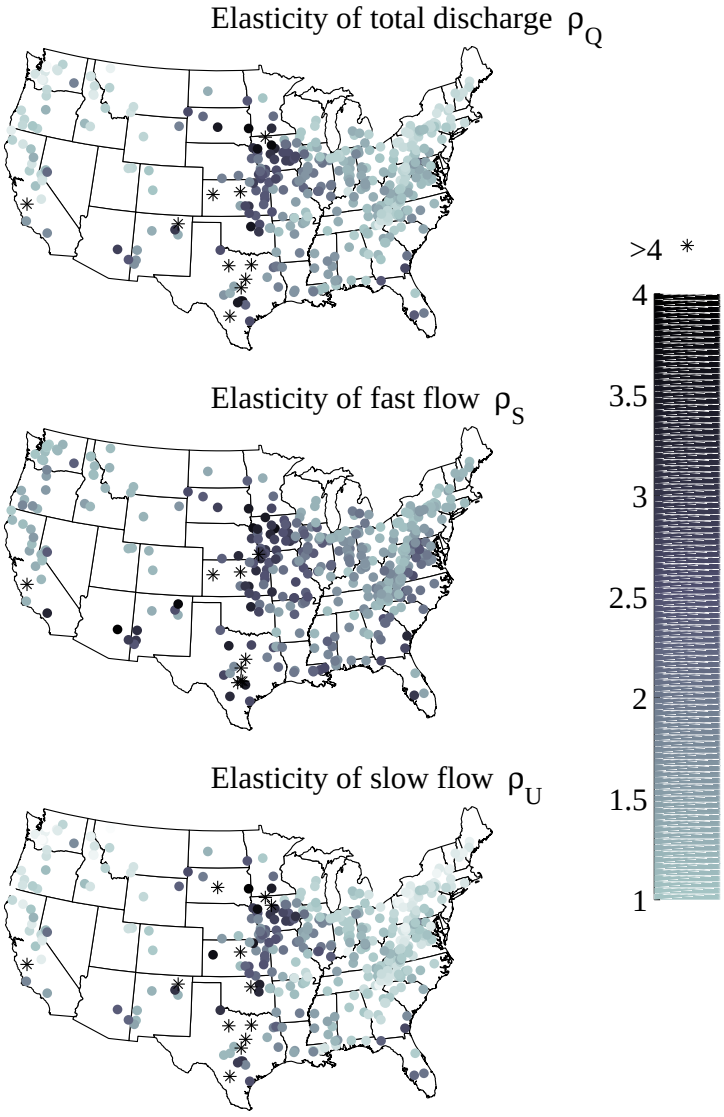

Figure 6.2: Elasticity of runoff components in the continental US.

6.3.2 Robustness of functional parameters and sensitivity results

Median absolute errors in the functional parameters were 907mm (or 19% of the best estimates of parameter values) for W_P, 364mm (24%) for V_P, 84mm (65%) for $\lambda_s W_P$, and 100mm (70%) for $\lambda_u V_P$. The percent errors for the thresholds are skewed because of the high relative error where the best estimate of the threshold is small, since an error of a given size is a large percentage of a 'best' value close to zero. Best estimates of parameters coincided closely with those in *Sivapalan et al.* (2010), which were fitted using a simple non-linear least-squares regression.

The median uncertainty in the elasticities were 8.0% (ρ_Q), 10.3% (ρ_S) and 11.8% (ρ_U), which is small compared to the range of variation between sites. This gives us confidence that we can make valid comparisons between sites. Absolute errors in the potentials were generally correlated with the best estimate, as were the errors in the threshold when they were less than approximately 50mm (results not shown).

6.3.3 Controls of the functional parameters on sensitivity

The runoff generation thresholds $\lambda_s W_P$ and $\lambda_u Vp$ had a much greater control over the elasticity than the wetting and vaporization potentials. We can illustrate the degree to which the differences in elasticity between sites are controlled by the functional parameters by plotting each elasticity against each parameter, as shown in Figure 6.3. Although both W_p and $\lambda_s W_P$ control ρ_S, and all four parameters control ρ_U and ρ_Q, the thresholds are by far the most important controls. In particular, the fast flow threshold almost uniquely determines the fast flow elasticity. Both exert very strong controls over the other elasticities.

The data suggest that the climate and long-term water balance exert some control on the thresholds. Plotting the threshold functional parameters, normalized by mean annual precipitation, against the mean annual Horton index (Figure 6.4), shows that in arid catchments (where Horton indicies ~ 1) the thresholds are a large proportion of annual precipitation, while in humid catchments (particularly where H is less than about 0.4), the thresholds are close to zero. Because the impact of the threshold on the water balance depends on its magnitude relative to the annual precipitation and wetting, this result implies that the thresholds exert a large control on the runoff in arid areas, and a smaller control in humid areas. To some extent the increasing relationship between the normalized threshold and H observed in Figure 6.4 is simply the result of the lower precipitation in arid areas used to do the normalization, rather than a systematic variation in the thresholds themselves, and so this result must be interpreted with care.

$$\frac{\lambda_s W_P}{\overline{P}} = \Lambda_S \approx \begin{cases} 1.46 \times (\overline{H} - 0.584) & \overline{H} > 0.584 \\ 0 & \overline{H} \leq 0.584 \end{cases} \quad (R^2 = 0.46) \tag{6.18}$$

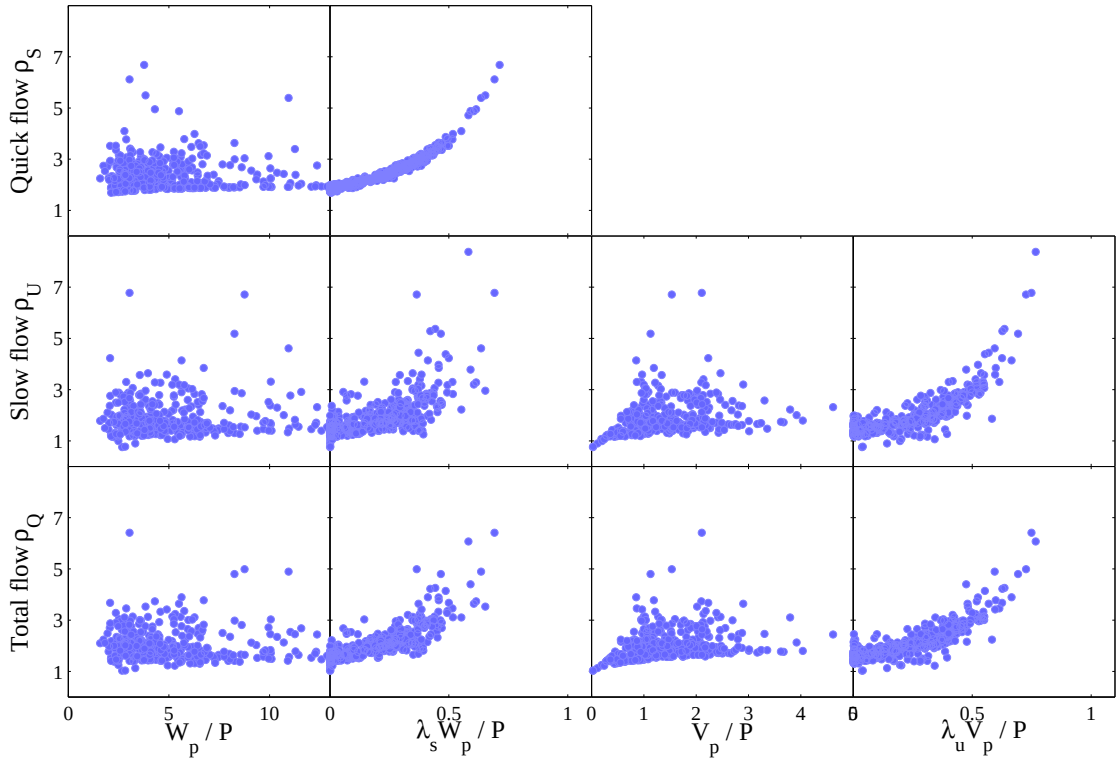

Figure 6.3: Relationship beween the predicted elasticity and the functional parameters (normalized by P). Differences between sites' sensitivity is mostly explained by differences in their threshold parameters $\lambda_s W_P$ and $\lambda_u V_P$. The upper potential W_P and V_P have less relative control.

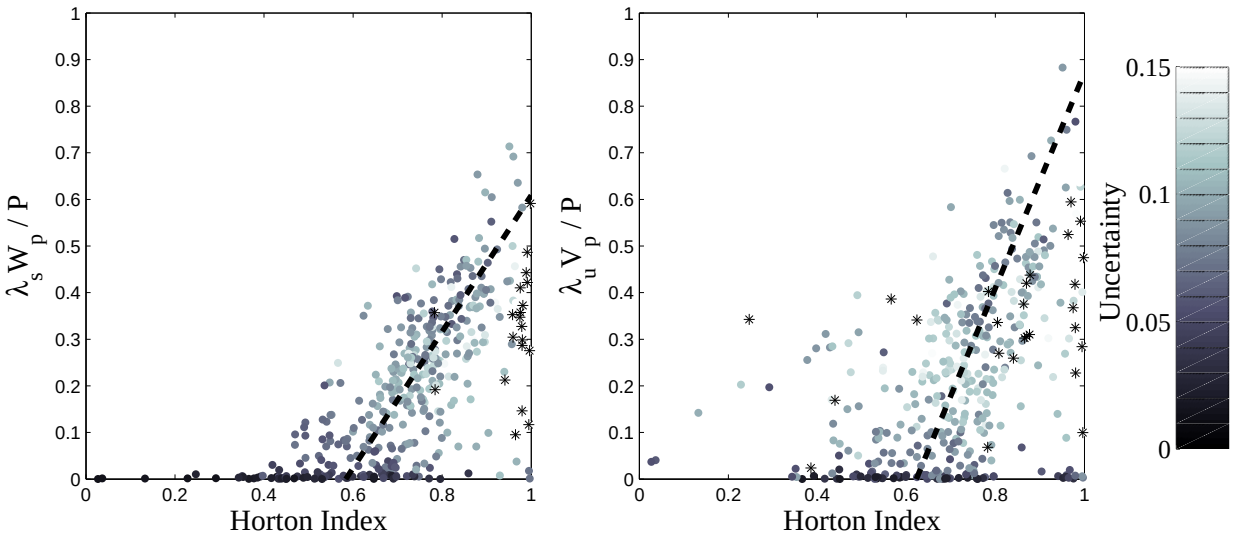

Figure 6.4: The thresholds for runoff production (normalized by annual precipitation) are directly correlated with the Horton index. Absolute uncertainty in the threshold parameters is shown by the tone (uncertainty greater than 0.15 is given by an asterix).

$$\frac{\lambda_u V_P}{\overline{P}} = \Lambda_U \approx \begin{cases} 2.30 \times (\overline{H} - 0.622) & \overline{H} > 0.622 \\ 0 & \overline{H} \leq 0.622 \end{cases} \quad (R^2 = 0.24) \tag{6.19}$$

6.4 Discussion: functional controls on climate sensitivity

Why are the thresholds such an important control on the elasticity, rather than the upper potentials? The importance of the thresholds arises largely because of the control they exert on the baseline amount of runoff generated and to which any increase is compared. This is illustrated in Figure 6.5, which shows the relationship between quickflow and precipitation at two sites. The two sites have very similar mean P and W_p, but different $\lambda_s W_P$. Both have a mean annual rainfall around 980mm, and have similar wetting potentials around 4000mm. The Genesee River site at Wellsville, NY has a threshold of $\lambda_s W_P = 100$mm, while the Embarras River at Sainte Marie, IL, has $\lambda_s W_P = 288$mm. Consequently the mean annual quickflow at the former site is larger: 165mm as opposed to 117mm. Under a 10% increase in precipitation (i.e. 98mm) both of these increase by about the same amount (34mm and 31mm). However because of the difference in the baseline amount of quick flow, the latter is a larger percentage increase. The value of ρ_S at the former is therefore lower at 2.0, while at the latter it is 2.6. Despite the scatter in the relationships shown in Figure 6.4, these sites follow the general pattern: the Genesee River site (with the lower threshold) is wetter than the Embarras River site, with a higher humidity index (1.4 versus 1.0) and lower Horton index (0.64 versus 0.81).

It could be argued that it is unsurprising to find a relationship between Horton index and the slow flow threshold, since this parameter was calibrated against the same data that was used to determine the mean Horton index. However, the threshold is determined by the interannual variability, and not just the mean of the data. Furthermore, there is no reason to expect a relationship between the Horton index and the fast flow threshold, because the Horton index is determined by the partitioning that occurs after the fast flow threshold has had its influence; yet this is the strongest of the relationships.

The relationship between the thresholds and the Horton index offers an opportunity to simplify the analysis of the links between the long-term water balance paritioning and the inter-annual variability. It is possible to express the sensitivities in terms of only two variables, the mean annual Horton index and a normalized wetting potential $W_P/\overline{P}$. This is achieved by using Equations 6.18 and 6.19 to eliminate the thresholds from the expressions for the elasticities (Equation 6.2), and then rearranging the P&S model predictions of the Horton index at the mean annual precipitation (given in *Sivapalan et al.* (2010)) to

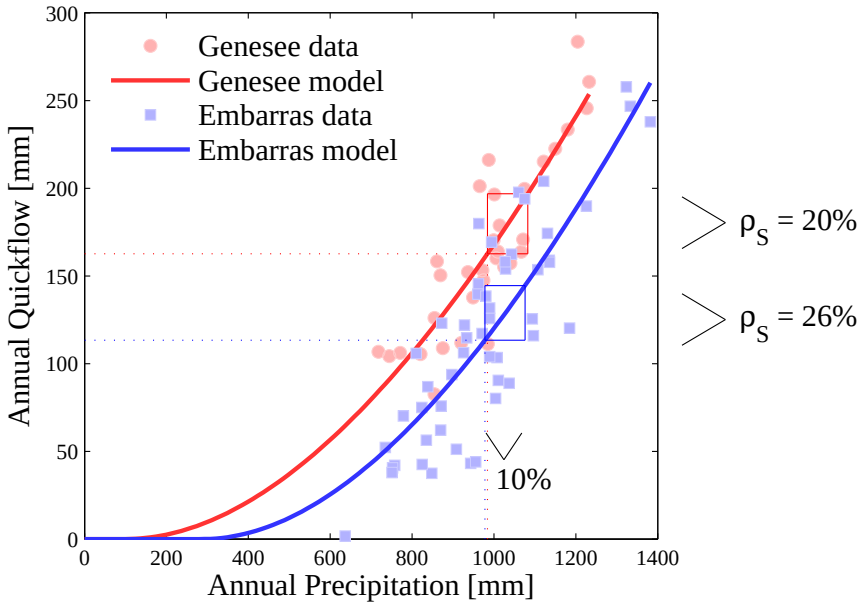

Figure 6.5: Quick flow as a function of precipitation for two very similar sites that differ mainly in their quick flow thresholds. See text for a discussion.

eliminate the vaporization potential V_P. With this procedure we obtain:

$$\frac{S}{P} = \frac{(1-\Lambda_S)^2}{W_P/\overline{P}+1-2\Lambda_S} \tag{6.20}$$

$$\frac{U}{P} = \frac{(1-H)\left(W_P/\overline{P}-\Lambda_S^2\right)}{W_P/\overline{P}+1-2\Lambda_S} \tag{6.21}$$

$$\rho_S = \frac{2W_P/\overline{P}+1-3\Lambda_S}{(1-\Lambda_S)(W_P/\overline{P}+1-2\Lambda_S)} \tag{6.22}$$

$$\rho_U = \frac{(W_P/\overline{P}-\Lambda_S)^2\left((H+1)W_P/\overline{P}+4\Lambda_S\Lambda_U-2\Lambda_U(W_P/\overline{P}+1)-(H+1)\Lambda_S^2\right)}{(W_P/\overline{P}+1-2\Lambda_S)\left(\Lambda_S^2-2\Lambda_S\Lambda_U+(\Lambda_U-1)W_P/\overline{P}+\Lambda_U\right)^2} \tag{6.23}$$

where for convenience we have used the shorthand Λ_S and Λ_U for the estimated normalized thresholds calculated using Equations 6.18 and 6.19. These expressions (plus Equation 6.9) can be used to predict the elasticity of runoff over the short term in terms of a long term average water balance property, the Horton index, and $W_P/\overline{P}$. Figure 6.6 compares the elasticities obtained from the MOPEX database with this function for fixed values of $W_P/\overline{P}$. The values of $W_P/\overline{P}$ used are representative of median (4.5) 10^{th} percentile (2.7) and 90^{th} percentile (10.1) in the MOPEX data. First, this figure demonstrates that the elasticities of all the components of runoff are functions of the mean Horton index. This is an interesting result, as it links the inter-annual variability of runoff to the long term average hydrologic functionality, as captured by the Horton index.

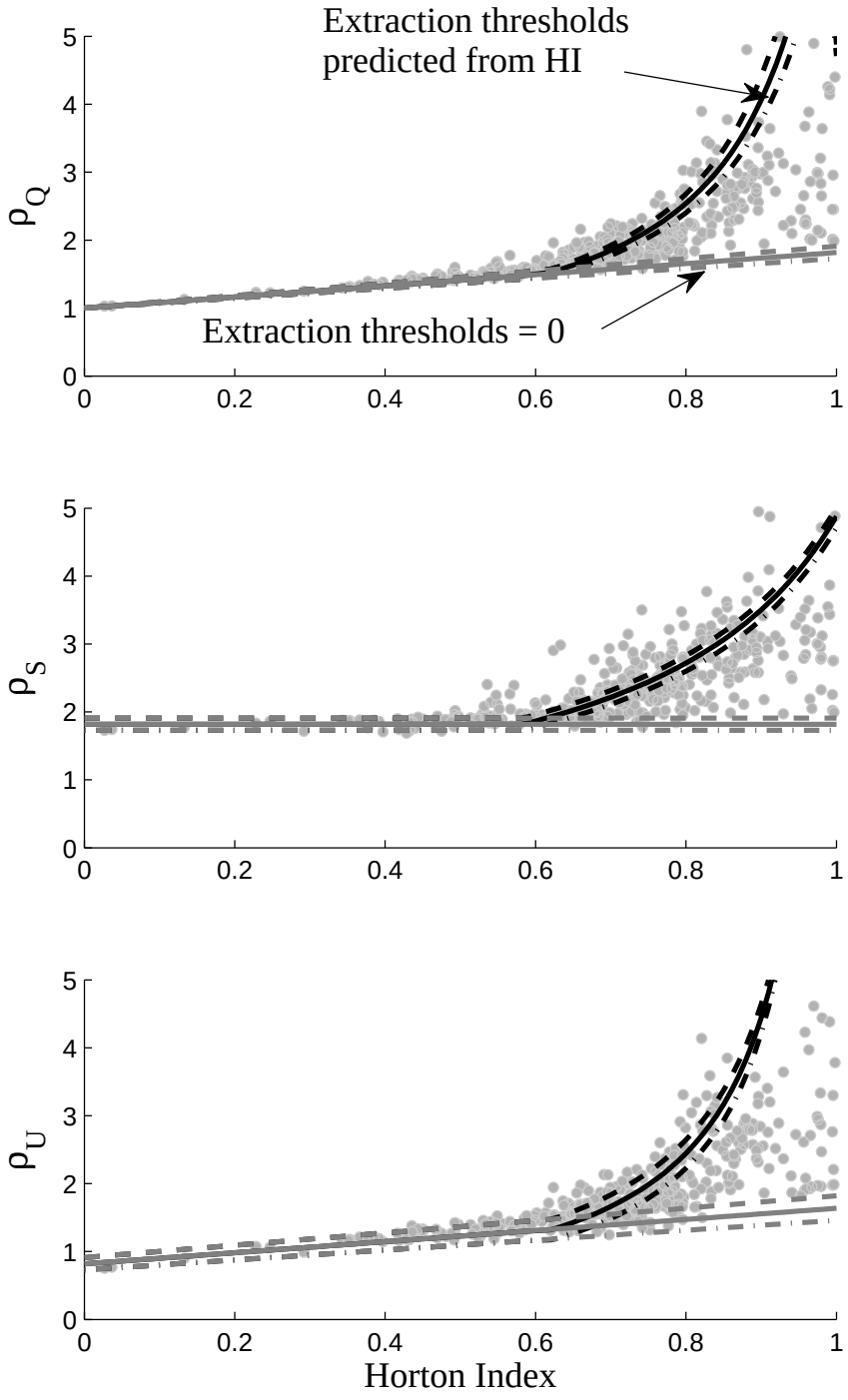

Figure 6.6: Relationship between the elasticity and the Horton index. Curves are gvien by equation 6.20. Black lines use thresholds predicted by regression, while the grey lines show the sensitivity when the thresholds are set to zero. The dashed, solid and dash-dot lines represent different values of $W_P/\overline{P}$. Values used are representative of median (4.5) 10^{th} percentile (2.7) and 90^{th} percentile (10.1) in the MOPEX data.

Second, it further demonstrates that the thresholds are the primary control on the runoff elasticity, particularly in dry climates. The gray lines illustrate the variation in the elasticity predicted by the P&S model if the thresholds are fixed at zero. In those cases, the elasticity is bounded at a maximum of 2 – in reality it can be much higher. The wetting potential $W_P/\overline{P}$ is a second-order control on the elasticity, at best. Much of the scatter in the relationship is therefore due to other processes affecting inter-annual variability that is not accounted for in this model.

6.5 Discussion: Comparison with other predictions of climate sensitivity

The results are directly comparable to other 'time for time' type analyses of precipitation sensitivity that appear in the literature. *Sankarasubramanian et al.* (2001) derived a map of streamflow sensitivities to changes in precipitation for the USA, based on at least 20 years of observations from 1291 catchments. They used a non-parametric estimator, compared it with model-based estimates of streamflow sensitivities in three catchments using Monte Carlo experiments and concluded that the non-parametric estimator is as or more robust, less biased and independent of model structure and parameter estimation procedures. Figure 6.7 compares the elasticites of total flow in the MOPEX dataset calculated using the P&S model and this non-parametric metric. The result shows that the methods are comparable, though the non-parametric method tends to predict lower values for the lower and upper ends of the distribution. The lower end values have greater uncertainty in the P&S model.

Based on the mapped results *Sankarasubramanian et al.* (2001) observed that snow dominated catchments tend to have the lowest streamflow sensitivities, as do catchments with very high humidity indices. Arid and semi-arid catchments tend to have the highest streamflow sensitivities, and regions where moisture and energy availability are out of phase have very high spatial variation of sensitivities. They compared their results with the results from *Dooge* (1992) who used the Budyko hypothesis to derive streamflow sensitivities, and concluded that the Budyko hypothesis is only valid in regions with high humidity indices but that in semi-arid catchments the non-parametric estimator yields considerable scatter around the theoretical values derived by *Dooge* (1992).

In Figure 6.1 we have plotted the sensitivities of total streamflow (a), quick flow (b) and slow flow (c) of all 377 catchments as functions of the mean humidity index. (Figure 6.1 can be compared to Figure 8 in *Sankarasubramanian et al.* (2001)). As in *Sankarasubramanian et al.* (2001), the streamflow sensitivity seems to converge to a value of 1 for very humid catchments. This result is consistent with *Dooge* (1992)

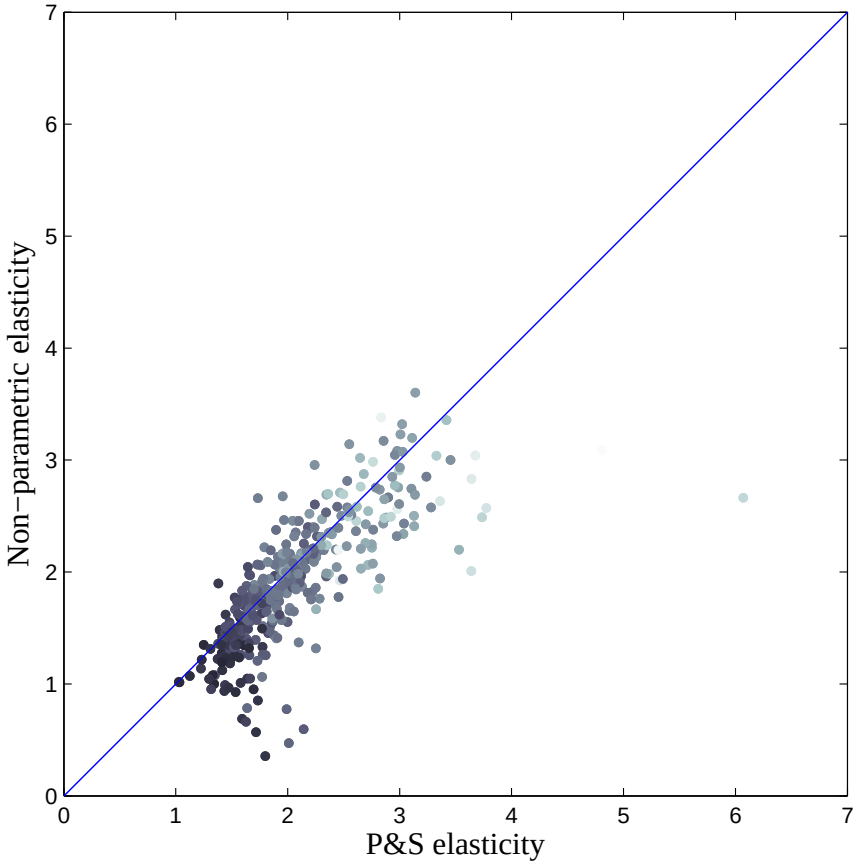

Figure 6.7: Comparison of estimated elasticity from the P&S model with the non-parametric approach of *Sankarasubramanian et al.* (2001). The non-parametric approach predicts lower elasticities at the upper and lower end of the distribution. Tone represents the relative uncertainty (light tone is higher relative uncertainty).

who derived analytical expressions of streamflow sensitivity to precipitation changes based on three empirical relationships (Ol'dekop, Turc-Pike, and Schreiber) that comply with Budyko's hypothesis. (These equations are empirical approximations of the Budyko relationship. The reader is referred to *Dooge* (1992) for details.) However, for very dry catchments our results indicate that streamflow sensitivity becomes very large and beyond the limit value of 3 as predicted by Ol'dekop and Turc-Pike parameterizations. The main difference between our results and those of *Sankarasubramanian et al.* (2001) is the predicted streamflow sensitivities for semi-arid regions. Our estimates never fall below the horizontal asymptote of 1, whereas the results reported in *Sankarasubramanian et al.* (2001) vary dramatically from very low (near zero) to high (4.5) sensitivities.

Sankarasubramanian et al. (2001) found that semi-arid catchments with very low streamflow sensitivity are located in Missouri and Pacific Northwest water resource regions (*Seaber et al.*, 1987). The western part of the Missouri water resource region is poorly covered by the MOPEX database, but MOPEX catchments located in the Pacific Northwest used in this study never exhibit streamflow sensitivities less than 1. The reason for this discrepancy is unclear. Part of it is due to the different method used, which introduces systematic differences at high and low values. It may also be due to the fact that different sets of catchments were used. The large variation of streamflow sensitivities can also be related to intra-annual variations in moisture and energy availability, as pointed out by *Sankarasubramanian et al.* (2001). Finally, it is possible that a negative covariance between annual precipitation and temperature that may exist in some of these semi-arid catchments (hot and dry versus cold and wet) is not taken into account in the P&S model. More research is needed to shed light on the possible causes of these differences, and to account for them.

In Dooge's work, Schreiber's method predicts infinite streamflow sensitivity as the humidity index approaches zero, and this seems to fit the general trend of our results well (Figure 6.1). Moreover, the general trend of all flow component sensitivities with humidity index is very similar. It is interesting to note that quick flow sensitivity seems to converge to a value slightly less than 2 for very humid catchments, while slow flow sensitivity converges to a value slightly more than 1. This suggests that for these humid regions, even though total streamflow changes proportionally to changes in precipitation, quick flow that will experience the greatest change.

6.6 Conclusions

While many previous studies have examined streamflow elasticity to changes in precipitation (*Schaake*, 1990; *Němec and Schaake*, 1982; *Dooge*, 1992; *Risbey and Entekhabi*, 1996; *Dooge et al.*, 1999; *Sankarasubramanian*

et al., 2001), the perspective and insights offered in this work are unique. The P&S (Ponce and Shetty) approach parameterizes the way catchments partition, store and release water; that is, their function, abstracted to a high level. This approach has allowed us to make the several new observations, which warrant reiteration.

The P&S model divides discharge into fast and slow components, allowing the sensitivity of these to be assessed independently. It was observed that in US catchments in the MOPEX database, estimates of the elasticity of total discharge were found to be around 2.1 on average; the fast component of streamflow tended to have a higher elasticity, at around 2.4 on average, indicating that this component was more sensitive to inter-annual variability in precipitation; the elasticity of slow flow was lower at around 1.9. The observation of different elasticities for each flow component is significant for understanding how the structure of the hydrograph may change under a changing climate.

The functional model allowed us to look for systematic controls on the observed elasticity in terms of the thresholds and the potentials that encapsulate the catchment function. We conclude that the threshold values exert the strongest control. In the case of quick flow the threshold for generating quick flow almost entirely controls the elasticity. This was found to be because these parameters are the primary determinants of the underlying amount of flow that any change is being compared to.

Moreover, there is a relationship between these threshold values and the long term hydrologic partitioning through the Horton index $H = V/W$. The thresholds were a high proportion of mean annual precipitation in arid sites (that is, with a low humidity index), and at sites where H is large. V is mainly water use by vegetation and W is related to water holding capacity of the catchment. Both V and W are determined by the catchment characteristics such as vegetation type and soils (see also (*Voepel et al.*, 2010) and (*Zanardo et al.*, 2010)). Specifically, H combines ecosystem and soil response to climate drivers (P and Ep) and as such captures how catchments have evolved (in terms of ecosystem dynamics and storage capacity) under prevailing climate (see also *Sivapalan et al.* (2010) and *Troch et al.* (2009b)).

We were able to derive analytical expressions that relate the elasticities to long term mean H, and those expressions capture very well the general relationship between sensitivity and H. These relations can form the basis for a space-for-time substitution to understand how catchments may respond to climate change. We thus effectively combined time-for-time with space-for-time approaches to hydrologic change analysis. The derived elasticities predict catchment response to short-term (decades) change in P while the relationships between the sensitivities and Horton index (i.e., humidity index) suggest how catchment response will change at larger time scales (centuries to millennia) when the system has had time to adapt to such changes in climate and have evolved towards an equilibrium state.

Deriving a more robust method for linking space-for-time and time-for-time, and deeper insights into the nature of the functional controls on catchment water balance, will depend on being able to better link the thresholds (and the upper potentials) to the landscape properties that control them. The thresholds are the result of many process interactions that may be unique to a particular place. Understanding how they emerge serves as a basis for making comparisons between catchments even where these processes differ. A full understanding of the physical controls on these emergent processes is an important avenue for future work. The functional parameters offer a basis for framing questions about controls on catchment behaviour that can be answered using more detailed physically-based hydrologic models.

The functional parameters used here arise from the interactions of a raft of processes and factors operating at sub-annual times scales, such as the seasonality of the climate, the timing of storm inputs and vegetation phenology. These processes are themselves subject to other sources of interannual variability, and these contribute to the scatter in the observed partitioning, and uncertainty in the appropriate functional parameters. An important example is the role of interannual variations in temperature on the amount of precipitation that falls as snow, and the rate and timing of snow-melt. It is possible to imagine an extension to the model that incorporates an additional partitioning of snowfall (separate from rainfall) into sublimation versus snowmelt. However, such an extension makes little sense without considering interannual variations in temperature, and must be left for future work.

The functional parameters also provide a basis for examining the kinds of changes in landscape biophysical properties over time that might occur either due to exogenous forces such as global climate change, or endogenous changes such as land use and land cover change. The difference in sensitivity between the fast and slow fow components identified here are especially interesting given that changes in the fast and slow flow components of the hydrograph are often associated with some distinct classes of water management issues (e.g. water quality issues are often associated with high flows, while in-stream habitat availability during dry periods are associated with low flows). Hypotheses can be quite easily generated in this framework. For example, many of the processes of urbanization in a catchment may lead to a reduction in the fast runoff threshold and wetting potential as impervious areas replace infiltrating surfaces. Replacement of deep-rooted perennials with shallow-rooted annual crops may lead to a reduction in the vaporization potential. Extraction of groundwater from superficial aquifers may lead to increases in the slow flow threshold, as more rainfall is required to generate significant subsurface flow towards streams. All these hypotheses can be easily tested given a sufficiently long pre- and post- treatment record. Alternatively, the framework described here can be used to interpret the effects of changes in parameters or inputs on detailed models of water balance, and so generate more generalizable insights.

More work is also required to investigate further controls on the annual water balance, and how these will shift in the future. In areas where snow is an important control on the water balance, shifts in snow versus rainfall and the timing of rainfall are known to be very important (*Leung and Wigmosta*, 1999; *Nijssen et al.*, 2001). It is also particularly important to understand how intra-annual variability (seasonality, phase of precipitation cycles relative to cycles of energy availability, etc.) further affects the sensitivity.

6.7 Acknowledgments

Work on this paper commenced during the Summer Institute organized at the University of British Columbia (UBC) during June-July 2009 as part of the NSF-funded Hydrologic Synthesis project, "Water Cycle Dynamics in a Changing Environment: Advancing Hydrologic Science through Synthesis" (NSF Grant EAR-0636043, M. Sivapalan, PI). We acknowledge the support and advice of numerous participants at the Summer Institute (students and faculty mentors). Partial support was provided by NSF grants EAR09-11205 (PI: Sivapalan) and EAR06-35752 (PI: Wagener). Special thanks due to Mateij Durcik for help with the background data preparation and analysis of the MOPEX dataset. Thanks also due to Marwan Hassan and the Department of Geography of UBC for hosting the Summer Institute and for providing outstanding facilities, without which this work would not have been possible. The authors would also like to thanks Andrew Neal, Paul Brooks and Sally Thompson, whose feedback on a draft manuscript greatly improved the final paper

Chapter 7

Scaling of ecohydrologically mediated water balance partitioning

[1] *Comparisons of point-scale and catchment-scale water balance is suggestive of systematic biases in water balance across scales. Thompson et al. (2011), hypothesized that feedbacks between A) vegetation as a driver of evapotranspiration, and B) water availability as a driver of vegetation distribution could generate non-trivial spatial scaling and organization in both the distribution of vegetation and water balance along a convergent network of flow paths. Here this hypothesis is explored using a simple network model of steady-state water-balance and vegetation density along a network. The model suggests that such organization is controlled by catchment properties related to aridity, the network topology, the sensitivity of the vegetation response to water availability, and the point-scale controls on partitioning between evapotranspiration and lateral drainage. Dimensionless numbers derived from the model capture the influence exerted by these controls. The feedbacks generated spatial dependence in catchment scale hydrologic variables, water balance and parameters describing hydrological partitioning. The proposed model suggests a theoretical framework to connect water balances at patch and catchment scales.*

7.1 Introduction

Prediction of hydrologic responses under change is made extremely challenging by the tremendous heterogeneity in landscape structure and climatic inputs; the tight interconnections between hydrological response and climatic, ecological, geomorphological, pedological and anthropological processes, all of which are subject to human alteration and endogenous and exogenous variability (*Istanbulluoglu and Bras*, 2005; *Vitousek*, 1994); and the multi-scale variability of resulting hydrological dynamics. Observations of hydrologic dynamics at the whole catchment scale are simplified by the lateral boundary conditions and flow aggregation through the river network. However, physical understanding of hydrological processes is often greatest at point scales where heterogeneity is reduced. Point-scale predictions are notoriously difficult to relate to catchment-scale responses (*Blöschl and Sivapalan*, 1995) leading to a gap between the scales at which processes occur and are understood, and the scale at which observations are made and prediction is needed.

Fortunately, the structure and dynamics of catchments results from long-term co-evolution, and catchments consequently display significant self-organization in hydrological and biophysical properties (*Hopp et al.*, 2009; *Wagener et al.*, 2004; *Koster et al.*, 2000). Identifying emergent properties or patterns in this organizational structure can constrain relationships across processes and scales, simplifying the problem of hydrological prediction (*Koster et al.*, 2000; *Ducharne et al.*, 2000; *McDonnell et al.*, 2007; *Blöschl*, 2006;

[1] An edited version of this work has been accepted for publication in Water Resources Research as: Thompson, S E, C J Harman, P A Troch, P Brooks and M Sivapalan, Spatial Scale Dependence of Ecohydrologically Mediated Water Balance Partitioning : A Synthesis Framework for Catchment Ecohydrology, *Water Resources Research*, 2011, in press. Copyright 2011 American Geophysical Union. Reproduced/modified by permission of American Geophysical Union. All figures, tables and data were created by Ciaran Harman unless otherwise indicated.

Sivapalan, 2003b). Two examples of this approach that have yielded considerable advances in hydrology are the geomorphological instantaneous unit hydrograph or GIUH (*Rodriguez-Iturbe and Valdes*, 1979; *Mesa and Mifflin*, 1986), which uses the characteristics of the channel network to predict catchment storm response; and the topographic wetness index, which uses topographic features to characterize spatial patterns of soil wetness and forms the basis for many current models (e.g. TOPMODEL and RHESSYs (*Beven and Kirkby*, 1979; *Band et al.*, 1991, 1993)). There is potential for other emergent patterns in catchment properties to be identified and used in a similar manner. In particular, the wide availability of high resolution aerial photography, as well as advances in aerial and ground based LIDAR (*Lefsky et al.*, 2002), now offers unprecedented levels of information about the spatial distribution of vegetation in catchments.

Motivated by the prospect that spatial organization of vegetation might form the basis for a new set of emergent relationships to constrain hydrological processes at catchment scales, *Thompson et al.* (2011) explored patterns of spatial scale dependence in the coupling of vegetation distribution and hydrological function in watersheds. Vegetation mapping suggests that vegetation cover and type in many catchments are influenced by patterns of water availability. These patterns may even persist in highly disturbed environments (see Figure 7.1). Thus, hydrological relationships inferred from vegetation patterns can be usefully applied across a wide array of sites and scales.

Moreover, understanding vegetation water use and its scaling has the potential to explain a significant proportion of the water balance and its variability. Point-scale controls on water balance and soil moisture due to vegetation are increasingly well understood (*Guswa et al.*, 2002; *Rodriguez-Iturbe et al.*, 2007) and can be envisaged as driving the partitioning between vertical and horizontal water fluxes (or 'green' and 'blue' water) at a point (*Falkenmark*, 1997). Spatial organization and scaling arise primarily due to spatial variation in the horizontal components of the flux, which, via either surface or subsurface redistribution subsidizes downstream or downslope points with water in addition to that supplied by rainfall (*Puigdefabregas et al.*, 1999; *Yu et al.*, 2008; *Valentin et al.*, 1999). The lateral subsidy reflects and integrates upslope or upstream structures and processes, including connectivity, slope, convergence and water balance partitioning. Spatial structures in vegetation are known to naturally arise in response to water availability (*Caylor et al.*, 2005; *Scanlon et al.*, 2007; *Rietkerk et al.*, 2004), at least in arid or semi-arid environments. Because of the two-way coupling between the lateral subsidy (as a driver of moisture availability) and the presence of vegetation (as a driver of local partitioning), vegetation spatial organization is hypothesized to be both a control and a signature of hydrological processes.

In this chapter we present a simple water balance model and use it to begin exploring the spatial organization of hydrology and vegetation around a convergent flowpath network, and the implications of this

organization for the scaling of the water balance. The model has two key features which create the potential for non-trivial spatial organization: i) the network defines a potential energy gradient and thus a direction of water accumulation, and (ii) vegetation cover and transpiration are treated as being co-dependent, allowing the patterns of vegetation organization and water balance along the imposed network structure to arise naturally along the network. In Section 2 the model is present and key results are derived. Following that the implications of these results for a catchment-scale understanding of eco-hydrology is discussed is Section 3.

7.2 A simple model of water balance and vegetation coupling on a hierarchical flowpath network

7.2.1 Model formulation

The water balance partitioning framework used in this network model is based on that suggested by *L'vovich* (1979), which formed the basis of the water balance model later developed by of *Ponce and Shetty* (1995b,a). The original model partitions rainfall into three components: vaporization V, equivalent to ET, the rapid runoff response Q_S which may be taken as consisting of overland flow , subsurface stormflow and interflow, and the slow runoff response Q_U, which approximates baseflow. Partitioning is treated as the outcome of competing demands for water in the catchment , e.g., between subsurface drainage and evapotranspiration, or between infiltration and overland flow: rainfall is firstly partitioned into wetting $W = Q_U + V$, and Q_S, and the wetting fraction is then partitioned between Q_U and V (see Figure 7.2). For example, *Ponce and Shetty* (1995b) described the partitioning in terms of assumed functional forms with associated coefficients that determine the potential for wetting W_P and vaporization V_P, and the thresholds needed to generate runoff $\lambda_{Q_S}\ W_P$ and $\lambda_{Q_U}\ V_P$. In this model the L'Vovich formulation is extended to allow an explicit treatment of vegetation, and investigation of water balance partitioning along a network.

Figure 7.2A illustrates the network structure applied in the model, which is assumed (for simplicity) to be a simple bifurcating network. The 'network' here is phenomenological in nature and should be thought of as representing the connectivity of all flow paths in the catchment, and not solely the channel network. The different process controls on water balance that apply on hillslopes, in the riparian zone and within the channel network are not explicitly resolved, and left for future research. The water balance equation for any link in the network at any level in the hierarchy is:

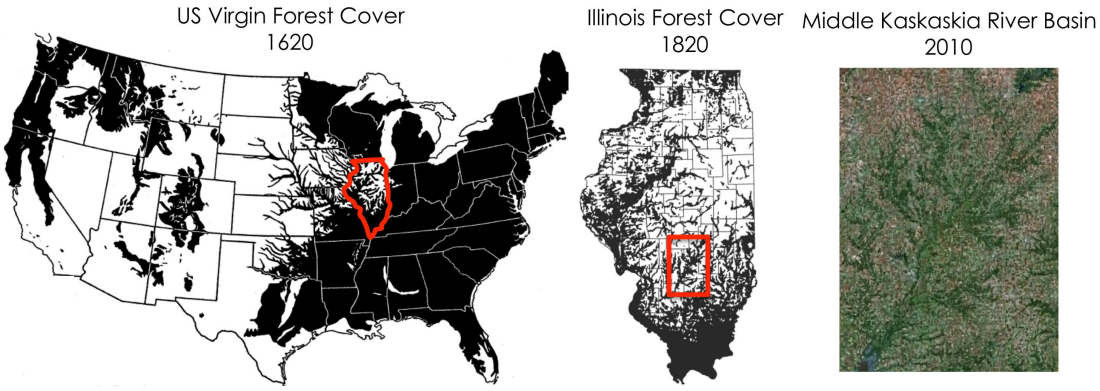

Figure 7.1: Virgin forest cover in the US at the time of colonization appears to follow a gradient from complete absence to complete presence across the continent, and was strongly organized by the river network in mesic climates. The self-similarity of this vegetation coverage is reflected in the historical forest cover of the state of Illinois. Interestingly, despite the high level of clearing and land disturbance in Illinois, contemporary patterns also preserve the remnants of this spatial pattern, although the degree to which this reflects water availability, the suitability of riverine land for agriculture or deliberate land management practices is unclear. Images sourced from *Greeley* (1925), *Iverson* (1991) and Google Earth (USDA Farm Service Imagery, ©2010 Digital Globe, ©2010 Google). Figure by Sally Thompson.

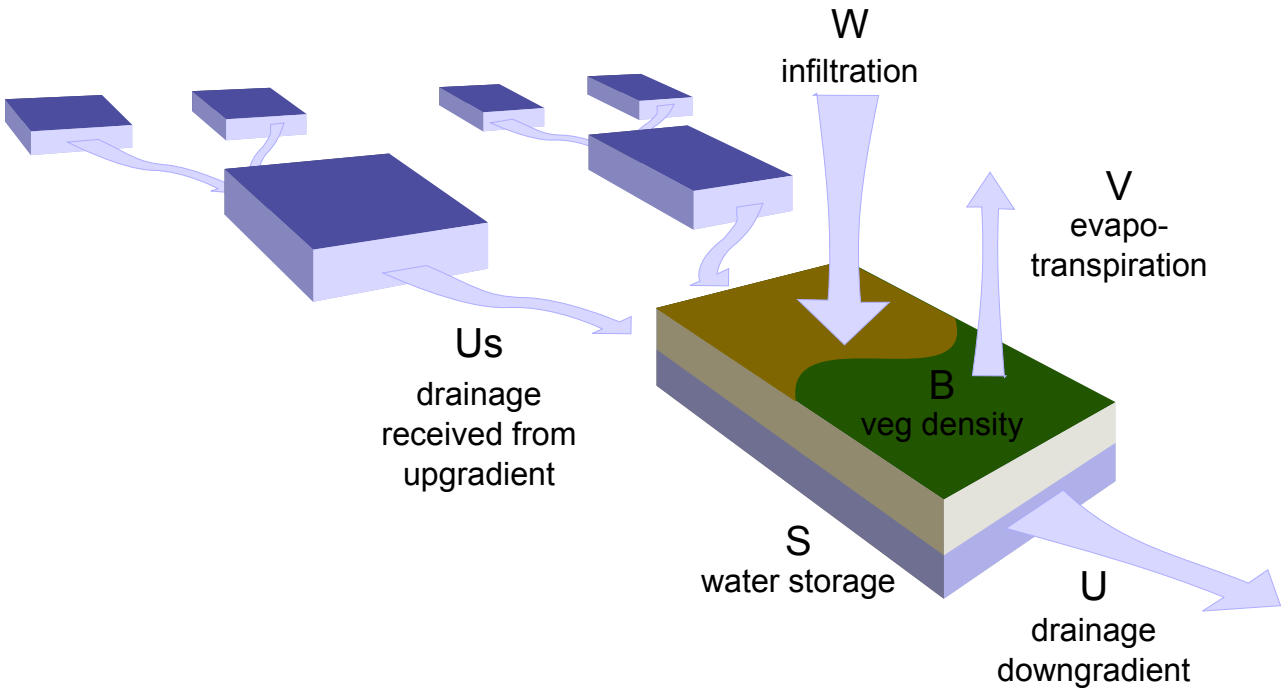

Figure 7.2: A) Vegetation mediates partitioning at a point. Flow paths in the catchment may be visualized as a network of links (each represented by a 'slab' in this figure). A downslope subsidy U_S provided by the sum of contributions from up-gradient contributing areas. The subsidy and the local wetting W are partitioned into vaporization V and an additional downslope contribution as mediated by local vegetative cover and properties. Local vegetation cover B controls partitioning and depends on water availability.

$$\frac{dS}{dt} = W + \sum Q_{U_s} - Q_U - V \tag{7.1}$$

where S is the local storage (a lumped term incorporating both saturated and unsaturated stores), W is the wetting due to rainfall, $\sum Q_{U_s}$ is the subsidy from links located immediately upstream of the local link, V is the local vaporization, and Q_U is discharge from the local link, which provides a water subsidy to the downstream link. In a bifurcating network, as used here, each link contributes Q_U to one downstream link and (with the exception of the exterior links) receives it from the two up-gradient links. For simplicity, we solve the model at steady state, neglecting the dynamics of Q_S or transients in the storage dynamics. Thus, Equation 7.1 can be re-written as:

$$Q_U = \sum Q_{U_s} + W - V \tag{7.2}$$

The steady-state water balance has to be solved iteratively on the network moving down-gradient from the exterior links. W is externally prescribed for the whole network, and the subsidy $\sum Q_{U_s}$ is generated from the upstream links, leaving 2 unknowns in the water balance: Q_U and V. Constitutive relations for Q_U and V are needed to close the system of equations. The flow and vaporization are treated as functions of the storage S in the link:

$$V = V_{max} B \times \begin{cases} \dfrac{S}{S_m} & 0 < S < S_m \\ 1 & S \geq S_m \end{cases} \tag{7.3}$$

$$Q_U = k_U S \tag{7.4}$$

We approximate vaporization V as transpiration, which has an upper limit given by the product of the fractional cover of perennial vegetation, B ($0 < B < 1$) and a maximum specific transpiration rate, V_{max}, set by atmospheric demand. We allow water stress to limit transpiration when storage S falls below a threshold value S_m. Under water-stressed conditions (i.e. when $S < S_m$), transpiration scales linearly with the fraction S/S_m. Similarly, we express Q_U as a linear function of S, which is often considered as a reasonable representation of the slow component of discharge (*Palmroth et al.*, 2010).

To complete the specification of the governing equations, we relate the fractional vegetation cover B to vaporization V at each link. This coupling represents the control of water availability for vaporization on carbon assimilation (*Sankaran et al.*, 2005; *Huxman et al.*, 2004):

$$B = \frac{V}{V + V_B} \tag{7.5}$$

Here V_B is a half-saturation parameter determining the water availability at which canopies close (lower for water tolerant species e.g. C4 grasses, or under strongly light limited conditions e.g. at high latitudes).

Equations 7.2 to 7.5 constitute a closed set equations linking water balance and vegetation cover. The feedback between water balance and vegetation cover generated by Equations 7.3 and 7.5, combined with the network structure, enables the generation of spatial patterns of vegetation cover and water balance. There are 4 parameters in the equations, representing the storage at which water stress begins (S_m), a drainage parameter which is a combination soil permeability and topographic slope (k_U), vegetation type (V_B) and evaporative demand (V_{max}). W is the main climatic driver, and is externally specified.

7.2.2 Solution of governing equations in a link of the network

To isolate the relationship of the fluxes and state variables to the parameters the equations can be solved for isolated links in the network. These solutions are most naturally expressed in terms of three non-dimensional similarity indices: the aridity index $R = V_{max}/W$; an index of the drainage competitiveness, $D = k_U S_m/V_{max}$; and an index of the vegetation adjustment to climate $G = V_B/V_{max}$. In addition we can define a 'locality index' $L = \sum Q_{U_s}/W$, which represents the relative importance of inputs of drainage from up-gradient. The solutions for the fluxes can then be expressed in normalized forms as Q_U/W and V/W. The normalized vaporization flux is equivalent to the local Horton index $H_L = V/W$.

Three solutions to the system of equations emerge. The first is a trivial solution that arises when vegetation is absent ($B = 0$) and transpiration is zero ($V = 0$). This is the only solution with non-negative values of V and B when $V_B > V_{max}$ (that is, $G > 1$) under unstressed conditions, or when $V_B > V_{max}(W + \sum Q_{U_s})/k_U S_m$ (that is $G > (1+L)/DR$) under stressed, suggesting that this case represents vegetation poorly adapted to the moisture conditions. Drainage in this case is simply equal to the sum of the inputs: $Q_U = W + \sum Q_{U_s}$, or in dimensionless terms: $Q_U/W = 1 + L$.

The other solutions correspond to the stressed and unstressed transpiration cases. It can be shown that stressed transpiration will occur when the inputs from wetting and the subsidy are sufficiently small,

specifically when $1 + L < R(1 - G + D)$. In this case the following solutions hold:

$$\frac{Q_U}{W} = \frac{D}{1+D} \cdot (1 + L + G \cdot R) \tag{7.6}$$

$$\frac{V}{W} = \frac{1 + L - D \cdot G \cdot R}{1 + D} \tag{7.7}$$

$$B = \frac{1 + L - D \cdot G \cdot R}{1 + L + G \cdot R} \tag{7.8}$$

In the unstressed case the solution is much simpler, and V and B do not depend on the subsidy L:

$$\frac{Q_U}{W} = 1 + L - R\,(1 - G) \tag{7.9}$$

$$\frac{V}{W} = R\,(1 - G) \tag{7.10}$$

$$B = 1 - G \tag{7.11}$$

In addition to parameters R, G and D, one further non-dimensional parameter β (where $0 < \beta < 1$) defines the network structure. A network with N links is generated by starting from the outlet and moving to the next confluence. At a confluence the remaining links are divided into two parts containing $\beta(N-1)$, and $(1-\beta)(N-1)$ parts, each assigned to one upstream branch of the confluence. This process is repeated recursively until the links are exhausted, generating a deterministic network that ranges from perfectly bifurcating when $\beta = 0.5$, to perfectly feathered (one main-stem surrounded by first-order channels) when $\beta = 0$ or 1.

7.2.3 Solving the model along the network

The model equations can be solved numerically on the network by iterating the solution to Equations 7.2 to 7.5 down-gradient from the exterior links to the outlet. For the special case of a symmetrically bifurcating network (i.e. $\beta = 0.5$) the network model may be solved analytically. In such a network every link of stream order k has two links of order $k-1$ upstream of it, for a total accumulated upstream area of $2^k - 1$ (including its own area). In this case, L in a link of order k is twice the value of Q_U/W in links of order $k-1$, i.e. $L = \sum Q_{U_s}/W = 2Q_{U_{k-1}}/W$. This creates a recurrence relation generating a geometric series in $2D/(1+D)$. For water-stressed conditions, this series can be solved to give Q_U, V and B as a function of scale k:

$$\frac{Q_{Uk}}{W} = \frac{1-\left(2\frac{D}{D+1}\right)^k}{1-D} D\,(1+GR) \tag{7.12}$$

$$\frac{V_k}{W} = \frac{\left(2\frac{D}{D+1}\right)^k (GR+1) - DGR - 1}{D-1} \tag{7.13}$$

$$B_k = 1 - \frac{(D-1)GR}{\left(\left(2\frac{D}{D+1}\right)^k - 1\right)(GR+1)} \tag{7.14}$$

The 'catchment' Horton index H at scale k, is determined by the ratio of mean vaporization over all up-gradient links to the wetting. This is simply one minus the ratio of the drainage Q_{Uk}, normalized by the up-gradient area $(2^k - 1)$ and the wetting W:

$$H_k = 1 - \frac{Q_{U_k}}{W(2^k-1)} = 1 - (GR+1)\left(\frac{\left(\frac{2D}{D+1}\right)^k - 1}{2^k - 1}\right)\frac{D}{D-1} \tag{7.15}$$

Expressions 7.12 to 7.15 are only valid under water stressed conditions where V is explicitly dependent on ΣU_S and consequently the network structure. The patterns that arise from this model are explored in the next section.

7.3 Discussion

7.3.1 Vegetation and water balance patterns along the network

The network model generates patterns of expanding vegetation cover (B) and water balance (expressed by the catchment Horton index H) in the down-gradient direction. Examples of such patterns are shown in Figure 7.3 (model parameters are given in the caption) which compares model output at each catchment scale to that obtained in the absence of the subsidy, and thus isolating the effects of the subsidy on catchment water balance. Figure 7.3 (A) shows a histogram of up-gradient contributing areas of a range of sizes, (B) shows the vegetation cover B, both in terms of its local value (computed numerically and analytically using Equation 7.14) and its spatial average over the up-gradient area, and (C) shows the local and catchment Horton index (V / W) computed using the numerical model and the analytical solution in Equations 7.13 and 7.15.

This example illustrates characteristic patterns driven by the subsidy of water down-gradient. The local value of the Horton index in the external links in this case is quite low at 0.5, indicating that only 50% of

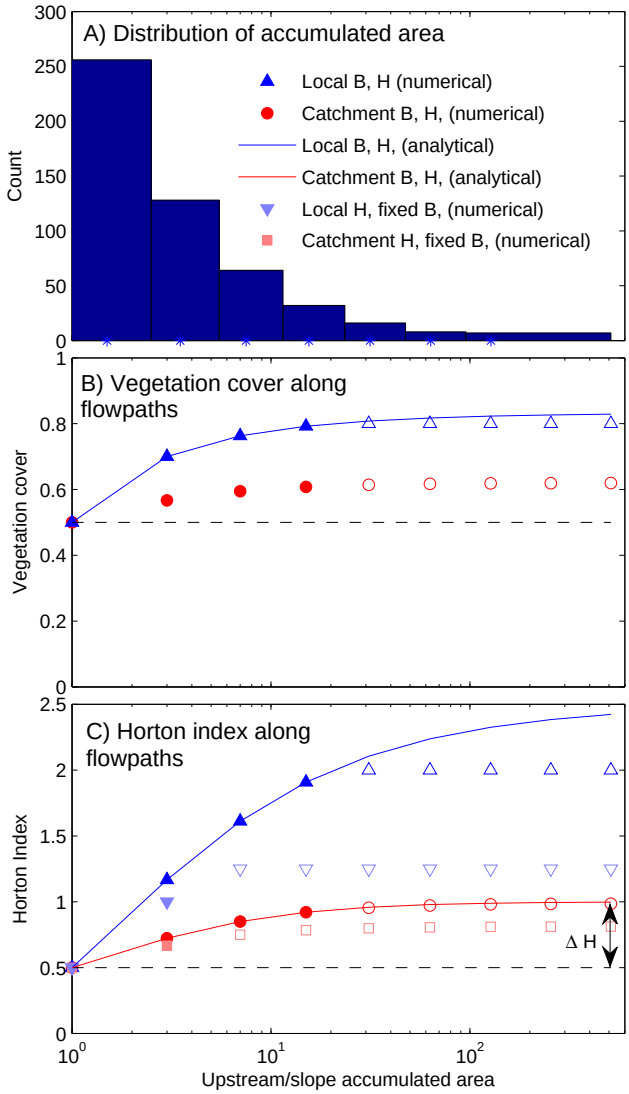

Figure 7.3: Model output for a system with $N = 511$ links, and $\beta = 0.5$, $R = 2.5$ (a dry system), $D = 1.5$ (Q_0/V_{max}), and $G = 0.2$ (V_B/V_{max}). (A) The proportion of the area with up-gradient contributing areas of different amounts (from 256 external links with area 1 to a single link with area 511 at the outlet), (B) vegetation index B, locally and averaged over the accumulated areas, as a function of accumulated area (closed symbols: water limited, open symbols: energy limited), and (C) Horton index for the accumulated areas (total V / total W) as a function of the accumulated area along the flowpath leading to each link in the system

W is used locally for vaporization, and the rest is passed down the network. Vegetation at this point is also relatively low, at $B = 0.5$, and is in the water stressed regime. In the case shown in Figure 7.3, these small order links comprise most of the catchment area. Further down the network, B increases as the subsidy effects increase water availability. Storage S also increases down-gradient, reducing the water stress and increasing transpiration rates, leading to a rapid increase in the local Horton index. The catchment Horton index also increases as a result of the increased V, and approaches 1. In the higher-order links ($k > 4$), the increased storage due to the up-gradient subsidy leads to a transition to unstressed transpiration, and local values of B and V stabilize.

The pattern of downstream changes in water balance and vegetation shown in the above example is for one specific case. More generally it can be shown that if the drainage efficiency is low ($D < 1-G$) and the system is sufficiently arid ($R > 1/(1 - D - G)$), the subsidy effect slowly increases down-gradient, asymptotically approaching a maximum value where the wetting and subsidy balances the increased vaporization due to the expanded vegetation cover. Otherwise, in wetter or more rapidly draining conditions, the system transitions to a locally unstressed condition at some scale. In unstressed conditions the flow Q_U/W exceeds the flow when $S = S_m$, which is defined as $D \cdot R$, allowing the onset of well watered conditions to be predicted as a threshold scale k_t (for $\beta = 0.5$) by rearranging equation 7.12:

$$k_t = \frac{\log\left(\frac{R(D+G-1)+1}{GR+1}\right)}{\log\left(\frac{2D}{D+1}\right)} \tag{7.16}$$

The accumulation of the subsidy downslope increases transpiration V under water-stressed conditions due to both an increase in storage and in biomass B. However as Figure 7.3C shows, if B were spatially uniform throughout the catchment and set only by external drivers (i.e. turning off the effect of the subsidy on the vegetation organization) then the spatial dependence of H is greatly reduced in terms of both the local and the catchment level Horton indices. Furthermore, a greater proportion of the system operates under well-watered conditions (i.e. k_t is reduced). The smaller value of H suggests the intriguing possibility that without the capacity for vegetation to organize, the catchment operates 'sub-optimally' , in the sense that less of the available water is utilized by vegetation to enable carbon fixation.

These patterns have clear implications for our understanding of the relationship between catchment and point-scale water balance patterns. There is a large difference between the value of Horton index in the unsubsidized exterior links and the value at the catchment outlet, a difference we will refer to as ΔH and investigate in more detail in the next section. There is an even larger difference between the values of the local Horton index near the outlet, which are affected by the subsidy, and the values in the exterior links,

which are not (but are otherwise identical). This behavior recapitulates the empirical difficulties associated with attempting to relate patch scale observations to catchment level responses (*Thompson et al.*, 2011), and suggests a possible rationale for this discrepancy (beyond blindly invoking within-catchment heterogeneity).

7.3.2 Controls of landscape and vegetation parameters on subsidy-based patterns

The patterns observed over various scales in the previous section are dependent on the parameters of the system, R, D, G, and β. Solving the model numerically over a wide range of parameter values reveals that the subsidy has the greatest effect for arid climates (large R), and intermediate values of drainage efficiency D and vegetation sensitivity G. This is shown in Figure 7.4, in which contours of ΔH (the difference in H at the network outlet and at the unsubsidized exterior links (c.f. Figure 7.3 C)) are shown as a function of R, D and G. This behavior can be readily understood as arising from the combination of parameters at which the presence of vegetation is sensitive to local storage. Where G is small or large, the vegetation cover is uniform across the catchment, saturating everywhere for small G ($B \sim 1$) or unable to establish for large G ($B \sim 0$). Similarly, where D is small, slow drainage favors vaporization, generating large H independently of the vegetation organization. Large D favors drainage, so V and H are small everywhere. For intermediate values of these parameters the spatial organization of vegetation is able to establish and significantly affect the water balance. This 'maximum organization in intermediate environments' is qualitatively reflected in the images of US pre-colonization vegetation cover in Figure 7.1, where the imprint of hydrological organization on vegetation pattern is most obvious in the Mid-West where forest cover transitions to grassland, driven in part by climatic factors.

Three regimes of model behavior can be identified in the ΔH plots in Figure 7.4. Firstly, for low D and high G, the catchment system is globally unstressed. In these circumstances subsidy effects do not alter the behavior of V and thus ΔH is zero. Secondly, for low G and low D, subsidy effects are not strong enough to alleviate water stress at any scale. Outside of these regions, H and the controls on V are both sensitive to the down-gradient subsidy. The boundaries of these regions are indicated by dashed lines in Figure 7.4. Although we have focused on the case with $\beta = 0.5$ in order to capitalize on the analytical results available in that case, the results presented are broadly representative of other bifurcating networks. An approximately 30-fold variation in the length of the main stem (as β deviating from ~ 0.5 to ~ 1 or ~ 0) results in variations in the peak values of ΔH of only $\sim 10\%$.

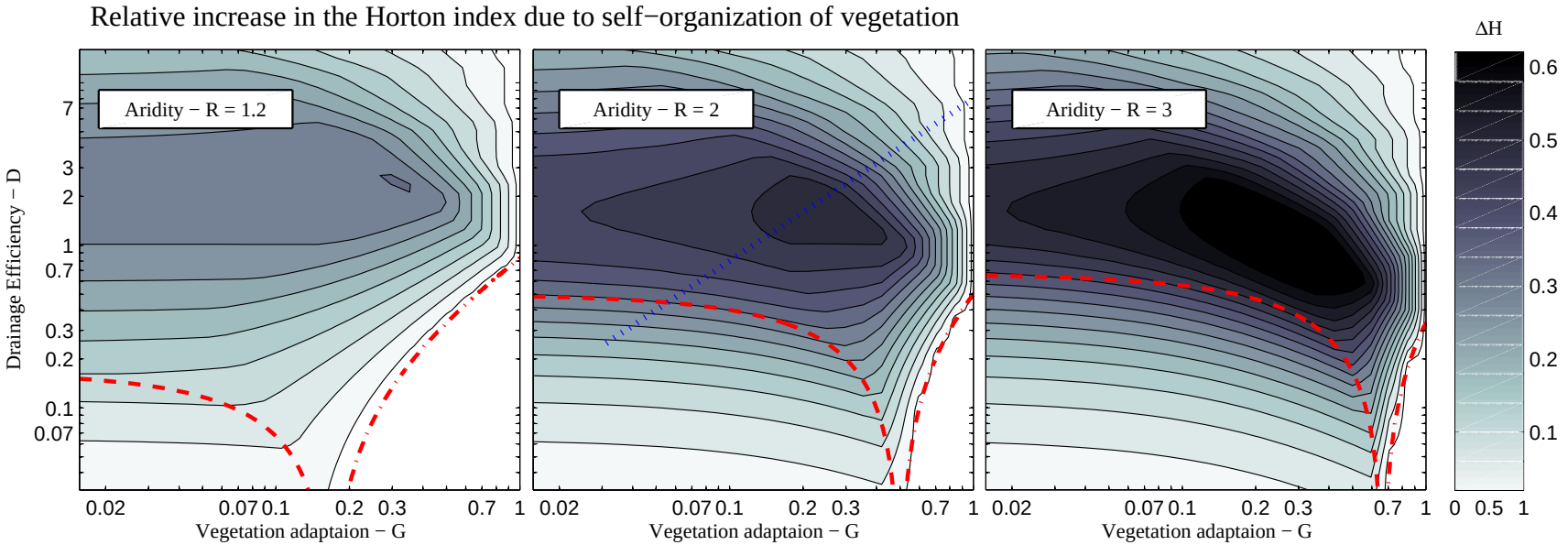

Figure 7.4: Contours of the difference in Horton index H (calculated at the system outlet) between the case with self-organized vegetation and the case with uniform vegetation, as a function of the three dimensionless ratios that determine the dynamics.

7.3.3 Effects on climate sensitivity of water balance

We can quantify this sensitivity with the derivative of H_K with respect to the aridity index R. In the analytical case this is obtained by noting that:

$$\frac{dH_k}{dR} = \frac{dH_k}{dV_{max}} \frac{dV_{max}}{dR} \tag{7.17}$$

From the definition of R, the second term on the right hand side is simply W. The first term can be obtained by differentiating Equation 7.15:

$$\frac{dH_k}{dR} = \left(G + \frac{1}{R}\right) \frac{D}{(D+1)} \left(\frac{D + 1 + \left(\frac{2D}{D+1}\right)^k (D(k-1) - k - 1)}{(D-1)^2 (2^k - 1)} \right) \tag{7.18}$$

The interpretation of this climate sensitivity is slightly different from the inter-annual variation explored by *Troch et al.* (2009c); *Sivapalan et al.* (2010) and *Harman et al.* (2011) in that it can be applied only over timescales long enough that the transient dynamics associated with vegetation self-organization have decayed and a steady state can again be assumed. However, the sign of the sensitivity is consistent with observations of H_k having a positive relationship to aridity. Note that G and $1/R$ simply amplify the effects of scale k and drainage D, so that where G is small (that is, vegetation cover is able to saturate when water is available) and R is large (the maximum vaporization rate is much larger than the available water) the sensitivity of the water balance to R is damped, since the vegetation is able to respond dynamically to changes in available water. This is broadly in accordance with the suggestions of *Troch et al.* (2009c). In addition, a close inter-twining of effects of scale and lateral flows on the water balance sensitivity is suggested by this relationship. Dividing the above equation by $(G+1/R)$ isolates the effects of D and k. The resulting values of $(\frac{dH_k}{dR})/(G + 1/R)$ from this analytical model, which is valid only in the stressed condition, and for the numerical model, which encompasses both stressed and unstressed conditions, are shown in Figure 7.5. Numerical results are shown for the subsidized case in a network with $\beta = 0.5$ and $k = 5$, and for the unsubsidized case (i.e. $k = 1$).

Intriguingly, the sensitivity is largest (least damped) for intermediate values of D. For the unsubsidized case ($k = 1$) $(\frac{dH_k}{dR})/(G+1/R)$ reduces to $D/(D+1)^2$, which has a maximum value when $D = 1$ (that is, when the drainage and transpiration are evenly matched). For the subsidized case ($k > 1$) this maximum occurs for larger D. This maximum sensitivity to climate for intermediate D arises due to the total dominance of landscape factors in determining partitioning when $D \gg 1$ and $D \ll 1$. In the former case, drainage is so efficient that vaporization is very small, and an increase in R will have negligible effect on the Horton

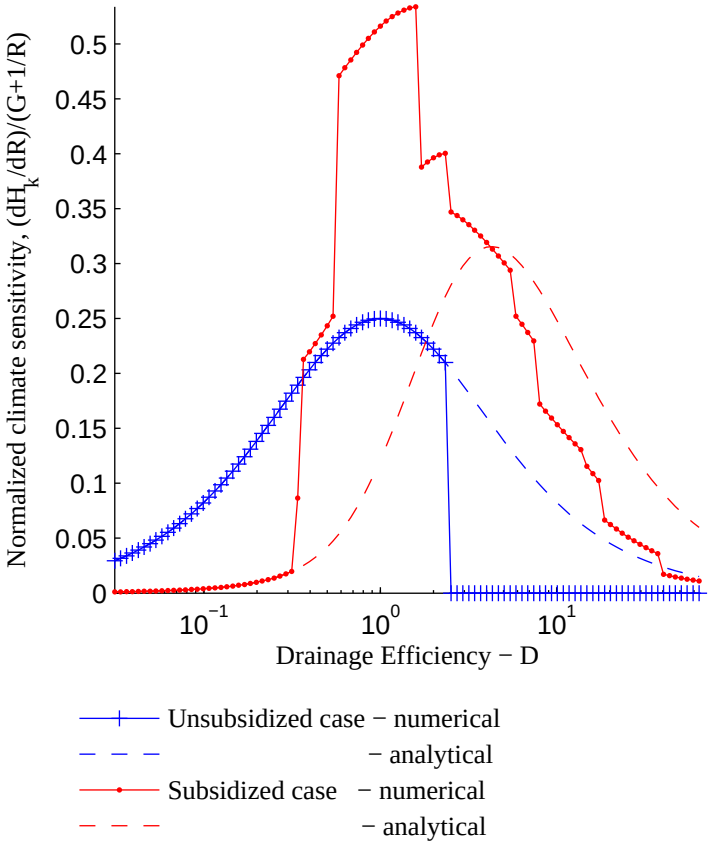

Figure 7.5: Sensitivity of the Horton Index to changes in aridity as a function of the drainage efficiency D. The multiple regimes of sensitivity are driven by a) thresholds in the capacity for vegetation to survive, b) the threshold between water stressed and unstressed transpiration and c) the symmetry of a perfectly bifurcating network, such that switching of either threshold induced by a change in D occurs synchronously at all links of a given order. In a more random network, the transitions between these regimes would be damped and would tend to confine the sensitivity of $(\frac{dH_k}{dR})/G$ to near zero at whole-catchment scales

index. In the latter, drainage is highly inefficient compared to vaporization, and so vaporization dominates the water-balance regardless of R. It is only when the vegetation controls on vaporization can compete with drainage (and vice-versa) does a change in R translate to a significant change in the water balance. The shift to higher D for larger catchments ($k > 1$) arises due to the fact that the increase in vegetation cover down-gradient depends on the accumulation of drainage. When $D > 1$ (drainage tends to dominate) an increase in R (towards a more arid climate) will produce a larger increase in V in the presence of a subsidy than if $D = 1$ because there is more water available from upstream that the vegetation can use to adapt to the new conditions.

The sensitivities captured in the analytical results are somewhat swamped, however, by the effects of transitions to alternative states along the network. These transitions cause the apparently erratic behavior of the unsubsidized case. As D increases, the subsidy to links at the downstream end of the network provides sufficient water that they become unstressed. In unstressed conditions V/W scales directly with R (Equation 7.10) and so sensitivity to variations in R becomes 1 for these parts of the network, and the sensitivity of the whole network jumps up. As D increases further, links at the upstream end of the network drain so efficiently that they cannot sustain vegetation, and transpiration drops to zero. Consequently they become insensitive to variations in climate. The number of links where these thresholds are crossed increases with D, leading to the complex behavior observed in Figure 7.5. The precise values of D at which the thresholds are crossed depends on the values of G and R, and the structure of the network.

These results provide intriguing insights into the way the landscape properties encapsulated in the model parameters affect the distribution of water in the landscape, and the sensitivity of that landscape to the climate.

7.4 Conclusions

This model aimed to test the hypothesis that a convergent network that allowed the accumulation of excess water, coupled with a two-directional feedback between vegetation and vaporization, would generate spatial organization of vegetation and of catchment water balance properties. Indeed, this simple framework generated spatial scaling in hydrological and ecological state variables and also in higher order metrics such as the Horton Index and the L'Vovich parameters. Three features of the model results are promising from the point of view of developing new scaling theories for catchments. The first is that the combination of lateral fluxes of water with a vegetation-vaporization feedback leads to interdependence between the spatial organization vegetation and hydrological partitioning. Although this model is far too simplistic to conclude that

observations of vegetation spatial distribution are sufficient to infer local hydrological states from, it suggests that as more complex and robust representations of plant-water feedbacks are accounted for, observations of vegetation may provide a way to improve predictions of catchment scaling behavior. Second, these effects are most significant in intermediate environments, where assumptions about the primacy of vertical fluxes between the atmosphere and land surface must give way to a more nuanced understanding of the controls on the partitioning between vertical and lateral fluxes. Thirdly, we have developed a basic scaling theory that incorporates this feedback for a perfectly bifurcating network, and shown that it exhibits the expected behavior.

Four dimensionless numbers dictated the sensitivity of the response. While R (aridity) and β (network bifurcation parameter) are observable at catchment scales, the drainage competitiveness parameter D and the vegetation sensitive parameter G reflect more complex relationships between slope, evapotranspiration dynamics, and the adaptations and acclimations of vegetation communities. Intriguingly, the locality index L has strong affinities to the topographic wetness index utilized in TOPMODEL. The strength of TOPMODEL is its ability to relate local measures of wetness to global properties of the catchment. The modeling approach suggests that it might be possible to define similar local - global relationships for other aspects of the water balance.

It must be acknowledged that the model presented here is simplistic from both physiological and hydrological points of view, and could potentially be criticized *ad infinitum*. The model results here should be interpreted as the outcomes of a thought experiment about the potential for organization along a network of flowpaths to occur at all, and in occurring, to influence the spatial scale dependence of hydrological and ecological parameters in catchments. The key conclusions are necessarily broad — that such an organization is indeed possible and has the potential to lead to strong scaling relationships — but motivate us to pursue refined investigations of the processes represented in this simple framework.

Chapter 8

Conclusions

8.1 Major contributions of the dissertation

Motivated by the need to understand and predict hydrologic behavior across scales in a changing world, this dissertation has sought to develop and apply a framework for understanding *why* particular types of hydrologic systems behave the way that they do. The objective was not to analyze a particular watershed in detail, but rather to develop insights that could apply across many watersheds. The major contributions of the dissertation are as follows:

- A framework for thinking about hydrologic questions across scales was developed. This framework calls for a renewal of the search for hydrologic 'laws' that apply at landscape scales, as proposed by *Dooge* (1986). It proposed that these laws can be found through a synthesis of pattern-based and process-based approaches to understanding the aggregate behavior of hydrologic systems. Furthermore this framework can provide a basis by which hydrologists can connect with other disciplines to understand the co-evolutionary processes that drive the organization of catchments, and to find explanations for the 'functional' patterns from emerge in the organization.

- Motivated by this framework, a simple model for predicting the travel time of a sorbing, reactive solute through the vadose was developed. This model was then used to demonstrate, in clear analytical statements, how the climate, soils and vegetation (through root water uptake) each determine the total travel time of the solute through the vadose zone. This work provides a clear demonstration of how simple models can be used to analyze the macro-scale controls on the hydrologic behavior of elements of landscape like the vadose zone.

- It was then demonstrated that similar ideas could be used to develop closure relations for predicting the flux of water through the landscape that captured the effects of unresolved spatial heterogeneity in a physically-defensible way without resolving that heterogeneity explicitly. Here a time-fractional kinematic wave equation was derived for subsurface lateral flow through a hillslope, and solutions

were shown to match the behavior of a fully resolved model where significant heterogeneity of the conductivity field was present.

- The effect of internal structure and heterogeneity on the behavior of aggregate hydrologic systems was then demonstrated for catchment discharge recession curves. It was shown that power-law type behavior could arise from the composition of many hillslopes and flowpaths exhibiting simpler exponential-type behaviors (which we might expect from physical principles). This interpretation challenged the commonly held interpretation that power-law recession curves arose from the hydraulics of flow in a single 'effective' hillslope presumed to represent the behavior of the whole catchment - an assumption that is difficult to defend in watersheds where hillslope gradients and lengths may vary considerably. The new interpretation was then shown to provide a meaningful interpretation of observed changes in the recession curve shape with scale.

- The different degrees of sensitivity of water-balance to precipitation in watersheds across the continental US was then presented as an example of a 'functional' pattern that may arise in part because of co-evolved landscape properties. Finding consistent explanations for the patterns of sensitivity with climate and geology would help us understand how co-evolution plays out in real landscapes. This work was also unique in that it is the first study of its type that has quantified and mapped the sensitivity of the 'fast' and 'slow' components of the discharge separately.

- Finally, an illustrative model of co-evolution at the watershed scale was then developed that shows how the interplay of hydrology and vegetation can lead to non-trivial patterns of scaling in water balance and vegetation cover along a convergent drainage network. Analytical solutions of this spatially-explicit model demonstrate how macro-scale controls of climate, geology and vegetation properties determine co-evolved functional patterns, in an analogous way to the analytical solutions for vadose zone travel time in Chapter 3.

8.2 Future research

A number of general points can be drawn from this analysis. The work in the first part of the dissertation demonstrated that many of the main landscape-structural controls on the propagation of climatic variability through the landscape could be functionally condensed into a timescale and/or a storage capacity (or rather a distribution of timescales and storages). The different regimes of behavior in each hydrologic system studied could be distinguished on the basis of whether A) the timescales of variability imposed by the climate were

much larger, much smaller, or were similar to the response timescales of the system, and B) the storage of water that accumulated in the system (which was a consequence of that balance of timescales) tended to reach the point at which a capacity (be it field capacity in Chapter 2 or the storage required to trigger lateral subsurface flow discussed in the introduction) was exceeded and water was partitioned along an alternative pathway out of the hydrologic system.

The essential requirement of an REW closure law is that is faithfully represent the way inflows of mass, energy, momentum etc. are stored, partitioned and filtered into outflows. As Chapters 2 and 4 demonstrate, simple models and closure relations that use the timescale and storage capacity concepts to represent these can be used to predict upscaled hydrologic behavior without resolving all the details of the structure and dynamics. These approaches can pave the way for developing operational REW-scale models with a rigorous physical justification.

The hydrologic systems studied here have been examined as individual units (the vadose zone, the saturated zone) disconnected from each other. This is in keeping with the REW modeling framework that has motivated that analysis. To understand the aggregate behavior of complete hydrologic systems would require us to consider how these units are connected together in a network, and how the timescales and storage capacities arranged along that network interact. The work presented in Chapter 5 hints at this sort of analysis, but considers only one pathway out of the catchment (i.e. there is no limit to the storage capacity) and makes the restrictive assumption that all the elements are arranged in parallel. A more complete analysis could draw on theory from circuit analysis and signal processing to develop a better understanding of the upscaled behavior of these stochastic-dynamic systems.

The results presented in Part Two, although very preliminary, suggest that the framework for understanding regimes and closure relations described above can also provide a rational basis for analyzing the evolution of hydrologic systems. If the dynamics of a hydrologic system can be analyzed in terms of storages and timescales, then hydrologic evolution can be understood by understanding how these storages and timescales change. The capacity of a hydrologic system to store water is determined by properties like the thickness of the soil and its hydraulic properties, the morphology of confining layers in hillslopes and valley-bottoms, and the properties of the underlying geology. The thresholds at which stored water is partitioned along alternative pathways is determined by structure of the surface topography and the depths to which roots penetrate and access water stored deeper in the soil. The timescales arise from the topography, soils, the energy available for evapotranspiration, and the dynamics of vegetation. With the exception of the underlying geological properties and the climatic factors, each of these is a co-evolved structure of the landscape.

A deeper understanding of co-evolution of landscape hydrology may therefore not only give us a deeper insight into the landscapes we live in, it may have very practical applications if connections can be made between co-evolved landscape structures and the closure laws needed for prediction.

But how can these connections be made? In the introductory Chapter it was suggested that what is needed is a combination of Process-based analysis of co-evolution and a Pattern-based approach built on catchment inter-comparison and historical reconstruction.

We could make a start by developing prototype model of co-evolving soil, vegetation and hydrologic dynamics built on the framework of *Istanbulluoglu and Bras* (2006). This model builds on the water-balance model of *Rodriguez-Iturbe et al.* (1999) and *Laio et al.* (2001a), incorporating a simple representation of vegetation cover growth and death coupled to water stress and a similarly simple prediction of overland flow erosion. The feedback between water availability and vegetation cover classifies this as a "co-evolutionary" model. It could be further extended to consider co-evolution over many timescales however through any of the following additions:

- Vegetation controls on soil hydraulic properties observed in the field work.
- Reductions in the soil thickness from denudation by overland flow erosion.
- Increases in the soil thickness through weathering of an underlying bedrock.

The addition of these components could be used to examine how, in contrast with the steady-state modeling presented earlier in the dissertation, the variability at short timescales created by individual rainfall events is an essential component driving the long-term co-evolution of the landscape. This interaction implies that in the co-evolutionary framework processes must be coupled across a very wide range of timescales. This was relatively easy to implement in this simple model, but will become more technically challenging is the model is made more complicated.

Indeed it is clear that to go beyond this toy modeling such complication is nessecary, as a model capable of examining the evolution of hydrologic processes must resolve the spatial relationships that control this evolution. As the results of Chapter 7 suggest at the catchment scale, modification of hydrologic fluxes by co-evolved properties of the landscape leads to non-trival self-organization along flowpaths. Moreover in many cases an assumption of the uni-directional networks of dependence along the flowpaths is not likely to be generally true for many landscape processes. In low topographic gradient areas ground-water and surface-water gradients can propagate against the direction of flow, producing a self-organization of flowpaths (*Harman*, 2007b). Furthermore, in areas where geomorphic processes of landscape evolution are

transport-limited (rather than detatchment-limited), changes in base level will create waves of erosion that propagate up topographic gradients (*Roering et al.*, 2007).

It must be understood that the development of co-evolutionary models is not an end in itself. Rather these models serve as tools for answering more fundamental questions. There is a risk that if the development of such models becomes divorced from its purpose, the natural tendency to want to improve model fidelity will drive the development of ever more complicated models.

The Pattern-based analysis of functional patterns in co-evolved landscape can provide a bulwark against this tendency, and ground the science in real-world observations. Seeking out and explaining the kind of patterns observed in Chapter 6 is a sure pathway to deeper insights into landscape organization and change. To achieve a synthetic understanding, falsifiable hypotheses that explain the existence and distribution (in space and time) of observed patterns of behavior must both be supported by independent evidence, and be shown to both arise naturally in process models.

Explaining patterns in stratigraphy and the distribution of rocks helped Hutton and Lyell found modern geology, and explaining patterns in the distribution of species helped Darwin found modern ecology and biology. These patterns were found only through the careful characterization, classification and mapping of observations of the landscape; in other words, through natural history. Hydrology does not have a heritage of natural history. The difficulties associated with characterizing flows through the landscape has meant that the hydrologic 'physiology' of only a handful of sites have been carefully characterized. An emphasis on modeling over perceptual understanding has also probably hindered the development of this kind of understanding (*Beven*, 2008; *Sivapalan*, 2009). At those experimental watersheds that have been examined, the complexities and unique characteristics of each individual site has tended to drive research, rather than the search for patterns that connect the behavior of many sites. Nor has there been an emphasis on reconstructing the trajectories of hydrologic change as it relates to hydrologic dynamics – streamflow reconstruction through, for example, tree-ring records do not resolve the shifts in the processes driving streamflow generation and variability.

Finally then, each piece of research presented in this dissertation has sought to provides insights that stand alone and contribute to our understanding of hydrology. Overarching this has been the objective to find new frameworks for thinking about hydrology. The frameworks presented here aim to deepen our understanding of the landscape, and to build better tools to help us manage those landscapes in a changing world.

References

Abramowitz, M., and I. A. Stegun, *Handbook of Mathematical Functions*, Dover, New York, 1972.

Arias-este, M., E. Lopez-Periago, E. Martinez-Carballo, J. Simal-Gandara, J.-C. Mejuto, and L. Garcia-Rio, The mobility and degradation of pesticides in soils and the pollution of groundwater resources, *Agriculture, Ecosystems and Environment*, *123*, 247–260, doi:10.1016/j.agee.2007.07.011, 2008.

Arnell, N., A simple water balance model for the simulation of streamflow over a large geographic domain, *Journal of Hydrology*, *217*(3-4), 314–335, 1999.

Baeumer, B., and M. Meerschaert, Fractional diffusion with two time scales, *Physica A*, *373*(237), 237–251, 2007.

Baeumer, B., D. Benson, M. Meerschaert, and S. Wheatcraft, Subordinated advection-dispersion equation for contaminant transport, *Water Resources Research*, *37*(6), 1543–1550, 2001.

Baeumer, B., M. M. Meerschaert, and S. Kurita, Inhomogeneous fractional diffusion equations, *Fractional Calculus and Applied Analysis*, *8*(4), 371 – 386, 2005.

Band, L., P. Patterson, R. Nemani, and S. Running, Forest ecosystem processes at the watershed scale - incorporating hillslope hydrology, *Agricultural and Forest Meterology*, *63*(1-2), 93–126, 1993.

Band, L. E., D. L. Peterson, S. W. Running, J. C. Coughlan, R. B. Lammers, J. Dungan, and R. Nemani, Forest ecosystem processes at the watershed scale: basis for distributed simulation, *Ecological Modeling*, *56*, 151–176, 1991.

Beck, C., and E. Cohen, Superstatistics, *Physica A: Statistical Mechanics and its Applications*, *322*, 267–275, doi:10.1016/S0378-4371(03)00019-0, 2003.

Bejan, A., *Shape and Structure, from Engineering to Nature*, Cambridge University Press, Cambridge, UK, 2000.

Bender, C. M., and S. A. Orszag, *Advanced Mathematical Methods for Scientists and Engineers*, McGraw-Hill, New York, 1978.

Bengough, A. G., M. F. Bransby, J. Hans, S. J. McKenna, T. J. Roberts, and T. A. Valentine, Root responses to soil physical conditions; growth dynamics from field to cell, *Journal of Experimental Botany*, *57*(2), 437–447, doi:10.1093/jxb/erj003, 2006.

Benjamin, J. R., and C. A. Cornell, *Probability, Statistics, and Decision for Civil Engineers*, McGraw-Hill, New York, 1970.

Benson, D., and M. M. Meerschaert, A simple and efficient random walk solution to multi-rate mobile/immobile mass transport equations, *Advances in Water Resources*, *32*(4), 532 – 539, 2009.

Benson, D., S. Wheatcraft, and M. Meerschaert, Application of a fractional advection-dispersion equation, *Water Resources Research*, *36*(6), 1403 – 1412, 2000.

Benson, D., S. Wheatcraft, and M. Meerschaert, Fractional dispersion, levy motion, and the made tracer tests, *Transport in Porous Media*, *42*, 211 – 240, 2001.

Berne, A., R. Uijlenhoet, and P. A. Troch, Similarity analysis of subsurface flow response of hillslopes with complex geometry, *Water Resources Research*, *41*(9), W09,410, doi:10.1029/2004WR003629, 2005.

Bertoin, J., *Levy Processes*, Cambridge Univ Press, Cambridge, UK, 1996.

Beven, K., Kinematic subsurface stormflow, *Water Resources Research*, *17*(5), 1419–1424, 1981.

Beven, K., On subsurface stormflow - predictions with simple kinematic theory for saturated and unsaturated flows, *Water Resources Research*, *18*(6), 1627–1633, 1982.

Beven, K., Searching for the Holy Grail of scientific hydrology: $Q_t = H(\overleftarrow{S}, \overleftarrow{R}, \Delta t)A$ as closure, *Hydrology and Earth System Sciences*, *10*(5), 609–618, 2006.

Beven, K., On doing better hydrological science, *Hydrological Processes*, *3553*(May), 3549–3553, doi: 10.1002/hyp, 2008.

Beven, K. J., Surface runoff at the Horton hydrologic laboratory (or not?), *Journal of Hydrology*, *293*, 219 – 234, 2004a.

Beven, K. J., Robert Horton?s perceptual model of infiltration, *Hydrological Processes*, *18*, 3447 – 3460, 2004b.

Beven, K. J., Robert Horton and abrupt rises of groundwater, *Hydrological Processes*, *18*, 3687 – 3696, 2004c.

Beven, K. J., and M. J. Kirkby, A physically-based variable contributing area model of basin hydrology, *Hydrological Sciences Bulletin*, *24*, 43–69, 1979.

Binley, A., J. Elgy, and K. Beven, A physically based model of heterogeneous hillslopes. 1. Runoff production, *Water Resources Research*, *25*(6), 1219–1226, 1989.

Blöschl, G., Hydrologic synthesis : Across processes, places, and scales, *Water Resources Research*, *42*, W03S02, doi:10.1029/2005WR004319, 2006.

Blöschl, G., and M. Sivapalan, Scale issues in hydrological modeling - a review, *Hydrological Processes*, *9*(3-4), 251–290, 1995.

Blöschl, G., and E. Zehe, On hydrological predictability, *Hydrological Processes*, *19*(October), 3923–3929, doi:10.1002/hyp.6075, 2005.

Bochner, S., Diffusion equations and stochastic equations, *Proceedings of the National Academy of Sciences*, *85*, 369 – 370, 1949.

Botter, G., A. Porporato, I. Rodriguez-Iturbe, and A. Rinaldo, Basin-scale soil moisture dynamics and the probabilistic characterization of carrier hydrologic flows: Slow, leaching-prone components of the hydrologic response, *Water Resources Research*, *43*(2), W02,417, doi:10.1029/2006WR005043, 2007.

Breshears, D. D., N. S. Cobb, P. M. Rich, K. P. Price, C. D. Allen, R. G. Balice, W. H. Romme, J. H. Kastens, M. L. Floyd, J. Belnap, J. J. Anderson, O. B. Myers, and C. W. Meyer, Regional vegetation die-off in response to global-change-type drought, *Proceedings of the National Academy of Sciences*, *102*(42), 15,144–8, doi:10.1073/pnas.0505734102, 2005.

Brutsaert, W., The unit response of groundwater outflow from a hillslope, *Water Resources Research*, *30*(10), 2759–2763, 1994.

Brutsaert, W., and J. Lopez, Basin-scale geohydrologic drought flow features of riparian aquifers in the southern great plains, *Water Resources Research*, *34*(2), 233–240, 1998.

Brutsaert, W., and J. L. Nieber, Regionalized drought flow hydrographs from a mature glaciated plateau, *Water Resources Research*, *13*(3), 637–644, 1977.

Budyko, M. I., *Climate and Life*, Elsevier, New York, 1974.

Cayar, M., and M. Kavvas, Ensemble average and ensemble variance behavior of unsteady, one-dimensional groundwater flow in unconfined, heterogeneous aquifers: an exact second-order model, *Stochastic Environmental Research and Risk Assessment*, pp. 1–10, doi:10.1007/s00477-008-0263-1, 2008.

Caylor, K., S. Manfreda, and I. Rodriguez-Iturbe, On the coupled geomorphological and ecohydrological organization of river basins, *Advances in Water Resources*, *28*(1), 69–86, doi:10.1016/j.advwatres.2004.08.013, 2005.

Chapman, T., A comparison of algorithms for stream flow recession and baseflow separation, *Hydrological Processes*, *13*(5), 701–714, 1999.

Chapman, T. G., Modelling stream recession flows, *Environmental Modelling and Software*, *18*(8-9), 683–692, doi:10.1016/S1364-8152(03)00070-7, 2003.

Chen, Z. Q., M. L. Kavvas, J. Y. Yoon, E. C. Dogrul, K. Fukami, J. Yoshitani, and T. Matsuura, Geomorphologic and soil hydraulic parameters for Watershed Environmental Hydrology (WEHY) model, *Journal of Hydrologic Engineering*, *9*, 465 – 479, doi:10.1061/(ASCE)(2004)9:6 (465), 2004.

Chiew, F., Estimation of rainfall elasticity of streamflow in Australia, *Hydrological Sciences Journal*, *51*(4), 613–625, 2006.

Clark, M. P., D. E. Rupp, R. A. Woods, H. J. T.-v. Meerveld, N. E. Peters, and J. E. Freer, Consistency between hydrological models and field observations: linking processes at the hillslope scale to hydrological responses at the watershed scale, *Hydrological Processes*, *23*(2), 311–319, doi:10.1002/hyp.7154, 2009.

Committee on Opportunities in the Hydrologic Sciences, W. S., and N. R. C. Technology Board, *Opportunities in the Hydrologic Sciences*, The National Academic Press, 1991.

Dagan, G., Analysis of flow through heterogeneous random aquifers: 2. Unsteady flow in confined formations, *Water Resources Research*, *18*(5), 1571–1585, 1982.

Destouni, G., Applicability of the steady state flow assumption for solute advection in field soils, *Water Resources Research*, *27*(8), 2129–2140, doi:10.1029/91WR01115, 1991.

Dietrich, W. E., D. G. Bellugi, L. S. Sklar, J. D. Stock, A. M. Heimsath, and J. J. Roering, Geomorphologic transport laws for predicting landscape form and dynamics, in *Prediction in Geomorphology, Geophysical Monograph 135*, American Geophysical Union, 2003.

Dogrul, E., M. Kavvas, and Z. Chen, Prediction of subsurface stormflow in heterogeneous sloping aquifers, *Journal of Hydrologic Engineering*, *3*(4), 258–267, 1998.

Dooge, J., Looking for hydrologic laws, *Water Resources Research*, *22*, S46–S58, 1986.

Dooge, J., Sensitivity of runoff to climate change - a Hortonian approach, *Bulletin of the American Meteorological Society*, *73*(12), 2013–2024, 1992.

Dooge, J., M. Bruen, and B. Parmentier, A simple model for estimating the sensitivity of runoff to long-term changes in precipitation without a change in vegetation, *Advances in Water Resources*, *23*(2), 153–163, 1999.

Dooge, J. C. I., Hydrology in perspective, *Hydrological Sciences Journal*, *33*(1), 61–85, 1988.

Drewry, D., P. Kumar, S. Long, C. Bernachi, X.-Z. Liang, and M. Sivapalan, Ecohydrological responses of dense canopies to environmental variability part 1: Interplay between vertical structure and photosynthetic pathway, *Journal of Geophysical Research - Biogeosciences*, *115*(25), G04,022, 2010.

Duan, Q., J. Schaake, V. Andrassian, S. Franks, G. Goteti, H. V. Gupta, Y. M. Gusev, F. Habets, A. Hall, L. Hay, T. Hogue, M. Huang, G. Leavesley, X. Liang, O. N. Nasonova, J. Noilhan, L. Oudin, S. Sorooshian, T. Wagener, and E. F. Wood, Model parameter estimation experiment (MOPEX): An overview of science strategy and major results from the second and third workshops, *Journal of Hydrology*, *320*(1-2), 3–17, 2006.

Ducharne, A., R. D. Koster, M. J. Suarez, M. Stieglitz, and P. Kumar, A catchment-based approach to modeling land surface processes in a general circulation model. 2. parameter estimation and model demonstration, *Journal of Geophysical Research Atmospheres*, *105*(D20), 24,823–24,838, 2000.

Dunne, T., Field studies of hillslope flow processes, in *Hillslope Hydrology*, edited by M. J. Kirkby, pp. 227 – 293, John Wiley, New York, 1978.

Dunne, T., T. R. Moore, and C. H. Taylor, Recognition and prediction of runoff-producing zones in humid regions, *Hydrological Sciences Bulletin*, *20*(3), 305 – 327, 1975.

Eagleson, P. S., Climate, soil, and vegetation - 6. Dynamics of the annual water balance, *Water Resources Research*, *14*(5), 749–764, doi:10.1029/WR014i005p00749, 1978.

El-kadi, A. I., and W. Brutsaert, Applicability of effective parameters for unsteady-flow in nonuniform aquifers, *Water Resources Research*, *21*(2), 183–198, 1985.

Falkenmark, M., Meeting water requirements of an expanding world population, *Phiosophical Transactions of the Royal Society of London Series B – Biological Sciences*, *352*(1356), 929–936, 1997.

Farmer, D., M. Sivapalan, and C. Jothityangkoon, Climate, soil, and vegetation controls upon the variability of water balance in temperate and semiarid landscapes: Downward approach to water balance analysis, *Water Resources Research*, *39*(2), 2003.

Feddes, R. A., P. J. Kowalik, and H. Zaradny, *Simulation of Field Water Use and Crop Yield*, John Wiley & Sons, New York, NY, 1978.

Feller, W., *An Introduction to Probability Theory and Its Applications*, vol. 2, 2 ed., John Wiley, New York, 1971.

Fiori, A., and D. Russo, Numerical analyses of subsurface flow in a steep hillslope under rainfall: The role of the spatial heterogeneity of the formation hydraulic properties, *Water Resources Research*, *43*(7), W07,445, doi:10.1029/2006WR005365, 2007.

Fiori, A., and D. Russo, Travel time distribution in a hillslope: Insight from numerical simulations, *Water Resources Research*, *44*(12), 1–14, doi:10.1029/2008WR007135, 2008.

Flury, M., Experimental evidence of transport of pesticides through field soils – a review, *Journal of Environmental Quality*, *25*(1), 25–45, doi:10.2134/jeq1996.00472425002500010005x, 1996.

Foussereau, X., W. D. Graham, G. Akpoji, G. Destouni, and P. S. C. Rao, Solute transport through a heterogeneous coupled vadose-saturated zone system with temporally random rainfall, *Water Resources Research*, *37*(6), 1577–1588, doi:10.1029/2000WR900389, 2001.

Ganti, V., A. Singh, P. Passalacqua, and E. Foufoula-Georgiou, Subordinated brownian motion model for sediment transport, *Physical Review E*, *80*, 011,111, doi:10.1103/PhysRevE.80.011111, 2009.

Ganti, V., M. M. Meerschaert, E. Foufoula-Georgiou, E. Viparelli, and G. Parker, Normal and anomalous diffusion of gravel tracer particles in rivers, *Journal of Geophysical Research*, *115*, F00A12, doi:10.1029/2008JF001222, in press.

Gellens, D., and E. Roulin, Streamflow response of belgian catchments to ipcc climate change scenarios, *Journal of Hydrology*, *210*(1-4), 242–258, 1998.

Gerke, H. H., Preferential flow descriptions for structured soils, *Journal of Plant Nutrition and Soil Science*, *169*(3), 382–400, doi:10.1002/jpln.200521955, 2006.

Greeley, W. B., The relation of geography to timber supply, *Economic Geography*, *1*, 1–11, 1925.

Green, W. G., and G. Ampt, Studies of soil physics, I: The flow of air and water through soils, *Journal of Agricultural Science*, *4*, 1–24, 1911.

Guardiola-Claramonte, M., P. Troch, D. Breshears, T. Huxman, M. Switanek, M. Durcik, and N. Cobb, Drought-induced tree die-off unexpectedly decreases stream flow in semi-arid basins, *Nature Communications*, *Under review*, 2010.

Gustafson, D. I., Groundwater ubiquity score: A simple method for assessing pesticide leachability, *Environmental Toxicology and Chemistry*, *8*(4), 339–357, doi:10.1002/etc.5620080411, 1989.

Guswa, A., M. Celia, and I. Rodriguez-Iturbe, Models of soil moisture dynamics in ecohydrology: A comparative study, *Water Resources Research*, *38*(9), 1166, doi:10.1029/2001WR000826, 2002.

Guswa, A. J., M. A. Celia, and I. Rodriguez-Iturbe, Effect of vertical resolution on predictions of transpiration in water-limited ecosystems, *Advances in Water Resources*, *27*(5), 467–480, 2004.

Harman, C., Effects of heterogeneity on subsurface flow in hillslopes and approaches to closure, Master's thesis, Department of Geography, University of Illinois at Urbana Champaign, 2007a.

Harman, C., and M. Sivapalan, Effects of hydraulic conductivity variability on hillslope-scale shallow subsurface flow response and storage-discharge relations, *Water Resources Research*, *45*(15), W01,421, doi:10.1029/2008WR007228, 2009a.

Harman, C., and M. Sivapalan, A similarity framework to assess controls on shallow subsurface flow dynamics, *Water Resources Research*, *45*, W01,417, doi:10.1029/2008WR007067, 2009b.

Harman, C., and M. Sivapalan, Effects of hydraulic conductivity variability on hillslope-scale shallow subsurface flow response and storage-discharge relations, *Water Resources Research*, *45*, W01,421, doi:10.1029/2008WR007228, 2009c.

Harman, C., and M. Sivapalan, A similarity framework to assess controls on shallow subsurface flow dynamics in hillslopes, *Water Resources Research*, *45*(1), 1–12, doi:10.1029/2008WR007067, 2009d.

Harman, C. J., Effects of heterogeneity on subsurface flow in hillslopes and approaches to closure, Masters thesis, University of Illinois at Urbana-Champaign, 2007b.

Harman, C. J., P. A. Troch, and M. Sivapalan, Functional model of water balance variability at the catchment scale: 2. elasticity of fast and slow runoff components to precipitation change in the continental united states, *Water Resources Research*, *47*, W02,523, doi:10.1029/2010WR009656, 2011.

Harte, J., Towards a synthesis of Newtonian and Darwinian worldviews, *Physics Today*, *October*, 29–34, 2002.

Hawk, K. L., and P. S. Eagleson, Climatology of station storm rainfall in the continental united states: Parameters of the Bartlett-Lewis and poisson rectangular pulses models, *Tech. rep.*, Ralph M. Parsons Lab, Department of Civil and Environmental Engineering, Mass. Inst. Tech, Cambridge, Mass., 1992.

Henderson, F. M., and R. A. Wooding, Overland flow and groundwater flow from a steady rainfall of finite duration, *Journal of Geophysical Research*, *69*, 1531–1540, 1964.

Hill, K. M., L. DellAngelo, and M. Meerschaert, Heavy tailed travel distance in gravel bed transport: An exploratory enquiry, *Journal of Geophysical Research*, *115*, F00A14, doi:10.1029/2009JF001276, 2010.

Hopp, L., C. Harman, S. L. E. Desilets, C. B. Graham, J. J. McDonnell, and P. A. Troch, Hillslope hydrology under glass: confronting fundamental questions of soil-water-biota co-evolution at biosphere 2, *Hydrology and Earth Systems Science*, *13*(11), 2105–2118, 2009.

Hornsby, A. G., R. D. Wauchope, and A. E. Herner, *Pesticide Properties in the Environment*, Springer-Verlag Inc., 1996.

Hurkmans, R., W. Terink, R. Uijlenhoet, P. Torfs, D. Jacob, and P. A. Troch, Changes in streamflow dynamics in the Rhine basin under three high-resolution regional climate scenarios, *Journal of Climate*, *23*(3), 679, doi:10.1175/2009JCLI3066.1, 2010.

Hurkmans, R. T. W. L., W. Terink, R. Uijlenhoet, E. J. Moors, P. a. Troch, and P. H. Verburg, Effects of land use changes on streamflow generation in the Rhine basin, *Water Resources Research*, *45*(6), 1–15, doi:10.1029/2008WR007574, 2009.

Huxman, T., M. Smith, P. Fay, A. Knapp, M. Shaw, M. Loik, S. Smith, D. Tissue, J. Zak, J. Weltzin, W. Pockman, O. Sala, B. Haddad, J. Harte, G. Koch, S. Schwinning, E. Small, and D. Williams, Convergence across biomes to a common rain-use efficiency, *Nature*, *429*, 651–654, doi:10.1038/nature02561, 2004.

Istanbulluoglu, E., and R. Bras, Vegetation-modulated landscape evolution: Effects of vegetation on landscape processes, drainage density, and topography, *Journal of Geophysical Research-Earth Surface*, *110*(F2), F02,012, doi:10.1029/2004JF000249, 2005.

Istanbulluoglu, E., and R. L. Bras, On the dynamics of soil moisture, vegetation, and erosion: Implications of climate variability and change, *Water Resources Research*, *42*(6), 1–17, doi:10.1029/2005WR004113, 2006.

Iverson, L., Forest resources of illinois: What do we have and what are they doing for us?, *Illinois Natural History Survey Bulletin*, *34*, 361–374, 1991.

Jothityangkoon, C., and M. Sivapalan, Framework for exploration of climatic and landscape controls on catchment water balance, with emphasis on inter-annual variability, *Journal of Hydrology*, *371*(1-4), 154–168, 2009.

Jury, W. A., Simulation of solute transport using a transfer function model, *Water Resources Research*, *18*(2), 363–368, 1982.

Jury, W. A., and J. Gruber, A stochastic analysis of the influence of soil and climatic variability on the estimate of pesticide groundwater pollution potential, *Water Resources Research*, *25*(12), 2465–2474, doi:10.1029/WR025i012p02465, 1989.

Kavvas, M. L., Z. Q. Chen, C. Dogrul, J. Y. Yoon, N. Ohara, L. Liang, H. Aksoy, M. L. Anderson, J. Yoshitani, K. Fukami, and T. Matsuura, Watershed Environmental Hydrology (WEHY) model based on upscaled conservation equations: Hydrologic module, *Journal of Hydrologic Engineering*, *9*, 450 – 464, doi:10.1061/(ASCE)1084-0699(2004)9:6(450), 2004.

Kirchner, J., Catchments as simple dynamical systems: catchment characterization, rainfall-runoff modelling, and doing hydrology backwards, *Water Resources Research*, *45*, W02,429, doi:10.1029/2008WR006912, 2009.

Kirchner, J. W., Getting the right answers for the right reasons: Linking measurements, analyses, and models to advance the science of hydrology, *Water Resources Research*, *42*(3), W03S04, doi:0.1029/2005WR004362, 2006.

Kirchner, J. W., X. Feng, and C. Neal, Catchment-scale advection and dispersion as a mechanism for fractal scaling in stream tracer concentrations, *Journal of Hydrology*, *254*, 82 – 101, 2001.

Koster, R. D., M. J. Suarez, A. Ducharne, M. Stieglitz, and P. Kumar, A catchment-based approach to modeling land surface processes in a general circulation model 1. Model structure, *Journal of Geophysical Research Atmospheres*, *105*(D20), 24,809 – 24,822, 2000.

Kuczera, G., and E. Parent, Monte carlo assessment of parameter uncertainty in conceptual catchment models: the metropolis algorithm, *Journal of Hydrology*, *211*(1-4), 69–85, doi:10.1016/S0022-1694(98)00198-X, 1998.

Kumar, P., Variability, feedback, and cooperative process dynamics: Elements of a unifying hydrologic theory, *Geography Compass*, *1*(6), 101,111/j1749–8198200700,068x, 2007.

Kuntz, D., and P. Grathwohl, Comparison of steady-state and transient flow conditions on reactive transport of contaminants in the vadose soil zone, *Journal of Hydrology*, *369*(3-4), 225–233, doi:10.1016/j.jhydrol.2009.02.006, 2009.

Laio, F., A vertically extended stochastic model of soil moisture in the root zone, *Water Resources Research*, *42*(2), W02,406, doi:10.1029/2005WR004502, 2006.

Laio, F., A. Porporato, L. Ridolfi, and I. Rodriguez-Iturbe, Plants in water-controlled ecosystems: Active role in hydrologie processes and responce to water stress ii. probabilistic soil moisture dynamics, *Advances in Water Resources*, *24*(7), 707–723, doi:10.1016/S0309-1708(01)00005-7, 2001a.

Laio, F., A. Porporato, L. Ridolfi, and I. Rodriguez-Iturbe, Mean first passage times of processes driven by white shot noise, *Physical Review E - Statistical, Nonlinear, and Soft Matter Physics*, *63*(3), 361,051 – 361,058, 2001b.

Laio, F., P. D'Odorico, and L. Ridolfi, An analytical model to relate the vertical root distribution to climate and soil properties, *Geophysical Research Letters*, *33*(18), L18,401, doi:10.1029/2006GL027331, 2006.

Larsbo, M., S. Roulier, F. Stenemo, R. Kasteel, and N. Jarvis, An improved dual-permeability model of water flow and solute transport in the vadose zone, *Vadose Zone Journal*, *4*(2), 398–406, doi:10.2136/vzj2004.0137, 2005.

Lefsky, M., W. Cohen, G. Parker, and D. Harding, LIDAR remote sensing for ecosystem studies, *Bioscience*, *52*(1), 19–30, 2002.

Leung, L., and M. Wigmosta, Potential climate change impacts on mountain watersheds in the pacific northwest, *Journal of the American Water Resources Association*, *35*(6), 1463–1471, 1999.

L'vovich, M., *World Water Resources and Their Future*, American Geophysical Union, 1979.

Mallants, D., B. P. Mohanty, D. Jacques, and J. Feyen, Spatial variability of hydraulic properties in a multi-layered soil profile, *Soil Science*, *161*(167 - 181), 1996.

Manga, M., On the timescales characterizing groundwater discharge at springs, *Journal Of Hydrology*, *219*(1-2), 56–69, 1999.

Maxwell, R. M., and S. J. Kollet, Quantifying the effects of three-dimensional subsurface heterogeneity on Hortonian runoff processes using a coupled numerical, stochastic approach, *Advances in Water Resources*, *31*(5), 807 – 817, doi:10.1016/j.advwatres.2008.01.020, 2008.

McDonnell, J. J., M. Sivapalan, K. Vache, S. Dunn, G. Grant, R. Haggerty, C. Hinz, R. Hooper, J. Kirchner, M. L. Roderick, J. Selker, and M. Weiler, Moving beyond heterogeneity and process complexity: A new vision for watershed hydrology, *Water Resources Research*, *43*(7), W07,301, doi:10.1029/2006WR005467, 2007.

McGrath, G., C. Hinz, and M. Sivapalan, Assessing the impact of regional rainfall variability on rapid pesticide leaching potential, *Journal of Contaminant Hydrology*, *113*(1-4), 56 – 65, doi:10.1016/j.jconhyd.2009.12.007, 2010.

McGrath, G. S., An exploration of rainfall controls on pesticide transport via fast flow pathways, Ph.D. thesis, School of Earth and Geographical Sciences, University of Western Australia, 156p, 2007.

McGrath, G. S., C. Hinz, and M. Sivapalan, Temporal dynamics of hydrological threshold events, *Hydrology and Earth System Sciences*, *11*(2), 923–938, doi:10.5194/hess-11-923-2007, 2007.

McGrath, G. S., C. Hinz, and M. Sivapalan, Modeling the effect of rainfall intermittency on the variability of solute persistence at the soil surface, *Water Resources Research*, *44*(9), W09,432, doi:10.1029/2007WR006652, 2008.

Meerschaert, M., and H.-P. Scheffler, *Limit Distributions For Sums of Independent Random Vectors: Heavy Tails in Theory and Practice*, John Wiley, New York, New York, 2001.

Meerschaert, M., and H.-P. Scheffler, Limit theorems for continuous time random walks with infinite mean waiting times, *Journal of Applied Probability*, *41*(3), 623 – 638, 2004.

Meerschaert, M., and H.-P. Scheffler, Triangular array limits for continuous time random walks, *Stochastic Processes and their Applications*, *118*, 1606 – 1633, doi:10.1016/j.spa.2007.10.005, 2008.

Meerschaert, M. M., D. A. Benson, and B. Baeumer, Multidimensional advection and fractional dispersion, *Physical Review E*, *59*, 5026 – 5028, 1999.

Meerschaert, M. M., D. A. Benson, and B. Baeumer, Operator levy motion and multiscaling anomalous diffusion, *Physical Review E*, *63*(1112 - 1117), 2001.

Mendoza, G., T. Steenhuis, M. Walter, and J. Parlange, Estimating basin-wide hydraulic parameters of a semi-arid mountainous watershed by recession-flow analysis, *Journal Of Hydrology*, *279*(1-4), 57–69, doi:10.1016/S0022-1694(03)00174-4, 2003.

Mesa, O., and E. Mifflin, *Scale Problems in Hydrology: Runoff Generation and Basin Response*, 1-17 pp., D. Reidel Publishing Co., Dordrecht, Holland, 1986.

Metropolis, N., A. Rosenbluth, M. Rosenbluth, and A. Teller, Equations of state calculations by fast computing machines. 1953, *Journal of Chemical Physics*, *21*(6), 1953.

Milly, P., Stability of the Green-Ampt profile in a delta function soil, *Water Resources Research*, *21*(3), 399–402, 1985.

Milly, P., Climate, soil water storage, and the average annual water balance, *Water Resources Research*, *30*(7), 2143–2156, 1994.

Milly, P. C. D., An analytic solution of the stochastic storage problem applicable to soil water, *Water Resources Research*, *29*(11), 3755–3758, doi:10.1029/93WR01934, 1993.

Moore, R. D., Storage-outflow models of streamflow recession, with application to a shallow-soil, forested catchment, *Journal of Hydrology*, *198*, 260–270, 1997.

Neuman, S. P., and V. D. Federico, Multifaceted nature of hydrogeologic scaling and its interpretation, *Reviews of Geophysics*, *41*(3), 1014, doi:10.1029/2003RG000130, 2003.

Nieber, J. L., and R. C. Sidle, Potential for enhanced seepage and subsurface erosion from discontinuous macropore networks, *American Geophysical Union*, 2008.

Nieber, J. L., and R. C. Sidle, How do disconnected macropores in sloping soils facilitate preferential flow?, *Hydrological Processes*, *24*(12), 1582–1594, doi:10.1002/hyp.7633, 2010.

Nijssen, B., G. O'Donnell, A. Hamlet, and D. Lettenmaier, Hydrologic sensitivity of global rivers to climate change, *Climatic Change*, *50*(1-2), 143–175, 2001.

Němec, J., and J. Schaake, Sensitivity of water resource systems to climate variation, *Hydrological Sciences Journal*, *27*(3), 327–343, 1982.

Oudin, L., V. Andreassian, J. Lerat, and C. Michel, Has land cover a significant impact on mean annual streamflow? An international assessment using 1508 catchments, *Journal of Hydrology*, *357*(3-4), 303–316, 2008.

Palmroth, S., G. Katul, D. Hui, H. McCarthy, R. Jackson, and R. Oren, Estimation of long-term basin-scale evapotranspiration from streamflow time series, *Water Resources Research*, *46*, W10,512, doi: dx.doi.org/10.1029/2009WR008838, 2010.

Paniconi, C., P. A. Troch, E. E. van Loon, and A. G. J. Hilberts, Hillslope-storage Boussinesq model for subsurface flow and variable source areas along complex hillslopes: 2. Intercomparison with a three-dimensional richards equation model, *Water Resources Research*, *39*(11), 1316, doi: 10.1029/2002WR001730, 2003.

Paola, C., E. Foufoula-Georgiou, W. Dietrich, M. Hondzo, D. Mohrig, G. Parker, M. Power, I. Rodriguez-Iturbe, V. Voller, and P. Wilcock, Toward a unified science of the earth's surface: opportunities for synthesis among hydrology, geomorphology, geochemistry, and ecology, *Water resources research*, *42*(3), W03S10, 2006.

Pauwels, V. R. N., N. E. C. Verhoest, and F. P. De Troch, A metahillslope model based on an analytical solution to a linearized Boussinesq equation for temporally variable recharge rates, *Water Resources Research*, *38*(12), 1297, doi:10.1029/2001WR000714, 2002.

Ponce, V., and A. Shetty, A conceptual model of catchment water balance. 2. Application to runoff and baseflow modelling, *Journal of Hydrology*, *173*(1-4), 41–50, 1995a.

Ponce, V., and A. Shetty, A conceptual model of catchment water balance: 1. Formulation and calibration, *Journal of Hydrology*, *173*(1-4), 27–40, doi:10.1016/0022-1694(95)02739-C, 1995b.

Porporato, A., F. Laio, L. Ridolfi, and I. Rodriguez-Iturbe, Plants in water-controlled ecosystems: Active role in hydrologie processes and responce to water stress III. Vegetation water stress, *Advances in Water Resources*, *24*(7), 725–744, doi:10.1016/S0309-1708(01)00006-9, 2001.

Porporato, A., E. Daly, and I. Rodriguez-Iturbe, Soil water balance and ecosystem response to climate change, *American Naturalist*, *164*(5), 625–632, doi:10.1086/424970, 2004.

Puigdefabregas, J., A. Sole, L. Gutierrez, G. del Barrio, and M. Boer, Scales and processes of water and sediment redistribution in drylands: results from the Rambla Honda field site in southeast Spain, *Earth Science Reviews*, *48*(1-2), 39–70, 1999.

Raats, P. A. C., Residence times of water and solutes within and below the root zone, *Agricultural Water Management*, *4*(1-3), 63 – 82, doi:10.1016/0378-3774(81)90044-5, 1981.

Ragan, R. M., An experimental investigation of partial area contributions, in *Hydrological Aspects of the Utilization of Water, Reports and Discussions*, vol. 76, pp. 241 – 251, IAHS Publications, 1968.

Rao, P. S. C., and J. M. Davidson, Estimation of pesticide retention and transformation parameters required in nonpoint source pollution models, in *Environmental Impact of Nonpoint Source Pollution*, edited by M. Overcash and J. Davidson, pp. 23–67, Ann Arbor Science Publishers, 1980.

Rao, P. S. C., G. Hornsby, and R. E. Jessup, Indices for ranking the potential for pesticide contamination of groundwater, *Proceedings of the Soil and Crop Science Society of Florida*, *44*, 1–8, 1985.

Rao, P. S. C., R. E. Jessup, and J. M. Davidson, Mass flow and dispersion, in *Environmental Chemistry of Herbicides*, vol. 1, edited by R. Grover, chap. 2, pp. 21–43, CRC Press, 1990.

Rao, P. S. C., N. B. Basu, and S. E. Thompson, Hydrologic and biogeochemical filtering of reactive solute export from catchments along human impact gradients, *Water Resources Research*, *Under Review*, 2010.

Reeves, D., D. Benson, and M. Meerschaert, Influence of fracture statistics on advective transport and implications for geologic repositories, *Water Resources Research*, *44*, W08,405, doi:10.1029/2007WR006179, 2008a.

Reeves, D., D. A. Benson, M. M. Meerschaert, and H.-P. Scheffler, Transport of conservative solutes in simulated fracture networks: 2. ensemble solute transport and the correspondence to operator-stable limit distributions, *Water Resources Research*, *44*, W05,410, doi:10.1029/2008WR006858, 2008b.

Reggiani, P., M. Sivapalan, and S. M. Hassanizadeh, A unifying framework for watershed thermodynamics: balance equations for mass, momentum, energy and entropy, and the second law of thermodynamics, *Advances in Water Resources*, *22*(4), 367–398, 1998.

Reggiani, P., M. Sivapalan, S. M. Hassanizadeh, and W. G. Gray, A unifying framework of watershed thermodynamics: constitutive relationships, *Advances in Water Resources*, *23*, 15–39, 1999.

Reggiani, P., M. Sivapalan, and S. M. Hassanizadeh, Conservation equations governing hillslope responses: Exploring the physical basis of water balance, *Water Resources Research*, *36*(7), 1845–1863, 2000.

Rietkerk, M., S. Dekker, P. de Ruiter, and J. van de Koppel, Self-organized patchiness and catastrophic shifts in ecosystems, *Science*, *305*(5692), 1926–1929, 2004.

Risbey, J., and D. Entekhabi, Observed sacramento basin streamflow response to precipitation and temperature changes and its relevance to climate impact studies, *Journal of Hydrology*, *184*, 209–223, 1996.

Robinson, J. S., and M. Sivapalan, Temporal scales and hydrological regimes: Implications for flood frequency scaling, *Water Resources Research*, *33*(12), 2981–2999, 1997.

Robinson, J. S., M. Sivapalan, and J. D. Snell, On the relative roles of hillslope processes, channel routing, and network geomorphology in the hydrologic response of natural catchments, *Water Resources Research*, *31*(12), 3089–3101, 1995.

Rodriguez-Iturbe, I., and J. Valdes, Geomorphologic structure of hydrologic response, *Water Resources Research*, *15*(6), 1409–1420, 1979.

Rodriguez-Iturbe, I., A. Porporato, L. Rldolfi, V. Isham, and D. R. Cox, Probabilistic modelling of water balance at a point: The role of climate, soil and vegetation, *Proceedings of the Royal Society A: Mathematical, Physical and Engineering Sciences*, *455*(1990), 3789–3805, 1999.

Rodriguez-Iturbe, I., P. D'Odorico, F. Laio, L. Ridolfi, and S. Tamea, Challenges in humid land ecohydrology: Interactions of water table and unsaturated zone with climate, soil, and vegetation, *Water Resources Research*, *43*(9), W09,301, doi:10.1029/2007WR006073, 2007.

Roering, J., J. T. Perron, and J. W. Kirchner, Functional relationships between denudation and hillslope form and relief, *Earth and Planetary Science Letters*, *264*(1-2), 245–258, doi:10.1016/j.epsl.2007.09.035, 2007.

Rupp, D., and J. Selker, Drainage of a horizontal boussinesq aquifer with a power law hydraulic conductivity profile, *Water Resources Research*, *41*(11), W11,422, doi:10.1029/2005WR004241, 2005.

Rupp, D., and J. Selker, Information, artifacts, and noise in dq/dt - q recession analysis, *Advances In Water Resources*, *29*(2), 154–160, doi:10.1016/j.advwatres.2005.03.019, 2006a.

Rupp, D. E., and J. S. Selker, On the use of the Boussinesq equation for interpreting recession hydrographs from sloping aquifers, *Water Resources Research*, *42*(12), W12,421, doi:10.1029/2006WR005080, 2006b.

Russo, D., and A. Fiori, Equivalent vadose zone steady state flow: An assessment of its capability to predict transport in a realistic combined vadose zone-groundwater flow system, *Water Resources Research*, *44*(9), 1–19, doi:10.1029/2007WR006170, 2008.

Russo, D., W. A. Jury, and G. L. Butters, Numerical analysis of solute transport during transient irrigation 2. The effect of immobile water, *Water Resources Research*, *25*(10), 2119–2127, doi: 10.1029/WR025i010p02119, 1989a.

Russo, D., W. A. Jury, and G. L. Butters, Numerical analysis of solute transport during transient irrigation 1. The effect of hysteresis and profile heterogeneity, *Water Resources Research*, *25*(10), 2109–2118, doi: 10.1029/WR025i010p02109, 1989b.

Sankaran, M., N. Hanan, R. Scholes, J. Ratnam, D. Augustine, B. Cade, J. Gignoux, S. Higgins, X. Le Roux, F. Ludwig, J. Ardo, F. Banyikwa, A. Bronn, G. Bucini, K. Caylor, M. Coughenour, A. Diouf, W. Ekaya, C. Feral, E. February, P. Frost, P. Hiernaux, H. Hrabar, K. Metzger, H. Prins, S. Ringrose, W. Sea, J. Tews, J. Worden, and N. Zambatis, Determinants of woody cover in african savannas, *Nature*, *438*(7069), 846–849, doi:10.1038/nature04070, 2005.

Sankarasubramanian, a., R. M. Vogel, and J. F. Limbrunner, Climate elasticity of streamflow in the United States, *Water Resources Research*, *37*(6), 1771–1781, doi:10.1029/2000WR900330, 2001.

Sato, K., *Levy Processes and Infinitely Divisible Distributions*, Cambridge Univ. Press, Cambridge, U. K, 1999.

Savenije, H. H. G., Equifinality, a blessing in disguise?, *Hydrological Processes*, *15*(14), 2835–2838, 2001.

Saxton, K. E., and W. J. Rawls, Soil water characteristic estimates by texture and organic matter for hydrologic solutions, *Soil Science Society Of America Journal*, *70*(5), 1569–1578, doi:10.2136/sssaj2005.0117, 2006.

Scanlon, T. M., K. K. Caylor, S. A. Levin, and I. Rodriguez-Iturbe, Positive feedbacks promote power-law clustering of kalahari vegetation, *Nature*, *449*(7159), 209–U4, doi:10.1038/nature06060, 2007.

Schaake, J., From climate to flow, *Climate Change and U.S. Water Resources*, pp. 177–206, 1990.

Schaake, J., S. Cong, and Q. Duan, The us MOPEX data set, *Tech. rep.*, Lawrence Livermore National Laboratory, 2006.

Schaefli, B., C. J. Harman, M. Sivapalan, and S. J. Schymanski, Hydrologic predictions in a changing environment: behavioral modeling, *Hydrology and Earth System Sciences Discussions*, *7*, 7779–7808, doi: 10.5194/hessd-7-7779-2010, 2010.

Schenk, H. J., The shallowest possible water extraction profile: A null model for global root distributions, *Vadose Zone Journal*, *7*(3), 1119–1124, doi:10.2136/vzj2007.0119, 2008.

Schumer, R., D. A. Benson, M. M. Meerschaert, and B. Baeumer, Fractal mobile/immobile solute transport, *Water Resources Research*, *39*(10), 1296, doi:10.1029/2003WR002141, 2003.

Schumer, R. A., M. M. Meerschaert, and B. Baeumer, Fractional advection-dispersion equaitons for modeling transport at the earth surface, *Journal of Geophysical Research*, *114*, F00A07, doi:10.1029/2008JF001246, 2009.

Seaber, P., F. Kapinos, and G. Knapp, Hydrologic unit maps (USA), *US Geological Survey Water-Supply Paper*, *2294*, 1987.

Shaw, S. B., A. A. Harpold, J. C. Taylor, and M. T. Walter, Investigating a high resolution, stream chloride time series from the Biscuit Brook catchment, Catskills, NY, *Journal Of Hydrology*, *348*(3-4), 245–256, doi:10.1016/j.jhydrol.2007.10.009, 2008.

Sivapalan, M., Computer models of watershed hydrology (book review), *Catena*, *29*(1), 88–90, 1997.

Sivapalan, M., Prediction in ungauged basins: A grand challenge for theoretical hydrology, *Hydrological Processes*, *17*(15), 3163–3170, 2003a.

Sivapalan, M., Process complexity at hillslope scale, process simplicity at the watershed scale: Is there a connection?, *Hydrological Processes*, *17*(5), 1037–1041, doi:10.1002/hyp.5109, 2003b.

Sivapalan, M., Pattern, process and function: Elements of a unified theory of hydrology at the catchment scale, *Encyclopedia of Hydrological Sciences*, pp. 193–219, 2005a.

Sivapalan, M., Encyclopedia of hydrological sciences, in *Encyclopedia of Hydrological Sciences*, edited by M. G. Anderson, chap. Pattern, process and function: elements of a unified theory of hydrology at the catchment scale, pp. 193–219, John Wiley & Sons, Ltd., 2005b.

Sivapalan, M., The secret to 'Doing better hydrological science': Change the question!, *Hydrological Processes*, *1396*(November 2008), 1391–1396, doi:10.1002/hyp, 2009.

Sivapalan, M., M. A. Yaeger, C. J. Harman, X. Xu, and P. A. Troch, Functional model of water balance variability at the catchment scale: 1. Evidence of hydrologic similarity and spacetime symmetry, *Water Resources Research*, *47*, WW02,522, doi:10.1029/2010WR009568, 2010.

Sloan, W., A physics-based function for modeling transient groundwater discharge at the watershed scale, *Water Resources Research*, *36*(1), 225–241, 2000.

Stark, C. P., E. Foufoula-Georgiou, and V. Ganti, A nonlocal theory of sediment buffering and bedrock channel evolution, *Journal of Geophysical Research*, *114*, F01,029, doi:10.1029/2008JF000981, 2009.

Struthers, I., C. Hinz, and M. Sivapalan, A multiple wetting front gravitational infiltration and redistribution model for water balance applications, *Water Resources Research*, *42*(6), W06,406, doi:10.1029/2005WR004645, 2006.

Struthers, I., C. Hinz, and M. Sivapalan, Conceptual examination of climate-soil controls upon rainfall partitioning in an open-fractured soil ii: Response to a population of storms, *Advances in Water Resources*, *30*(3), 518 – 527, doi:10.1016/j.advwatres.2006.04.005, 2007.

Szilagyi, J., and M. Parlange, Baseflow separation based on analytical solutions of the Boussinesq equation, *Journal Of Hydrology*, *204*(1-4), 251–260, 1998.

Szilagyi, J., M. Parlange, and J. Albertson, Recession flow analysis for aquifer parameter determination, *Water Resources Research*, *34*(7), 1851–1857, 1998.

Tague, C., and L. Band, RHESSys: Regional hydro-ecologic simulation system: An object-oriented approach to spatially distributed modeling of carbon, water and nutrient cycling, *Earth Interactions*, *8*(19), 1–42, 2004.

Tague, C., and G. Grant, A geological framework for interpreting the low-flow regimes of cascade streams, Willamette River Basin, Oregon, *Water Resources Research*, *40*(4), W04,303, doi:10.1029/2003WR002629, 2004.

Tallaksen, L. M., A review of baseflow recession analysis, *Journal Of Hydrology*, *165*(1-4), 349–370, 1995.

Thompson, S., and G. Katul, Plant propagation fronts and wind dispersal: An analytical model to upscale from seconds to decades using superstatistics., *American Naturalist*, *171*(4), 468?479, doi:10.1103/PhysRevE. 71.016131, 2008.

Thompson, S. E., C. J. Harman, P. A. Troch, P. Brooks, and M. Sivapalan, Spatial scale dependence of ecohydrologically mediated water balance partitioning : A synthesis framework for catchment ecohydrology, *Water Resources Research*, *in press*, doi:10.1029/2009WR008821, 2011.

Touchette, H., and C. Beck, Asymptotics of superstatistics, *Physical Review E - Statistical, Nonlinear, and Soft Matter Physics*, *71*(1), 016,131, doi:10.1103/PhysRevE.71.016131, 2005.

Troch, P., F. Detroch, and W. Brutsaert, Effective water-table depth to describe initial conditions prior to storm rainfall in humid regions, *Water Resources Research*, *29*(2), 427–434, 1993a.

Troch, P., M. Mancini, C. Paniconi, and E. Wood, Evaluation of a distributed catchment scale water-balance model, *Water Resources Research*, *29*(6), 1805–1817, 1993b.

Troch, P., E. van Loon, and A. Hilberts, Analytical solutions to a hillslope-storage kinematic wave equation for subsurface flow, *Advances in Water Resources*, *25*(6), 637–649, 2002.

Troch, P. A., C. Paniconi, and E. E. van Loon, Hillslope-storage Boussinesq model for subsurface flow and variable source areas along complex hillslopes: 1. Formulation and characteristic response, *Water Resources Research*, *39*(11), doi:10.1029/2002WR001728, 2003.

Troch, P. A., A. H. van Loon, and A. G. J. Hilberts, Analytical solution of the linearized hillslope-storage Boussinesq equation for exponential hillslope width functions, *Water Resources Research*, *40*(8), W086,011–W086,016, doi:10.1029/2003WR002850, 2004.

Troch, P. A., G. A. Carrillo, I. Heidbüchel, S. Rajagopal, M. Switanek, T. H. M. Volkmann, and M. Yaeger, Dealing with landscape heterogeneity in watershed hydrology : A review of recent progress toward new hydrological theory, *Geography Compass*, *1*, 375–392, 2009a.

Troch, P. A., G. F. Martinez, V. R. N. Pauwels, M. Durcik, M. Sivapalan, C. Harman, P. D. Brooks, H. Gupta, and T. Huxman, Climate and vegetation water use efficiency at catchment scales, *Hydrological Processes*, *23*(16), 2409–2414, doi:10.1002/hyp.7358, 2009b.

Troch, P. A., G. F. Martinez, V. R. N. Pauwels, M. Durcik, M. Sivapalan, C. J. Harman, P. D. Brooks, H. V. Gupta, and T. E. Huxman, Climate and vegetation water use efficiency at catchment scales, *Hydrological Processes*, *23*(16), 2409–2414, 2009c.

Tromp-van Meerveld, H. J., and J. J. McDonnell, Threshold relations in subsurface stormflow 1: A 147 storm analysis of the panola hillslope trench, *Water Resources Research*, *42*, W02,410, doi: 10.1029/2004WR003778, 2006a.

Tromp-van Meerveld, H. J., and J. J. McDonnell, Threshold relations in subsurface stormflow: 2. The fill and spill hypothesis, *Water Resources Research*, *42*(2), W02,411, doi:10.1029/2004WR003800, 2006b.

Tromp-van Meerveld, H. J., A. L. James, J. J. McDonnell, and N. E. Peters, A reference data set of hillslope rainfall-runoff response, panola mountain research watershed, united states, *Water Resources Research*, *44*(6), 1–4, doi:10.1029/2007WR006299, 2008.

Uchida, T., K. Kosugi, and T. Mizuyama, Effects of pipeflow on hydrological process and its relation to landslide: a review of pipeflow studies in forested headwater catchments, *Hydrological Processes*, *15*(11), 2151–2174, doi:10.1002/hyp.281, 2001.

Uchida, T., I. T.-v. Meerveld, and J. J. Mcdonnell, The role of lateral pipe flow in hillslope runoff response: An intercomparison of non-linear hillslope response, *Journal of Hydrology*, *311*(1-4), 117–133, 2005.

Valentin, C., J. d'Herbes, and J. Poesen, Soil and water components of banded vegetation patterns, *Catena*, *37*(1-2), 1–24, 1999.

van Der Werf, H. M. G., Assessing the impact of pesticides on the environment, *Agriculture, Ecosystems and Environment*, *60*, 81–96, doi:10.1016/S0167-8809(96)01096-1, 1996.

Vitousek, P., Beyond global warming - ecology and global change, *Ecology*, *75*(7), 1861–1876, 1994.

Voepel, H., B. Ruddell, R. Schumer, P. Troch, P. Brooks, A. Neal, M. Durcik, and M. Sivapalan, Hydrologic controls on catchment-scale vegetation productivity, *Water Resources Research*, *Under review*, 2010.

Vogel, R. M., and C. N. Kroll, Regional geohydrologic-geomorphic relationships for the estimation of low-flow statistics, *Water Resources Research*, *28*(9), 2451–2458, 1992.

Šimůnek, J., M. Šejna, H. Saito, M. Sakai, and M. T. van Genuchten, The HYDRUS-1D software package for simulating the movement of water, heat, and multiple solutes in variably saturated media, *Tech. rep.*, Department Of Environmental Sciences University Of California Riverside Riverside, California, 2009.

Wagener, T., M. Sivapalan, J. J. McDonnell, R. Hooper, V. Lakshmi, X. Liang, and P. Kumar, Predictions in ungauged basins (PUB): A catalyst for multi-disciplinary hydrology, *EOS, Newsletter of the American Geophysical Union*, *85*(44), 451, 457, 2004.

Wagener, T., M. Sivapalan, P. A. Troch, and R. Woods, Catchment classification and hydrologic similarity, *Geography Compass*, *1*(4), 901–931, doi:10.1111/j.1749-8198.2007.00039.x, 2007.

Wagener, T., M. Sivapalan, P. A. Troch, B. L. McGlynn, C. J. Harman, H. V. Gupta, P. Kumar, P. S. C. Rao, N. B. Basu, and J. S. Wilson, The future of hydrology: An evolving science for a changing world, *Water Resources Research*, *46*(5), 1–10, doi:10.1029/2009WR008906, 2010.

Wang, P., P. Quinlan, and D. M. Tartakovsky, Effects of spatio-temporal variability of precipitation on contaminant migration in the vadose zone, *Geophysical Research Letters*, *36*(12), L12,404, doi: 10.1029/2009GL038347, 2009.

Western, A., S. Zhou, R. Grayson, T. Mcmahon, G. Bloschl, and D. Wilson, Spatial correlation of soil moisture in small catchments and its relationship to dominant spatial hydrological processes, *Journal of Hydrology*, *286*(1-4), 113–134, doi:10.1016/j.jhydrol.2003.09.014, 2004.

Whipkey, R. Z., Subsurface stormflow from forested slopes, *Bulletin of the International Association of Scientific Hydrology*, *10*(2), 74 – 85, 1966.

Whipkey, R. Z., Theory and mechanics of subsurface stormflow, in *International Symposium on Forest Hydrology*, edited by W. E. Sopper and H. W. Lull, pp. 255 – 259, Pergamon,, New York, 1967.

Wierenga, P. J., Solute distribution profiles computed with steady-state and transient water movement models1, *Soil Science Society of America Journal*, *41*(6), 1050–1055, doi: 10.2136/sssaj1977.03615995004100060006x, 1977.

Wittenberg, H., Baseflow recession and recharge as nonlinear storage processes, *Hydrological Processes*, *13*(5), 715–726, 1999.

Woods, R., The relative roles of climate, soil, vegetation and topography in determining seasonal and long-term catchment dynamics, *Advances in Water Resources*, *26*(3), 295–309, 2003.

Yang, D., F. Sun, Z. Liu, Z. Cong, G. Ni, and Z. Lei, Analyzing spatial and temporal variability of annual water-energy balance in nonhumid regions of china using the budyko hypothesis, *Water Resources Research*, *43*(4), W04,426, 2007.

Yu, M., Q. Gao, H. E. Epstein, and X. Zhang, An ecohydrological analysis for optimal use of redistributed water among vegetation patches, *Ecological Applications*, *18*(7), 1679–1688, 2008.

Zanardo, S., C. J. Harman, P. A. Troch, P. S. C. Rao, and M. Sivapalan, Climatic and landscape controls on inter-annual variability of water balance and vegetation water use : a stochastic approach, *Water Resources Research*, *Under review*, 2010.

Zecharias, Y. B., and W. Brutsaert, Recession characteristics of groundwater outflow and base-flow from mountainous watersheds, *Water Resources Research*, *24*(10), 1651–1658, 1988.

Zhang, L., W. Dawes, and G. Walker, Response of mean annual evapotranspiration to vegetation changes at catchment scale, *Water Resources Research*, *37*(3), 701–708, 2001.

Zhang, Y., D. Benson, and B. Baeumer, Predicting the tails of breakthrough curves in regional-scale alluvial systems, *Groundwater*, *45*(4), 473 – 484, 2007.

Vita

Ciaran Harman was born in Perth, Western Australia, where he received a Bachelor of Arts and a Bachelor of Environmental Engineering with First Class Honours from the University of Western Australia in 2003. He worked as a research assistant for the Cooperative Research Center for Catchment Hydrology, based at the University of Melbourne from 2003 to 2005. He received an M.S. in Geography at the University of Illinois in 2007.